Investigating the Role of FOSL2 and JUND in the Molecular Adaptation to Hypoxia in Colorectal Cancer

Submitted by:

Tammy Potgieter, BSc (Hons), MSc

School of Medicine

Department of Translational Medical Sciences

A thesis submitted to the University of Nottingham for the degree of Doctor of Philosophy

Abstract

Colorectal cancer is a major cause of cancer-related death worldwide, overall ranking third in terms of cancer incidence but second in terms of cancer mortality. Many solid tumours including approximately one third of colorectal tumours feature regions of tumour hypoxia, or low oxygen. Tumour hypoxia arises due to the increased metabolic and proliferative rates of tumour cells, alongside the poor oxygen supply delivered through aberrant tumour neovasculature. Whilst once considered a mere consequence of tumour expansion, tumour hypoxia is now recognised as a driving force of malignancy, contributing to factors such as invasion, metastasis and therapy resistance. The HIF transcription factors are the canonical regulators of the transcriptional response to hypoxia. However, it is becoming increasingly recognised that many other transcription factors play a role in regulating the molecular adaptation to hypoxia, despite this network being under-investigated and not fully elucidated. Preliminary data suggests that the AP1 transcription factor plays an important role in mediating hypoxic colorectal cancer survival. In cancer, AP1 deregulation is implicated in many pathways including differentiation, proliferation and apoptosis. However, the role of AP1 in tumour hypoxia is not well understood. It was hypothesised that the AP1 subunits FOSL2 and JUND mediate crucial aspects of the hypoxic response in CRC. Both FOSL2 and JUND were found to be upregulated under hypoxic conditions, and knockdown of both subunits led to significantly reduced 3D spheroid volume and cell survival in a clonogenic assay. RNA-sequencing identified FOSL2 in particular as a novel regulator of the hypoxic transcriptional response, significantly associating with 333 hypoxia-inducible genes involved in processes such as tumour metabolism and invasion. FOSL2 was therefore taken forward to analyse clinical relevance, where FOSL2 expression was significantly correlated with pro-metastatic variables such as high tumour budding and an infiltrative tumour edge in a large CRC tissue micro array. However, FOSL2 was not a significant prognostic indicator for 5-year survival and FOSL2 knockdown did not significantly impact tumour growth in a sub-cutaneous *in vivo* model. Further work is needed to validate the role of FOSL2 in the hypoxic response.

Acknowledgements

Principally, I would like to thank my supervisors Alan McIntyre and Andy Benest for the opportunity to complete this research and for ongoing support throughout.

Thank you to the BBSRC for funding this work and to the Nottingham BBSRC DTP Team for their excellent management of the programme.

I am extremely grateful to Dr Abhik Mukherjee and Declan Sculthorpe for their time and expertise in helping me to analyse the TMA. My gratitude extends to Alison Ritchie and Pam Collier for their support with the *in vivo* work within this project.

I would like to thank all members of the BDI Technical Team, in particular Vicky Norris, for their ability to keep the labs running smoothly and safely, even in the toughest of times, whilst also managing to keep everyone happy and motivated.

A big thank you to members of my lab group both past and present for the help and support we provided each other. A special thank you goes out to Eric Vancauwenberghe, for his infinite knowledge, wisdom and motivation, and for being an invaluable mentor from the first day and until the end. Thank you to friends along the way, notably Lou and Charlie, for encouragement and support which kept me going throughout.

Finally, this thesis would not have been possible without the love and support of my family. Thank you to my parents for providing me with the best example of hard work and resilience. Thank you to Austin for the love and encouragement, for many weekend trips into the lab and for supplying me with unlimited cups of tea. Thank you to my cats, Piper and Banjo, for hours of amusement which served as a welcome distraction, despite their attitude of indifference toward my work.

COVID Impact Statement

Unfortunately, the work submitted in this thesis was impacted significantly by the COVID-19 pandemic. The PhD project began in April 2019, and by March 2020 the research laboratories were closed for 5 months until August 2020. Following return to the laboratory, further research time was lost due to the intensive logistical issues that arose from the pandemic, including capacity restrictions and reagent supply problems. While all efforts were made to mitigate the lost research time, this was not always possible due to the practical nature of the research. This work has been completed within the original deadline and an extension has not been taken, and therefore represents a project completed with an interrupted period of around 6 months.

List of Abbreviations

ADP	Adenosine diphosphate
AKT	Protein kinase B
ANGPLT4	Angiopoietin-like 4
AP1	Activator protein 1
APC	Adenomatous polyposis coli
ATP	Adenosine triphosphate
bHLH	Basic helix-loop-helix
BME	Beta-mercaptoethanol
BSA	Bovine serum albumin
CA9	Carbonic anhydrase 9
cAMP	Cyclic adenosine monophosphate
CAS9	CRISPR-associated protein 9
c-Fos	C-Fos proto-oncogene
CIMP	CpG island methylator phenotype
CIN	Chromosomal instability
c-Jun	C-Jun proto-oncogene
CMS	Consensus molecular subtype
CRC	Colorectal cancer
CRE	cAMP-responsive element
CREB	cAMP-response element-binding protein
CRISPR	Clustered regularly interspaced short palindromic repeats
DBD	DNA-binding domain
dH_2O	Distilled H_2O
DNA	Deoxyribonucleic acid
dNTP	Deoxynucleotide triphosphate
ECM	Extracellular matrix
EDTA	Ethylenediaminetetraacetic acid

EGFR	Epidermal growth factor receptor
EMT	Epithelial to mesenchymal transition
ER	Estrogen receptor
ERK	Extracellular signal-related kinase
ETS	E26 transformation-specific family
FBS	Foetal bovine serum
FOSB	FosB proto-oncogene
FOSL1	FOS-like 1
FOSL2	FOS-like 2
GO	Gene ontology
gRNA	Guide RNA
GTP	Guanosine triphosphate
HAF	Hypoxia-associated factor
HAP	Hypoxia-activated pro-drug
HGF	Hepatocyte growth factor
HIF1	Hypoxia-inducible factor 1
HIF2	Hypoxia-inducible factor 2
HNPCC	Hereditary non-polyposis colorectal cancer
HRE	Hypoxia-response element
HSP60	Chaperonin
IF	Immunofluorescence
JNK	c-Jun N-terminal kinase
JUNB	JunB proto-oncogene
JUND	JunD proto-oncogene
KEGG	Kyoto encyclopaedia of genes and genomes
KD	Knockdown
LOH	Loss of heterozygosity
LZ	Leucine-zipper
MAPK	Mitogen-activated protein kinase

mCRC	Metastatic colorectal cancer
MEK	Mitogen-activated protein kinase kinase
MET	Hepatocyte growth factor receptor
miRNA	Micro RNA
MMR	Mismatch repair
MOI	Multiplicity of infection
mRNA	Messenger RNA
MSI	Microsatellite instability
MSS	Microsatellite stabile
mTOR	Mammalian target of rapamycin
NFκB	Nuclear factor kappa-light-chain-enhancer of activated B cells
PAM	Protospacer adjacent motif
PBS	Phosphate buffered saline
PCR	Polymerase chain reaction
PFA	Paraformaldehyde
PHD	Prolyl hydroxylase domain
PI3K	Phosphoinositide 3-kinase
PIC	Protease inhibitor cocktail
PIP_2	Phosphatidylinositol 4,5-biphosphate
PIP_3	Phosphatidylinositol (3,4,5)-triphosphate
PRAS40	Proline-rich AKT substrate of 40kDa
PTEN	Phosphatase and tensin homolog
RAF	Raf proto-oncogene serine/threonine kinase
RAS	Ras proto-oncogene GTPase
REST	RE1 silencing transcription factor
RIPA	Radioimmunoprecipitation assay buffer
RNA	Ribonucleic acid
RNA-SEQ	RNA-sequencing
rRNA	Ribosomal RNA

RTK	Receptor tyrosine kinase
SDS	Sodium dodecyl sulphate
SDS-PAGE	Sodium dodecyl sulphate polyacrylamide gel electrophoresis
SOS	Son of sevenless homolog 1
STAT	Signal transducer and activator of transcription
TBS	Tris buffered saline
TCS2	Tuberous sclerosis complex 2
TCA	Tricarboxylic acid cycle
TNM	Tumour-node-metastasis
TMA	Tissue micro-array
TP53	Tumour protein 53
UPW	Ultrapure water
UV	Ultraviolet
VEGF	Vascular endothelial growth factor
VHL	Von Hippel-Landau
WNK1	Lysine deficient protein kinase 1
WT	Wild-type

Table of Contents

Abstract 2

Acknowledgements 3

COVID Impact Statement 4

List of Abbreviations 5

Table of Contents 9

List of Figures and Tables 14

1.0 Introduction 19

1.1 Cancer 19

1.2 Colorectal Cancer 20

1.2.1 Incidence and Survival of Colorectal Cancer 20

1.2.2 Development of Colorectal Tumours 21

1.2.3 CRC and Genomic Instability 22

1.2.4 Consensus Subtypes of CRC 24

1.3 Transcriptional Signalling in Colorectal Cancer 26

1.3.1 General Mechanism of Transcription 26

1.3.2 Transcriptional Dysregulation in Cancer 27

1.3.3 Transcriptional Dysregulation in CRC 28

1.4 Tumour Hypoxia 29

1.4.1 Development of Hypoxia Within Tumours 29

1.4.2 Hypoxia and Therapy Resistance 31

1.4.3 Hypoxia Inducible Factors 32

1.4.3.1 HIF Structure and Isoforms 32

1.4.3.2 HIF Regulation 33

1.4.4 HIF-Regulated Pathways in Cancer 36

1.4.5 Targeting Tumour Hypoxia 38

1.4.5.1 Hypoxia-Activated Pro-drugs 38

1.4.5.2 Targeting HIF Signalling 39

1.5 Additional Transcriptional Regulators of Tumour Hypoxia 41

1.5.1 NFκB 41

1.5.2 ETS 41

1.5.3 p53 42

1.5.4 REST 43

1.5.5 Additional Factors Regulating the Hypoxic Response 44

1.6 The Role of AP1 in Cancer 45

1.6.1 AP1 Family and Structure 45
1.6.2 The Dual Role of AP1 in Cancer 46
1.6.3 AP1 in Hypoxia 47
1.7 Project Aims and Hypotheses 49
2.0 Materials and Methods 50
2.1 Cell Culture 50
2.1.1 Maintenance of Cells 50
2.1.2 Passaging of Cell Lines 50
2.1.3 Hypoxic Culture Conditions 51
2.1.4 Cryopreservation of Cell Lines 51
2.1.5 Cell Counting 51
2.2 3D Cell Culture 51
2.3 Clonogenic Assay 52
2.4 Generation of Inducible Knockdown Pooled Populations 53
2.4.1 Generation of Inducible Cas9 Cell Lines 53
2.4.2 Generation of Inducible Knockdown Cell Pools 54
2.5 Generation of Knockdown Clones 55
2.5.1 Lipofection with Synthetic gRNAs 55
2.5.2 Single Clone Selection 56
2.6 DNA Extraction and Sequencing 57
2.6.1 DNA Extraction 57
2.6.2 Polymerase Chain Reaction 58
2.6.3 Agarose Gel Electrophoresis 59
2.6.4 Gel Extraction of DNA 59
2.7 Western Blot 60
2.7.1 Protein Extraction 60
2.7.2 Protein Quantification 61
2.7.3 Gel Electrophoresis 61
2.7.4 Gel Transfer and Immunoblotting 62
2.8 Phos-Tag 63
2.8.1 Protein Extraction 63
2.8.2 Sample Preparation 64
2.8.3 Gel Electrophoresis and Transfer 64
2.8.4 Immunoblotting 65
2.9 Immunocytochemistry 65
2.10 Proteome Profiler Phospho-Kinase Array 66

2.11 RNA Extraction and Quantitative PCR 67
2.11.1 RNA Extraction 67
2.11.2 cDNA Synthesis 67
2.11.3 Quantitative PCR 68
2.12 RNA-Sequencing 69
2.12.1 Sample Preparation 69
2.12.2 Sequencing 70
2.13 Tissue Micro-Array 71
2.14 In Vivo Study 71
2.15 Statistical Analyses 71
3.0 Investigating the Role of FOSL2 and JUND in Regulating the Hypoxic Transcriptome 72
3.1 Introduction 72
3.1.1 Investigating Tumour Hypoxia by Transcriptomics 72
3.2 Aims and hypotheses 74
3.3 Results 75
3.3.1 FOSL2 Expression in Hypoxia 75
3.3.2 Generation of Inducible FOSL2 Knockdown Cell Lines 76
3.3.3 Effect of FOSL2 Knockdown on 3D Spheroid Growth 87
3.3.4 Effect of FOSL2 Knockdown on Cell Survival 90
3.3.5 The FOSL2-Associated Hypoxic Transcriptome 92
3.3.6 JUND Expression in Hypoxia 106
3.3.7 Generation of Inducible JUND Knockdown Cell Lines 107
3.3.8 Effect of JUND Knockdown on 3D Spheroid Growth 111
3.3.9 Effect of JUND Knockdown on Cell Survival 115
3.3.10 The JUND-Associated Hypoxic Transcriptome 116
3.3.11 FOSL2 and JUND Co-association with Hypoxic Targets 124
3.3.12 FOSL2 Knockdown Xenograft Experiment 127
3.4 Discussion 136
3.4.1 Phenotypic Role of FOSL2 and JUND in CRC 136
3.4.2 FOSL2-Associated Hypoxic Transcriptome 137
3.4.3 JUND-Associated Hypoxic Transcriptome 139
3.4.4 FOSL2 and JUND Co-associated Hypoxic Targets 140
3.4.5 Role of FOSL2 in Tumour Growth *in vivo* 141
4.0 Investigating the Clinical Relevance of FOSL2 in CRC 143
4.1 Introduction 143
4.1.1 AP1 as a Prognostic Biomarker in Cancer 143

4.1.2 AP1 Inhibitors to Target Cancer 144
4.2 Aims and hypotheses 147
4.3 Results 148
4.3.1 H-Scoring Method for Immunohistochemistry 148
4.3.2 FOSL2 Clinical Associations Across the Whole Tumour 152
4.3.3 FOSL2 Clinical Associations in the Tumour Centre 159
4.3.4 FOSL2 Clinical Associations in the Advancing Edge 161
4.3.5 FOSL2 Clinical Associations in Immune Cell Staining 162
4.3.6 Alternative Method of Analysis 164
4.3.7 Clinicopathological Analysis Split by Gender 166
4.3.8 FOSL2 Correlation with Additional Markers 168
4.4 Discussion 171
4.4.1 Association of FOSL2 with Pro-Metastatic Variables 171
4.4.2 Association of FOSL2 with Patient Survival 173
4.4.3 Role of FOSL2 in Immune Cells 174
5.0 Investigating the Role of FOSL2 in Hypoxic Phospho-Signalling 175
5.1 Introduction 175
5.1.1 Targeting Signal Transduction in CRC 175
5.1.2 Signal Transduction in Hypoxia 176
5.1.3 AP1 Signalling 177
5.2 Aims and hypotheses 179
5.3 Results 180
5.3.1 FOSL2 Phosphorylation in Hypoxia 180
5.3.2 FOSL2 Localisation in Hypoxia 181
5.3.3 Generation of HIF1α and HIF2α knockdown clones 185
5.3.4 Investigating the role of HIF1α, HIF2α and FOSL2 in hypoxic phospho-signalling 188
5.4 Discussion 207
5.4.1 FOSL2 Phosphorylation in Hypoxia 207
5.4.2 HIF-Associated Hypoxic Signalling 209
5.4.3 FOSL2 Association with Hypoxic Signalling 211
6.0 Discussion and Future Directions 212
6.1 Overall Conclusions 212
6.2 Future Directions 214
6.2.1 Validating the Role of FOSL2 as a Hypoxic Target in CRC 214
6.2.2 Investigating the FOSL2 Hypoxic Interactome 216
6.2.3 Investigating the Role of JUND in Associating with the Hypoxic Response 217

6.3 Limitations of Methodology 218
7.0 Appendix 220
7.1 Supplementary Experimental Information 220
7.2 Professional Internship Placement: Reflective Statement 224
8.0 Bibliography 227

List of Figures and Tables

Figure 1.1 Categorisation of colorectal tumours into 4 CMS subtypes

Figure 1.2 Development of tumour hypoxia

Figure 1.3 Regulation of HIFs in normoxia and hypoxia

Figure 2.1 Schematic map of the Edit-R Inducible Lentiviral Cas9 Nuclease vector

Figure 2.2 Schematic map of the Sanger Lentivirus LV04 vector

Table 2.1 gRNA sequences for JUND and FOSL2 purchased in the LV04 vector format

Table 2.2 gRNA sequences for HIF1α and HIF2α purchased as synthetic gRNAs

Table 2.3 Optimisation of CRISPR-Cas9 approaches

Table 2.4 Components for PCR per DNA sample

Table 2.5 PCR cycling protocol

Table 2.6 Details of antibodies used in this project

Table 2.7 Reverse transcription Mastermix components per sample

Table 2.8 Cycling programme for the cDNA synthesis reaction

Table 2.9 qPCR Mastermix components per reaction well

Table 2.10 Cycling programme for qPCR

Figure 3.1 FOSL2 and CA9 protein expression under normoxic (21% O_2), physoxic (8.5% O_2) and hypoxic (1% O_2) conditions in Ls174T across multiple time points.

Figure 3.2 Illustrative qPCR data demonstrating discrepancies between the siRNA and clonal knockdown approach in Ls174T

Figure 3.3 Illustrative qPCR data demonstrating clonal heterogeneity across several genes in Ls174T

Figure 3.4 Schematic diagram depicting both CRISPR-Cas9 approaches optimised for this project

Figure 3.5 Generation of inducible FOSL2 knockdown cell lines representing the CMS3 subtype

Figure 3.6 Generation of inducible FOSL2 knockdown cell lines representing the CMS4 subtype

Figure 3.7 Effect of FOSL2 knockdown on 3D spheroid growth in HCT116

Figure 3.8 Attempts to form Ls174T spheroids with images shown at the day 5 time-point

Figure 3.9 Effect of FOSL2 knockdown on Ls174T cell survival in the clonogenic assay

Table 3.1 RNA purity and integrity values for HCT116 control and FOSL2 knockdown samples submitted for RNA-sequencing

Figure 3.10 Validation of HCT116 control and FOSL2 knockdown RNA samples prior to RNA-sequencing

Figure 3.11 RNA-sequencing sample correlation and gene expression distributions

Figure 3.12 Co-expressed and differentially expressed genes between control hypoxia and control normoxia

Table 3.2 Top 20 DEGs upregulated in control hypoxia vs control normoxia

Table 3.3 AP1 subunits upregulated in control hypoxia vs control normoxia

Figure 3.13 KEGG pathway analysis of significantly upregulated genes in control hypoxia compared to control normoxia

Figure 3.14 Co-expressed and differentially expressed genes between control hypoxia and FOSL2 knockdown hypoxia

Table 3.4 Top 30 DEGs associated with FOSL2 and upregulated in hypoxia compared to normoxia

Figure 3.15 KEGG pathway analysis of significantly downregulated genes in FOSL2 knockdown hypoxia compared to control hypoxia

Table 3.5 KEGG pathways significantly associated with both FOSL2 and induced by hypoxia

Table 3.6 Differentially expressed genes comprising the significant KEGG pathways that are both induced by hypoxia and associated with FOSL2

Figure 3.16 JUND and CA9 protein expression under normoxic (21% O_2), physoxic (8.5% O_2) and hypoxic (1% O_2) conditions in Ls174T across multiple time points

Figure 3.17 Generation of inducible JUND knockdown cell lines representing the CMS3 subtype

Figure 3.18 Generation of inducible JUND knockdown cell lines representing the CMS4 subtype

Figure 3.19 Effect of JUND knockdown on 3D spheroid growth in HCT116

Figure 3.20 Effect of JUND knockdown on Ls174T cell survival in the clonogenic assay.

Table 3.7 RNA purity and integrity values for HCT116 control and JUND knockdown samples submitted for RNA-sequencing

Figure 3.21 Validation of HCT116 control and JUND knockdown RNA samples prior to RNA-sequencing

Figure 3.22 Co-expressed and differentially expressed genes between control hypoxia and JUND knockdown hypoxia

Table 3.8 Top 30 DEGs associated with JUND and upregulated in hypoxia compared to normoxia

Figure 3.23 KEGG pathway analysis of downregulated genes in JUND knockdown hypoxia compared to control hypoxia

Figure 3.24 GO analysis of downregulated genes in JUND knockdown hypoxia compared to control hypoxia

Table 3.9 Hypoxia-induced DEGs associated with both FOSL2 and JUND

Table 3.10 Associations of co-associated FOSL2 and JUND DEGs with biological functions

Table 3.11 Experimental groups for FOSL2 KD/Control HCT116 and Ls174T xenograft experiment (CSU1909)

Figure 3.25 Average tumour volumes for HCT116 FOSL2 knockdown and control experiment

Figure 3.26 Average growth rate for HCT116 FOSL2 knockdown and control experiment

Figure 3.27 Average tumour volumes for Ls174T FOSL2 knockdown and control experiment

Figure 3.28 Average growth rate for Ls174T FOSL2 knockdown and control experiment

Figure 3.29 Western blots showing FOSL2 and CA9 expression in HCT116 control and FOSL2 knockdown clone tumours (CSU1869D)

Figure 3.30 Analysis of CA9 and FOSL2 expression in HCT116 control and FOSL2 knockdown tumour samples

Figure 4.1 Summary of current AP-1-targeting approaches

Figure 4.2 Organisation of the colorectal cancer TMA slides

Figure 4.3 Distinguishing tumour from normal colonic epithelium

Figure 4.4 Categorising stain intensity scores for the H-scoring method

Figure 4.5 Calculating the H-score

Table 4.1. Descriptive statistics for FOSL2 H-scores valid for analysis

Figure 4.6 Histogram depicting the distribution of FOSL2 H-scores

Table 4.2 Clinicopathological variables that FOSL2 expression was analysed against including their respective categories

Figure 4.7 Statistically significant associations of FOSL2 expression averaged across all tumour regions

Figure 4.8 Kaplan-Meier plot of cumulative survival against overall survival/month for FOSL2 expression

Figure 4.9 Statistically significant associations of FOSL2 expression in the central tumour

Figure 4.10 Statistically significant associations of FOSL2 expression at the advancing edge of the tumour

Figure 4.11 Example immune cell staining for FOSL2

Figure 4.12 Statistically significant associations of FOSL2 absence or presence of immune cell staining in the luminal cores

Figure 4.13 Statistically significant associations of FOSL2 absence or presence of immune cell staining at the tumour advancing edge

Figure 4.14 Statistically significant associations of FOSL2 expression with additional markers

Table 4.3 Statistically significant associations of FOSL2 expression across the average of the tumour regions when comparing the highest FOSL2 expressor tertile vs all others

Table 4.4 Statistically significant associations of FOSL2 expression across the average of the tumour regions when comparing male highest FOSL2 expressor tertile vs all others

Table 4.5 Statistically significant associations of FOSL2 expression across the average of the tumour regions when comparing female highest FOSL2 expressor tertile vs all others

Table 4.6 A summary of all statistically significant results when analysing FOSL2 expression associations with clinicopathological variables

Figure 5.1 Regulation of AP1 expression and activity by the MAPK pathway

Figure 5.2 Phosphorylated FOSL2 protein levels under normoxic (21% O_2) or hypoxic (1% O_2) conditions in HCT116 and Ls174T cell lines across multiple time-points

Figure 5.3 Representative images of FOSL2 localisation in normoxic (A, 21% O_2) or hypoxic (B, 1% O_2) conditions in HCT116

Figure 5.4 Representative images of FOSL2 localisation in normoxic (A, 21% O_2) or hypoxic (B, 1% O_2) conditions in Ls174T

Figure 5.5 Generation of HIF1α and HIF2α knockdown cell lines in Ls174T

Figure 5.6 Validation of Ls174T HIF1α and HIF2α knockdown clones by Sanger sequencing

Figure 5.7 Experimental process for the phospho-kinase array experiment

Figure 5.8 Phospho-kinase array targets normalising control hypoxia (1% O_2) to control normoxia (21% O_2) in Ls174T cells

Figure 5.9 Phospho-kinase array targets normalising HIF1α knockdown and HIF2α knockdown hypoxia conditions to control hypoxia in Ls174T cells

Figure 5.10 Phospho-kinase array targets normalising FOSL2 knockdown hypoxia to control hypoxia in Ls174T cells

Figure 5.11 Heatmap depicting changes induced by HIF1α, HIF2α and FOSL2 knockdown in hypoxia normalised to control hypoxia

Figure 5.12 Significantly associated FOSL2 targets alongside values for HIF1α and HIF2α knockdown conditions

Table 5.1 Significantly associated FOSL2 target parameters

Figure 5.13 Schematic diagram demonstrating FOSL2 association with phospho-signalling pathways

Figure 5.14 Validation of phospho-array target hypoxic induction in Ls174T in 10% and 0.5% FBS

Figure 5.15 Validation of phospho-array target hypoxic induction in HCT116 in 10% and 0.5% FBS

1.0 Introduction

1.1 Cancer

Cancer is a set of diseases arising from a complex multistep process in which successive genetic alterations drive the transformation of healthy into malignant cells. These alterations will firstly confer a selective advantage to allow for initial clonal expansion, as well as providing genomic instability to lead to subsequent mutations in other genes required for malignancy. In addition to genetic mutation, these alterations are often a combination of changes which also involve chromosomal rearrangements, gene amplification and epigenetic modifications, predominantly occurring in proto-oncogenes and tumour-suppressor genes[1]. The activation of proto-oncogenes and the inactivation of tumour suppressor genes enable the cancer cells to sustain proliferative signalling, leading to uncontrolled cell division and the formation of a tumour mass in the case of solid tumours. TP53 is an example of a classical tumour suppressor gene with an antiproliferative role in response to various stresses. It is therefore unsurprising that somatic mutations in TP53 are present in almost all human cancers[2]. In addition to *de novo* mutation, inherited mutations in many cancer-associated genes predispose individuals to cancer. For example, TP53 germline mutations cause the Li-Fraumeni Syndrome, associated with a wide range of early-onset tumours including brain tumours, breast tumours and sarcomas[3]. An important consideration for clinical oncology is mutational intratumour heterogeneity, where research has mapped the clonal evolution of tumours and their metastases through multi-region sequencing, revealing the presence of oncogenic driver mutations that are distinct to certain tumour or metastatic regions, as well as those that are ubiquitous[4]. More recent research has highlighted the importance of additional levels of heterogeneity, including transcriptomic and immunogenic as well as genetic heterogeneity within tumours[5].

In addition to increased and uncontrolled proliferation, cancer cells acquire additional traits that enable tumour growth and subsequent metastatic dissemination, in an organising principle termed the 'hallmarks of cancer'[6,7]. Such traits include the

induction of angiogenesis, evasion of the immune system and activation of invasion and metastasis. These fundamental characteristics of cancer cells are facilitated by genome instability and the tumour microenvironment. Over the last decade, research has directed a paradigm shift in our perception of cancer away from a mass of proliferating cells, and towards a complex and dynamic structure of multiple distinct cell types. Tumour cells are able to recruit and reprogram normal cells including fibroblasts, vascular cells and immune cells which form the tumour-associated stroma, and heterotypic interactions between neoplastic and normal cell types contribute to tumourigenesis[8]. For example, tumour cells are able to recruit fibroblasts which are reprogrammed into 'cancer-associated fibroblasts', or CAFs. CAFs play an important role in the deposition and remodelling of extracellular matrix (ECM). Following dissemination of cancer cells, CAF activation at secondary sites help to establish macrometastases through the production of matrix components such as periostin which provide supportive signals to cancer cells[9]. Other factors are able to stimulate tumour cell proliferation directly, such as the secretion of hepatocyte growth factor (HGF) from some stromal cells results it activation of the MET receptor and mitogen-activated protein kinase (MAPK) signalling. In this context, signalling from the tumour-associated stroma can have important implications for targeted therapy, as the tumour cells display innate resistance to RAF inhibition, for example to BRAF inhibition in BRAF-mutant melanoma cells[10].

1.2 Colorectal Cancer

1.2.1 Incidence and Survival of Colorectal Cancer

Colorectal cancer (CRC) encompasses cancers of the colon and rectum. CRC is a major cause of cancer-related death worldwide, overall ranking third in terms of cancer incidence but second in terms of cancer mortality. In 2020 it is estimated that over 1.9 million new CRC cases occurred, resulting in 935,000 deaths and accounting for around 1 in 10 cancer cases and deaths[11]. Globally, the distribution of incidences of CRC varies widely, with up to a 9-fold variation in incidence rates by world regions, with the most

cases seen in Western countries[12]. In this regard, CRC can be considered a marker of socioeconomic development, with incidence rates rising uniformly with the Human Development Index (HDI) in countries undergoing major development transition. This increase in incidence is mainly attributed to an increased exposure to environmental risk factors that arise from a shift in lifestyle and diet towards westernisation[13]. On the contrary, higher developed countries over the last decade have seen a decreasing trend in the numbers of new cases of CRC. This is likely due to a number of factors including the implementation of nationwide screening programmes. Despite this, increasing numbers of CRC cases coupled with a rising incidence among younger generations remains a concern and a significant public health challenge. The global number of CRC cases is expected to reach 3.2 million in 2040 based on projections of aging, population growth and human development[14].

Using data collected from the last decade, CRC in the UK had a 5-year survival rate of 61% for males and 63% for females, averaged over all stages. CRC staging is primarily based on the tumour-nodes-metastasis (TNM) system. For stage I CRC, the 5 year survival rate is 94% in males and 97% in females[15]. Mortality rates increase dramatically for those diagnosed with metastatic disease (mCRC), and patients with unresectable metastases have a limited median survival of around 5 months when treated only with supportive care[16]. While the survival of mCRC has been improved, progress is hindered by the highly heterogeneous nature of the disease. CRC is driven by a great variety of driving mutations, and as such a 'catch-all' molecular therapy is not possible to develop, and precision medicine based on individual tumour profiling becomes more important.

1.2.2 Development of Colorectal Tumours

As with other forms of cancer, colon tumours develop through a multi-step process involving a sequential acquisition of genetic and epigenetic changes that accumulate over time[17]. Typically, CRC begins with the non-cancerous proliferation of mucosal epithelial cells that form localised growths of abnormal cells known as polyps. Polyps form within the intestinal mucosa, and only around 10% of these growths will progress

to an invasive cancer. The risk of this progression increases as the benign growth grows larger and can take many years due to the number of alterations required to drive the transformation of the cells to invasive and metastatic disease[18]. Where invasive tumours do arise from benign polyps, these are termed adenocarcinomas, and account for 96% of all CRCs[19].

Mutations in specific oncogenes, tumour suppressor genes and DNA repair genes can provide certain mucosal cells with a selective advantage and lead to increased and uncontrolled proliferation. CRCs can be classified as sporadic, inherited or familial depending on how these mutations arise. Inherited CRCs are rare and account for only 5% of all CRCs. Patients inherit one mutated allele of a gene, and a point mutation arising in the normal allele later in life triggers the onset of carcinogenesis. Two groups of inherited CRCs have been classified. These include familial adenomatous polyposis (FAP), and hereditary non-polyposis colorectal cancer (HNPCC)[20,21]. FAP is characterised by the formation of many malignant polyps in the colon, and is caused by the autosomal dominant inheritance of a germline mutation in the APC (adenomatous polyposis coli) gene. APC plays a key role in the Wnt signalling pathway which is important to the pathogenesis of CRC[22]. APC leads to the degradation of oncogenic β-catenin through the formation of a destruction complex in partnership with GSK-3β and Axin/Axin2. A loss of APC function therefore leads to β-catenin accumulation. β-catenin then translocates to the nucleus, complexes with Tcf/Lef and activates the transcription of downstream oncogenic target genes involved in cellular growth and proliferation[23]. Due to the important contribution of APC inactivation to the pathogenesis of hereditary CRC, it is unsurprising that APC mutation is also found in up to 85% of sporadic CRCs[24]. HNPCC on the other hand, is related to inherited mutations in genes encoding DNA repair proteins, such as PMS1, PMS2, MLH1, MLH6 and MSH2[20].

1.2.3 CRC and Genomic Instability

At the DNA level, CRCs are heterogeneous and can be classified according to their status of genomic instability, which represents an important hallmark of cancer. The

aforementioned DNA repair mutations featuring prominently in HNPCC as well as many sporadic tumours lead to microsatellite instability (MSI). Around 15% of primary CRCs are characterised by MSI. Patients with MSI-positive CRCs display a high level of DNA replication errors, particularly within the repetitive DNA sequences known as microsatellites[25]. These are tandem repeats of one to five base pairs. A standard panel of five microsatellite markers is used to assess the MSI status of a CRC patient, with MSI-high (MSI-H) tumours exhibiting instability in ≥ 30% of markers. In contrast, patients with MSI-low (MSI-L) tumours display instability in <30% of markers. Finally, patients with no apparent MSI are referred to as microsatellite stable (MSS)[26]. MSI is associated with a higher mutation rate and subsequent increased risk for malignancy through replication errors caused by an impaired DNA mismatch repair (MMR) system[27,28]. In sporadic cases of MSI-H CRC, hypermethylation of the MLH1 promoter is responsible for over 50% of cases, whereas a somatic mutation of MLH1 and MSH2 accounts for only around 15% of cases[29]. Thus, impairment of the MMR system can occur through epigenetic inactivation as well as somatic mutation. This represents an overlap between MSI and CpG Island Methylator Phenotype (CIMP), another form of genomic instability that features in CRC. CIMP tumours are characterised by widespread hypermethylation of CpG islands, and can be found in approximately 30-35% of CRCs[30]. Similarly to assessing MSI status, CIMP status can be assessed by a panel of methylation markers, characterising CRC as exhibiting or not exhibiting DNA methylation to the level of certain standards[31]. Tumours designated as CIMP-high have associations with MSI status (80%) and over half featuring BRAF mutations[32]. In contrast, CIMP-low CRCs are associated with a very high frequency of the KRAS mutation (>90%), and a typically high rate of TP53 mutations (~70%)[33].

The most common form of genomic instability in CRC is chromosomal instability (CIN), present in around 85% of all cases of CRC[34]. CIN is characterised by alterations of chromosome number and structure, which may include gains and losses of whole chromosomes or chromosomal segments, rearrangements of chromosomes and loss of heterozygosity (LOH) events[35]. These chromosomal changes affect the expression of tumour-associated genes, in turn activating pathways essential to CRC initiation[36]. It is unsurprising that CIN tumours display a high frequency of LOH and allelic loss at

the loci of tumour suppressor genes, including APC on chromosome 5q and TP53 on chromosome 17p[37]. In addition, an allelic loss at chromosome 18q is a common event detected in nearly 70% of CRCs during late carcinogenesis[38,39]. Located within this region are the SMAD2 and SMAD4 genes, encoders of downstream transforming growth factor-β (TGF-β) signal transducers. Loss of SMAD2 and SMAD4 may therefore contribute to tumourigenesis through conferring a resistance to TGF-β[40,41]. As well as chromosomal gains and losses, CIN tumours are also recognised by the accumulation of mutations in certain oncogenes and tumour suppressors. For example, as well as being lost through allelic loss or LOH, somatic APC mutations are frequent events in CIN-positive CRCs[42]. Similarly, somatic TP53 mutations are common in the majority of CRC cases and appear to be important in the transition of adenoma to carcinoma, given the increased frequency in the carcinoma stages of development, often occurring as missense mutations[43]. Finally, oncogenic mutations are also characteristic of CIN-positive CRCs, most notably occurring in the KRAS oncogene. The KRAS protein is a membrane-bound GTP/GDP-binding protein with intrinsic GTPase activity which mutations often impair, causing accumulation of active GTP-bound KRAS and constitutive downstream activation of proliferative pathways. Activating KRAS mutations feature in 35-40% of CRCs, mostly occurring in codons 12 and 13[44].

1.2.4 Consensus Subtypes of CRC

CRC is a highly heterogeneous set of diseases, and the concept of molecular subtyping these tumours is advantageous to the progression of personalised treatments as well as to aid better understanding of tumour development and characteristics. Many different classification systems have been proposed for CRC over the years, including defining tumour characteristics such as genetic features, tumour microenvironment and immunological characters[45]. The identification of four consensus molecular subtypes (CMS) gained attention within the field for its potential to stratify CRCs into four distinct groups[46]. Briefly, CMS1 tumours (known as MSI immune) make up 14% of CRCs and display MSI-H, hypermethylation and hypermutation. CMS1 tumours are also characterised by immune infiltration and activation alongside frequent BRAF mutations. CMS2, or canonical subtype, encompasses around 37% of all CRCs and

exhibit an MSS status, activated Wnt and Myc pathways, mutated TP53 and an elevated EGFR expression. CMS3 (metabolic) tumours make up 13% of CRCs and show elevated multiple metabolic signatures, moderately activated Wnt/Myc signalling and mutation of KRAS and PIK3CA. The final subtype, CMS4 (mesenchymal), is characterised by activation of the TGF-β pathway and epithelial-mesenchymal transition (EMT), contributing to chemoresistance[46]. Figure 1.1 summarises these key characteristics. Importantly, colorectal cancer cell lines used to study CRC *in vitro* have been successfully classified into CMS subtypes and have been shown to accurately recapitulate the genomic profiles of primary carcinomas, allowing for a more targeted approach to basic CRC research and drug screening[47].

CMS1 MSI immune	CMS2 Canonical	CMS3 Metabolic	CMS4 Mesenchymal
14%	37%	13%	23%
MSI, CIMP high, hypermutation	SCNA high	Mixed MSI status, SCNA low, CIMP low	SCNA high
BRAF mutations		*KRAS* mutations	
Immune infiltration and activation	WNT and MYC activation	Metabolic deregulation	Stromal infiltration, TGF-β activation, angiogenesis
Worse survival after relapse			Worse relapse-free and overall survival

Figure 1.1 Categorisation of colorectal tumours into 4 CMS subtypes. CMS1-4 incorporate key pathological features of CRCs such as microsatellite stability status, key driving mutations, involvement of immune cells and key activated pathways. Figure taken from Guinney et al., 2015.

The ability to identify key oncogenic changes characteristic to these subtypes is of important clinical relevance. For example, it has been found that for CMS1 CRCs exhibiting defective MMR tumours, mutant neoantigen expression contributes to the efficiency of immune checkpoint blockade therapy. This achieved an expected response in 53% of tumours and a complete response in 21% of patients[48]. However, identifying individual mutations common across a subtype of CRC and using this to guide personalised treatment may pose too simplistic of an approach. For example, EGFR mutation status does not seem to predict efficacy of anti-EGFR monoclonal

antibody therapies such as cetuximab and panitumumab that have provided clinical benefit to a subset of patients with mCRC[49,50]. Instead, resistance to this form of therapy is mediated through somatic KRAS mutations, which result in constitutive activation of the RAS-MEK-ERK pathway functioning downstream of the EGFR receptor[51–53]. It is therefore necessary to determine the mutation status of RAS prior to anti-EGFR therapies[54]. However, even in CRC patients with wild-type RAS, cetuximab treatment is effective in less than 10% of patients, with most showing further disease progression as the cancer cells further mutate and develop acquired resistance to targeted therapies[55,56]. Combination therapy approaches are therefore likely to be necessary to overcome these acquired resistance strategies of CRC cells[57,58]. In addition to this, the CMS subtyping would consider wild-type RAS status as a homogenous state for deciding therapeutic options. Despite this, wild-type RAS has been found across multiple different CMS groups with significant biological differences, which will inevitably translate into heterogeneous drug efficacies. A more individual and combinatorial approach will therefore be necessary for truly efficacious personalised treatment, however subtyping such as the CMS system has been important in applying gene classifications to cell lines and organoids with drug sensitivity data[46].

1.3 Transcriptional Signalling in Colorectal Cancer

1.3.1 General Mechanism of Transcription

The process of mRNA synthesis is known as transcription, and it is responsible for the cell-specific expression of protein-coding genes. Transcription occurs within the nuclei of cells and can be broadly categorised into four stages: pre-initiation, initiation, elongation and termination[59]. Transcription begins with the assembly of a large pre-initiation complex (PIC), triggered by the binding of transcription factor II D (TFIID) to the promoter of the gene that is being regulated. Other proteins within this large complex are recruited, and these include transcription factors, cofactors, RNA polymerase II (Pol II), mediator complexes and the TFIIH complex. TFIIH contains

subunits with intrinsic helicase and ATPase activities which are necessary for the unwinding of the DNA double helix at the gene promoter region[60]. After transcription of the initial nucleotides, elongation then begins which consists of releasing the gene promoter, binding of elongation factors, and phosphorylation of the Pol II C-terminal domain (CTD) by CDK7[61]. The stability of the transcriptional machinery is increased and elongation continues until the site of polyadenylation has been transcribed, and mRNA is cleaved away from the transcriptional machinery in a process known as termination[62]. Additional factors are involved in mRNA processing prior to translation. Transcription factors themselves are proteins with DNA-binding domains that are able to bind to specific consensus sequences within the promoter and/or enhancer regions of their target genes in order to regulate transcription. Additional domains within the structure of transcription factors allows for interactions with additional cofactors, the presence or absence of which helps to tightly regulate transcription and contributes to cell-specific transcriptomes[59].

1.3.2 Transcriptional Dysregulation in Cancer

The tightly regulated process of transcription can be deregulated in cancer through a variety of mechanisms. When the list of 1571 known or candidate oncogenic proteins is cross-referenced to the 1988 documented human transcription factors, a significant 19% of all known oncogenes are in fact characterised as transcription factors[63]. As transcription factors are considered the terminal effectors of signalling pathways, a deregulation of just a few transcription factors can have a significant impact on gene expression profiles in cancer. Not only can the transcription factors themselves be oncogenic, but oncogenes representing other upstream categories of cellular proteins such as signal transducers and growth factor receptors can lead to aberrant activation of transcription factors and their downstream effectors[64]. Cancer cells rely on constitutive activation of oncogenic transcription factors for many hallmarks of cancer, including tumour initiation, progression and metastasis. Conversely, tumour suppressive transcription factors undergo loss of function in cancer, allowing for sustained proliferative signalling to drive tumour progression. Most notably, around 50% of all cancers exhibit a loss of function mutation in p53, a key regulator of many

target genes involved in cell cycle arrest and apoptosis[65]. As well as inhibiting proliferation, tumour suppressive transcription factors are able to suppress metastasis. For example, KLF4 maintains the expression of E-cadherin in breast cancer cells, and also reduces the expression of Slug in prostate cancer, preventing EMT activation[66]. However, it is also well known that transcription factors are able to paradoxically perform both oncogenic and tumour suppressive functions. In fact, 50% of genes identified to exhibit paradoxical functions in cancer were identified as transcription factors[67].

1.3.3 Transcriptional Dysregulation in CRC

In CRC specifically, emerging evidence suggests that certain transcription factors drive key events in the progression of colorectal tumours. These TFs are deregulated by a variety of means, including through genetic and epigenetic alterations leading to changes in their transcriptional activity[68]. Oncogenic TFs are activated in CRC and contribute to the tumourigenesis of colorectal tumours, facilitating processes such as EMT, angiogenesis and drug resistance. For example, NFκB is a transcription factor with a known role in CRC in the regulation of tumourigenesis and inflammation. Constitutive activation of NFκB has been identified in CRC, in particular the RelA subunit, which has been shown to suppress apoptosis *in vitro* and leads to limited tumour formation *in vivo* upon knockdown[69]. NFκB is known to regulate a variety of genes involved in cell growth, for example Cyclin-D1 and cMyc, and anti-apoptosis, such as Bcl-2[70]. In addition to regulating these pathways, NFκB has also been shown to be involved in invasion and metastasis through the regulation of EMT-regulated genes, such as matrix metalloproteinases (MMPs), as well as angiogenic genes such as VEGF[71]. Interestingly, NFκB has also been shown to mediate its pro-tumourigenic effects through regulating the tumour microenvironment. Whilst NFκB promotes an anti-apoptotic phenotype within the intestinal epithelial cells, it has also been shown to act within the myeloid cells to increase expression of pro-inflammatory mediators that may act as tumour-promoting factors within the microenvironment[72]. This therefore represents an example of the complex and multifaceted way in which a transcription factor may play an oncogenic role in cancer.

Many other transcription factors have been identified as playing an oncogenic role in CRC. These include the STAT family of transcription factors, involved in the regulation of genes controlling cell cycle progression, such as cyclins D1/D2, apoptosis inhibitors, such as Bcl-XL, and angiogenic factors such as VEGF[73]. STAT3 seems to play the most prominent role in CRC pathogenesis, with the highest incidence of STAT3 constitutive activity in CRC biopsies. Furthermore, STAT3 has been shown to accelerate the proliferation of colorectal cancer cells and to promote tumour growth[74]. The importance of the STAT family in CRC tumourigenesis is demonstrated by the efficacy of JAK/STAT3 inhibition, which has been shown to induce G1 cell cycle arrest and apoptosis in addition to reduced cell invasion[75]. Many other TFs have been identified as playing an oncogenic role in CRC. For example, NFAT2 expression in human CRC has been associated with invasion, and inhibition of NFAT2 results in downregulation of metastasis-related genes[76]. The transcription factor CREB is also involved in CRC metastasis, and activated levels are increased in colorectal cancer cells and intestinal adenomas. Additionally, CREB overexpression has been associated with KRAS-mutant tumours. When CREB is silenced within KRAS-mutant tumours the malignant phenotype is reversed, suggesting that KRAS-induced CRC may be CREB-dependent[77]. Tumour suppressor TFs also play an important role in CRC. Unsurprisingly, TP53 is among the most commonly mutated genes in CRC, occurring in approximately 40-50% of sporadic CRCs and associated with tumour invasion and aggressiveness[78]. Interestingly, transcriptional crosstalk exists in which mutant p53 mediates pro-oncogenic functions. For example, mutated p53 has been shown to promote STAT3 phosphorylation, leading to tumour growth and an invasive phenotype[79].

1.4 Tumour Hypoxia

1.4.1 Development of Hypoxia Within Tumours

Oxygen is of central importance in maintaining intracellular ATP levels as well as serving as an electronic acceptor in many biochemical reactions. Physiological oxygen concentrations (termed ‘physoxia’) vary considerably within the different tissues of the body and typically range from around 3% to 7.4% O_2[80]. Within the colon

epithelium, physoxia is around 6.8% O_2. Within tissues, low oxygen or 'hypoxia' is generally defined as pO_2 9mmHg or a cellular concentration of 0.1-1% O_2. Anoxia is defined as the absence of oxygen[80]. Solid tumours are the most common form of cancer, and the majority of solid tumours including a third of colon cancers display regions of hypoxia. Hypoxic regions develop within solid tumours via several different mechanisms resulting in an imbalance between oxygen supply and oxygen demand[81,82]. Chronic or diffusion-limited hypoxia is due to the uncontrolled cellular proliferation of tumour cells, where rapid tumour expansion results in tumour cells positioned 70-150μM away from functioning blood vessels. The increased diffusion distance means that these tumour cells receive inadequate oxygen supply to meet their increased demand[83]. At distances exceeding 150μM, cells may become anoxic and give rise to patches of necrotic tissue, a common feature found in the centre of many large solid tumours, depicted schematically in Figure 1.2. Hypoxic tumour cells are able to stimulate the growth of their own neovasculature through a process termed angiogenesis. Paradoxically, oxygen supply to the tumour cells neighbouring this neovasculature often remains deficient, due to the poorly organised, leaky and aberrant nature of the new vessels[84]. Repeated cycles of closing and opening of these vessels leads to localised fluctuations of acute hypoxia and reoxygenation cycles as reperfusion of hypoxic tissue with oxygenated blood occurs. Increased tissue damage and activation of a stress response as free-radical concentrations increase is known as reoxygenation injury[85,86]. Hypoxia would typically result in the death of both normal and cancer cells. Importantly, cancer cells are able to adapt to the presence of hypoxia and are able to survive and proliferate within a hypoxic tumour microenvironment. The molecular adaptation of cancer cells to hypoxia contributes to many of the hallmarks of cancer, including a malignant and aggressive tumour phenotype[87].

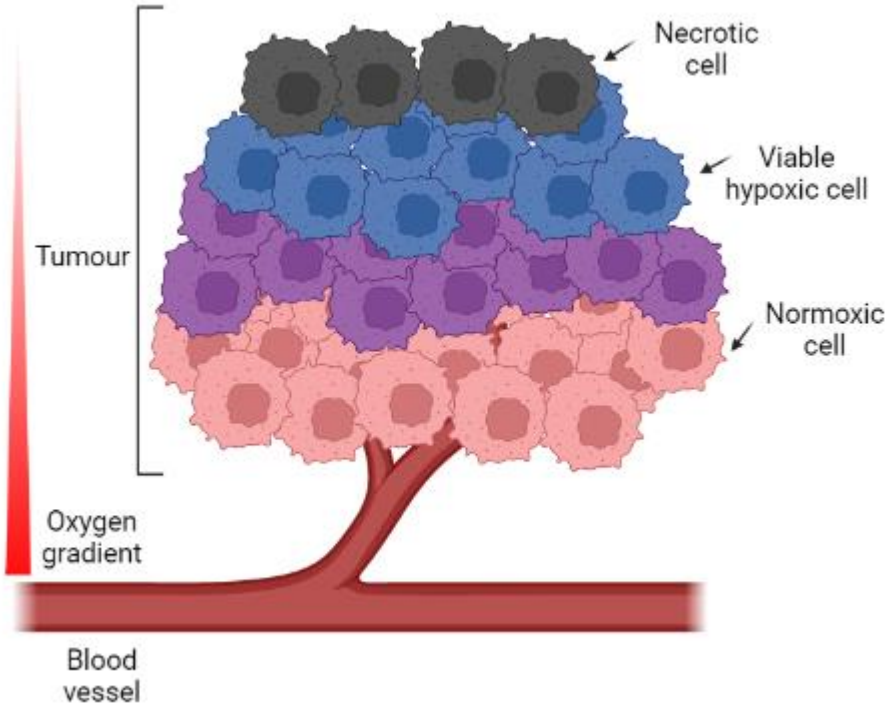

Figure 1.2 Development of tumour hypoxia. Tumour cells positioned close to blood vessels remain normoxic. As the tumour grows due to uncontrolled cellular proliferation in addition to increased metabolic demands, tumour cells positioned further away from the vasculature become hypoxic. At distances exceeding 150µM, cells may become anoxic and give rise to patches of necrotic tissue. Figure created in BioRender.

1.4.2 Hypoxia and Therapy Resistance

In addition to promoting an aggressive tumour phenotype, tumour hypoxia is associated with therapeutic resistance which contributes to hypoxia featuring as an independent prognostic factor in cancer, irrespective of parameters such as cancer grade or stage[88]. Several mechanisms contribute to chemoresistance in hypoxic tumours. In physical terms, viable hypoxic tumour cells have been found positioned up to 250µM away from their nearest blood vessel and it is difficult for large chemotherapy agents to penetrate through multiple cellular layers, meaning that lower levels of active drug will reach hypoxic cells in the core of solid tumours. This is further compounded by the opening and closing of dysfunctional blood vessels leading to poor tissue perfusion and uneven distribution of drugs[89,90]. Mechanistically, most chemotherapeutic drugs including alkylating agents and antimetabolites act mainly by initiating apoptosis through induction of DNA damage during DNA synthesis. Hypoxia

causes cells to progress through the cell cycle more slowly than normoxic cells and so these drugs have less efficacy against hypoxic tumour regions[91]. Drug resistance is also mediated through a lack of apoptotic potential as hypoxia has been found to select for cells that have lost sensitivity to p53-mediated apoptosis[92]. Additional molecular mechanisms for hypoxia-mediated chemoresistance include upregulation of proteins that mediate drug resistance. For example, the MDR gene product p-glycoprotein is a transmembrane drug efflux pump that has been found to be associated with resistance to chemotherapy drugs including adriamycin. Hypoxia was shown to induce MDR1 expression and subsequent P-gp expression in both normal and tumour cells[93]. Furthermore, it was found that inhibiting HIF1α was able to reverse multidrug resistance in colon cancer cells through the downregulation of P-gp[94]. In addition to chemoresistance, hypoxia has a well-established link to radiotherapy resistance, observed by Gray et al. in 1953[95]. The physiochemical oxygen fixation hypothesis suggests that molecular oxygen has a high affinity for and covalently binds to free radicals produced by radiation in cellular molecules including DNA. This generates a peroxy radical that 'fixes' the damage, leading to DNA strand breaks and base damage. However, under hypoxic conditions, the free radicals are restored to their undamaged form as cellular nonprotein sulfhydryls, namely glutathione, can donate a hydrogen atom to the radical[96]. Due to the oxygen enhancement effect with radiotherapy, the radiation dose required to achieve the same biological effect is 2.8 to 3 times higher in the absence of oxygen[97].

1.4.3 Hypoxia Inducible Factors

1.4.3.1 HIF Structure and Isoforms

The molecular adaptation to hypoxia is governed in a major part by transcription factors known as the hypoxia inducible factors (HIFs). The HIFs elicit a transcriptional response involving over 150 hypoxia-inducible genes involved in many pathways that contribute to the hallmarks of cancer. The HIFs exist as an oxygen sensitive α-subunit which heterodimerises with a constitutively expressed β-subunit[98]. In mammals, three

HIF-α subunits are expressed: HIF1α, HIF2α and HIF3α, whilst one form of the β-subunit exists, known as HIF1β. All HIF subunits are members of the bHLH-PAS (basic helix-loop-helix PER-ARNT-SIM) superfamily of transcription factors, and it is through their PAS domains that they are able to dimerise to form intact heterodimers[99]. HIF1α and HIF2α are the best described of the HIF-α subunits, sharing a high level of DNA sequence and structural homology, and both contain the DNA-binding bHLH domain within their N-terminus[100]. Importantly, with the high level of sequence similarity between their bHLH domains and with sharing HIF1β as a binding partner, HIF1 and HIF2 recognise the same consensus motif within the DNA, defined as RCGTG and termed the hypoxic response element (HRE)[101]. Further domains conserved between the two HIF-α subunits include two transactivation domains important in the regulation of transcriptional activity, an NH2-terminal (N-TAD) and COOH-terminal (C-TAD)[98]. In contrast, the HIF3α subunit undergoes extensive alternative splicing and many of the resulting splice variants do not contain a functional transactivation domain. In this regard, HIF3α can competitively inhibit transcriptional activation of target genes by the transcriptionally active HIFα isoforms[102]. Despite recognising the same HRE in order to activate the expression of their respective target genes, HIF1 and HIF2 are distinct in their patterns of expression and induction in response to hypoxia. HIF1 is often considered to be the canonical HIF due to its significant number of hypoxic target genes and ubiquitous expression in response to reduced oxygen[103,104]. HIF2 on the other hand, exhibits a tissue-specific pattern of expression, indicative of a more specialised function[105,106]. In addition to the different pattern of expression, HIF1 and HIF2 also differ in their time-course of hypoxic induction. The induction of HIF1 is an event occurring transiently and at the onset of hypoxia, whilst it has been found that the HIF2 protein gradually accumulates following the reduction of oxygen and governs a more sustained or chronic response[107].

1.4.3.2 HIF Regulation

The transcriptional activity of HIFs is largely regulated through the protein stability of the oxygen-sensitive α subunit, which is continuously degraded under normoxic conditions by a well-defined mechanism. In the presence of oxygen, members of the

2-oxoglutarate-dependent prolyl hydroxylase domain (PHD) family of enzymes catalyse the hydroxylation of HIFα at one, or both, of two highly conserved prolyl residues (Pro402 and Pro564)[108]. These residues are located within the oxygen-dependent degradation domain (ODDD) of the α subunit in close proximity to the N-TAD[109]. Hydroxylation at these residues creates a binding site for the E3 ubiquitin ligase von Hippel-Landau (pVHL), leading to the polyubiquitination of HIFα and targeting for proteasomal degradation[110]. As the hydroxylation reaction requires oxygen, HIFα degradation is therefore coupled directly to oxygen availability. Under hypoxic conditions, HIFα hydroxylation is suppressed, leading to accumulation of HIFα, dimerisation with HIF1β, translocation to the nucleus and subsequent transactivation of hypoxia-responsive target genes. This process is depicted schematically in Figure 1.3. In addition to this pathway, many other mechanisms are involved in the regulation of HIF stability and transcriptional activity. A third residue present in the C-TAD of HIF1α (Asn-803) is hydroxylated by another 2-oxoglutarate-dependent dioxygenase known as Factor Inhibiting HIF1 (FIH-1). This modification inhibits the interaction of HIF1 with its transcriptional coactivator p300, leading to a repression of HIF1 transactivation activity in the presence of oxygen[111]. This represents an example of regulatory mechanisms that differ between HIF1 and HIF2, despite their molecular similarity. Another is the Hypoxia Associated Factor (HAF), an E3 ubiquitin ligase that interacts with HIF1α and contributes to its oxygen-dependent degradation[112]. In contrast, the interaction that occurs between HAF and HIF2α leads to an increase in the transactivation potential of HIF2, with an overexpression of HAF therefore shifting the balance in hypoxic signalling toward HIF2-regulated pathways[113].

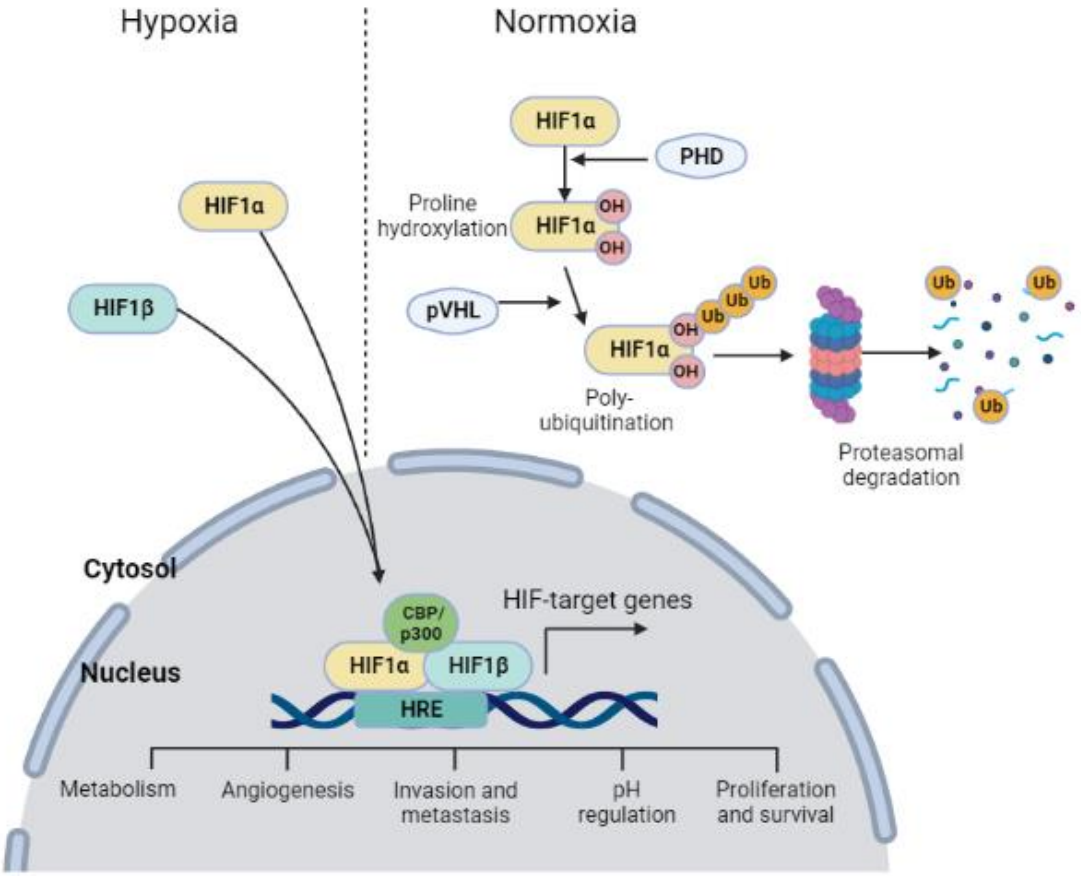

Figure 1.3 Regulation of HIFs in normoxia and hypoxia. Under normoxic conditions, HIFα is hydroxylated on conserved prolyl residues by PHD enzymes, leading to poly-ubiquitination and subsequent proteasomal degradation by pVHL. Under hypoxic conditions, HIFα hydroxylation is suppressed, leading to accumulation of HIFα subunits, dimerisation with HIF1β and binding of the dimer to the HRE of hypoxia-inducible gene promoters. Figure created in BioRender.

Interestingly, oxygen-independent mechanisms for the regulation of HIF1α have also been identified on multiple regulatory levels beyond protein stabilisation. Activation of the PI3K pathway has been shown to upregulate the protein translation of HIF1α through the activation of mTOR[114]. Upon activation, mTOR phosphorylates the eukaryotic translation initiation factor 4E (eIF-4E) binding protein (eIF4E-BP1). These components are essential for inhibition of cap-dependent mRNA translation, and their phosphorylation by mTOR disrupts this inhibitory interaction, leading to enhanced translation of HIF1α[115]. Enhanced translation of HIF1α can also be achieved through direct phosphorylation of eIF-4E by MAP kinase interacting kinase (MNK), a downstream target of phosphorylated ERK. ERK is an interesting example of multi-level regulation of HIF, as it is able to enhance HIF1α translation through the above

described mechanism but also to promote HIF1α transcriptional activity through phosphorylation of the CBP/p300 coactivator to promote HIF1α/p300 complex function[116].

1.4.4 HIF-Regulated Pathways in Cancer

HIF activation within tumours can occur via several of the aforementioned regulatory mechanisms. While the HIFs have important conserved physiological functions including roles in development, the pathways aiming to adapt to intratumoural hypoxia become important drivers of cancer hallmarks and increased malignancy. The HIFs therefore represent important clinical targets in cancer. Immunohistochemical analyses of human primary tumours and metastases demonstrate increased levels of HIF1α, HIF2α or both in comparison to normal surrounding tissue and correlated with decreased patient survival across many cancer types including colon cancer[117,118]. However, the role of the HIFs in cancer progression is variable, with the relative contributions of HIF1 and HIF2 differing depending on the tumour context. For example, HIF2 has been shown to act as an important renal oncoprotein in pVHL-defective clear cell renal carcinomas, whereas most of these tumours do not express HIF1 which has been shown to have tumour suppressive functions[119]. Importantly, HIF1 and HIF2 have also been shown to have divergent roles within colon cancer. HIF1 has been shown to promote tumourigenesis *in vivo* and cell growth *in vitro*, where a loss of HIF1 has been shown to decrease proliferation and migration of colorectal cancer cells. Conversely, HIF2 has shown opposing effects in colon cancer, where loss of HIF2 has been strongly correlated with advanced tumour stage[120]. It is therefore important that any therapeutics developed against HIF signalling consider their tumour-specific roles. Cell type and HIF-isoform specificity is mediated in part through the interactions of HIF1 and HIF2 with cis-acting non-HIF transcription factors, leading to differential expression of HIF1 and HIF2 target gene expression dependent on cell type and additional factors present. For example, HIF2 has been found to cooperate with the Ets-1 transcription factor to regulate VEGF-2, an important receptor involved in angiogenesis[121]. Interestingly, HIF1 and HIF2 have also been shown to bind to distinct regions of the genome, with HIF1 demonstrating a preference for promoter-

proximal binding whilst HIF2 demonstrated bias for promoter distant or enhancer binding[122]. These distant sites occur in a cell type-specific manner and likely contribute to differential regulation of HIF1 and HIF2 target genes.

Several large-scale expression profiling studies have helped to identify hypoxic pathways regulated by HIF1 and HIF2 either cooperatively or independently that contribute to many of the hallmarks of cancer[123–125]. These include (but are not limited to) altered metabolism, increased proliferation, angiogenesis, cellular immortality and promoting invasion and metastasis. Metabolic reprogramming is one of the most notable pathways regulated by HIF1 in response to hypoxia, more specifically involving a metabolic switch from oxidative phosphorylation toward anaerobic glycolysis. Through shifting metabolism from the oxygen-dependent TCA cycle to the oxygen-independent glycolytic pathway, hypoxic cells utilise glucose as their primary source of ATP generation and therefore maintain energy production through a mechanism termed the Warburg effect[126]. HIF1 mediates this metabolic switch through activation of target genes involved in glucose uptake and glycolysis. These include the GLUT1 and GLUT3 transporters involved in the uptake of glucose into the cell, and the lactate dehydrogenase A (LDHA) enzyme responsible for the conversion of pyruvate into lactate during glycolysis as well as many other components of the glycolytic pathway[127–129]. Another function of this glycolytic switch is to prevent an excess of ROS that can form when hypoxia leads to a reduced efficiency in electron transport. Another important metabolic feature of hypoxic tumour cells is an increased intracellular pH termed acidosis, and an accompanying decreased extracellular pH, which have been shown to promote cell proliferation and invasion respectively. HIF1 mediates this altered acid-base balance through activation of genes including the gene encoding carbonic anhydrase 9, which has been shown to have an important role in colorectal tumour growth[130].

1.4.5 Targeting Tumour Hypoxia

1.4.5.1 Hypoxia-Activated Pro-drugs

The outlined importance of tumour hypoxia as a prognostic factor and contributor to therapy resistance means that targeting the hypoxic tumour cells specifically is an important clinical aim. Approaches to targeting tumour hypoxia began in the 1980s with the development of hypoxia-activated pro-drugs (HAPS), also known as bioreductive alkylating agents[96]. HAPS are inactive compounds that, once activated, become cytotoxic drugs within hypoxic cells. The general mechanism by which this occurs is through intracellular reductases, which convert the inert pro-drug into a cytotoxic radical that produces DNA damage under hypoxic conditions. In aerobic cells, back-oxidation of the radical leads to the re-formation of the inactive pro-drug and a greatly reduced toxicity[131]. Tirapazamine (TPZ) is an example of an early HAP that has shown antitumour activity in clinical trials. Importantly, TPZ has also been shown to enhance the anticancer activity of the chemotherapeutic drug cisplatin, demonstrated in a phase III clinical trial with advanced non-small-cell lung cancer where TPZ in addition to cisplatin doubled overall response rate and prolonged patient survival[132]. More recently, evofosfamide (TH-302) was developed as a pro-drug reduced in hypoxia to release isophosphoramide mustard (IPM) which alkylates DNA. As with TPZ, TH-302 monotherapy and combination therapies were shown to increase overall survival in advanced pancreatic cancer in phase II[133] and III clinical trials[134].

Whilst many different HAP formulations have been developed, results of clinical trials remain mixed and often disappointing, and no current FDA-approved HAP exists for the treatment of cancer. An important consideration for clinical trial failures is the lack of patient stratification based on the presence or severity of intratumoural hypoxia. Patients with a low hypoxic fraction would not be expected to improve with HAP therapy and this likely confounds trial results[135]. This raises another important issue within the field of tumour hypoxia which is the need for hypoxic biomarkers in order to assess the level of hypoxia present within a patient's tumour and use this information to aid therapeutic decisions. Current examples of hypoxic assessment include exogenous injectable markers such as pimonidazole, PET tracers for hypoxia

such as HX4, and more recently the establishment of hypoxic gene expression signatures used to characterise the hypoxic state of a tumour[136].

1.4.5.2 Targeting HIF Signalling

Due to the vast number of hypoxic pathways regulated by the HIF transcription factors that contribute directly to the hallmarks of cancer, it is unsurprising that the HIFs themselves represent attractive molecular targets for a range of cancers. HIF signalling can be targeted at various regulatory levels, and represents a good example of multi-level targeting of transcription factors in general[137]. These include inhibition of HIF1α expression, for example through the development of the EZ-2968 antisense oligonucleotide that specifically binds and inhibits HIF1α mRNA expression and downstream target gene expression as a result. EZ-2968 has been shown to attenuate tumour progression in various models[138,139]. As well as at the RNA level, HIF1α can also be targeted at the protein level. This can occur at the level of protein translation or protein stability. One approach to inhibiting the translation of HIF1α is through the inhibition of mTOR. The PI3K/Akt/mTOR growth factor signalling pathway is known to regulate HIF1α translation in over 70% of human cancer cell lines[115]. For colon cancer specifically, inhibition of mTOR has been shown to lead to a significant reduction in tumour growth and represents an important mechanism for inhibiting hypoxic adaptation[140,141]. Other inhibitors of HIF1α act mechanistically to prevent its transcriptional activity at various levels, including preventing HIF1α and HIF1β dimerisation, HIF1 DNA binding or the formation of the active transcriptional complex. Some anthracycline chemotherapeutic agents such as doxorubicin have been shown to disrupt the binding of HIF1 to DNA in hypoxic cancer cells through intercalation with DNA and the induction of strand breaks[142]. For cancers such as prostate which exhibit increased levels of HIF1 protein, anthracycline inhibition of HIF1 has been shown to reduce HIF1 target gene expression such as VEGF, leading to decreased tumour vascularisation as well as decreased tumour growth[143]. The recruitment of the HIF1 cofactor p300/CREB is another molecular target that may be inhibited to prevent transactivation of HIF1 target genes. Bortezomib is an agent which is able to induce the interaction between HIF1 and FIH, leading to an increase in FIH-mediated

repression of p300 recruitment and subsequent inhibition of an active transcriptional complex[144].

Whilst multiple levels of direct HIF inhibition are being explored clinically, HIF signalling is also being targeted indirectly and more specifically through inhibition of important downstream target effectors of HIF-regulated pathways. Due to the important nature of tumour context and heterogeneity, targeting specific downstream targets of HIF which are driving tumour progression may lead to more effective clinical outcomes and reduce off-target and undesirable effects of targeting HIF signalling globally[145]. Perhaps the most successful approach to date has been the targeting of angiogenesis through inhibition of VEGF signalling. Anti-angiogenic monoclonal antibodies (mAbs) or small-molecule inhibitors of VEGF receptors have both been utilised against many cancers with the aim of preventing the formation of tumour neovasculature[146]. For example, bevacizumab is an anti-VEGF mAb that has been approved for a range of metastatic and recurrent cancers[147,148]. However, early in the development of anti-VEGF therapeutics it became clear that the blockage of VEGF signalling was largely ineffective when utilised as a monotherapy due to drug resistance arising through adaptive and compensatory mechanisms[149]. Not only does restricted tumour blood flow resulting from anti-angiogenic therapy lead to poor drug penetration and the selection of drug-resistant phenotypes, but cancer cells are often able to activate alternative angiogenic signalling pathways through the upregulation of alternative pro-angiogenic factors in the absence of VEGF[150]. Current research therefore focuses on dual or multi-therapy combinations to overcome this resistance. For example, FGFs are pro-angiogenic factors that are able to increase the proliferation of endothelial cells, and anti-VEGF therapy has been shown to increase levels of FGF or FGF receptor in many cancers[151]. Dual inhibition of the FGF and VEGF pathways is a promising combination to increase anti-cancer efficacy[152]. The compound S49076 is able to simultaneously target MET, AXL and FGF, and has been shown to induce tumour growth arrest in bevacizumab-resistant tumours[153].

1.5 Additional Transcriptional Regulators of Tumour Hypoxia

1.5.1 NFκB

It is being increasingly recognised within the field of transcriptional regulation of hypoxia that the HIFs are not the only transcription factors involved in mediating the hypoxic response. In fact, a dynamic network of interacting factors appear to work together in order to regulate hypoxic pathways, although this network is yet to be fully elucidated. The aforementioned NFκB transcription factor that plays an important role in CRC pathology has also been found to play a role in the regulation of the hypoxic response, and may mediate some of its pro-tumourigenic effects in a hypoxia-dependent manner In the canonical NFκB pathway, the inhibition of κB Kinase (IKK) complex is activated in response to stimuli, and in turn phosphorylates the IκB inhibitor protein responsible for sequestering NFκB in the cytosol[154]. NFκB free dimers then translocate to the nucleus to mediate the regulation of specific target genes. An important cross-talk between HIF and NFκB has been demonstrated. In colorectal cancer, HIF1 and NFκB have been found to co-regulate Twist and Snail in order to drive EMT[155]. These co-regulations also feature across other cancer types. For example, in hypoxic prostate cancer cells, both HIF1 and NFκB promote cell survival through upregulation of interleukin-8 receptor CXCR1[156]. The precise mechanisms of NFκB activation in hypoxia are not well defined, yet it has been suggested to involve oxygen sensors such as PHD1, which may mediate NFκB activation through mediating the IKK complex[157]. Interestingly, NFκB has been identified as a direct modulator of HIF1α expression, with the HIF1α promoter demonstrating responsiveness to NFκB[158]. Upon hypoxic induction, NFκB has been shown to induce the expression of invasive genes such as MMPs and apoptotic regulators such as Bcl-2[159].

1.5.2 ETS

Other transcription factors demonstrated to regulate aspects of the hypoxic response include those within the ETS family, one of the largest evolutionary conserved groups of TFs, with over 28 reported factors in humans. The family is defined by a DNA-binding

ETS domain, and are involved in the regulation of a wide range of physiological pathways including cell growth, metabolism and differentiation[160]. ETS1 in particular has been shown to play an important role as a prognostic biomarker for colorectal cancer[161], and has also been investigated in the context of tumour hypoxia. Hypoxia is known to activate ETS1, via the activity of HIF1. More specifically, the promoter region for ETS1 was found to contain an HRE, to which HIF1 was reported to bind under hypoxic conditions[162]. Interestingly, studies have found that the ETS TF Elk-1 is most importantly involved in co-regulating HIF2 target genes as opposed to HIF1 target genes. For example, in a breast cancer cell line, a small group of hypoxia-inducible genes were identified as being regulated by HIF2. All of these genes were found to contain putative binding sites for ETS transcription factors, with 10 of 11 of these genes featuring ETS-binding sites in proximity to an HRE. Knockdown of Elk-1 reduced hypoxic induction of HIF2-dependent genes, and a physical interaction between Elk-1 and HIF2 was confirmed through coimmunoprecipitation[163]. This represents an interesting observation that additional TFs and their cell-and stimulus-specific availability may aid differential regulation of HIF1 and HIF2 target pathways. Additional studies have confirmed the interactions between HIF2 and ETS transcription factors. For example, the interaction between HIF2 and ETS1 was found to be required for full transcriptional activation of Flk1 (VEGF receptor-2) in endothelial cells, presenting an important co-regulatory mechanism for the regulation of angiogenesis[164]. The hypoxia-induced regulation of angiogenesis by ETS1 was later confirmed by an additional study which identified miR-200b as a hypoxia-sensitive miRNA involved in the induction of angiogenesis via direct targeting of ETS1 in endothelial cells[165].

1.5.3 p53

It is well known that the tetrameric tumour suppressive transcription factor p53 is activated in response to various forms of cellular stress such as DNA damage, heat shock or even tumour hypoxia in order to maintain genomic stability. In the absence of cellular stress, p53 is targeted for degradation by a ubiquitin ligase known as MDM2[166]. Within a tumour, the hypoxic cells are typically radioresistant and induce a

replication-mediated DNA damage response (DDR), which includes the activation of the p53 tumour suppressor gene[167]. Hypoxia is able to induce a DNA damage response in the absence of detectable DNA damage, potentially functioning as one of the earliest drivers of p53 mutation in tumourigenesis. While an increase in p53 protein in hypoxia has been shown to be dependent on the presence of HIF1α, HIF1α upregulation alone is not sufficient for p53 stabilisation[168]. Decreased expression of the E3 ubiquitin-protein ligase MDM2 facilitates hypoxia-mediated p53 stabilisation, leading to a transrepression activity that is essential for p53-induced apoptosis in hypoxia[169].

As with NFκB, extensive crosstalk between HIF1 and p53 is described. As well as its transrepression capability, p53 induces the expression of a subset of its target genes in hypoxia including BNIP3 and FAS/CD95, both of which contain the HRE and may involve the cooperative binding of both p53 and HIF1 for full hypoxic induction[170]. Further evidence for direct interactions between p53 and HIF1 has been provided, with one study demonstrating that p53 promotes MDM2-mediated ubiquitination and proteasomal degradation of the HIF1 α subunit. Conversely, a loss of p53 in tumour cells was shown to enhance HIF1α levels and augment HIF-1-dependent expression of VEGF[171]. However, such hypotheses are controversial, with research showing that MDM2 can in fact increase HIF1α abundance and activity in hypoxia[172]. Interesting new research has highlighted the existence of a HIF1/mutant p53 complex able to control the transcription of pro-tumourigenic genes including ECM components[173].

1.5.4 REST

Another transcription factor demonstrated to play an important role in the molecular adaptation to hypoxia in several tumour types is the repressor element-1 silencing transcription factor (REST). Whilst initially implicated in neurogenesis, REST has since been shown to be important in many cell types including tumour cells[174]. In fact, REST has been identified as a master transcriptional repressor in hypoxia, regulating a significant 20% of all hypoxia-repressed genes in HEK293 cells[175]. In response to hypoxia, REST translocates to the nucleus and induces transcriptional repression of

target genes, binding to the repressor element 1 (RE1) element within the promoter region and causing repression through chromatin remodelling or inhibition of transcriptional machinery[176]. As with many TFs, REST may act in an oncogenic or tumour suppressor role depending on cell type and context. For example, over 30% of glioblastomas rely on high REST expression for growth and invasive phenotype, largely attributed to its repression of miR-124a, leading to an increase in expression of the miRNA targets involved in cell proliferation[177]. However, in certain cancers including colon, REST has been shown to function as a tumour suppressor, where rapid proliferation of colon cancer cell lines can be reduced through transfection of exogenous REST[178]. Interestingly in hypoxia, a crosstalk between HIF and REST has also been observed, with REST shown to repress HIF-1α mRNA expression and negatively regulate some HIF-regulated target genes involved in metabolism during hypoxia in HEK293 and prostate cancer cells[179].

1.5.5 Additional Factors Regulating the Hypoxic Response

The transcription factors described above are in no way exhaustive in depicting the transcriptional regulation of the hypoxic response in cancer. In fact, a large number of additional TFs have been identified as regulating aspects of the tumour hypoxic response in a range of cancers. These include the aforementioned CREB, which has been shown to be upregulated by hypoxia in cancers including breast and hepatocellular carcinoma, and contributes to the neoplastic phenotype at multiple levels[180,181]. Members of the STAT TF family have also been investigated in terms of the hypoxic response. In particular, STAT5a has been linked to advanced tumour growth following hypoxic exposure in prostate cancer[182], whilst STAT5b has been shown to regulate expression of HSP90 under hypoxic conditions, contributing to malignancy in breast cancer[183]. Interestingly, STAT5 has been shown to promote HIF2-dependent expression of genes involved in glucose metabolism such as GLUT1 and GLUT3[184]. It's apparent therefore that a significant number of TFs are involved in hypoxia-inducible gene expression in both a HIF-dependent and HIF-independent manner dependent on the cellular context.

1.6 The Role of AP1 in Cancer

1.6.1 AP1 Family and Structure

Activator protein 1 (AP1) represents a dimeric transcription factor comprised of members from four transcription factor sub-families: Fos, Jun, ATF and MAF. Fos and Jun represent the most well-defined of the sub-families and are known to play important roles in cancer. Fos consists of FosB, c-Fos, FOSL1 and FOSL2, whilst Jun comprises JunB, c-Jun and JunD[185]. The AP1 complex may therefore exist as many combinations of homo- or heterodimers, the precise dynamics of which determine the downstream targets and pathways regulated by AP1. All members of the AP1 superfamily share a leucine-zipper motif through which subunits are able to dimerise, and a basic domain for interaction with DNA, and as such are known as bZip proteins[186]. AP1 subunits are activated in response to a range of growth factors and external stimuli, mediated in a large part through MAPK signalling as discussed further in the project. Upon activation and depending on the dimer composition, AP1 binds to palindromic regulatory sequences of DNA in order to mediate transactivation of specific target genes. Fos:Jun and Jun:Jun dimers have been found to preferentially bind to TRE DNA motifs (TPA-responsive elements) and, with a slightly lower affinity, to CRE DNA motifs (cAMP-responsive elements), with respective sequences 5'-TGA(C/G)TCA and 5'- TCACGTCA[187,188]. Interestingly, the members of the AP1 family show great variation in their ability to form dimers and transactivate AP1-regulated target genes. For example, whilst Jun is able to form homodimers or heterodimers with other Jun family members, Fos is unable to do so and must heterodimerise with a non-Fos AP1 subunit[189]. Accumulating evidence suggests that, depending on the specific cellular context, differential expression of AP1 subunits will lead to the switching on or off of different transcriptional programs, thus making the study of AP1 highly complex[190].

1.6.2 The Dual Role of AP1 in Cancer

Given the important role of AP1 in regulating many physiological pathways governing cell growth, differentiation and apoptosis, it is unsurprising that many AP1 proteins are implicated in tumourigenesis. In fact, members of the Fos and Jun families have been identified as oncogenes, and can be defined by their transactivation potential. c-Fos, c-Jun and FosB contain potent transactivation domains identified by their efficiency in transforming cells in culture. On the other hand, FOSL1 and FOSL2 show weak transforming activity, whilst JunB and JunD lack a potent transactivation domain and show no transforming activity[191]. All, however, have been shown to play a role in cancer development and progression through specific dimer formations. Many cancers feature an overexpression of Jun subunits. Consistent with the efficient transforming capabilities of c-Jun, c-Jun is well known to promote tumourigenicity, with overexpression of this particular subunit observed in some aggressive CD30-positive lymphomas[192]. Furthermore, c-Jun is important in the development of skin and liver tumours, the latter demonstrated by inactivation of c-Jun which interferes with the development of chemically-induced tumours within the liver[193,194]. In contrast, c-Fos has been demonstrated to play a role in the formation of osteosarcomas. When overexpressed widely in mice, c-Fos causes osteosarcoma formation through the transformation of osteoblasts and chondroblasts[195].

Despite the lack of potent transformation ability, overexpression of FOSL1 and FOSL2 leads to the development of lung and epithelial tumour in transgenic mice, likely mediated through dimerisation with AP1 subunits containing an intact transactivation domain[196]. More recent research has highlighted an additional role of FOSL1 in malignancy, whereby high FOSL1 expression in aggressive cancer cells mediated through autocrine/paracrine feedback leads to enhanced proliferation and metastasis[197]. In breast cancer, FOSL1 and c-Jun expression has been found to be significantly higher in aggressive breast cancer cell lines compared to non-invasive cell lines, with FOSL1 and c-Jun-induced genes including those involved in cell migration and invasion such as the matrix metalloproteinases MMP2 and MMP9[198,199].

Interestingly, in many cases AP1 has been shown to have tumour suppressive as well as oncogenic functions in cancer, highlighting a double-edged nature to AP1

transcription factors, highly dependent on dimer composition and cellular context. For example, whilst c-Fos was originally considered a canonical oncogene, it has now been found that a loss of c-Fos is associated with ovarian cancer progression through the regulation of cell adhesion pathways[200]. Additionally, a loss of c-Fos has been associated with advanced stage and metastasis of gastric carcinoma[201]. It is also reported that JunB and JunD, lacking potent transactivation domains, have context-dependent tumour suppressing functions. In the case of JunB, it was shown that the absence of JunB expression through epigenetic silencing resulted in progressive myeloid leukaemia[202]. Differential regulation of processes crucial to cancer, such as apoptosis, is a common theme in AP1 TFs. For example, in neuronal cells, c-Jun regulates the expression of pro-apoptotic Bim[203], whereas Jun proteins are able to exert protective signals in T cells through the induction of anti-apoptotic Bcl3[204]. It is therefore important that the role of AP1 in cancer progression is examined within the context of a complex network of differential regulation dependent on dimer composition and cell type-specific regulatory factors. In colon cancer, AP1 activity has been linked to increased proliferation and may be stimulated as previously described through activation of the upstream MAPK pathway, or through the Wnt signalling pathway which is often activated through mutation of the APC gene or microsatellite instability[205]. However, the contribution of the AP1 subunits to the regulation of tumourigenic pathways in CRC has not yet been fully elucidated.

1.6.3 AP1 in Hypoxia

As with the other aforementioned TFs involved in the adaptation of cancer cells to hypoxia, AP1 activation is also induced by hypoxic stress. A study in HT29 colon cancer cells showed an increased expression of c-Jun and JunD during hypoxia[206]. Mechanisms for AP1 activation include a hypoxia-induced increase of intracellular calcium leading to induction of calcium-dependent AP1 subunit expression, as demonstrated with c-Fos expression[207,208]. Further research shows that AP1 binding induced by hypoxia regulates the expression of important hypoxic-response genes such as tyrosine hydroxylase (TH)[209], VEGF and NDRG-1, IL-8 through cooperation with NFκB[210], and endothelin-1[211]. However, as the magnitude of AP1 induction by hypoxia

does not always correlate with the level of induction of AP1 response genes, many other factors are likely to cooperate with AP1 in hypoxia to regulate the response. Importantly, AP1 has been showed to cooperate with HIF1 in either a direct or indirect manner to promote target gene expression in hypoxia[212]. For example, it was shown that calcium-induced c-Jun and HIF1 cooperate in the hypoxic response to regulate VEGF expression[213]. Furthermore, c-Jun is able to associate with the oxygen-dependent degradation domain (ODD) of HIF1, masking the ubiquitination sites and preventing the proteasomal degradation of HIF1[214]. In a reciprocal manner, it has also been found that a functional relationship exists concerning HIF1-dependent c-Jun N-terminal phosphorylation in hypoxia involved with glucose metabolism[215]. AP1 therefore functions as another important TF in the hypoxic response and as is the case with many TFs, undergoes complex interactions with other factors to facilitate the regulation of target genes.

1.7 Project Aims and Hypotheses

Preliminary data for this project was obtained by Alan McIntyre who identified FOSL2 as a key mediator of hypoxic cell viability in a colorectal lentiviral shRNA viability screen. Eric Vancauwenberghe gathered data to support this hypothesis, demonstrating that many AP1 proteins were induced by hypoxia across several colorectal cancer cell lines and were regulating the expression of hypoxia-inducible targets such as CA9. It was demonstrated by co-immunoprecipitation that hypoxia increased heterodimerisation of FOSL2 with Jun proteins, and that knockdown of FOSL2 using an siRNA approach decreased clonogenic viability.

Whilst FOSL2 had been validated as playing a role in hypoxia in colorectal cancer cell lines, this role is yet to be fully elucidated. The aim of the current project is to identify FOSL2 as an important mediator of the hypoxic response through both the regulation of the CRC transcriptome and phospho-signalling pathways. Through CRISPR-Cas9, FOSL2 knockdowns will be produced to assess the impact of loss of FOSL2 on colorectal cancer spheroid growth. Alongside, the phenotypic and transcriptomic role of JUND in hypoxia will be investigated, as a subunit shown to be consistently upregulated by hypoxia in CRC cell lines. Finally, the clinical relevance and prognostic significance of FOSL2 will be investigated through a CRC tissue micro-array and subcutaneous xenograft experiment.

Specifically, this thesis will address the following:

1. To identify the role of JUND and FOSL2 in spheroid growth and clonogenic viability in hypoxia and to investigate their hypoxia-regulated transcriptomes in CRC.
2. To investigate the clinical relevance of FOSL2 through analysis of a large CRC tissue micro-array and growth of FOSL2-knockdown tumours within a mouse xenograft experiment.
3. To determine the activation of FOSL2 in hypoxia, and to investigate phospho-signalling pathways associated with FOSL2 in hypoxia and their HIF-dependence or -independence.

2.0 Materials and Methods

2.1 Cell Culture

2.1.1 Maintenance of Cells

Cell culture was carried out under sterile conditions in a Class II Microbiological Safety Cabinet (BioMAT$_2$, Contained Air Solutions, Manchester, UK). The following colorectal cancer cell lines used in this project were originally purchased from American Type Culture Collection (ATCC): HCT116 (CCL-247), Ls174T (CL-188), HT-29 (HTB-38) and SW620 (CCL-227), and the cells underwent routine mycoplasma testing. Cells were cultured in high-glucose Dulbecco's Modified Eagle Medium (DMEM, Sigma-Aldrich, MO, USA) supplemented with 10% [v/v] fetal bovine serum (FBS, Sigma-Aldrich, MO, USA). For experiments involving the study of phosphorylated proteins, cells were serum starved in 0.5% FBS 24 hours prior to beginning the experiment. Cell lines were maintained in a humidified tissue culture incubator at 5% CO_2 and a temperature of 37°C.

2.1.2 Passaging of Cell Lines

Cell lines were routinely sub-cultured every 2-3 days prior to reaching 70% confluence in a T-75cm^2 tissue culture flask (Corning, Fisher Scientific, MA, USA). Cell culture media was aspirated from the flask and cells were washed once with phosphate buffered saline (PBS, Sigma-Aldrich, MO, USA). Cells were detached from the tissue culture flask using 1X Trypsin- Ethylenediaminetetraacetic acid (EDTA) solution (Sigma-Aldrich, MO, USA) at 37°C for 5 minutes. Dissociation of cells was confirmed by microscopy and the trypsin solution was quenched using the appropriate volume of fresh complete media pre-warmed to 37°C. Cells were pelleted by centrifugation for 5 minutes at 1200rpm. Pellets were resuspended in 10ml of complete media and typically re-seeded 1:10 into a new tissue culture flask made up to the appropriate volume of fresh complete media.

2.1.3 Hypoxic Culture Conditions

In order to induce hypoxia, cells were incubated at 1% O_2 in an *invivo*$_2$ 400/500 hypoxic workstation (Baker Ruskinn, South Wales, UK). CO_2 levels were maintained at 5% and the temperature at 37°C. The length of hypoxic incubation varied by experiment. For experiments utilising physoxic levels of oxygen, cells were incubated at 8.5% O_2 (5% CO_2, 37°C) in an *invivo*$_2$ 400 hypoxic workstation (Baker Ruskinn, South Wales, UK).

2.1.4 Cryopreservation of Cell Lines

For long term storage of cell lines, flasks of cells were grown to 70% confluence, trypsinised and pelleted by centrifugation as described above. Cell pellets were resuspended in freezing media (90% [v/v] FBS, 10% [v/v] dimethyl sulfoxide (DMSO, Sigma-Aldrich, MO, USA)). 0.5ml of resulting suspension was added to each cryovial (Brooks Life Sciences, Manchester, UK). Vials were inserted into 'Mr Frosty' freezing containers (Thermo Scientific, MA, USA) containing 100% isopropanol (Sigma-Aldrich, MO, USA) filled to the recommended level. These containers were incubated overnight at -80°C and transferred the following day to Brooks Biostore III Cryo (Azenta Life Sciences, MA, USA) for long-term storage.

2.1.5 Cell Counting

Cells were counted prior to experimental seeding in order to achieve the desired cell density. Cells were trypsinised, pelleted and resuspended as previously described. 10µl of the resulting cell suspension was transferred into both chambers on the Dual-Chamber TC10/TC20 cell counting slide (Bio-Rad, CA, USA). The slide was inserted into the TC10 automated cell counter (Bio-Rad, CA, USA), and the cells/ml reading was used to calculate dilutions of cells required for downstream experiments.

2.2 3D Cell Culture

For *in vitro* spheroid formation, cells were trypsinised and counted as previously described. A cell suspension was prepared containing enough cells per condition for

12 technical replicates, with the final concentration being 1000 cells per well in 100µl volume. 100µl of cell suspension was added to each well of an ultra-low attachment 96-well plate (Corning Costar, Fisher Scientific, MA, USA). 200µl of sterile PBS was added to each outside well to prevent edge evaporation effects. Plates were spun for 20 minutes at 2500rpm in order to promote spheroid formation. The day of plating and centrifugation is denoted Day 0. On Day 1, an additional 100µl of fresh complete medium was added to each well. On Day 3, 5, 7, 9, 12 and 14, spheroids underwent medium changes and imaging. For medium changes, 100µl of medium was removed from each well and replaced with 100µl of fresh complete medium, ensuring the spheroid is not aspirated or disaggregated. Spheroids were imaged on a widefield microscope (NiKDn Eclipse Ti) using the NIS-elements Imaging Software (NiKDn, NY, USA). Images were exported to ImageJ (NIH, MD, USA) for analysis. Briefly, the area of the spheroid was measured in pixels and converted into mm^2 using a factor calculated by the number of pixels equating to $1mm^2$ of a haemocytometer. The spheroid area was then used to calculate spheroid radius, diameter and volume, and the average volume was plotted against time in days.

2.3 Clonogenic Assay

For the clonogenic assay, cells were trypsinised and counted as previously described. Cells were seeded at a concentration of 500 cells in 7ml complete medium per T-$25cm^2$ cell culture flask (Corning, Fisher Scientific, MA, USA). Two flasks were seeded per experimental condition in order to obtain an average of technical repeats per biological replicate. All conditions were left overnight in the cell culture incubator in order to allow cells to adhere to the flask. The following day, flasks belonging to hypoxic experimental conditions were transferred into the hypoxic chamber and left for 72 hours. Following this, flasks were transferred back to normoxic culture conditions and colonies were left to grow for a further 10 days with minimal disturbance of flasks within the incubator. Flasks were removed from the incubator and the medium was aspirated. The colonies were fixed and stained by covering the surface of the flask with 1% methylene blue solution (Sigma-Aldrich, MO, USA) for one hour at room temperature. Methylene blue was removed from the flasks, and flasks

were rinsed three times in tap water. Flasks were left to dry overnight and then colonies were counted manually.

2.4 Generation of Inducible Knockdown Pooled Populations

2.4.1 Generation of Inducible Cas9 Cell Lines

For this project, cell lines were generated to express Cas9 under a doxycycline inducible promoter by transduction with Dharmacon Edit-R lentiviral hEF1a-Blast-Cas9 nuclease expression particles (Dharmacon, CO, USA) (Figure 2.1). Cells were trypsinised and counted as previously described and prepared at a density of 20,000 cells in 200µl of medium per well in a 48-well cell culture plate (Corning, Falcon, Fisher Scientific, MA, USA). Polybrene (Sigma-Aldrich, MO, USA) was added to the cell suspension at a final concentration of 8 µg/ml to enhance the lentiviral transduction through neutralising the charge repulsion between viral particles and cell surface. Lentiviral particles were used at a multiplicity of infection (MOI) of 10 and were reverse transduced by adding the cell suspension on top of the lentivirus. One well was transduced per cell line, with an additional 2 control wells included per cell line for non-transduced, plus or minus blasticidin conditions in order to monitor cell selection. 24-hours post transduction, remaining viral particles were washed away with 3 washes of PBS and cells were given 200µl of fresh medium. 24 hours later (48 hours post-transduction) blasticidin (Santa Cruz Biotechnology, TX, USA) selection began in order to kill the non-transduced cells. Blasticidin concentrations for cell selection were determined by prior antibiotic kill curves. Cas9 induction was confirmed in each cell line prior to knockdown generation by induction with 2 µg/ml doxycycline (Sigma-Aldrich, MO, USA) for 48 hours before protein extraction and western blotting for the Cas9 protein.

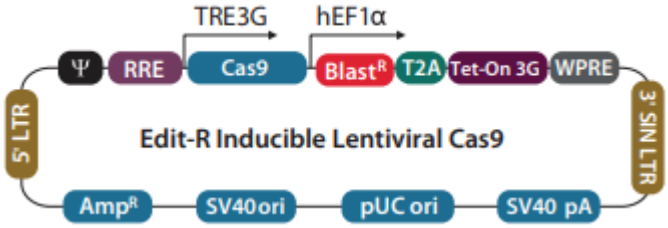

Figure 2.1 Schematic map of the Edit-R Inducible Lentiviral Cas9 Nuclease vector. The vector contains a human codon-optimised version of the *S.pyogenes Cas9 (csn1)* gene under the control of a doxycycline inducible promoter TRE3G. The Tet-On 3G trans-activator protein is constitutively expressed alongside the blasticidin resistance gene ($Blast^R$). When doxycycline is present, the trans-activator protein binds to the TRE3G promoter and activates the expression of the Cas9 nuclease. (Figure from Dharmacon).

2.4.2 Generation of Inducible Knockdown Cell Pools

The above stable inducible Cas9 cell lines were used for further lentiviral transductions of guide RNA sequences in order to generate inducible knockdown cell lines. The lentiviruses purchased were Sigma's Guaranteed Predesigned CRISPR gRNA, purchased in lentiviral format with the LV04 U6-gRNA:hPGK-puro-2A-tBFP backbone (Sigma-Aldrich, MO, USA), (Figure 2.2) to allow for antibiotic selection of transduced cells with puromycin. Two guide RNA sequences for each gene were selected based on specificity and efficiency ratings provided by Sigma, with the sequences of these provided in Table 2.1. In addition to the targeting sequences, Sigma's 'Lenti CRISPR Universal Non-Target Control#1 Transduction Particles' containing the same LV04 backbone as the guide RNA sequences was used as a non-targeting negative control (Sigma-Aldrich, MO, USA). The transductions were performed as described above. 48 hours post-transduction, cells were selected with puromycin (Gibco, Fisher Scientific, MA, USA). Puromycin concentrations for cell selection were determined by prior antibiotic kill curves. Gene knockdowns were tested and used for experiments by inducing cells with doxycycline for 4 days prior to cell seeding. Doxycycline was renewed after the first 48 hours.

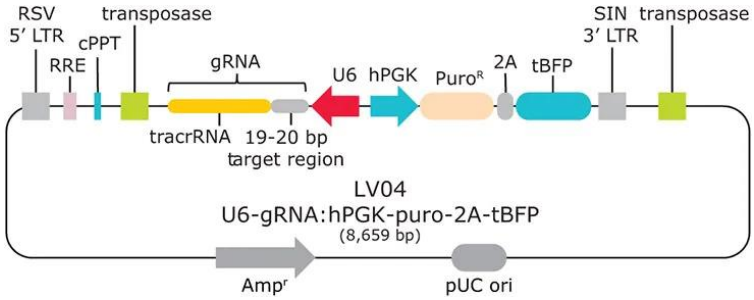

Figure 2.2 Schematic map of the Sanger Lentivirus LV04 vector. The vector uses a dual-component system which consists of a U6-driven gRNA and hPGK-driven puromycin resistance cassette along with blue fluorescence protein (BFP). (Figure from Sigma-Aldrich).

Target	Sequence (5'-3')	Transcripts Hit
JUND g1	GCGAACCTGAGCAGCTACG	2/2
JUND g2	TCGCCGAAGCTCGGCACGT	2/2
FOSL2 g1	GACGCTTCTCCTCCTCTTCAGG	4/4
FOSL2 g2	GCTGGCTGCAGCCAAGTGCCGG	4/4

Table 2.1 gRNA sequences for JUND and FOSL2 purchased in the LV04 vector format.

2.5 Generation of Knockdown Clones

2.5.1 Lipofection with Synthetic gRNAs

The knockdown clones used in this study were generated using lipofection of oligonucleotide guide RNAs as opposed to the previously described lentiviral guide RNA delivery system. Sigma's Guaranteed Predesigned CRISPR gRNA was purchased in synthetic RNA format, with the gRNA sequences selected listed in Table 2.2. Cas9-inducible cell lines created as outlined above were treated with 2 µg/ml doxycycline for 48 hours in order to induce Cas9 expression at 70% confluence in a T-75cm^2 flask. Cells were trypsinised, centrifuged and resuspended in OPTI-MEM reduced serum medium (Thermo Fisher, MA, USA). Cells were then counted and diluted to the correct density for 85,000 cells in a total of 200µl of OPTI-MEM per well of a 24-well cell culture plate (Corning, Falcon, Fisher Scientific, MA, USA). Transfection complexes were prepared in sterile 1.5ml Eppendorf tubes (Starlab, Hamburg, Germany). 2.5µl of

10µM gRNA was diluted into 22.5µl OPTI-MEM. In a separate tube, 1.5µl of lipofectamine RNAiMAX reagent (Thermo Fisher, MA, USA) was diluted in 23.5µl of OPTI-MEM. The oligonucleotide and lipofectamine tubes were gently mixed together, and the resulting 50µl of transfection mix was added dropwise to the surface of the well. 200µl of cell suspension was added directly on top of the transfection mix using the reverse transfection method. 6 hours post-transfection, the cell/transfection mixture was aspirated from the cells and replaced with 500µl of complete medium containing 2 µg/ml doxycycline in order to maintain levels of Cas9 expression.

Target	Sequence (5'-3')	Transcripts Hit
HIF1α g1	CTTTGTCTAGTGCTTCCAT	3/3
HIF1α g2	AGCGACAGATAACACGTTA	3/3
HIF1α g3	AGTGTACCCTAACTAGCCG	3/3
HIF2α g1	CGAATCTCCTCATGGTCGC	2/2
HIF2α g2	GTTCTCGGAGTCTAGCGCA	2/2
HIF2α g3	ACCCTATATCCCCATGGAC	2/2

Table 2.2 gRNA sequences for HIF1α and HIF2α purchased as synthetic gRNAs.

2.5.2 Single Clone Selection

24-hours post-transfection, cells were diluted to single clones. The cell culture medium was removed, and the cells were washed with PBS. Cells were trypsinised for 5 minutes and the trypsin quenched with fresh complete medium. The cells were centrifuged, resuspended in 1ml of medium and counted as previously described. Cells were serially diluted to a final concentration of 1 cell per 200µl of medium in a 96-well cell culture plate (Corning, Falcon, Fisher Scientific, MA, USA). 24 hours later, each well was observed by light microscopy for the presence of a single colony. Wells containing multiple or no colonies were discarded. Single colonies were expanded until protein could be extracted in order to assess gene knockdown. The table below summarises optimisation steps taken for the CRISPR-Cas9 work within this project, as well as the pros and cons of each approach (Table 2.3).

Stage of Optimisation	Synthetic gRNA Delivery	Lentiviral gRNA Delivery
Targets optimised	HIF1α and HIF2α	FOSL2 and JUND
Best targeting sequence (5'-3')	HIF1α: CTTTGTCTAGTGCTTCCAT HIF2α: GTTCTCGGAGTCTAGCGCA	FOSL2: GCTGGCTGCAGCCAAGTGCCGG JUND: TCGCCGAAGCTCGGCACGT
Most efficient knockdown achieved	Clones produced with >90% knockdown of both HIF1α and HIF2α (Ls174T)	78% reduction in FOSL2 expression (HT-29) 88% reduction in JUND expression (Ls174T)
Amount of gRNA/virus	50nM gRNA	Transduced with MOI of 10
Number of cells transfected/transduced	HCT116: 85,000 cells/well Ls174T: 100,000 cells/well (24-well format)	HCT116: 20,000 cells/well Ls174T: 20,000 cells/well (48-well format)
Clones vs pools	Clonal approach used	Pooled approach used
Pros of approach	**Synthetic gRNA** is cheap and quick to use and avoids random integration of DNA into the genome	**Lentiviral gRNA** is the most efficient method of introducing gRNA into hard-to-transfect cell lines
	Clonal approach allows for clones to be screened based on % knockdown so greater efficiencies can be achieved	**Pooled approach** overcomes the limitations of clonal heterogeneity as the population is mixed
Cons of approach	**Synthetic gRNA** lipofection yields a lower efficiency of gRNA entry into cells than lentiviral methods	**Lentiviral gRNA** enables random integration of gRNA into the genome which can lead to off-target effects
	Clonal approach can lead to issues of clonal heterogeneity	**Pooled approach** allows for out-competing of the gene knockdown and lower efficiency over time

Table 2.3 Optimisation of CRISPR-Cas9 approaches used within this project along with the pros and cons of each approach

2.6 DNA Extraction and Sequencing

2.6.1 DNA Extraction

DNA was extracted from knockdown clones generated as described in order to sequence the predicted cutting region. Firstly, predicted knockdown clones were pelleted down as previously described, with pellets stored short-term at -80°C until use. DNA extraction was performed using the DNAzol reagent (Sigma-Aldrich, MO, USA). Cell pellets were maintained on ice and washed once with ice-cold PBS followed by centrifugation at 12,000rpm for 5 minutes. The PBS was aspirated and 500µl of DNAzol was added to each pellet which was then resuspended with a pipette and incubated at room temperature for 3 minutes. The resulting lysate was transferred to

a fresh 1.5ml Eppendorf tube and 250µl of 100% ethanol was added in order to precipitate the DNA. DNA precipitates were gathered onto a pipette tip by spooling and adhering onto the Eppendorf tube wall. The DNA precipitates were then washed twice with 800µl of 75% ethanol before removing all ethanol and allowing precipitates to air-dry briefly for 30 seconds. Finally, DNA was solubilised in 8mM NaOH (50-200µl depending on precipitate size). DNA was quantified using the Nanodrop 2000 (Thermo Fisher, MA, USA) through absorbance measurement taken at 260nm.

2.6.2 Polymerase Chain Reaction

DNA extracted as described above was diluted to 100 ng/µl in 8mM NaOH and amplified using polymerase chain reaction (PCR). PCR reactions were set up in 50µl reactions according to Table 2.4. The polymerase used was the Q5 High-fidelity DNA polymerase (New England Biolabs, MA, USA). Primers spanning the gRNA site were purchased from Sigma, see Appendix for details. Reactions were placed into a Veriti 96-well thermal cycler (Applied Biosystems, Fisher Scientific, MA, USA) according to the cycling programme shown in Table 2.5. Upon completion, DNA was stored at -20°C.

Reagent	**Volume (µl)**
H_20	27
5X Q5 reaction buffer	10
dNTPs (10mM)	1
Forward primer (5µM)	5
Reverse primer (5µM)	5
Q5 High-fidelity DNA polymerase	1
DNA	1
Total volume	**50**

Table 2.4 Components for PCR per DNA sample.

Step	Temperature (°C)	Time
Initial denaturation	98	30 seconds
25-35 cycles	98 50-72 72	5-10 seconds 10-30 seconds 20-30 seconds/kb
Final extension	72	2 minutes
Final hold	4	-

Table 2.5 PCR cycling protocol.

2.6.3 Agarose Gel Electrophoresis

PCR products generated as above were separated using agarose gel electrophoresis. Samples were prepared by adding 10µl of 6X purple loading dye (New England Biolabs, MA, USA) to the PCR product. Samples were run on a 1.5% [w/v] agarose gel, prepared by dissolving 3g agarose powder in 200ml of 1X Tris-acetate-EDTA (TAE) buffer. Ethidium bromide was added at a concentration of 0.5 µg/ml to stain the DNA. Samples were loaded into the wells alongside the Quick-load 1kb DNA ladder (New England Biolabs, MA, USA), leaving a well empty between samples to avoid contamination during gel extraction. The gel was run at 80V for 2 hours and imaged using the Gel-Doc EZ Imager (Bio-Rad, CA, USA).

2.6.4 Gel Extraction of DNA

The PCR products run on agarose gels as described above next underwent excision from the gel in order to proceed with sequencing. Extraction was performed using the GenElute gel extraction kit (Sigma-Aldrich, MO, USA) according to the kit protocol with centrifugations performed at 12,000rpm. Briefly, the DNA band corresponding to the correct size for the PCR product was visualised using a UV transilluminator, and a clean scalpel was used to excise the band for each sample. Each gel slice was then weighed in a clean 1.5ml Eppendorf tube, to which 3 volumes of gel solubilisation was added followed by incubation at 55°C for 10 minutes in order to dissolve the gel. During incubation, DNA binding columns were prepared by adding 500µl of column

preparation solution to the binding column in a 2ml collection tube followed by a 1 minute centrifugation and discard of the flow-through. 1 gel volume of 100% isopropanol was added to the dissolved gel, which was mixed thoroughly and transferred to the prepared binding column and centrifuged for 1 minute before discarding flow-through. Next, columns were washed by adding 700µl of wash solution and centrifuged for 1 minute. Flow-through was discarded and columns were centrifuged for a further minute to remove residual ethanol. Binding columns were transferred into a clean 1.5ml Eppendorf tube and 35µl elution buffer was added to the centre of the membrane and incubated for 1 minute. Columns were centrifuged for a final minute to elute DNA, which was quantified as described and stored at -20°C.

2.7 Western Blot

2.7.1 Protein Extraction

Protein was extracted from cells growing at 70% confluence in a 10cm cell culture dish (Corning, Fisher Scientific, MA, USA). Dishes were removed from either the cell culture incubator or the hypoxic chamber and immediately placed onto ice. Cell culture medium was aspirated, and the cells were washed with 5ml of ice-cold PBS. The PBS was removed and 250µl of 1X radioimmunoprecipitation assay buffer (RIPA) (Cell Signalling Technology, MA, USA) supplemented with protease inhibitor cocktail (PIC) (Sigma Aldrich, MO, USA) (10 µl/ml) was added to the dish. The cells were scraped from the dish using a cell scraper (Corning, Fisher Scientific, MA, USA) and the lysate was collected into a 1.5ml Eppendorf tube. Cell lysates were homogenised by sonication using a Bioruptor® Pico sonication device (Diagenode, Belgium). Lysates were then cleared by centrifugation for 10 minutes at 12,000rpm in a 4°C centrifuge. The supernatant was transferred to a fresh 1.5ml Eppendorf and stored at -80°C for quantification and downstream analysis.

2.7.2 Protein Quantification

Protein sample concentration was determined using the Bradford assay. Briefly, a standard curve of bovine serum albumin (BSA) (Lee BioSolutions, MO, USA) was created by firstly producing a 50 mg/ml BSA stock through dissolving 0.5g BSA into 10ml dH_20. The top concentration of 4000 µg/ml BSA was produced by adding 80µl of 50 mg/ml BSA stock to 920µl PBS. Serial dilutions of the 4000 µg/ml BSA was performed by adding 100µl of the previous stock concentration to 100µl PBS to achieve the following range of concentrations: 2000 µg/ml, 1000 µg/ml, 500 µg/ml, 250 µg/ml, 125 µg/ml, 62.5 µg/ml, 31.25 µg/ml, 15.625 µg/ml. A PBS-only condition was used to provide the negative control. Experimental samples were diluted 1:10 in PBS. 10µl of the standards and unknown samples were added into triplicate wells of a 96-well plate (Falcon, Corning, Fisher Scientific, MA, USA). Immediately prior to use, the Bradford assay dye reagent (Bio-Rad, CA, USA) was diluted 1:5 with dH_2O. 200µl of diluted assay reagent was pipetted into each well. The plate was read at 620nm using the Infinite F50 absorbance microplate reader (Tecan, Männedorf, Switzerland) and the Magellan data analysis software. The raw data was exported to Microsoft Excel for analysis.

2.7.3 Gel Electrophoresis

Protein samples were separated using sodium dodecyl sulphate-polyacrylamide gel electrophoresis (SDS-PAGE) based on their size. Quantified protein samples were prepared for western blotting by adding the calculated volume of protein lysate (typically equal to 40µg) to 4X Laemmli sample buffer (Bio-Rad, CA, USA) and making all samples up to an equal volume with dH_2O in order to create a 1X working solution. The 4X Laemmli sample buffer was prepared prior to use by adding 100µl of β-mercaptoethanol (Sigma Aldrich, MO, USA) to 900µl 4X Laemmli sample buffer. Prepared protein samples were then boiled at 95°C for 5 minutes. 1mm polyacrylamide gels were prepared using the Mini-PROTEAN Tetra Handcasts system (Bio-Rad, CA, USA) at varying percentages of polyacrylamide depending on the sizes of the target proteins to be resolved. The gels were assembled in a running module in

the gel tank which was then filled with 1X running buffer. 4µl of Precision Plus Protein Dual Color Standards (Bio-Rad, CA, USA) was pipetted into the first well of the gel, followed by the protein samples. Electrophoresis was performed at 80V for 60 minutes followed by 120V until the dye front had reached the bottom of the gel.

2.7.4 Gel Transfer and Immunoblotting

After protein resolution through the gel, proteins were transferred from the gel onto a nitrocellulose membrane (0.45µM pore size, Bio-Rad, CA, USA) using the Bio-Rad Turbo Transfer system (Bio-Rad, CA, USA). 1L of 1X transfer buffer was made up by mixing 600ml of dH_2O with 200ml ethanol and 200ml of 5X transfer buffer. This was used to soak the tissue stacks and nitrocellulose membrane prior to assembly in the transfer cassette. Proteins were transferred on either a high molecular weight or mixed molecular weight transfer programme depending on the size of the target proteins. Following transfer, membranes were blocked for 1 hour in 5% BSA or 3% milk [w/v] in 1X Tris-buffered saline (TBS) containing 0.1% Tween20 (TBS-T) (Sigma Aldrich, MO, USA). After blocking, membranes were incubated with primary antibody solution (either diluted in 5% BSA or 3% milk [w/v]-TBST as per blocking) overnight at 4°C on a rocking platform. Table 2.6 details the antibodies used for this project alongside the dilution. The following day, membranes were washed 3 times for 5 minutes each with TBS-T 0.1% [v/v] on a rocking platform. The membranes were incubated for 1 hour at room temperature with the appropriate fluorescent secondary antibody, protected from light with foil. IRDye 680RD and 800CW (LI-COR Biosciences, NE, USA) secondary antibodies were used, diluted 1:10,000 in either 5% BSA or 3% milk [w/v]-TBST solution. Membranes were washed for a final 3 times, 5 minutes each with TBS-T on a rocking platform. Finally, membranes were imaged using the Odyssey FC Imaging System (LI-COR Biosciences, NE, USA) and band densitometry analysis was performed using the ImageStudio Lite software (LI-COR Biosciences, NE, USA). β-actin was used as a loading control for gene-of-interest normalisation.

Target	Company	Catalogue #	Dilution
β-Actin	Santa Cruz Biotechnology	sc-47778	1:1000
HIF1α	BD Biosciences	610959	1:500
HIF2α	Cell Signalling Technology	7096S	1:500
FOSL2	Cell Signalling Technology	19967S	1:1000
JUND	Cell Signalling Technology	5000S	1:1000
Cas9	Cell Signalling Technology	14697S	1:1000
CA9	Absolute Antibodies	Ab00414-1.4	1:500
Akt (pan)	Cell Signalling Technology	2920S	1:1000
p-Akt (Ser473)	Cell Signalling Technology	4060S	1:1000
Erk1/2	Cell Signalling Technology	4696S	1:1000
p-Erk1/2 (Thr202/Tyr204)	Cell Signalling Technology	9101S	1:1000

Table 2.6 Details of antibodies used in this project.

2.8 Phos-Tag

2.8.1 Protein Extraction

The Phos-Tag Acrylamide (Fujifilm WaKD Chemicals, Germany) system was used in order to study levels of protein phosphorylation where phospho-antibodies against the target protein were not commercially available. When combined with SDS-PAGE, the Phos-Tag acrylamide system can be used to separate phosphorylated from non-phosphorylated proteins. Cells were counted and seeded for protein extraction as previously described under 0.5% FBS [v/v] conditions. For each condition, a duplicate dish was seeded for lysis in 4M urea buffer. This is because the samples need to be lysed directly in Laemmli sample buffer for use with the Phos-Tag, and this is not compatible with the Bradford quantification assay. Dishes were removed from the incubator or hypoxic chamber and placed directly on ice. Cells were washed once with ice-cold 1X TBS. For Phos-Tag sample dishes, 250µl of laemmli sample buffer (62.5mM Tris pH 6.8, 2% SDS, 10% glycerol, 0.03% bromophenol blue and 5% β-

mercaptoethanol, BME) supplemented with protease inhibitor cocktail (10 µl/ml) was added to the dish. Dishes were scraped using a cell scraper and the lysate collected into a 1.5ml Eppendorf tube. Samples were boiled at 95°C for 5 minutes. Samples were passed through a syringe 10 times and then centrifuged at 12,000rpm for 10 minutes at 4°C. The supernatant was transferred to a fresh 1.5ml Eppendorf and stored at -80°C. For the duplicate dishes, 250µl of 4M urea buffer supplemented with protease inhibitor cocktail (10 µl/ml) was added to the dish after 1 wash with ice-cold TBS. Cells were scraped, collected into a 1.5m Eppendorf tube and passed through a syringe 10 times. Cells were centrifuged for 10 minutes at 12,000rpm at 4°C and the supernatant was transferred to a fresh 1.5ml Eppendorf tube. The sample was used in a Bradford assay immediately as previously described and the resulting concentrations were used to prepare the equivalent conditions of the Phos-Tag samples for electrophoresis.

2.8.2 Sample Preparation

A dephosphorylation negative control sample is generated for each Phos-Tag gel to be run using Lambda Protein Phosphatase (New England Biolabs, MA, USA). 20µg of protein sample is added to 1µl 10X NEB buffer, 1µl of 10mM $MnCl_2$, 1µl of lambda protein phosphatase and made up to 10µl with dH_2O. The reaction is incubated at 30°C for 90 minutes. 20µg of Phos-Tag samples are similarly prepared in 10µl reactions containing 1µl of 10X NEB buffer. Prepared dephosphorylation and Phos-Tag samples are then boiled at 95°C for 5 minutes.

2.8.3 Gel Electrophoresis and Transfer

Initially, the Phos-Tag compound was prepared as per the manufacturer's instructions with methanol and dH_2O to generate 5.0mmol/L of Phos Tag solution containing 3% [v/v] methanol and the resulting solution was protected from light. 50µM Phos-Tag acrylamide gels containing 100µM zinc were hand-cast and stored at 4°C until use. See appendix for Phos-Tag gel and buffer recipes used. Gels were assembled into running modules and loaded with ladder and sample as previously described for a classical

western blot. The gels were run at 80V until 45 minutes after the blue dye front had migrated out of the gel. Gels are then prepared for transfer by undergoing 3 x 10 minute washes in transfer buffer (made up as previously described) containing 3mM EDTA (Sigma Aldrich, MO, USA). Following this, gels are washed once for 10 minutes in transfer buffer without EDTA to remove excess EDTA. Gels are then transferred onto nitrocellulose membranes as previously described for a classical western blot.

2.8.4 Immunoblotting

After gel transfer, Phos-Tag membranes were blocked in 5% BSA [w/v]-TBS-T 0.1% [v/v] for 1 hour at room temperature on a rocking platform. Antibody incubations, washes and imaging were performed as previously described for a classical western blot.

2.9 Immunocytochemistry

Cells were grown to 70% confluence on a µ-slide 8-well coverslip (Ibidi, Germany) in either 10% or 0.5% [v/v] FBS conditions. Cell medium was aspirated, and cells were washed once with PBS. Cells were fixed in 300µl 4% paraformaldehyde (PFA) (Thermo Fisher, MA, USA) in PBS for 10 minutes at room temperature. The fixative was removed, and cells were washed three times with PBS-0.1% Tween [v/v]. Cells were permeabilised in 300µl PBS-0.5% saponin (Sigma Aldrich, MO, USA) [w/v] for 5 minutes at room temperature, followed by three washes with PBS-0.1% Tween [v/v]. Cells were blocked for 1 hour at room temperature in 300µl 1% BSA in TBS [w/v] containing 0.5% saponin [w/v]. Cells were washed three times with PBS-0.1% Tween [v/v]. Cells were incubated at 4°C overnight with primary antibody diluted in 300µl 1% BSA in TBS [w/v] containing 0.5% saponin [w/v] per well. The following day, cells were washed three times with PBS-0.1% Tween [v/v]. Cells were incubated in 100µl of the appropriate secondary antibody diluted in 1% BSA in TBS [w/v] containing 0.5% saponin [w/v] for 45 minutes at room temperature, protected from light. Cells were washed a further three times with PBS-0.1% Tween [v/v]. The nuclei of the cells were stained with 100µl of 1 µg/ml Hoechst stain (Thermo Fisher, MA, USA) diluted in PBS for 10 minutes at

room temperature, protected from light. Cells were washed a final three times with PBS-0.1% Tween [v/v]. Microscope slides were imaged using the Leica Confocal TCS SPE (Leica Microsystems, Germany). Images were exported to ImageJ for analysis.

2.10 Proteome Profiler Phospho-Kinase Array

The Proteome Profiler Human Phospho-Kinase Array kit (R&D Systems, MN, USA) was used to assess protein phosphorylation of 39 proteins across different conditions, according to the protocol provided. Briefly, 2 x 10^6 Ls174T cells were seeded in 10cm^2 cell culture dishes. The following day, dishes were either placed into 1% O_2 or 21% O_2. 24 hours later, dishes were washed with PBS and lysed with 250µl Array Buffer 6 supplemented with protease inhibitor cocktail (10 µl/ml). Samples were agitated for 30 minutes at 4°C and then centrifuged at 4°C for 5 minutes at 14,000rpm. The supernatant was transferred to a fresh 1.5ml Eppendorf tube and quantified immediately using the Bradford assay previously described. Part A and Part B membranes (1 pair per sample) were blocked in 1ml Array Buffer 1 in the multi-well dish provided for 1 hour at room temperature. 600µg of protein lysate was diluted in 2ml Array Buffer 1 and 1ml of sample was added to each Part A and Part B membrane after aspiration of the block solution. The sample was incubated with the membranes overnight at 4°C on a rocking platform. The following day, membranes were removed from the multi-well dish and both Part A and Part B were washed together three times in 20ml 1X Wash Buffer for 10 minutes at room temperature. Membranes were returned to the multi-well dish and incubated for 2 hours at room temperature with either Detection Antibody Cocktail A or Detection Antibody Cocktail B diluted in 1ml 1X Array Buffer 2/3. Membranes were washed separately 3 times with 20ml 1X wash buffer for 10 minutes each. Streptavidin-HRP was diluted 1:2000 in 1X Array Buffer 2/3 and membranes were incubated in 1ml of the reagent for 30 minutes at room temperature. Part A and Part B membranes were washed a final 3 times together for 3 x 10 minutes in 20ml 1X Wash Buffer. Membranes were aligned on a sheet of Parafilm and were covered in 1ml of prepared Chemi Reagent mix per membrane pair for 1 minute. Membranes were imaged using the Odyssey FC Imaging System and densitometry analysis was performed using the ImageStudio Lite software.

2.11 RNA Extraction and Quantitative PCR

2.11.1 RNA Extraction

Cells were grown to 70% confluency in a 10cm dish under experimental conditions. Dishes were removed from the cell culture incubator or hypoxic chamber and placed onto ice. Cell culture medium was aspirated and 1ml TRI Reagent (Sigma Aldrich, MO, USA) was added per 10cm dish and incubated for 5 minutes at room temperature. The resulting lysate was removed from the dish and transferred into a 1.5ml Eppendorf tube. 200µl of chloroform was added and the samples were shaken by hand before a 20 minute centrifugation at 12,000rpm in a 4°C centrifuge. 400µl of the upper aqueous layer was carefully aspirated from the sample and added to a 1.5ml Eppendorf tube containing 500µl isopropanol. Samples were shaken by hand and incubated at -80°C for 2 hours. Samples were then pelleted by centrifugation for 20 minutes at 12,000rpm at 4°C. The supernatant was removed from the tube and pellets were washed with 800µl of 75% ethanol and centrifuged for 5 minutes at 8500rpm at 4°C. The supernatant was removed, and the RNA pellet was dissolved in 20µl of RNase-free water. RNA samples were quantified using the Nanodrop 2000 and stored at -80°C for downstream analysis.

2.11.2 cDNA Synthesis

cDNA synthesis was performed using the High Capacity cDNA Reverse Transcription Kit (Applied Biosystems, Fisher Scientific, MA, USA). The calculated volume for 2µg RNA was diluted to 10µl with RNase-free water per reaction. The final reaction volume was made up to 20µl by adding 10µl of cDNA Mastermix per sample. Table 2.7 provides the Mastermix components per sample.

Reagent	Volume (µl)
10X RT buffer	2.0
25X dNTP mix (100mM)	0.8
10X Random RT Primers	2.0
RNase-free water	4.2
MultiScribe Reverse Transcriptase	1.0
Total volume per reaction	**10.0**

Table 2.7 Reverse transcription Mastermix components per sample.

Samples were placed into a Veriti 96-well thermal cycler (Applied Biosystems, Fisher Scientific, MA, USA) and the cDNA cycling programme was selected. Details are shown in Table 2.8. Upon completion of the programme, samples were removed and diluted 1:10 by the addition of 180µl RNase-free water and stored at -20°C for later analysis by qPCR.

Step	Temperature (°C)	Time (Minutes)
1	25	10
2	37	120
3	85	5
4	4	-

Table 2.8 Cycling programme for the cDNA synthesis reaction.

2.11.3 Quantitative PCR

Quantitative PCR (qPCR) was performed using the Viia7 Real-Time PCR System (Applied Biosystems, Fisher Scientific, MA, USA). The reagent used was the Light Cycler 480 SYBR Green I Master Mix (Roche, Switzerland). A Mastermix was prepared for each gene to be analysed, with β-actin used as a control housekeeping gene on each plate run. qPCR primers were purchased from Sigma Aldrich and sequences are listed in the Appendix. Table 2.9 details the components of the Mastermix and the volume of each component per reaction well on a clear 96-well plate (Applied Biosystems, Fisher

Scientific, MA, USA). These volumes were multiplied by the number of samples to be tested in triplicate.

Reagent	Volume (µl)
Forward primer (10µM)	1
Reverse primer (10µM)	1
RNase-free water	6
SYBR green I master mix	10
cDNA	2
Total volume per reaction	**20.0**

Table 2.9 qPCR Mastermix components per reaction well.

Plates were spun down and run on the Viia7 Real-Time PCR System. Programme details are shown in Table 2.10. Upon completion of the programme, the Ct values generated were exported to an Excel file for analysis by the ΔCt method.

Step	Temperature (°C)	Time (seconds)
Initial denaturation	95	30
40 cycles	95 58 72	5 15 10
Final hold	4	-

Table 2.10 Cycling programme for qPCR.

2.12 RNA-Sequencing

2.12.1 Sample Preparation

Unlike RNA extraction for qPCR using TRI Reagent, for RNA-sequencing samples were prepared using the Qiagen RNeasy Mini Kit (Qiagen, Germany). This is because column extraction techniques were the preference of Novogene due to enhanced purity and integrity of the RNA. Cells were grown to 70% confluence in 10cm dishes under the relevant experimental conditions. Cell culture medium was aspirated, and the dishes

washed once with ice-cold PBS which was subsequently removed. 600µl of Buffer RLT supplemented with 10 µl/ml BME was added to each dish which was scraped with a cell scraper. The lysate was transferred to a 1.5ml Eppendorf tube and homogenised by passing through a syringe 10 times. 600µl of 70% ethanol was added to the lysate which was mixed and transferred (700µl at a time) into a spin column placed inside a collection tube. Columns were centrifuged for 15 seconds at 10,000rpm and the flow-through was discarded. 700µl Buffer RW1 was added to each column which were then centrifuged for 15 seconds at 10,000rpm and the flow-through was discarded. On-column DNase-digestion was performed by adding 10µl DNase I stock to 70µl Buffer RDD and adding the 80µl mixture directly onto the centre of the membrane, incubated for 15 minutes at room temperature. 350µl Buffer RW1 was added to each column followed by centrifugation for 15 seconds at 10,000rpm and the flow-through was discarded. 500µl Buffer RPE was added to each column followed by centrifugation for 15 seconds at 10,000rpm and the flow-through was discarded. This step was repeated with a 2 minute centrifugation to dry the column. The columns were transferred into a new collection tube and 30µl RNase-free water was added to the centre of each membrane. Columns were centrifuged for 1 minute at 10,000 rpm and the resulting eluate was quantified as previously described and stored at -80°C.

2.12.2 Sequencing

RNA prepared as above was diluted to 200 ng/µl and shipped to Novogene for their sequencing service. This consisted of a 150bp-paired end sequencing with a depth of 20 million reads, performed using the Illumina NovaSeq 6000 Sequencing System (Illumina, CA, USA). Bioinformatics analysis was included in the service, with the Homo Sapiens (GRCh38/hg38) reference genome used. Prior to sequencing, RNA sample quality was assessed by Novogene using agarose gel electrophoresis and RIN number to assess quality and Nanodrop to assess purity of samples.

2.13 Tissue Micro-Array

Human colorectal cancer microarray slides were obtained from the Nottingham and Health Sciences Biobank in collaboration with Declan Sculthorpe and Dr Abhik Mukherjee. Slides were stained for FOSL2 by Declan using standard immunohistochemical technique. H-scoring of the array was performed by myself with a selection of scores reviewed by Dr Mukherjee, an independent histopathologist. When scoring was complete, data was passed onto Declan for analysis relating to the patient clinical characteristics from which the cores were derived.

2.14 In Vivo Study

Seven week old immunocompromised CD-1 nude mice were injected subcutaneously into the left flank with 2 x 10^6 HCT116 or Ls174T cells in a 100µl dosing volume prepared with Matrigel. The cells were either control or FOSL2 knockdown cells generated *ex vivo* prior to implantation. The study was identified as CSU1909 and carried out under project license number P435A9CF8. Mice were weighed weekly and tumours were measured every 3-4 days using Vernier callipers in order to calculate tumour volume. The cells were generated by me, whilst the implantation, measurements and animal care were performed by senior *in vivo* research manager Alison Richie and experienced research technician Pam Collier.

2.15 Statistical Analyses

Data presented represent the mean ± standard error of the mean (SE). Statistical analyses were carried out using two-tailed Student's *t*-test or ANOVA with Tukey's *post hoc* test when appropriate. $p < 0.05$ was considered significant. The chi-squared test was performed for the analysis of the TMA scores.

3.0 Investigating the Role of FOSL2 and JUND in Regulating the Hypoxic Transcriptome

3.1 Introduction

3.1.1 Investigating Tumour Hypoxia by Transcriptomics

Tumour hypoxia has become an increasingly recognised clinical biomarker for a range of characteristics including patient prognosis and resistance to therapy. However, the recognition and quantification of tumour hypoxia in a clinical setting is challenging, and so research into non-invasive and accurate hypoxic biomarkers is needed. For example, whilst HIF over-expression is closely associated with hypoxia and patient prognosis, HIF itself is not considered to be a useful hypoxic biomarker alone due to mechanisms of oxygen-independent mechanisms of activation[216]. Over the past decade due to advancements in bioinformatics, research has turned to the powerful tool of transcriptomics in order to identify hypoxic gene signatures that can characterise tumour hypoxia. This would be especially useful to incorporate into existing molecular categorisation of tumour subtypes, as the stratification of hypoxic patients will allow for more targeted therapy.

Hypoxic gene signatures have been generated for a wide range of cancers known to feature tumour hypoxia, where stratification of the hypoxic fraction of tumours would be beneficial for therapeutic decisions. For example, in glioblastoma which is often characterised by extensive tissue hypoxia. One study utilised TGCA datasets and produced a 20-gene hypoxic signature, featuring well known hypoxia-inducible genes such as VEGFA and LDHA. When the hypoxic signature genes were mapped onto STRING to identify potential hypoxic protein interaction networks, interestingly both FOS and JUN appeared among the 20 highest with the most potential hypoxic interactions[217]. This is also the case for a study that produced a 28-gene hypoxic prognostic gene signature for prostate cancer, where FOSL2 was included among the list of genes comprising the signature[218].

The use of hypoxic gene signatures have also been utilised in studies of colorectal cancer. One study constructed a hypoxic gene signature utilising transcriptomic data from 309 CRC patients with clinical information. A 14-gene signature was developed and validated across multiple cohorts, accurately predicting disease-free survival following treatment[219]. They identified an enrichment of cell cycle and metabolic genes and functions including mTORC1, E2F transcription factors and mitosis in the high-risk group, identifying targets that has been previously correlated to CRC but not to hypoxia, highlighting the value of the transcriptomic approach in identifying novel hypoxic targets. Interestingly in colorectal cancer, hypoxia-related miRNAs have also been considered for use in hypoxic signatures given research suggesting the crucial role of hypoxia-related miRNAs across many cancers including CRC. One study utilising the HT-29 cell line under normoxic and hypoxic conditions identified 52 differentially expressed miRNAs, developing a hypoxia-related miRNA signature consisting of just 4 of these involved in several pathways including MAPK signalling[220]. The use of the miRNA hypoxic signature was able to successfully discriminate high-risk patients in a TCGA cohort and was determined to be an independent prognostic indicator for CRC.

More recently, a paradigm shift in tumour hypoxia transcriptomics has focused on the role of hypoxia in modulating the immune system within the tumour microenvironment. For example, an 8-gene hypoxic signature in pancreatic cancer was found to predict survival, including genes such as VEGFA and P4HA1 as identified in the cervical cancer hypoxic signature, in addition to genes such as DDIT4 involved in the DNA damage response. Interestingly, the hypoxic signature was also indicative of an immunosuppressed tumour microenvironment, with an almost global mutual exclusivity existing between hypoxia and immune reactivity[221]. This highlights an important implication of establishing hypoxic signatures which may be correlated to additional phenotypes that aids the treatment of cancer. For example, through reversal of the hypoxic state in the patients identified by the hypoxic signature, the immune system would become reactive and open the path for immune checkpoint inhibition. Similar outcomes have been found in a prognostic model developed for colorectal adenocarcinoma, where the overall degree of hypoxia present, as defined through a hypoxic gene signature, is correlated with immunosuppressive activity[222].

3.2 Aims and hypotheses

The role of FOSL2 and JUND in mediating the hypoxic response in colorectal cancer has not yet been explored. I hypothesise that both FOSL2 and JUND will be upregulated in hypoxia in CRC cell lines, and knockdown of these subunits will decrease 3D spheroid growth and clonogenic formation. I hypothesise that, through RNA-sequencing, FOSL2 and JUND will be identified as master regulators of the transcriptomic response to hypoxia, through associating and co-associating with hypoxic pathways. Finally, I hypothesise that FOSL2 will play a role in *in vivo* tumour growth.

In order to test these hypotheses I will use the following aims:

1. Determine the upregulation of FOSL2 and JUND following exposure to multiple time-points of hypoxia (1% O_2) or normoxia (21% O_2) in Ls174T.
2. Optimise an inducible CRISPR-Cas9 knockdown system and produce inducible FOSL2 and JUND knockdowns in a panel of CRC cell lines.
3. Investigate the effect of FOSL2 and JUND knockdown on the growth of 3D spheroids in Ls174T.
4. Investigate the effect of FOSL2 and JUND knockdown on the ability of cells to form colonies in a clonogenic assay featuring normoxic (21% O_2) and hypoxic (1% O_2) conditions.
5. Generate and validate FOSL2 and JUND knockdown samples for RNA-sequencing generated at a 24 hour time-point in normoxia (21% O_2) or hypoxia (1% O_2).
6. Investigate through RNA-sequencing the top genes and pathways associated with FOSL2 and JUND in hypoxia and where co-association of hypoxic targets occurs.
7. Analyse the effect of FOSL2 knockdown on xenograft tumour growth in Ls174T and HCT116 knockdown-implanted mice.
8. Extract protein from xenograft tumour samples to establish FOSL2 association with CA9 expression *in vivo*.

3.3 Results

3.3.1 FOSL2 Expression in Hypoxia

It was first determined whether FOSL2 protein levels were upregulated in hypoxia in Ls174T colorectal cancer cells. Wild-type Ls174T cells were exposed to hypoxic (1% O_2), physoxic (8.5% O_2) or normoxic (21% O_2) cell culture conditions for various time-points: 12, 24, 48 and 72 hours, prior to protein extraction. As normoxic oxygen levels have been used throughout this project, it was important here to include physoxic conditions to compare FOSL2 expression at normoxic and the more physiologically relevant physoxic levels. FOSL2 protein levels are significantly upregulated at the 24 hour and 48 hour hypoxic time-points (24 hours $p<0.001$, 48 hours $p<0.05$) when compared to 12 hour normoxic levels as shown in Figure 3.1A and 3.1B. Non-significant hypoxic inductions are apparent at the 12 hour and 72 hour time-points. The highest hypoxic induction of FOSL2 is seen at the 24-hour time-point, where FOSL2 expression is 5.5 fold higher compared to the normoxic control. This decreases at the 48-hour hypoxic time-point, where FOSL2 levels are 3.8 fold higher than the normoxic control. CA9 is used as a hypoxic control, as described in the introduction as a HIF-1 target that is upregulated in hypoxia over time and is used to establish that the samples are hypoxic. CA9 is significantly upregulated at the 24, 48 and 72 hour hypoxic time-points compared to the normoxic control ($p<0.0001$) with a nonsignificant induction at the 12 hour hypoxia time-point (Figure 3.1C). No significant differences were found between normoxic and physoxic levels of either FOSL2 or CA9.

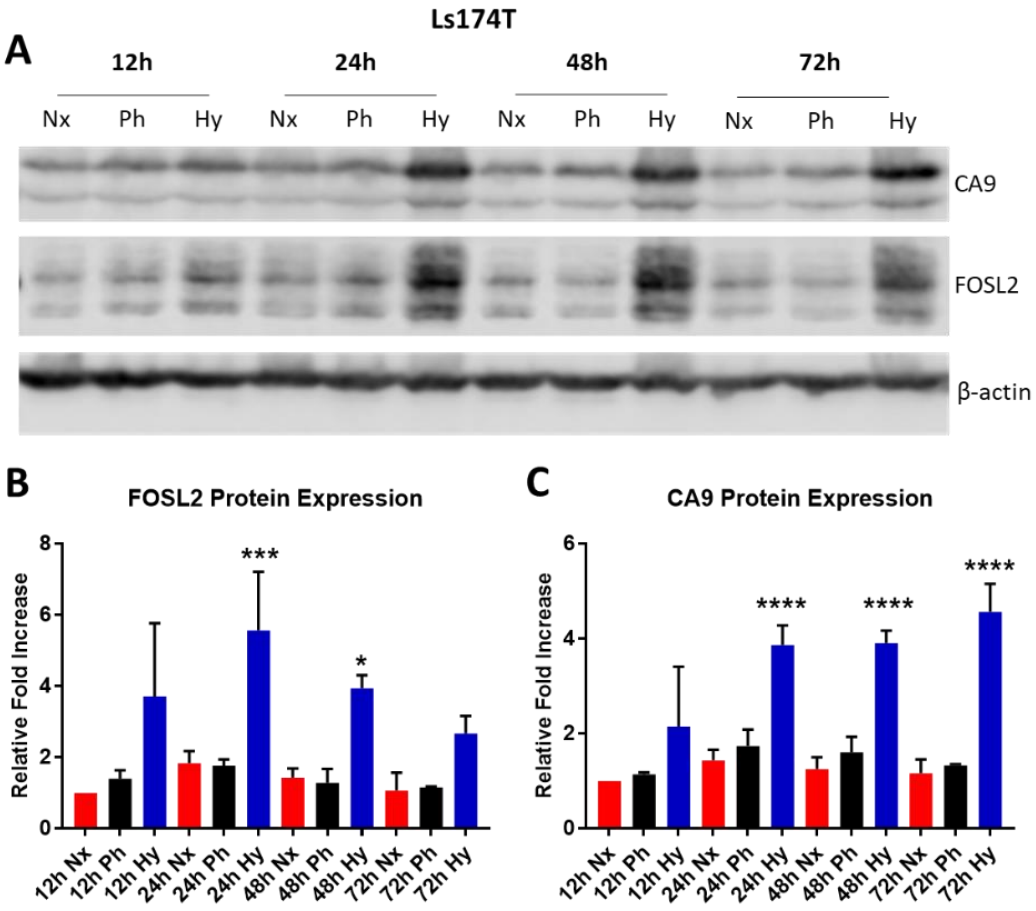

Figure 3.1 FOSL2 and CA9 protein expression under normoxic (21% O_2), physoxic (8.5% O_2) and hypoxic (1% O_2) conditions in Ls174T across multiple time points. (A) Representative immunoblot images of CA9 and FOSL2. (B) Quantification of FOSL2 expression. (C) Quantification of CA9 expression. Error bars indicate ± SEM. Data analysed using a one-way ANOVA. N=3. *p<0.05, **p<0.01, ***p<0.001, ****p<0.0001.

3.3.2 Generation of Inducible FOSL2 Knockdown Cell Lines

As shown in the above data, FOSL2 expression is induced by hypoxic conditions, suggesting that as a transcription factor, FOSL2 associates with targets of the hypoxic transcriptome. In order to investigate this role, FOSL2 knockdown cell lines were generated to be used as models to determine the targets or pathways that FOSL2 associated with in hypoxia in colorectal cancer. Two simultaneous CRISPR-Cas9 approaches were utilised in order to generate FOSL2 knockdown cell lines. The first clonal approach was already being utilised within the lab group, and this was used to generate the knockdown clones that are used and described in Chapter 5. For this

chapter, an alternative CRISPR-Cas9 approach was optimised because data that was being generated from experiments conducted in parallel to this work was suggesting an issue with clonal heterogeneity from the original clonal technique utilised for generating the HIF1α and HIF2α knockdown clones described later. These issues were found in the work described here but also across other projects from within the McIntyre lab that were utilising the same clonal technique.

In order to illustrate these issues, data has been selected from qPCR validation experiments conducted on a previous RNA-sequencing experiment that was performed by Eric Vancauwenberghe of the McIntyre lab. The RNA-seq conditions included siRNA knockdowns for FOSL2, HIF1α and HIF2α in hypoxic conditions (1% O_2, 24 hours) as well as an siRNA control in both hypoxia and normoxia (21% O_2, 24 hours) and FOSL2 knockdown in normoxia. The RNA used to perform the sequencing was passed onto myself and I used this material to perform qPCR to validate several top hits that were found to be associated with FOSL2 in hypoxia. In addition to this, I performed the same validation using material from FOSL2 clonal knockdowns (generated by Eric) and HIF1α and HIF2α knockdowns (generated by myself as described in Chapter 5) to assess the robustness of the clonal knockdown approach.

Figure 3.2 shows qPCR data from 4 targets selected from the RNA-sequencing study performed in Ls174T, from both the siRNA approach and the clonal knockdown approach. Several issues with the clonal approach are evident. Panels 3.2A and 3.2B show CA9 mRNA expression in siRNA and clonal approaches respectively. The siRNA approach demonstrates the observed effects: the highest level of association with HIF1α, no association with HIF2α and some association with FOSL2 (demonstrated previously in work conducted by Eric Vancauwenberghe). However, when clones are used, significant association with HIF2α is apparent. This highlights an important clonal effect where not all single clones are found to express CA9, a significant limitation to the use of single clones in the study of the hypoxic response. Clonal effects are also found in the regulation of SORBS1, where the siRNA approach demonstrates significant association of this target with both HIFs and FOSL2 (Figure 3.2C). However, this effect of FOSL2 is not present in the FOSL2 knockdown clone, and instead a significant upregulation of SORBS1 is apparent upon knockdown of HIF1α (Figure

3.2D). Similarly, when validating DEPTOR, the regulatory effect of FOSL2 found in the siRNA material is lost in the clone, and again significant association with HIF2α is apparent (Figure 3.2E-F). Finally, validation of PCK1 demonstrates significant association with FOSL2 in hypoxia using the siRNA approach (Figure 3.2G), and again the HIF2α association found using the knockdown clones (Figure 3.2H). In order to investigate further how single clones generated using the described approach vary from wild-type Ls174T cells, material was generated from both wild-type cells, control clones, and several knockdown clones per gene. As Figure 3.2I demonstrates, the control clones are not behaving as wild-type Ls174T cells in the context of PCK1 expression. The wild-type cells show robust hypoxic induction of the gene, which is lost in all single clones and overall levels are significantly lower. This effect was seen to a greater extent in some genes that others.

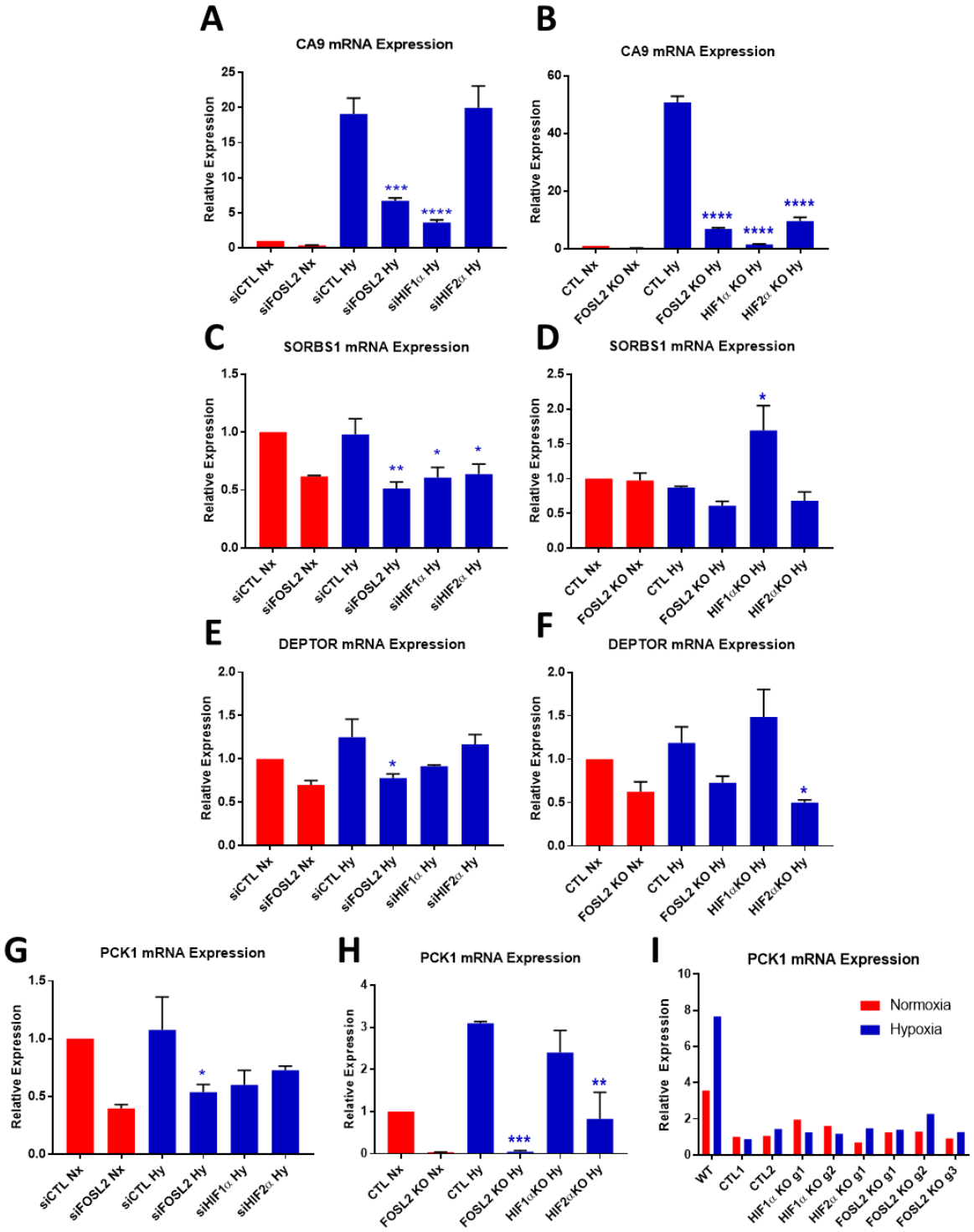

Figure 3.2 Illustrative qPCR data demonstrating discrepancies between the siRNA and clonal knockdown approach in Ls174T. CA9 mRNA expression in siCTL and siFOSL2 in normoxia (21% O_2, 24 hours) and siCTL, siFOSL2, siHIF1α and siHIF2α in hypoxia (1% O_2, 24 hours) (A) compared to the same conditions as clonal knockdowns in (B). The same is shown for SORBS1 (C-D), DEPTOR (E-F) and PCK1 (G-H). (I) Demonstrates additional conditions including wild-type cells. Error bars indicate ± SEM. Data analysed using a one-way ANOVA. N=3 (A-H) N=1 (I). *p<0.05, **p<0.01, ***p<0.001, ****p<0.0001. Significance level shown for knockdown conditions normalised to control hypoxia only.

Figure 3.3 demonstrates further examples (n=1) of genes where the wild-type was compared to control clones and multiple knockdowns for the same gene were tested. For CA9 (Figure 3.3A), control clone 2 showed a greater hypoxic induction than control clone 1, and FOSL2 KD 3 displayed around a third less induction than FOSL2 KD 2. EGLN3 displayed greater similarity of hypoxic induction between clones (Figure 3.3B), whilst CLIC4 and SAV1 demonstrated considerable variation between knockdowns within the same gene and between controls (Figure 3.3C – Figure 3.3D). It was therefore concluded that clonal heterogeneity arose from the use of single knockdown clones and that a new system should be optimised for further downstream work.

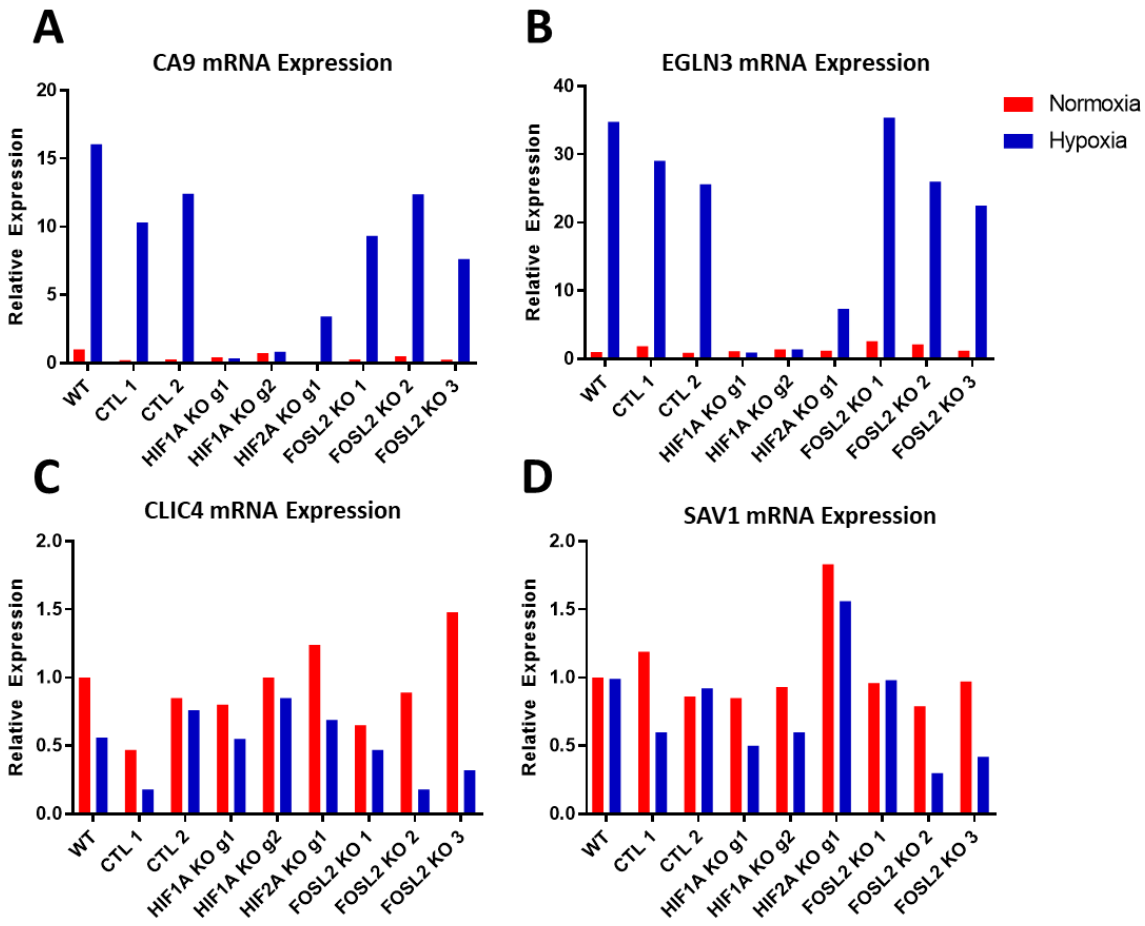

Figure 3.3 Illustrative qPCR data demonstrating clonal heterogeneity across several genes in Ls174T. qPCR data for 4 representative genes in normoxia (21% O_2, 24 hours) or hypoxia (1% O_2, 24 hours) in wild-type, control clones and a range of knockdown clones. (A) CA9 mRNA expression (B) EGLN3 mRNA expression (C) CLIC4 mRNA expression (D) SAV1 mRNA expression. N=1. Data normalised to WT normoxia condition.

A schematic diagram of both CRISPR-Cas9 approaches optimised for this project is shown in Figure 3.4 and described further in Methods. Briefly, the same inducible Cas9 cell lines generated by lentiviral transduction were used as the Cas9 system for both approaches. The clonal approach utilised doxycycline induction (2 μg/ml, 48 hours) to induce Cas9 followed by lipofection of synthetic gRNAs and clonal expansion. This meant that individual cells were expanded and tested for the presence of the gene knockdown. In contrast, the second approach starts with a second lentiviral transduction on top of the iCas9 cell lines, this time to transfer the gRNA into the target cells under the selection of puromycin. Following puromycin selection, doxycycline (2 μg/ml, 96 hours) was used to induce Cas9 expression in the mixed pool population. The mixed knockdown pool resulting from this was used for downstream analysis. Importantly, following transduction of the gRNA, Cas9 is only induced with doxycycline immediately prior to experimental use, and cells that have been previously exposed to doxycycline were not used for new experiments. This is to ensure that each knockdown population is generated fresh and that cells were not given time to compensate in response to gene knockdown.

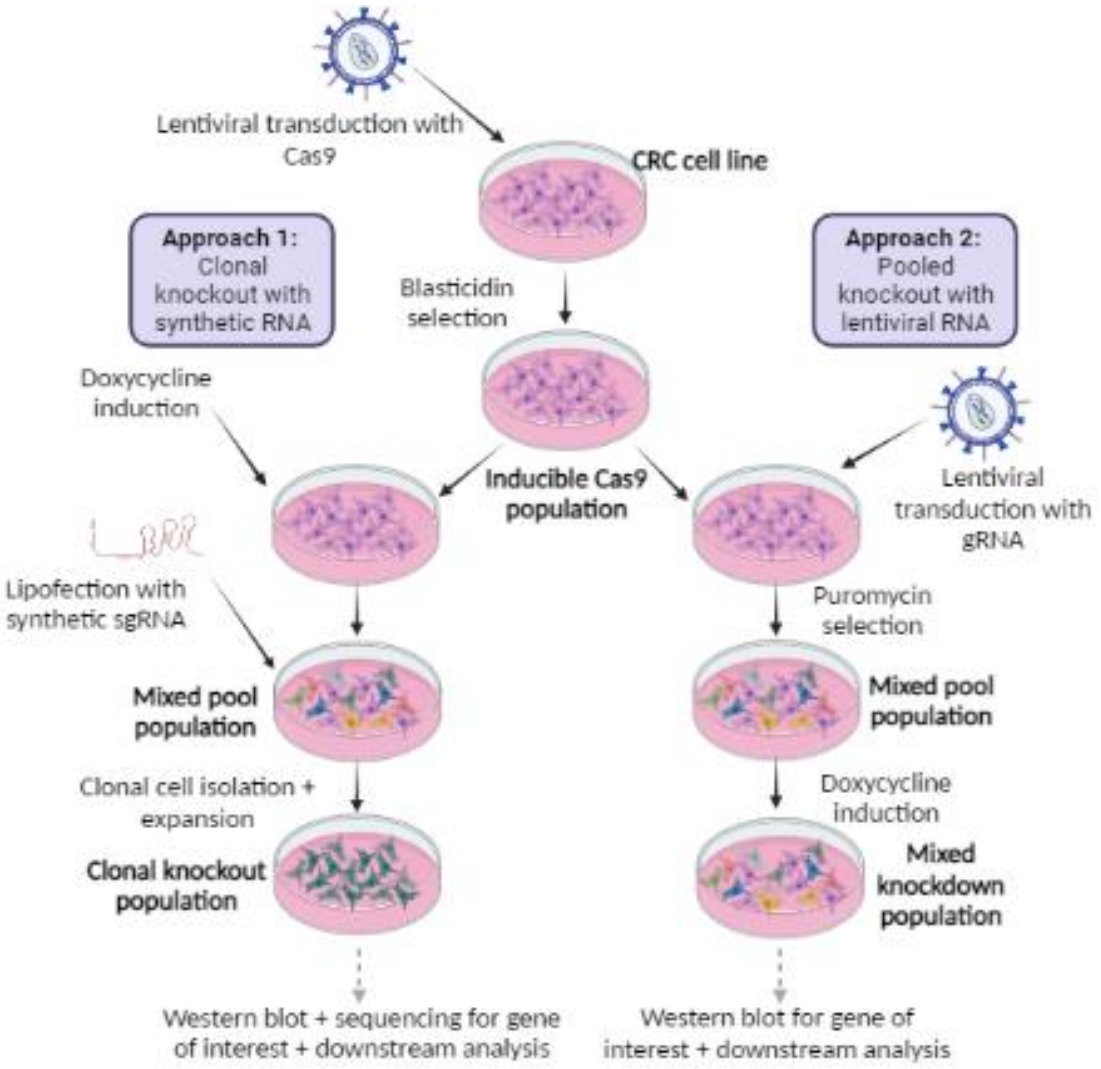

Figure 3.4 Schematic diagram depicting both CRISPR-Cas9 approaches optimised for this project. The approach on the right is used for the generation of the inducible FOSL2 knockdown cell lines as described below. Figure created in BioRender.

Initially, 4 cell lines were used for the creation of the inducible FOSL2 knockdowns, with Ls174T and HT-29 representing the CMS3 colorectal cancer subtype and HCT116 and SW620 representing the CMS4 colorectal cancer subtype. The Cas9-inducible cell lines were transduced with either a non-targeting control or one of two FOSL2-targeting gRNA lentiviruses. Cells were seeded in 6-well format with + doxycycline groups treated with 2 µg/ml doxycycline for 5 days prior to protein extraction to assess knockdown efficiency in each cell line. Controls without doxycycline were included to assess potential impact of doxycycline on FOSL2 expression.

The representative immunoblots show that Cas9 is induced by doxycycline treatment but is absent in the conditions without doxycycline, showing that the inducible system can be effectively switched on and off (Figure 3.5A and 3.5D). For HT-29 representing CMS3, there was no significant difference in FOSL2 expression between control and control plus doxycycline, and so the doxycycline treatment does not alter FOSL2 expression. When normalising each guide RNA or non-targeting control plus doxycycline to its isogenic control (the same gRNA but minus the doxycycline treatment), both FOSL2-g1 and FOSL2-g2 plus doxycycline are significantly lower than without doxycycline (g1 $p<0.001$, g2 $p<0.0001$). However, FOSL2-g1 is only achieving a 40% reduction in FOSL2 expression whereas FOSL2-g2 is achieving a 78% reduction in FOSL2 expression when treated with doxycycline (Figure 3.5B). All conditions were also normalised separately to control minus doxycycline in order to assess if FOSL2-g1 and FOSL2-g2 expression levels were lower than the control in the absence of doxycycline, however these conditions were not significantly different from the control (Figure 3.5C). Similarly, for Ls174T, no significant difference was observed in FOSL2 expression between control and control plus doxycycline conditions. Both FOSL2-g1 and FOSL2-g2 plus doxycycline were significantly lower than their isogenic controls (FOSL2-g1 $p<0.05$, FOSL2-g2 $p<0.0001$) but similarly to HT-29, FOSL2-g1 effects were lower at only a 27% reduction in FOSL2 expression, whereas FOSL2-g2 achieved a 48% reduction in FOSL2 levels (Figure 3.5E). When normalised to control minus doxycycline, FOSL2-g2 minus doxycycline is also significantly decreased by 42% ($p<0.001$), demonstrating that gene cutting may be taking place in the absence of doxycycline (Figure 3.5F).

FOSL2 knockdown cell lines were also generated as described in SW620 and HCT116, representing colorectal cancer CMS4 subtype. For SW620, no significant difference was found in FOSL2 protein expression between control with and without doxycycline. Only a 35% decrease in FOSL2 expression is observed with FOSL2-g1 plus doxycycline ($p<0.001$) and a 66% decrease is observed in FOSL2-g2 plus doxycycline ($p<0.01$) compared to isogenic controls (Figure 3.6A and 3.6B). No significant differences were found between FOSL2-g1 or FOSL2-g2 without doxycycline when compared to control without doxycycline (Figure 3.6C). Finally, FOSL2 knockdown cells were also generated

in HCT116 (Figure 3.6D). This time, a significant increase was found in control plus doxycycline compared to control without doxycycline ($p<0.01$) suggesting that doxycycline may be inducing FOSL2 in this cell line. There is no significant reduction in FOSL2 expression with FOSL2-g1 with doxycycline compared to without, however FOSL2-g2 with doxycycline is 68% reduced compared to FOSL2-g2 without doxycycline ($p<0.0001$) (Figure 3.6E). When all conditions are compared to control without doxycycline, neither FOSL2-g1 nor FOSL2-g2 without doxycycline are significantly different from the control (Figure 3.6F).

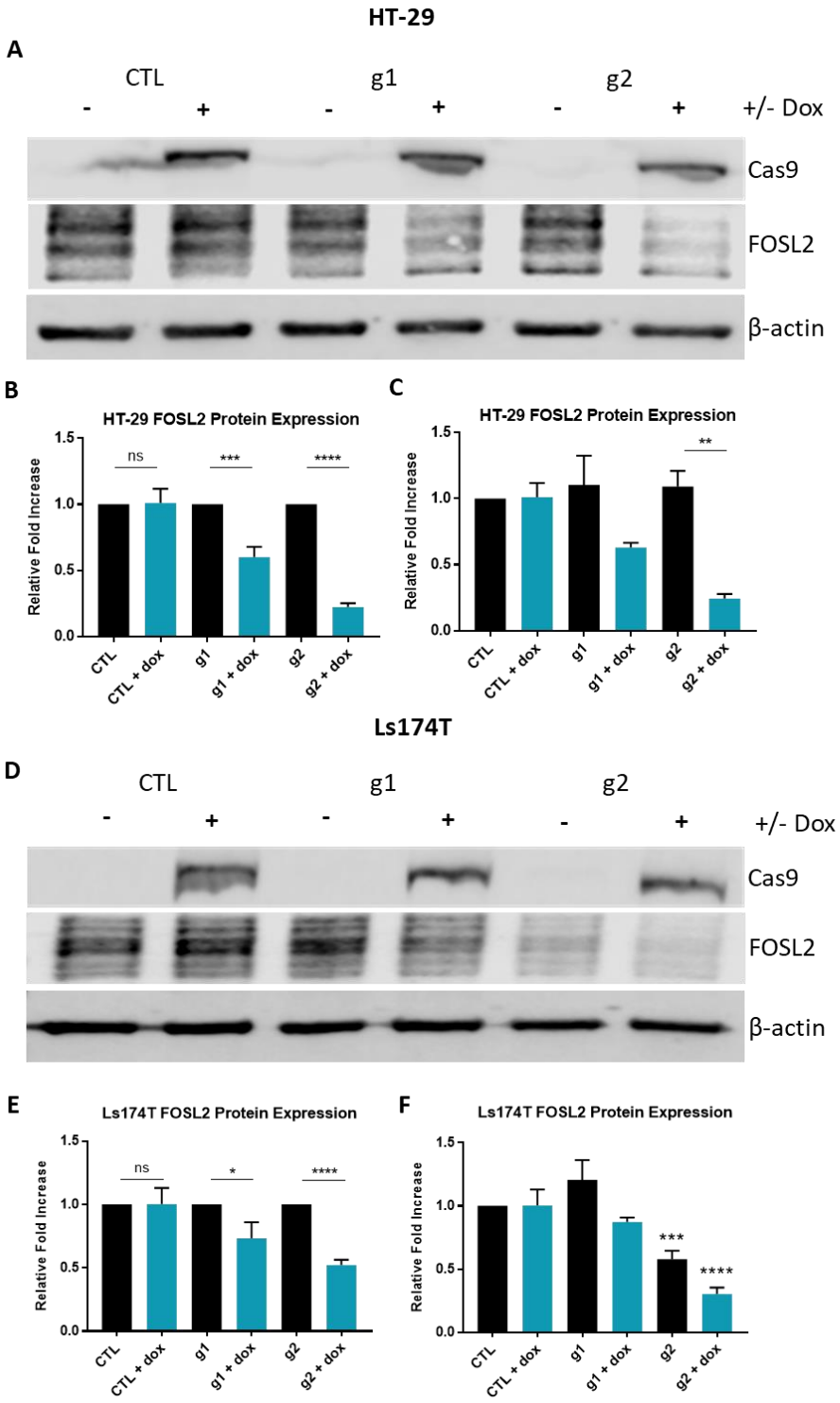

Figure 3.5 Generation of inducible FOSL2 knockdown cell lines representing the CMS3 subtype. Conditions include a non-targeting control and two gRNA sequences for FOSL2, in the presence or absence of doxycycline (2 µg/ml). Representative immunoblots are shown for Cas9 and FOSL2 in HT-29 (A) with quantification (B-C). Representative immunoblots are shown for Cas9 and FOSL2 in Ls174T (D) with quantification (E-F). Error bars indicate ± SEM. Data analysed using a one-way ANOVA. N=3. *p<0.05, **p<0.01, ***p<0.001, ****p<0.0001.

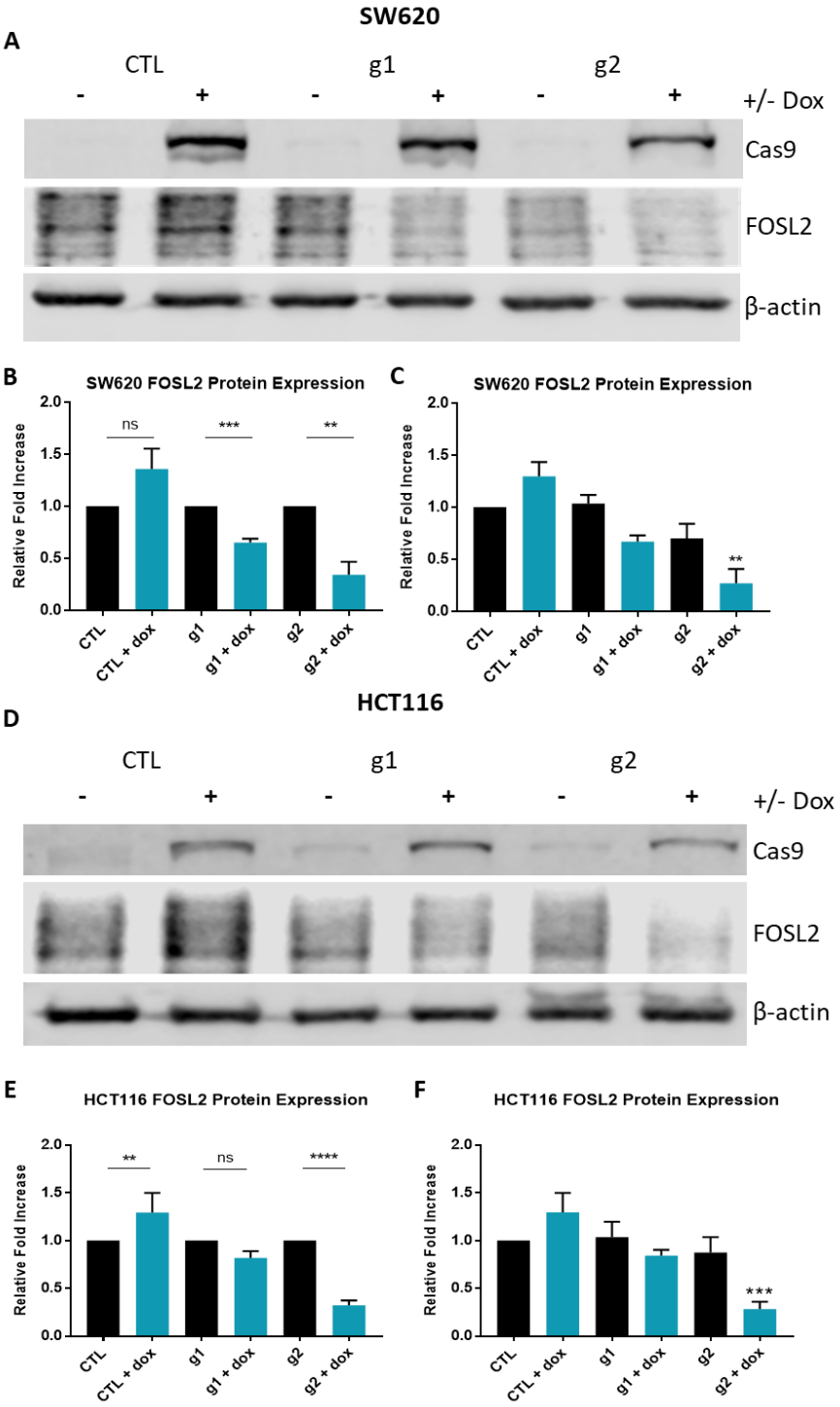

Figure 3.6 Generation of inducible FOSL2 knockdown cell lines representing the CMS4 subtype. Conditions include a non-targeting control and two gRNA sequences for FOSL2, in the presence or absence of doxycycline (2 µg/ml). Representative immunoblots are shown for Cas9 and FOSL2 in SW620 (A) with quantification (B-C). Representative immunoblots are shown for Cas9 and FOSL2 in HCT116 (D) with quantification (E-F). Error bars indicate ± SEM. Data analysed using a one-way ANOVA. N=3. *p<0.05, **p<0.01, ***p<0.001, ****p<0.0001

3.3.3 Effect of FOSL2 Knockdown on 3D Spheroid Growth

The role of FOSL2 in 3D colorectal cancer spheroid growth was investigated in HCT116 and Ls174T FOSL2 knockdown cell lines. In each case, FOSL2-g2 was identified as generating the most efficient FOSL2 knockdown and as such was used for downstream investigations. Spheroids were generated in HCT116 control and FOSL2-g2 cell lines as validated previously and as described in Methods. Plus and minus doxycycline (2 µg/ml, 5 day treatment) conditions were included for both groups in order to determine whether doxycycline treatment may be affecting spheroid growth. Representative images of HCT116 spheroids are shown in Figure 3.7A. The average spheroid volume was calculated for each group after using the ImageJ Wand Tool to draw around the circumference of each spheroid. Analysis is shown in Figure 3.7B, where no significant differences were found between the control without doxycycline and control with doxycycline spheroid groups, demonstrating that the doxycycline treatment is not impacting spheroid growth. The FOSL2-g2 knockdown (with doxycycline) group grew to a significantly lower volume than the isogenic control without doxycycline ($p<0.05$) at day 14. Furthermore, the FOSL2 knock down group was also significantly smaller by $0.12mm^3$ than the control plus doxycycline group ($p<0.001$), indicating a true effect irrespective of doxycycline treatment.

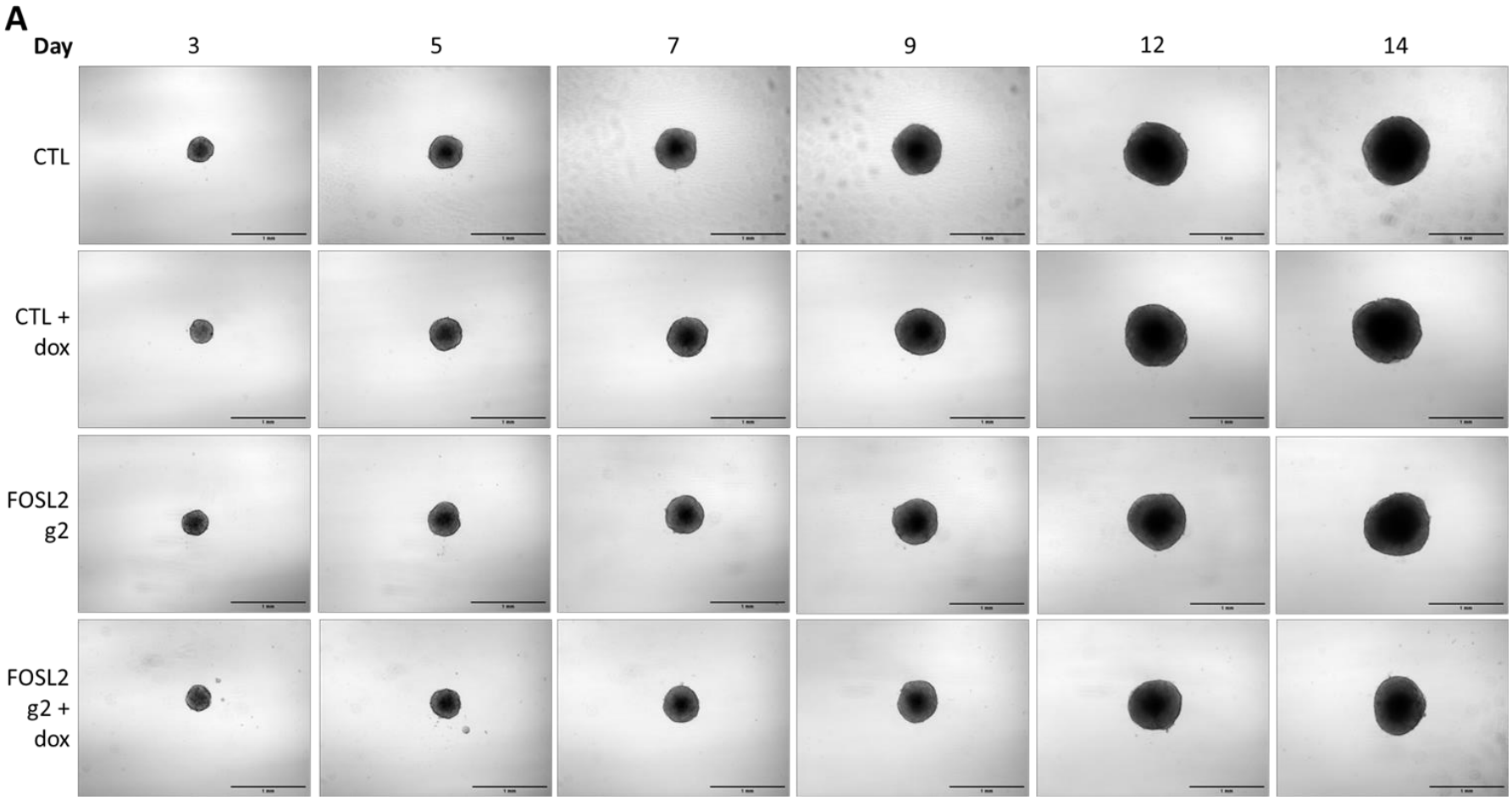
A
Day
3
5
7
9
12
14
CTL
CTL + dox
FOSL2 g2
FOSL2 g2 + dox

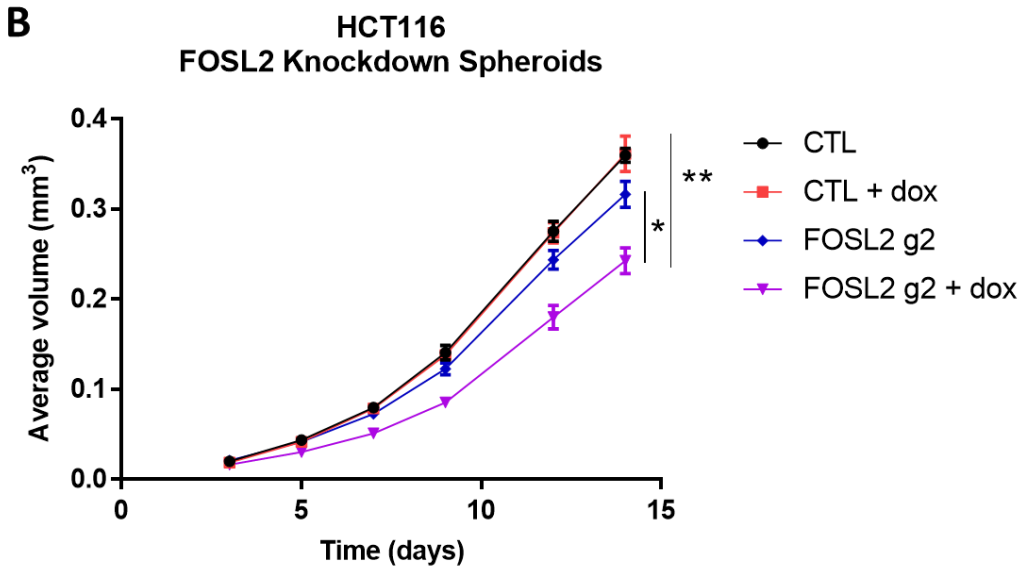

Figure 3.7 Effect of FOSL2 knockdown on 3D spheroid growth in HCT116. (A) Representative images of control and FOSL2 knockdown spheroids in HCT116. Spheroids were formed and imaged as described. Control and FOSL2-g2 spheroids are shown with their respective isogenic controls (+/- doxycycline 2 µg/ml). Images taken at 10X magnification. Scale bar represents 1mm. (B) Analysis of spheroid average volume at the 14 day time-point. N=3. Error bars indicate ± SEM. Data analysed using a t-test. N=3. *p<0.05, **p<0.01.

The same experiment was performed for the inducible Ls174T knockdown cell lines, however issues were encountered when attempting to form the spheroids. As it is known that the Ls174T cell line are more difficult to generate 3D spheroids from than the previously shown HCT116, cultrex basement membrane extract (BME) was included in the suspension at a final concentration of 500 µg/ml in order to promote spheroid formation. Despite this, cells from all conditions were still forming aggregates rather than defined spheroids. Illustrative data is shown in Figure 3.8. An example is shown for each condition at the day 5 time-point. Aggregates of significantly different sizes form within each group, creating large-scale variation. Even when a spheroid-like structure does form, as shown for the FOSL2 + dox condition, by the later days the spheroid has budded. This meant that analysis was extremely difficult as almost all spheroids had to be discounted from analysis leaving data that could not be considered robust. Therefore, analysis is not shown for this cell line and further

optimisation is required to generate spheroids from Ls174T, with varying concentrations of either BME or Matrigel.

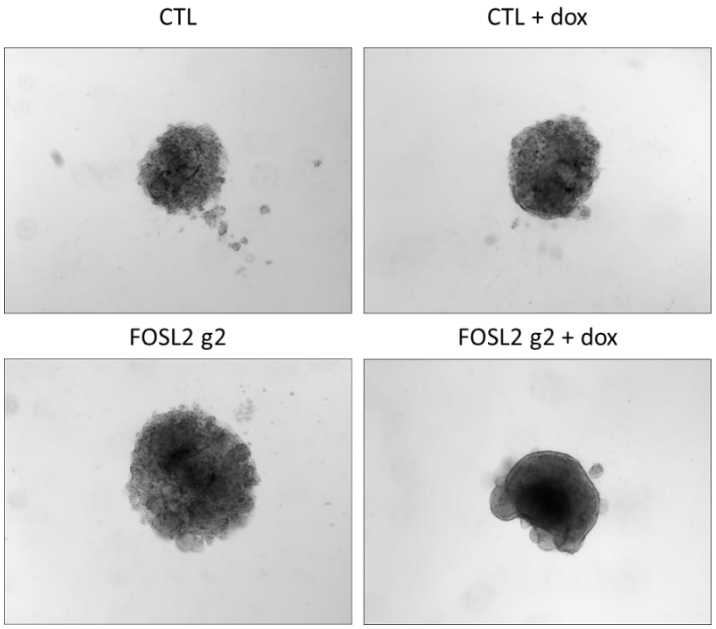

Figure 3.8 Attempts to form Ls174T spheroids with images shown at the day 5 time-point. Images were taken at day 5 from Ls174T spheroids formed with the addition of 500 µg/ml BME. Images taken at 10X magnification.

3.3.4 Effect of FOSL2 Knockdown on Cell Survival

The role of FOSL2 in cell survival was also assessed using the clonogenic assay, which represents an *in vitro* survival assay measuring the ability of a single cell to form a colony. Ls174T cells were used as the spheroids did not form, and so a phenotypic effect observed in this cell line would indicate a role for FOSL2 that is applicable to more than one cell lines. Ls174T control – or control + doxycycline (2 µg/ml), were placed into either hypoxia (1% O_2) or normoxia (21% O2) for 72 hours. FOSL2-g2 was selected as for the spheroids due to the highest level of cutting efficiency. Only FOSL2-g2 + dox in hypoxic conditions were used, as the control normoxia vs hypoxia would identify differences in hypoxic colony formation, and the control + or – doxycycline would identify any effect of the doxycycline on colony formation. Figure 3.9 displays the raw and analysed data. No significant differences were identified between either control normoxia and control hypoxia, or control plus doxycycline against control minus doxycycline. This indicates that neither the hypoxic condition nor doxycycline treatment is impacting the cell survival. However, when analysed against control

hypoxia plus doxycycline, the FOSL2-g2 + doxycycline in hypoxia condition exhibited significantly reduced colony counts of 42% ($p<0.0001$). FOSL2 therefore plays a role in hypoxic cell survival, although without the corresponding normoxic condition it cannot be determined to be hypoxia-specific.

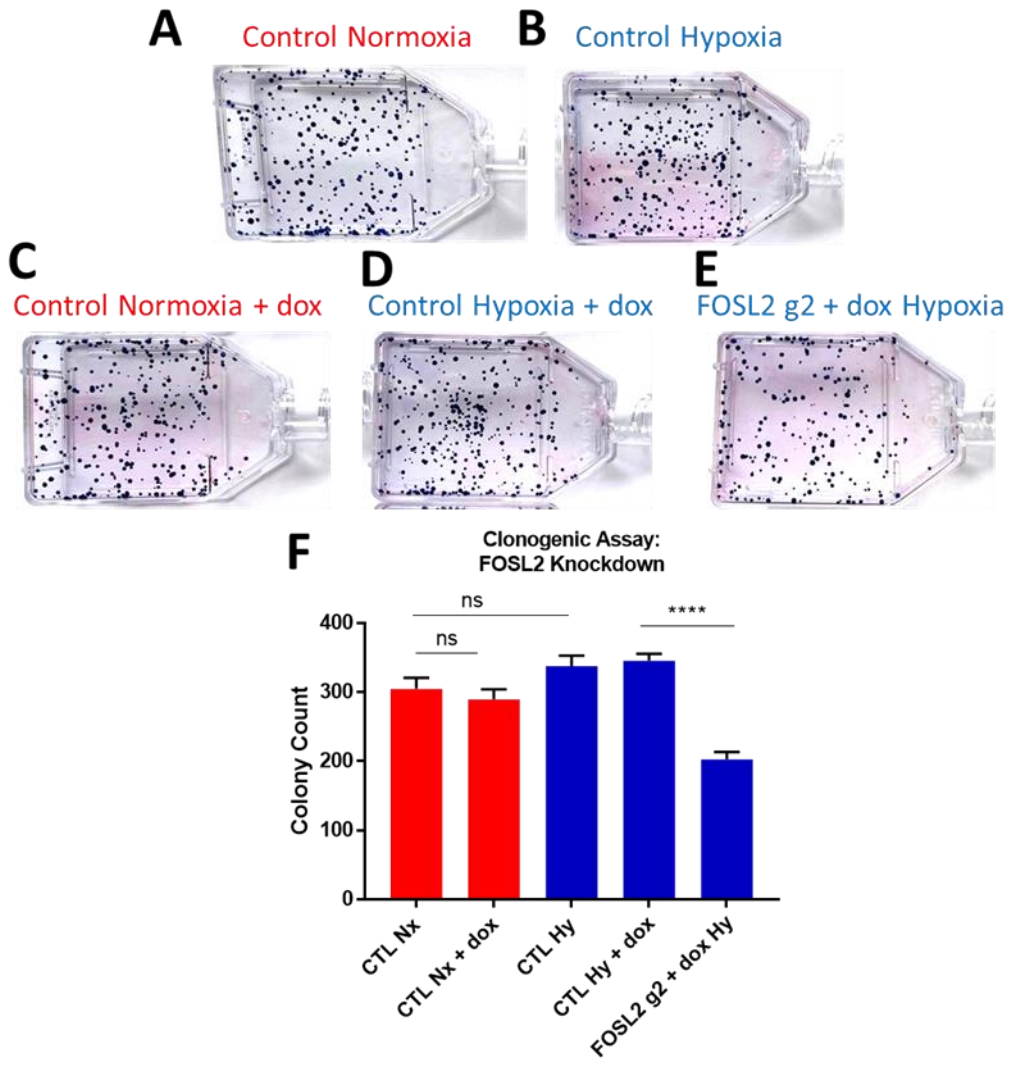

Figure 3.9 Effect of FOSL2 knockdown on Ls174T cell survival in the clonogenic assay. FOSL2 knockdown was induced as previously described. (A-E) depict raw data images as labelled with the colonies visible. (F) Quantification of colony counts. Error bars represent mean ± SEM. Data analysed by one-way ANOVA. **** $p<0.0001$. N=3.

3.3.5 The FOSL2-Associated Hypoxic Transcriptome

HCT116 FOSL2-g2 knockdown and control cell lines generated as previously described were incubated in normoxia (21% O_2) or hypoxia (1% O_2) for 24 hours prior to RNA extraction as described in Methods. Total RNA extracts were tested for purity and degradation prior to sending for sequencing in line with Novogene's sample requirements. The 260/280 ratio was assessed by Nanodrop, with a ratio of 1.8 or above indicating the absence of protein or DNA contamination. All samples had a 260/280 ratio of above 2.0, indicating samples that can be considered pure for downstream applications (Table 3.1).

RNA samples of 200 ng/µl were provided to the Deep-Seq facility (University of Nottingham) for the assessment of RNA integrity using the Agilent Bioanalyser and TapeStation System. An RNA Integrity Number (RIN) was obtained for each sample, which ranges from 1-10 with 1 representing the most degraded RNA profile and 10 representing the most intact RNA profile. A RIN value of >9 is considered acceptable for sequencing. All RNA samples had a RIN of 10.0 aside from one sample which had a RIN of 9.9 (Table 3.1).

Sample	260/280 Ratio	RIN
n1 Control Normoxia	2.08	10.0
n1 Control Hypoxia	2.06	10.0
n1 FOSL2 KD Normoxia	2.08	10.0
n1 FOSL2 KD Hypoxia	2.08	10.0
n2 Control Normoxia	2.08	10.0
n2 Control Hypoxia	2.10	10.0
n2 FOSL2 KD Normoxia	2.07	10.0
n2 FOSL2 KD Hypoxia	2.08	10.0
n3 Control Normoxia	2.08	10.0
n3 Control Hypoxia	2.06	9.9
n3 FOSL2 KD Normoxia	2.06	10.0
n3 FOSL2 KD Hypoxia	2.08	10.0

Table 3.1 RNA purity and integrity values for HCT116 control and FOSL2 knockdown samples submitted for RNA-sequencing.

Samples for sequencing were analysed by qPCR following cDNA synthesis of the RNA. CA9 was used as both a hypoxic marker and a known AP-1-regulated gene to test that the level of hypoxia was consistent among experimental repeats and the level of knockdown impacted the expression of CA9. Figure 3.10A shows a significant 1.87 fold increase of FOSL2 mRNA in control hypoxia compared to control normoxia ($p<0.001$). CA9 was also significantly upregulated by over 80-fold compared to control normoxia ($p<0.0001$) (Figure 3.10B). CA9 was significantly downregulated in the FOSL2 knockdown hypoxia compared to control hypoxia ($p<0.001$), with a 27% decrease of CA9 expression upon FOSL2 knockdown (Figure 3.10B).

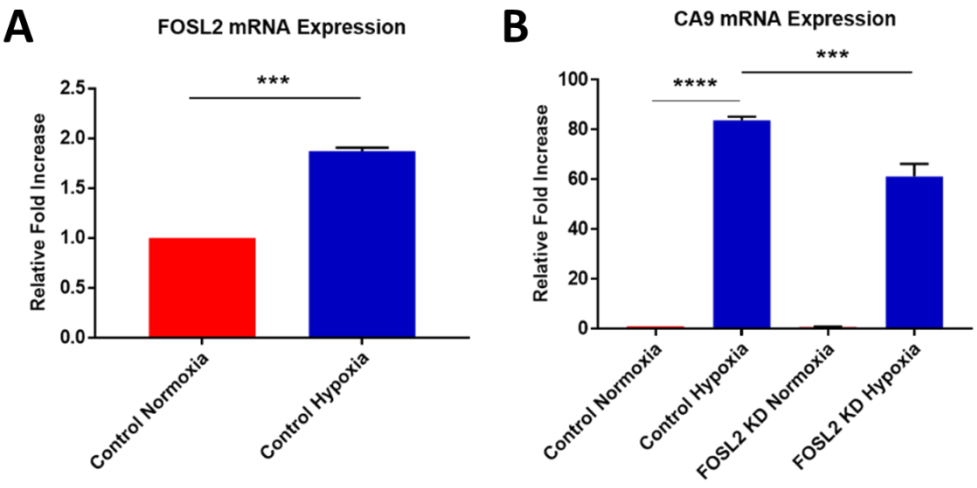

Figure 3.10 Validation of HCT116 control and FOSL2 knockdown RNA samples prior to RNA-sequencing. RNA samples were generated as previously described following 24 hour exposure to hypoxic (1% O_2) or normoxic (21% O_2) conditions. (A) FOSL2 mRNA expression in control hypoxia compared to normoxia samples. (B) CA9 mRNA expression in control and FOSL2 knockdown samples in both normoxia and hypoxia. Error bars indicate ± SEM. Data analysed using a one-way ANOVA. N=3. *p<0.05, **p<0.01, ***p<0.001, ****p<0.0001.

RNA samples were submitted to Novogene for RNA-sequencing. Several QC checks were completed prior to sample sequencing including sequencing error rate distribution checks, A/G/C/T distribution check and sequence data filtering. Figure 3.11 displays an assessment of sample variability. Figure 3.11A shows the Pearson correlation matrix between samples. All correlation coefficients are above 0.96, indicating a strong positive correlation between samples and no evident outliers. Figure 3.11B displays the distribution of overall gene expression levels across all samples. Overall gene expression levels are very similar across all samples, indicating that the hypoxic or knockdown conditions are not influencing overall gene expression levels.

Before analysing the FOSL2-associated hypoxic transcriptome, the first analysis completed was to compare the control normoxia and control hypoxia conditions. As control hypoxia will be compared against for the FOSL2 knockdown in hypoxia condition, it is important to assess that the condition is enriched for hypoxia-inducible

genes. Figure 3.12A displays co-expressed genes between control hypoxia and control normoxia. 407 genes are found to be expressed only in control hypoxia, whilst 12173 genes are expressed in both conditions. Figure 3.12B shoes the volcano plot for control hypoxia vs control normoxia. 1774 genes were significantly upregulated in control hypoxia compared to normoxia, whilst 1629 genes were significantly downregulated. 24106 genes were not significantly differentiated between the two conditions. Table 3.2 shows the top 20 significant differentially expressed genes (DEGs) that were upregulated in control hypoxia vs control normoxia. The DEG upregulated to the highest extent in hypoxia was CA9 (Log2 fold change 4.88). Other hypoxia inducible genes featured, such as ANGPLT4 and LDHC (lactate dehydrogenase C). Interestingly, HIF1α does not feature in the top 20 but does appear on the list in the form of HIF1A antisense RNA-2 (HIF1A-AS2). Further down from the top 20, other DEGs were significantly upregulated in hypoxia including VEGFA (Log2 fold change 0.71, p=4.64e-21) and BNIP3 (Log2 fold change 2.94, p=0). The list was also examined for the AP1 subunits in order to investigate their upregulation. FOSL2 was found to be significantly upregulated in hypoxia (Log2 fold change 0.87, p=3.07e-31). JUND was significantly upregulated in hypoxia (Log2 fold change 0.56, p=6.81e-10), as was JUNB (Log2 fold change 0.49, p=1.49e-07) and c-Jun (Log2 fold change 0.72, p=8.70e-11). These findings are summarised in Table 3.3.

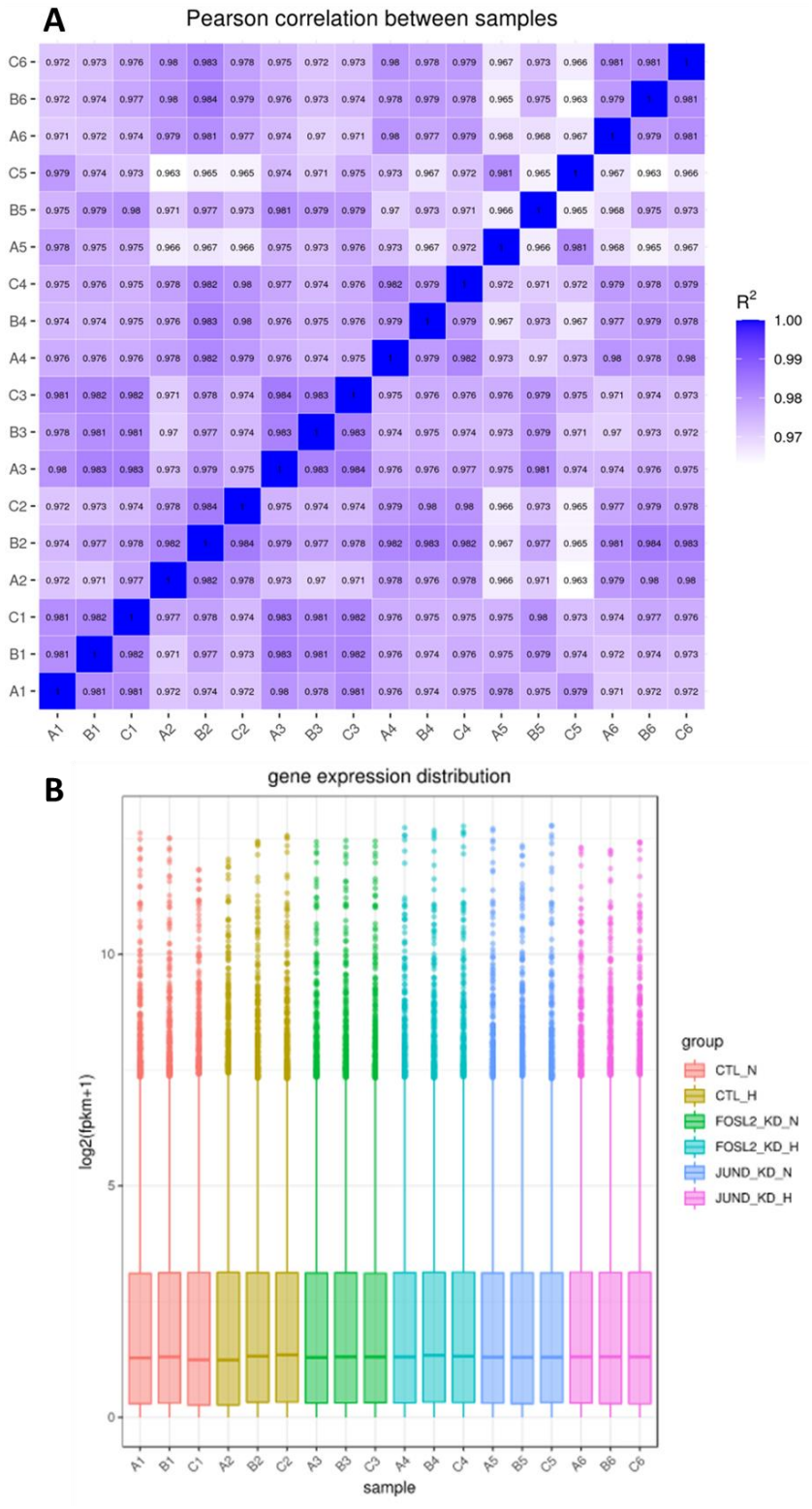

Figure 3.11 RNA-sequencing sample correlation and gene expression distributions. (A) Pearson correlation matrix displaying correlation coefficient values for each of the 18 samples against each other. (B) Violin plot demonstrating overall levels of gene expression in all 18 samples. FPKM is the unit used to report estimated gene expression levels.

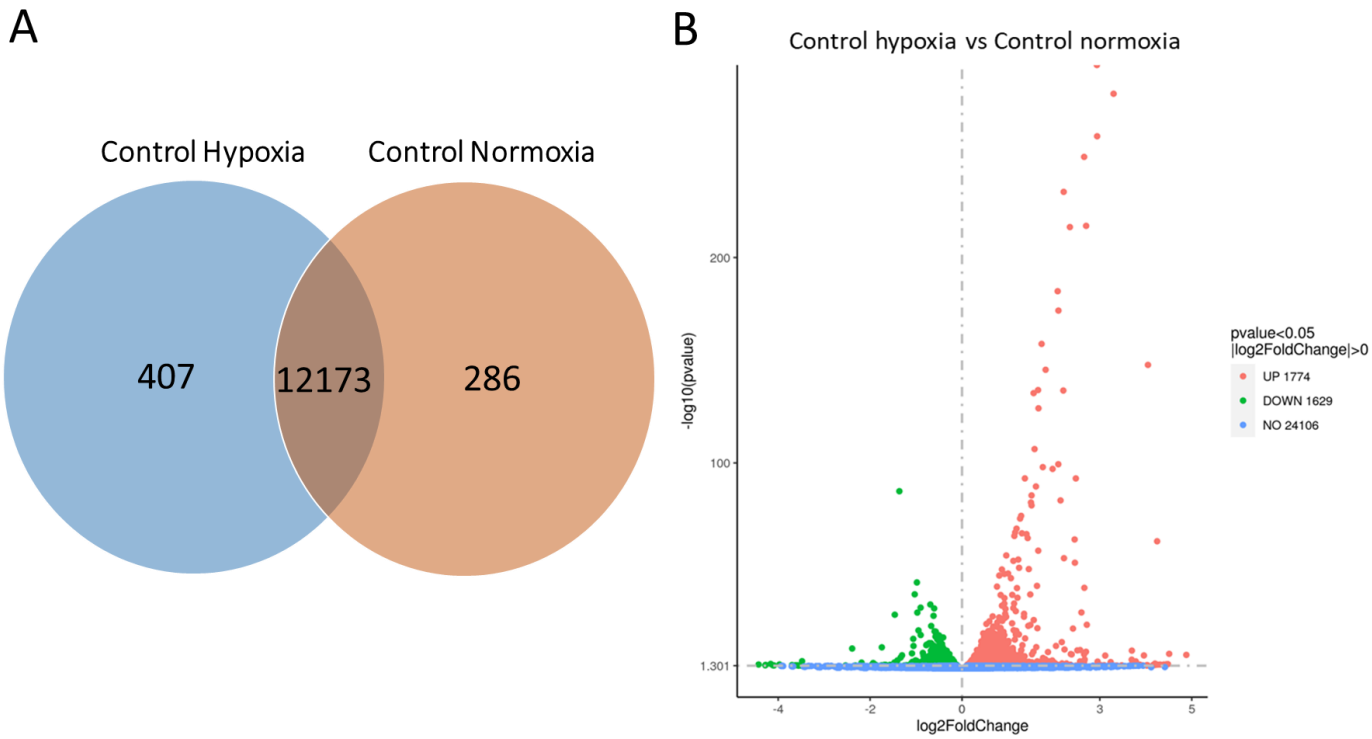

Figure 3.12 Co-expressed and differentially expressed genes between control hypoxia and control normoxia. (A) Venn diagram depicting co-expressed genes. (B) Volcano plot indicating DEGs. The level of significance is given on the y-axis whilst the log2 fold change is presented on the x-axis.

Gene Name	Control Hypoxia	Control Normoxia	Log2 Fold Change	p value
CA9	32.27	1.11	4.88	2.77e-07
PTPRN	32.73	1.42	4.51	8.34e-08
LDHAP3	4.05	0	4.31	0.014
HMX1	3.84	0	4.26	0.015
HIF1A-AS2	7.07	0.37	4.2	0.005
PTPRO	3.66	0	4.17	0.02
TMEM211	3.68	0	4.16	0.024
ANGPLT4	884.0	53.5	4.05	1.88e-148
AMZ1	3.24	0	4.04	0.03
LDHC	3.26	0	4.03	0.03
SLC8A3	3.26	0	4.02	0.03
TPRKBP2	3.25	0	4.02	0.04
RAPGEF4	28.16	1.81	3.96	5.08e-07
LDHAP7	3.07	0	3.93	0.04
VTCN1	15.24	1.09	3.78	0.0004
HLA-V	42.14	3.23	3.70	2.29e-09
DIRC3	18.82	1.45	3.69	5.88e-05
ELN	5.00	0.35	3.68	0.02
PLPP7	4.03	0.36	3.38	0.05
ALDOC	3155.41	320.60	3.30	1.88e-280

Table 3.2 Top 20 DEGs upregulated in control hypoxia vs control normoxia. The average read counts are presented for both conditions alongside the Log2 fold change and p-value.

Gene Name	Control Hypoxia	Control Normoxia	Log2 Fold Change	p value
FOSL2	1975.23	1081.45	0.87	3.07e-31
c-Jun	587.56	356.81	0.72	8.70e-11
JUND	2231.07	1512.67	0.56	6.81e-10
JUNB	1601.50	1138.91	0.49	1.49e-07

Table 3.3 AP1 subunits upregulated in control hypoxia vs control normoxia. The average read counts are presented for both conditions alongside the Log2 fold change and p-value.

KEGG pathway analysis was used to explore which pathways are significantly enriched in control hypoxia compared to control normoxia. Pathway enrichment analysis identifies significantly enriched pathways associated with differentially expressed genes, compared to the whole genome background. Figure 3.13 displays a KEGG dotplot diagram featuring pathways that are significantly upregulated in control hypoxia compared to control normoxia. The size of the dot reflects the gene count enriched in the pathway, whilst the colour shows the pathway enrichment significance. KEGG analysis identified 22 significantly upregulated pathways in hypoxia, with the top 20 displayed in Figure 3.13. The most significant of the upregulated pathways is MAPK signalling (p=3.18e-07), featuring 54 DEGs upregulated in hypoxia. MAPK signalling is activated upon many forms of cellular stress including hypoxia. Many MAP kinases are upregulated in this pathway in the hypoxic condition, including MAPK3, MAPK7 and MAPK13. Upstream kinases are also upregulated, such as MAP2K1, MAP3K1 and MAP3K2. Other pathways feature in the KEGG analysis, including the HIF-1 signalling pathway, where 24 of the pathway genes are significantly upregulated (p=7.10e-06), acting as a good control for the hypoxic condition. Another upregulated pathway in hypoxia is glycolysis/gluconeogenesis, featuring significant upregulation of 18 genes from this pathway (p=8.54e-06). It is well known that under hypoxic conditions cancer cell metabolism switches from oxidative phosphorylation to anaerobic glycolysis, many of the enzymes of which are regulated in a HIF1-dependent manner. Many of the proteins are enriched in hypoxia including LDHA, LDHC, HK1 and HK2.

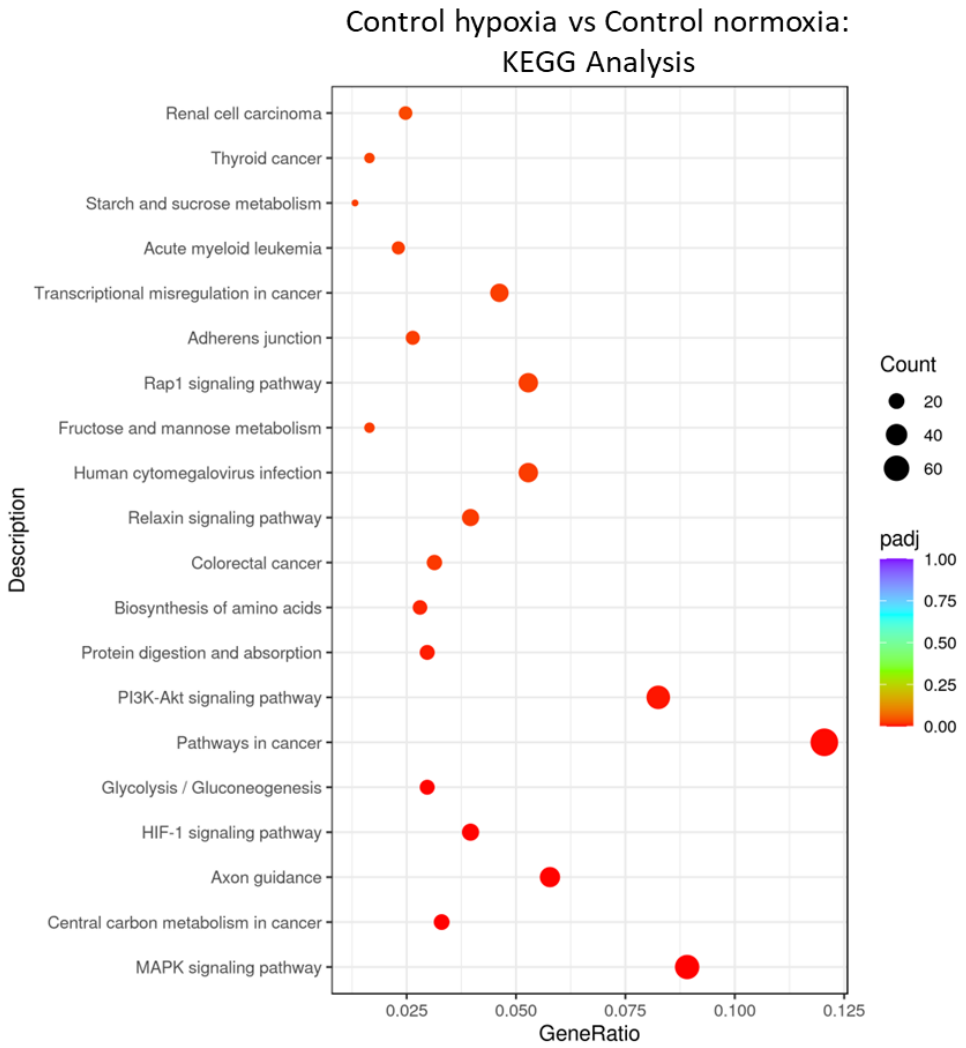

Figure 3.13 KEGG pathway analysis of significantly upregulated genes in control hypoxia compared to control normoxia. The x-axis shows the gene ratio, which reflects the number of enriched genes compared to all genes featuring in the pathway. The size of the dot shows the gene count, while the colour reflects the level of significance.

Control hypoxia was therefore determined to be an appropriate comparison for the FOSL2 knockdown condition in order to determine FOSL2-associated targets in hypoxia, due to the DEGs and pathways that were upregulated compared to normoxia. Figure 3.14A displays co-expressed genes between FOSL2 knockdown hypoxia vs control hypoxia and Figure 3.14B is a volcano plot depicting DEGs. 576 genes were significantly upregulated upon FOSL2 knockdown in hypoxia compared to control hypoxia, 872 genes were significantly downregulated upon FOSL2 knockdown in hypoxia compared to control hypoxia, and 26311 genes were not significantly differentiated between the two conditions.

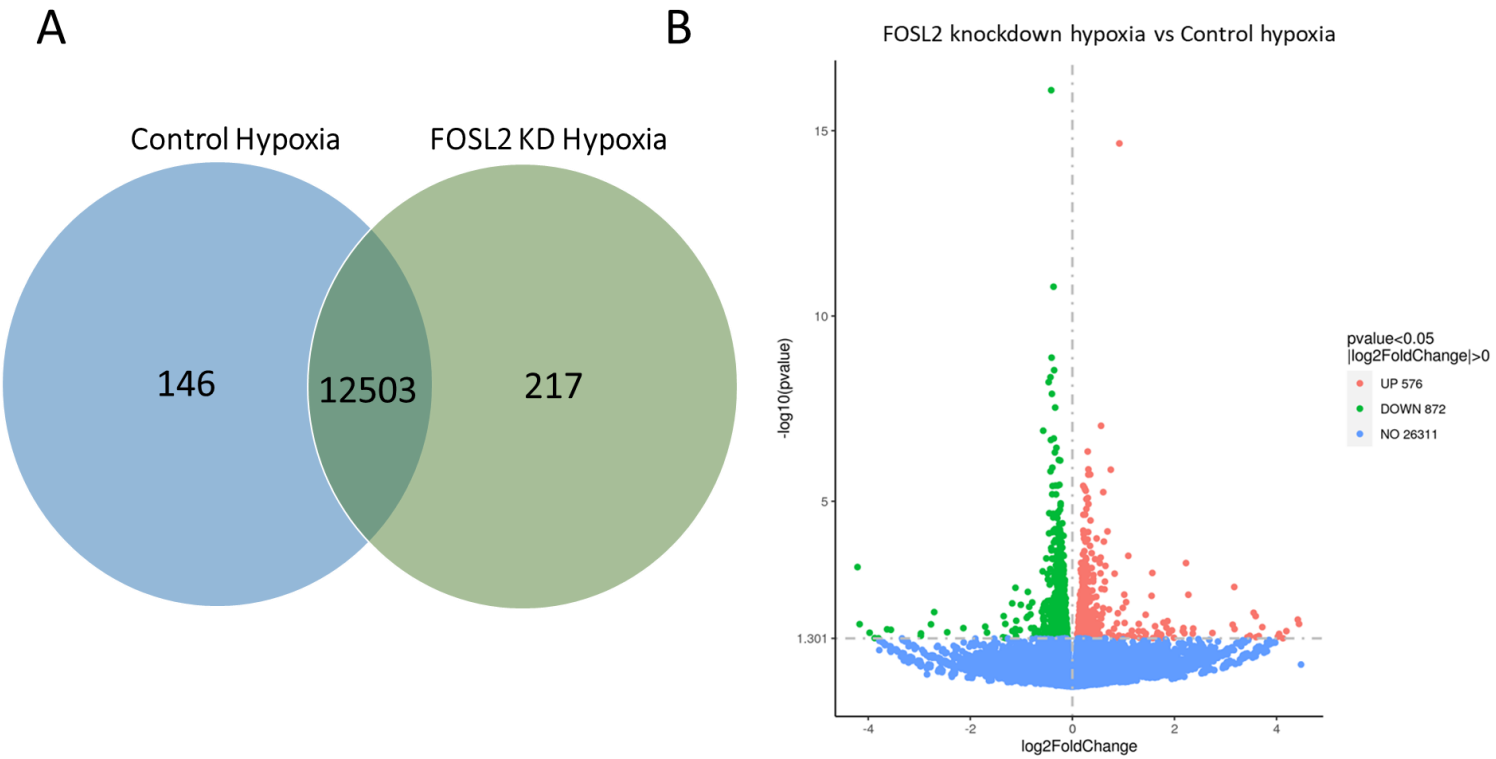

3.14 Co-expressed and differentially expressed genes between control hypoxia and FOSL2 knockdown hypoxia. (A) Venn diagram depicting co-expressed genes. (B) Volcano plot indicating DEGs. The level of significance is given on the y-axis whilst the log2 fold change is presented on the x-axis.

The DEGs that were downregulated upon FOSL2 knockdown in hypoxia compared to control hypoxia were investigated as these represent DEGs whose expression is associated with FOSL2. FOSL2 itself did not feature on the list of downregulated genes, despite prior analysis of lysates extracted alongside the RNA-sequencing samples demonstrating FOSL2 knockdown. Of the 872 genes significantly downregulated upon FOSL2 knockdown, the top 150 based on Log2 fold change were selected. This resulted in a list with Log2 fold values ranging from -4.21 to -0.34. This list of 150 downregulated DEGs was then cross-referenced to DEGs that were upregulated in control hypoxia vs control hypoxia, as the FOSL2-associated hypoxic transcriptome is the focus of this study. 30 resulting DEGs are presented in Table 3.4, in order of smallest (highest negative) Log2Fold change upon FOSL2 knockdown.

Gene Name	Log2 Fold Change: FOSL2 Knockdown Hypoxia vs Control Hypoxia	p-value	Log2 Fold Change: Control Hypoxia vs Control Normoxia	p-value
CYP2W1	-4.209908	0.000596	1.567748	0.034322
CFAP57	-1.0296667	0.029823	1.036568	0.019105
DEGS2	-0.8936385	0.013954	1.385993	0.000637
ALOX12B	-0.8732501	0.012838	1.3106	0.000742
NAT16	-0.8465259	0.007045	1.195177	0.000542
AK4P3	-0.598723	0.009517	2.171836	1.63E-13
CD82	-0.5822064	0.000777	0.487112	0.006929
RBBP8NL	-0.573043	0.007757	0.887819	0.000141
ZSWIM4	-0.5658865	0.01598	0.839835	0.000567
COL13A1	-0.5648927	0.013141	0.746739	0.001288
SMTNL2	-0.5484937	0.016024	0.901571	0.000238
KAZALD1	-0.5375654	0.005533	0.568315	0.004213
DNER	-0.5360333	0.029454	0.513685	0.034262
DPP4	-0.5305883	0.007418	1.291847	1.27E-09
CDKN1C	-0.5114179	0.000348	0.970692	2.56E-10
SEMA3A	-0.4866126	0.000911	0.369284	0.015697
SGPP2	-0.4766039	0.046455	0.639535	0.010961
MMP14	-0.44218	0.004799	0.397085	0.011505
BDH2	-0.4406205	0.027838	0.575894	0.006227
KIF3C	-0.4344866	0.001472	0.682936	1.86E-06
IFI27L2	-0.4309405	0.016602	0.421608	0.006719
PCSK9	-0.4291186	4.49E-09	0.277595	0.000297
MSLNL	-0.4281579	0.029334	0.583754	0.004539
ADAM19	-0.4215434	2.22E-07	0.241359	0.00215
SCD	-0.414776	8.07E-17	0.262652	4.88E-06
C1QL4	-0.4007819	0.008863	0.530581	0.00179
ZBTB22	-0.3942689	0.005756	0.323697	0.016626
CAVIN3	-0.3906794	0.012571	0.805099	1.18E-05
EMP1	-0.3876437	6.79E-05	0.33782	0.000477
ANGPTL4	-0.387583	3.86E-06	4.047352	1.9E-148

Table 3.4 Top 30 DEGs associated with FOSL2 and upregulated in hypoxia compared to normoxia. The Log2 fold change for FOSL2 knockdown hypoxia vs control hypoxia is presented alongside the corresponding p-value, and the Log2 fold change for control hypoxia vs control normoxia is also presented alongside the corresponding p-value.

The gene most downregulated upon FOSL2 knockdown in hypoxia compared to control hypoxia is the cytochrome P450 enzyme CYP2W1 (log2 fold change -4.21, p=0.0006) which also happens to be the third most upregulated in control hypoxia compared to control normoxia (log2 fold change 1.57, p=0.03) of those associated with FOSL2. Such genes represent interesting targets for further validation, as they are both

induced by hypoxia and associated with FOSL2 in hypoxia. DEGS2, involved in biosynthesis of phytosphingolipids, represents another of these targets, being the third most associated with FOSL2 in hypoxia (log2 fold change -0.89, p=0.01) and the fourth most upregulated in control hypoxia compared to normoxia (log2 fold change 1.39, p=0.0006) of those associated with FOSL2. Other interesting targets feature in the list, such as the well-known hypoxia-inducible gene ANGPLT4 that displays the highest upregulation in hypoxia (log2 fold change 4.05, p=1.9e-148) and some degree of association with FOSL2 in hypoxia (log2 fold change -0.39, p=3.86e-06). Some of the DEGs identified are not known to be FOSL2-associated, and so represent novel FOSL2-associated targets. For example, ADAM19, known to be upregulated in colon cancer and involved in cancer progression, as discussed further in the chapter conclusions, is associated with FOSL2 and upregulated in hypoxia. Interestingly, matrix metallopeptidase 14 (MMP14), well known to promote invasion in cancer, is also associated with both FOSL2 (log2 fold change -0.44, p=0.005) and hypoxia (log2 fold change 0.4, p=0.01).

Other DEGs of interest appear further down the list and so are not present in the table but are worthy of note. For example, upon FOSL2 knockdown in hypoxia, both JUND and JUNB are significantly downregulated (log2 fold change -0.18, p=0.01) (log2 fold change -0.2, p=0.005) respectively. This may suggest an association with JUN subunits and FOSL2 in hypoxia. Another finding of interest is in the DEGs significantly upregulated upon FOSL2 knockdown in hypoxia compared to control hypoxia. This includes FOSL1 (log2 fold change 0.2, p=0.005), representing a possible contribution toward a compensatory mechanism upon knockdown of FOSL2.

KEGG pathway analysis was used to explore which pathways are significantly downregulated in FOSL2 knockdown hypoxia compared to control hypoxia. Figure 3.15 displays this analysis as a dotplot. 13 pathways were significantly downregulated upon FOSL2 knockdown in hypoxia, whilst those above ‘Huntington disease’ in the dotplot figure do not meet the threshold for significance. By far the pathway most associated with FOSL2 in terms of both significance and number of genes enriched is ‘ribosome’, where 45 genes are downregulated upon FOSL2 knockdown, including many proteins comprising ribosomal subunits. However, this pathway and indeed the genes within

are not significantly upregulated in control hypoxia compared to control normoxia. As the aim of the study is to investigate hypoxia-induced pathways associated with FOSL2, the KEGG pathways upregulated in control hypoxia compared to control normoxia (Figure 3.13) were cross-referenced against those downregulated upon FOSL2 knockdown in hypoxia compared to control hypoxia. 4 pathways are found within this overlap: Central carbon metabolism in cancer, Biosynthesis of amino acids, Fructose and mannose metabolism, and Carbon metabolism. These are boxed in red on the Kegg dotplot shown in Figure 3.15, and summarised in Table 3.5.

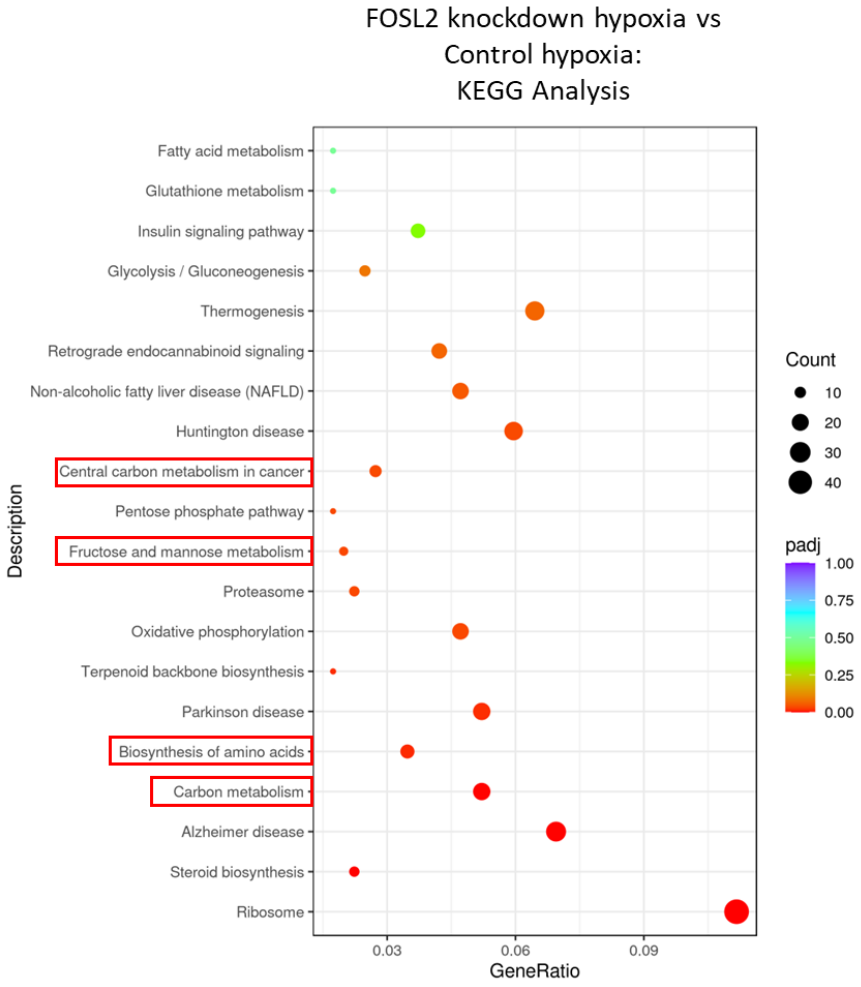

Figure 3.15 KEGG pathway analysis of significantly downregulated genes in FOSL2 knockdown hypoxia compared to control hypoxia. The x-axis shows the gene ratio, which reflects the number of enriched genes compared to all genes featuring in the pathway. The size of the dot shows the gene count, while the colour reflects the level of significance. The pathways highlighted in red are also found to be significantly upregulated in control hypoxia vs control normoxia.

		FOSL2 Knockdown Hypoxia vs Control Hypoxia: Downregulated		Control Hypoxia vs Control Normoxia: Upregulated	
KEGG ID	**Description**	**Number of Genes**	**p-value**	**Number of Genes**	**p-value**
hsa01200	Carbon metabolism	21	0.0006	21	0.03
hsa01230	Biosynthesis of amino acids	14	0.01	17	0.01
hsa00051	Fructose and mannose metabolism	8	0.03	10	0.02
hsa05230	Central carbon metabolism in cancer	11	0.03	20	0.0001

Table 3.5 KEGG pathways significantly associated with FOSL2 and induced by hypoxia. The KEGG pathway ID and description is provided as well as the number of differential genes and corresponding p-value for both FOSL2 knockdown hypoxia vs control hypoxia and control hypoxia vs control normoxia.

The 4 KEGG pathways identified above were investigated for their DEGs, and those featuring in both the FOSL2 knockdown hypoxia vs control hypoxia and control hypoxia vs control normoxia comparison were selected. The results for these DEGs are summarised in Table 3.6, which represents interesting targets associated with FOSL2 and induced by hypoxia, by the pathway that the genes are enriched in. As evident, there is much overlap between these metabolic genes, for example PFKL appears in all 4 pathways, whilst ALDOC, HK1 and TPI1 appear in 3 pathways. This suggests a core group of metabolic genes that are both hypoxia-inducible and associated with FOSL2, and co-regulate various metabolic pathways.

Carbon Metabolism	Biosynthesis of Amino Acids	Central Carbon Metabolism in Cancer	Fructose and Mannose Metabolism
ALDOC	ALDOC	HK1	ALDOC
ENO1	ENO1	PFKL	HK1
ENO2	ENO2	PGAM1	PFKL
H6PD	IDH2	PKM	TKFC
HK1	PFKL	SLC16A3	TPI1
IDH2	PGAM1	SIRT3	PFKFB4
PFKL	PGK1	MAPK3	
PGAM1	PKM		
PGK1	TPI1		
PKM			
TKFC			
TPI1			

Table 3.6 Differentially expressed genes comprising the significant KEGG pathways that are both induced by hypoxia and associated with FOSL2.

3.3.6 JUND Expression in Hypoxia

The next aims of the project were to identify whether JUND demonstrated the same role in associating with targets of the hypoxic response as identified for FOSL2. It was therefore first determined whether JUND protein levels were upregulated in hypoxia in Ls174T cells. The same protein lysates generated for Figure 3.1 were used again here to allow direct comparison. These lysates were extracted from Ls174T wild-type cells exposed to hypoxic (1% O_2), physoxic (8.5% O_2) or normoxic (21% O_2) cell culture conditions for various time-points: 12, 24, 48 and 72 hours. JUND protein levels are significantly upregulated at both the 24 hour ($p<0.05$) and 48 hour ($p<0.01$) hypoxic time-points when normalised to 12 hour normoxia, the same finding as for FOSL2 hypoxic induction (Figure 3.16A-B). Non-significant hypoxic inductions are apparent at the 12 hour and 72 hour time-points. Whilst the highest induction for FOSL2 was found at the 24-hour time-point, the fold increases for JUND were similar for both 24 and 48 hour time-points at 2.2 and 2.3 respectively. Again, no significant differences were found between normoxic and physoxic levels of JUND, supporting the use of normoxic oxygen levels for further experiments. The CA9 data shown in Figure 3.1 is replicated in Figure 3.16 to show a hypoxic positive control alongside JUND expression (Figure 3.16C).

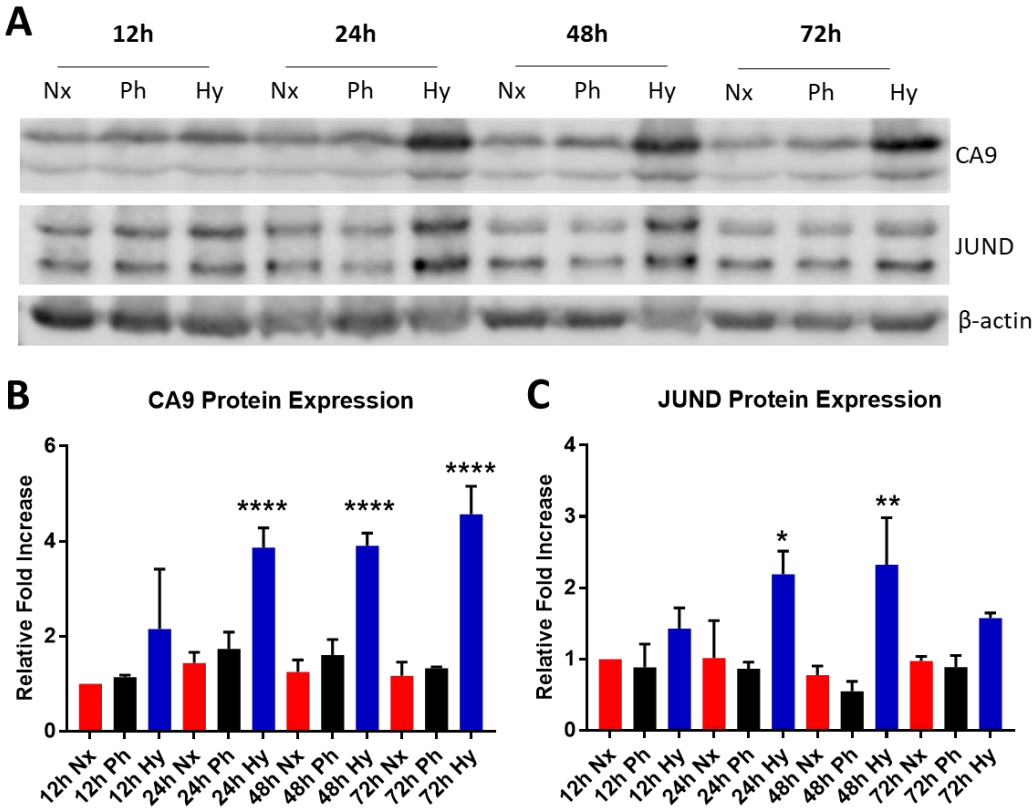

Figure 3.16 JUND and CA9 protein expression under normoxic (21% O_2), physoxic (8.5% O_2) and hypoxic (1% O_2) conditions in Ls174T across multiple time points. (A) Representative immunoblot images of CA9 and JUND. (B) Quantification of JUND expression. (C) Quantification of CA9 expression. Error bars indicate ± SEM. Data analysed using a one-way ANOVA. N=3. *p<0.05, **p<0.01, ***p<0.001, ****p<0.0001.

3.3.7 Generation of Inducible JUND Knockdown Cell Lines

The described approach to generating FOSL2 inducible knockdowns was repeated with gRNAs targeting JUND in order to generate inducible JUND knockdown cell lines to investigate the role of JUND in the hypoxic response. Similarly, Ls174T and HT-29 representing the CMS3 colorectal cancer subtype were used and for CMS4, HCT116 and SW620 were used. HT-29 knockdowns are shown in Figure 3.17A and representative blots for Ls174T in Figure 3.17B. No significant differences were found between control with and without doxycycline and so JUND expression was not impacted by doxycycline treatment. When comparing isogenic controls, JUND-g1 plus doxycycline achieved a 70% reduction in JUND expression compared to JUND-g1 without doxycycline (p<0.0001). JUND-g2 was even more efficient, achieving an 88%

knockdown compared to the isogenic control ($p<0.0001$) (Figure 3.17C). However, when all conditions were normalised to control minus doxycycline, JUND-g1 without doxycycline showed a 45% decrease in JUND expression, demonstrating potential Cas9 leakage in the absence of doxycycline ($p<0.01$) (Figure 3.17D). This effect was not seen with JUND-g2 without doxycycline. For Ls174T, a significant 1.5 fold increase in JUND expression was observed in control plus doxycycline compared to control without doxycycline ($p<0.05$), and so the doxycycline treatment may be impacting JUND expression in this cell line. In Figure 3.17E, all conditions were compared only to control without doxycycline due to the observation that each guide targeting JUND, with or without doxycycline, had significantly lower JUND expression compared to the controls. JUND-g1 plus doxycycline achieved an 80% reduction in JUND expression ($p<0.001$) and JUND-g2 plus doxycycline achieved an 84% reduction in JUND expression ($p<0.0001$). However, JUND-g1 without doxycycline also reduced JUND expression (70%, $p<0.001$) as did JUND-g2 without doxycycline (66%, $p<0.001$).

For the CMS4 subtype cell lines, SW620 JUND knockdowns showed a lower efficiency than the previous cell lines (Figure 3.18A). There were no significant differences between control and control plus doxycycline, JUND-g1 plus doxycycline reduced JUND expression by only 31% ($p<0.05$), and JUND-g2 plus doxycycline reduced JUND expression by 53% ($p<0.0001$) (Figure 3.18B). As seen with the previous cell lines, both JUND-g1 and JUND-g2 without doxycycline also show significantly lower expression of JUND (50%, $p<0.0001$ and 26%, $p<0.01$ respectively) (Figure 3.18C). Finally, for HCT116, there were no significant differences between control and control plus doxycycline. JUND-g1 plus doxycycline reduced JUND expression by 63% ($p<0.0001$). JUND-g2 plus doxycycline showed the best knockdown efficiency by reducing JUND expression by 82% ($p<0.0001$) (Figure 3.18D and 3.18E). JUND-g2 without doxycycline was not significantly different to control minus doxycycline, however JUND-g1 without doxycycline was reduced by 60% ($p<0.0001$) (Figure 3.18F).

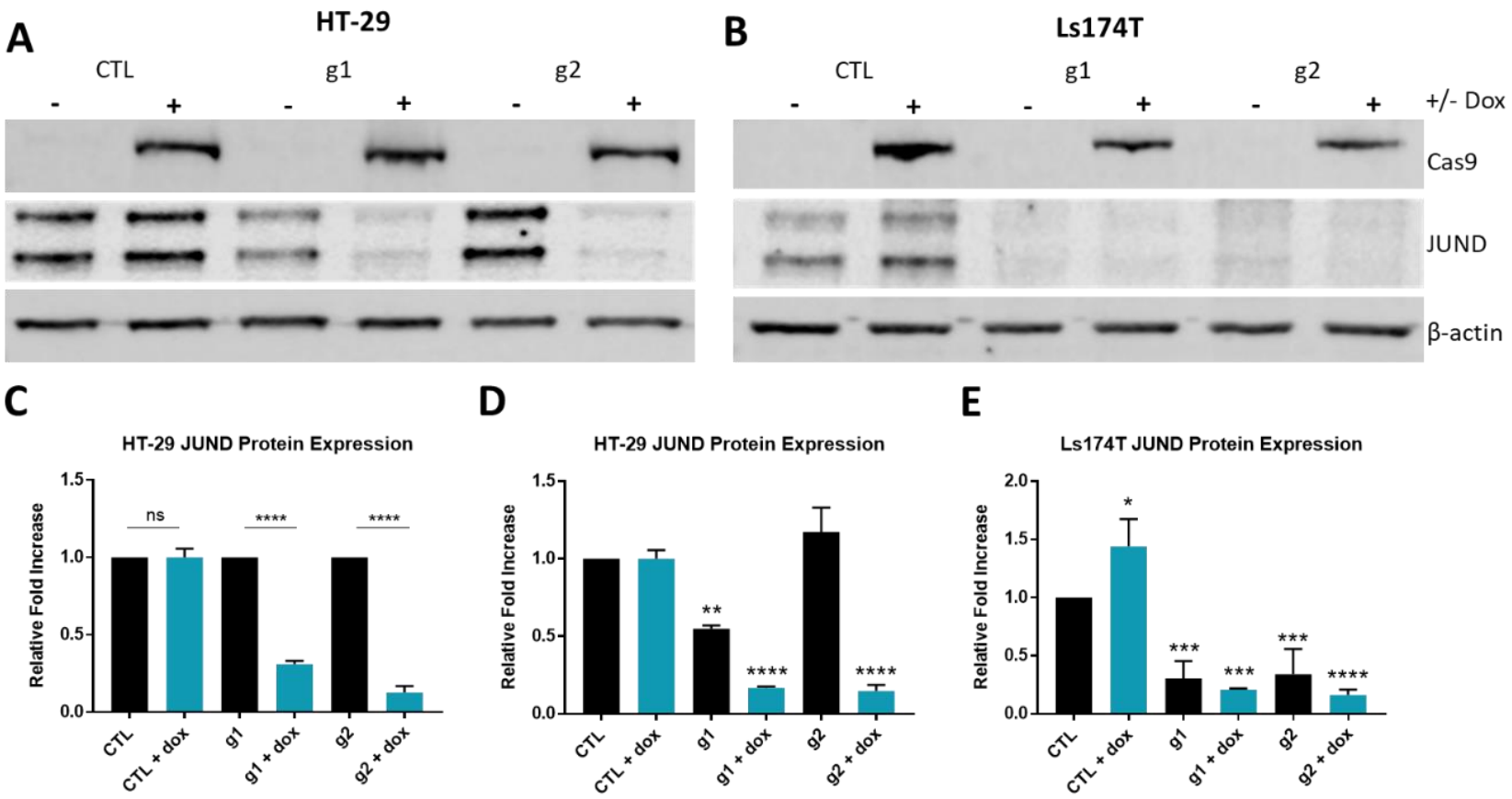

Figure 3.17 Generation of inducible JUND knockdown cell lines representing the CMS3 subtype. Conditions include a non-targeting control and two gRNA sequences for JUND, in the presence or absence of doxycycline (2 µg/ml). Representative immunoblots are shown for Cas9 and JUND in HT-29 (A) with quantification (C-D). Representative immunoblots are shown for Cas9 and JUND in Ls174T (B) with quantification (E). Error bars indicate ± SEM. Data analysed using a one-way ANOVA. N=3. *p<0.05, **p<0.01, ***p<0.001, ****p<0.0001.

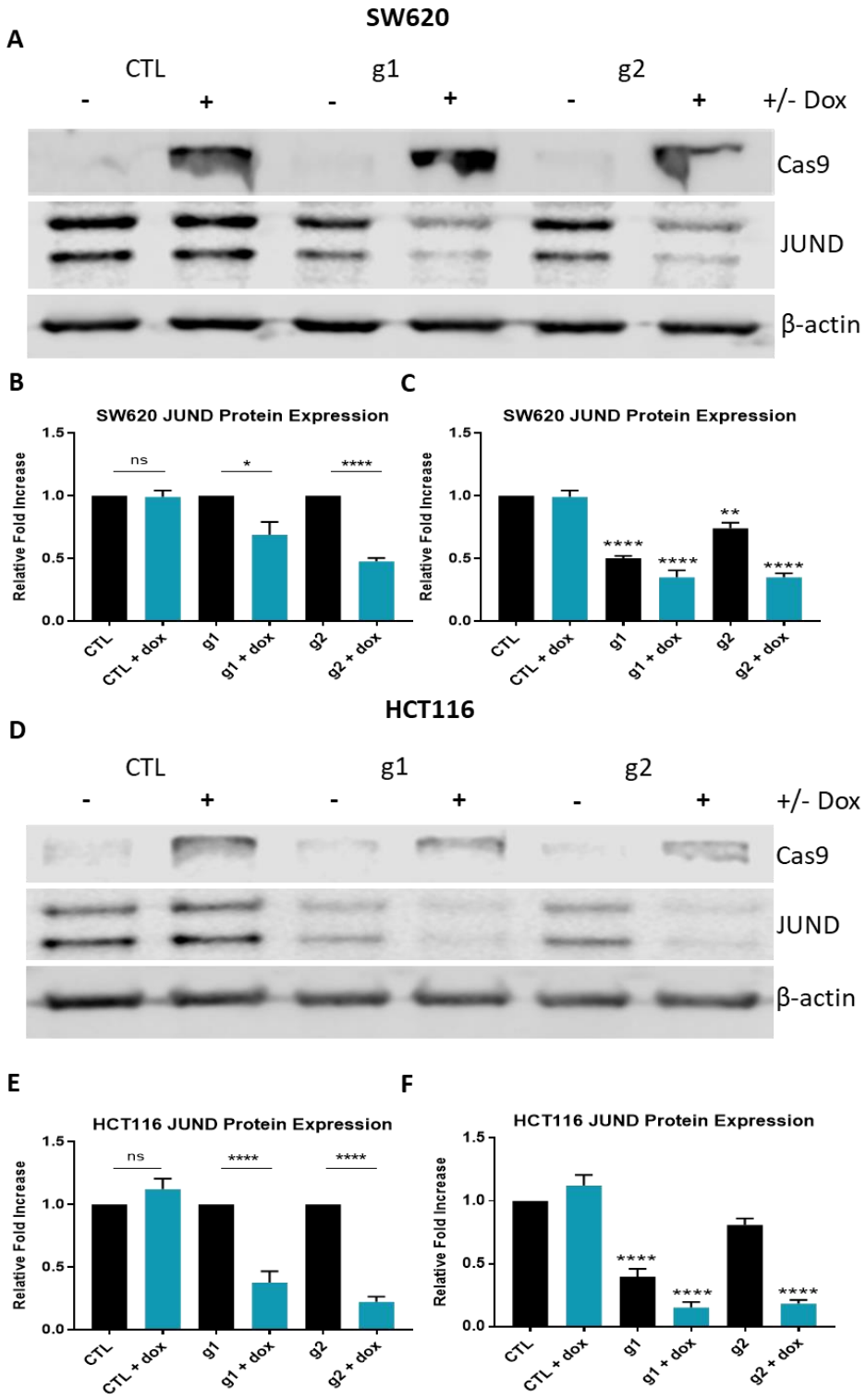

Figure 3.18 Generation of inducible JUND knockdown cell lines representing the CMS4 subtype. Conditions include a non-targeting control and two gRNA sequences for JUND, in the presence or absence of doxycycline (2 µg/ml). Representative immunoblots are shown for Cas9 and JUND in SW620 (A) with quantification (B-C). Representative immunoblots are shown for Cas9 and JUND in HCT116 (D) with quantification (E-F). Error bars indicate ± SEM. Data analysed using a one-way ANOVA. N=3. *p<0.05, **p<0.01, ***p<0.001, ****p<0.0001.

3.3.8 Effect of JUND Knockdown on 3D Spheroid Growth

The role of JUND in 3D colorectal cancer spheroid growth was investigated in the same manner as described for FOSL2 in HCT116. Unlike FOSL2, JUND knockdown efficiencies were reasonable with both targeting gRNAs, and so both JUND-g1 and JUND-g2 were used in spheroid experiments to see if any effect on spheroid growth may be observed in a guide-independent manner. The same control spheroids were used as for the FOSL2 investigation as experiments were performed simultaneously. Representative images of HCT116 spheroids are shown in Figure 3.19A for JUND-g1 and 3.18B for JUND-g2. In each case, plus and minus doxycycline conditions were once again included as additional controls. Analysis for JUND-g1 knockdown is shown in Figure 3.19C. There were no significant differences in spheroid volume found between control and control plus doxycycline, or JUND-g1 plus doxycycline when compared to either control plus doxycycline or JUND-g1 minus doxycycline. However, for the JUND-g2 analysis shown in Figure 3.19D, spheroid growth is significantly smaller by 0.06mm^3 in the JUND-g2 plus doxycycline condition than the control plus doxycycline group ($p<0.05$), indicating an effect on spheroid size irrespective of doxycycline treatment. No significant differences were found between control plus or minus doxycycline or JUND-g2 plus or minus doxycycline.

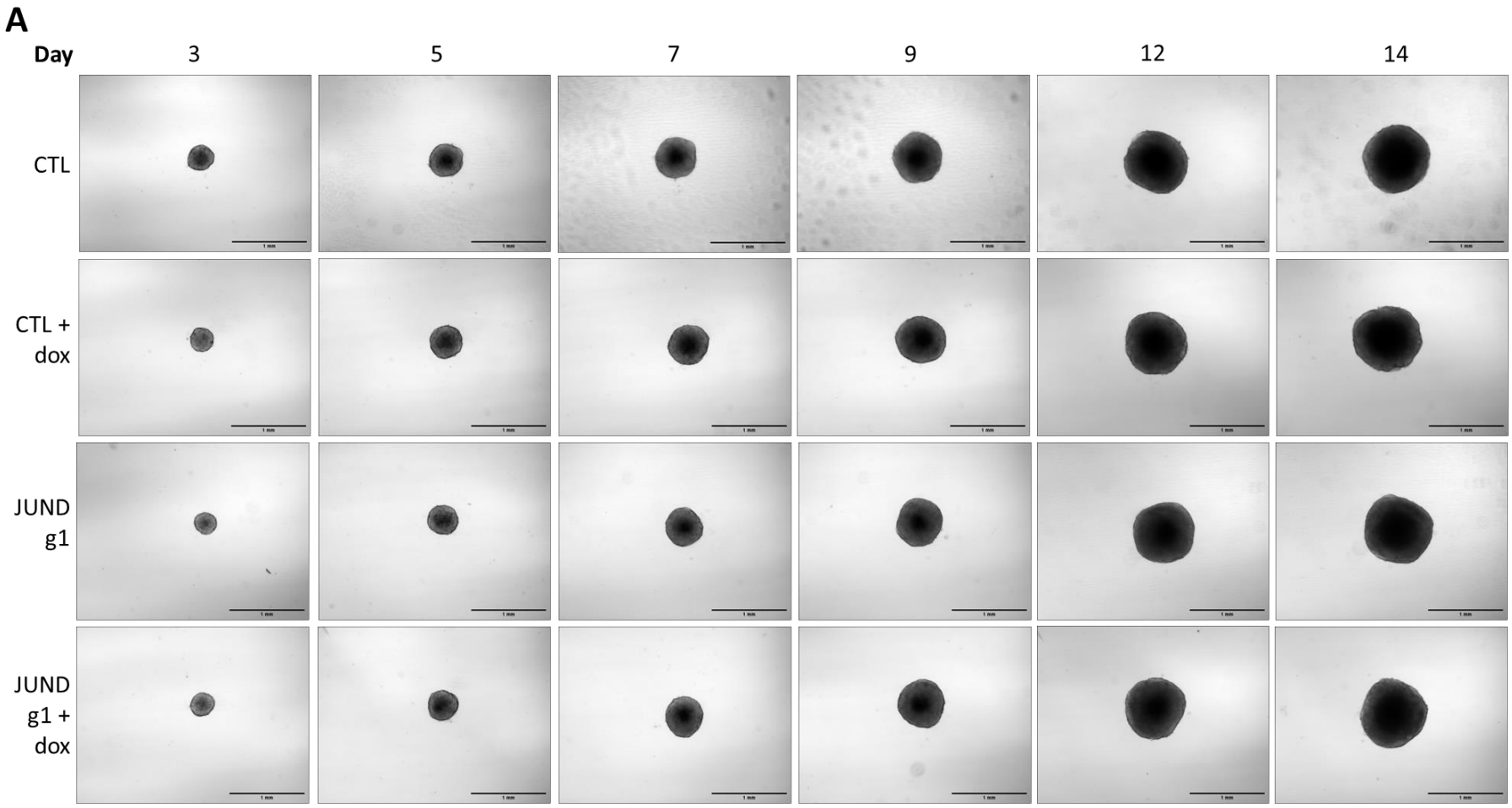
A
Day
3
5
7
9
12
14
CTL
CTL + dox
JUND g1
JUND g1 + dox

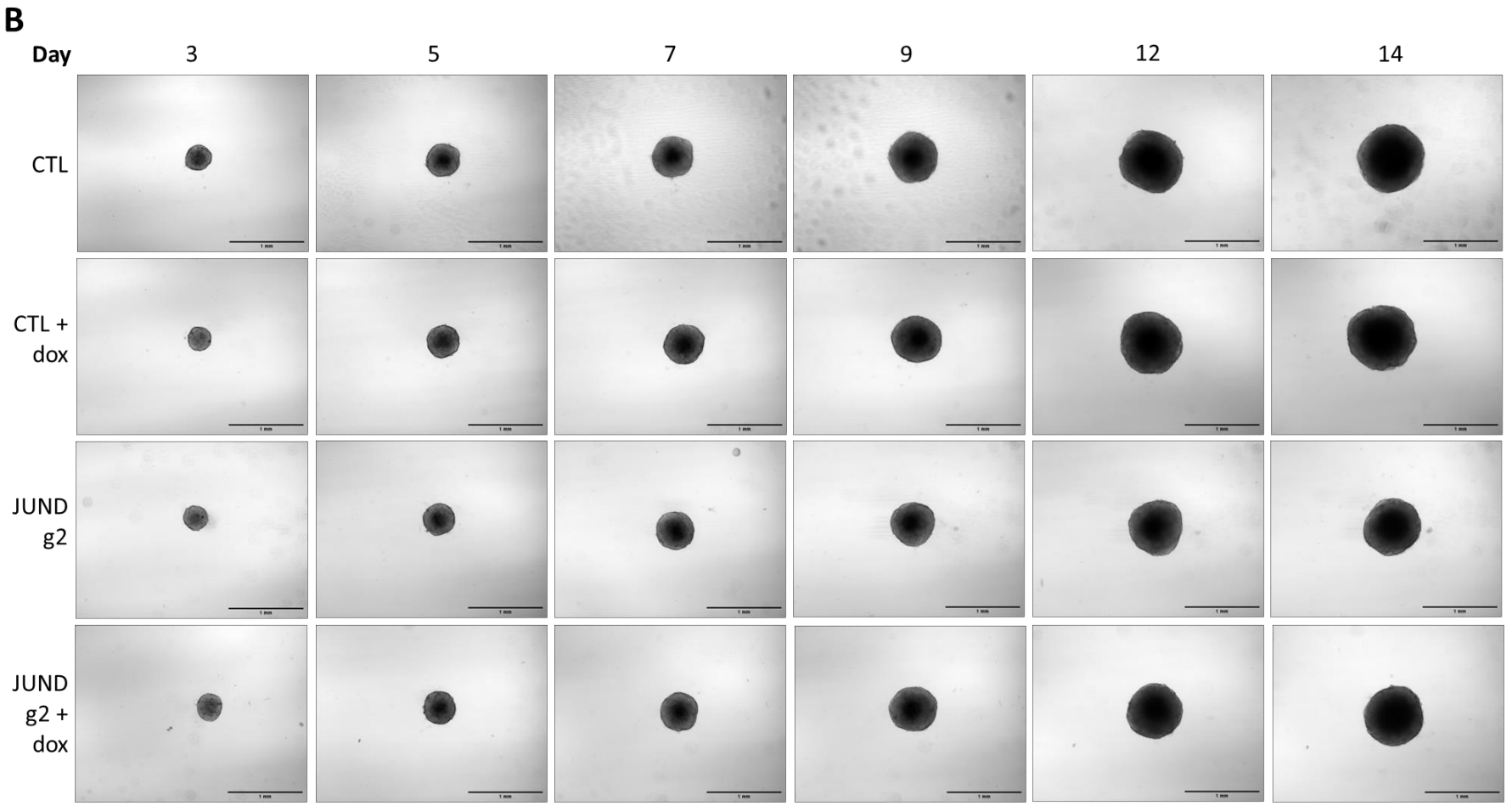
B
Day
3
5
7
9
12
14
CTL
CTL + dox
JUND g2
JUND g2 + dox

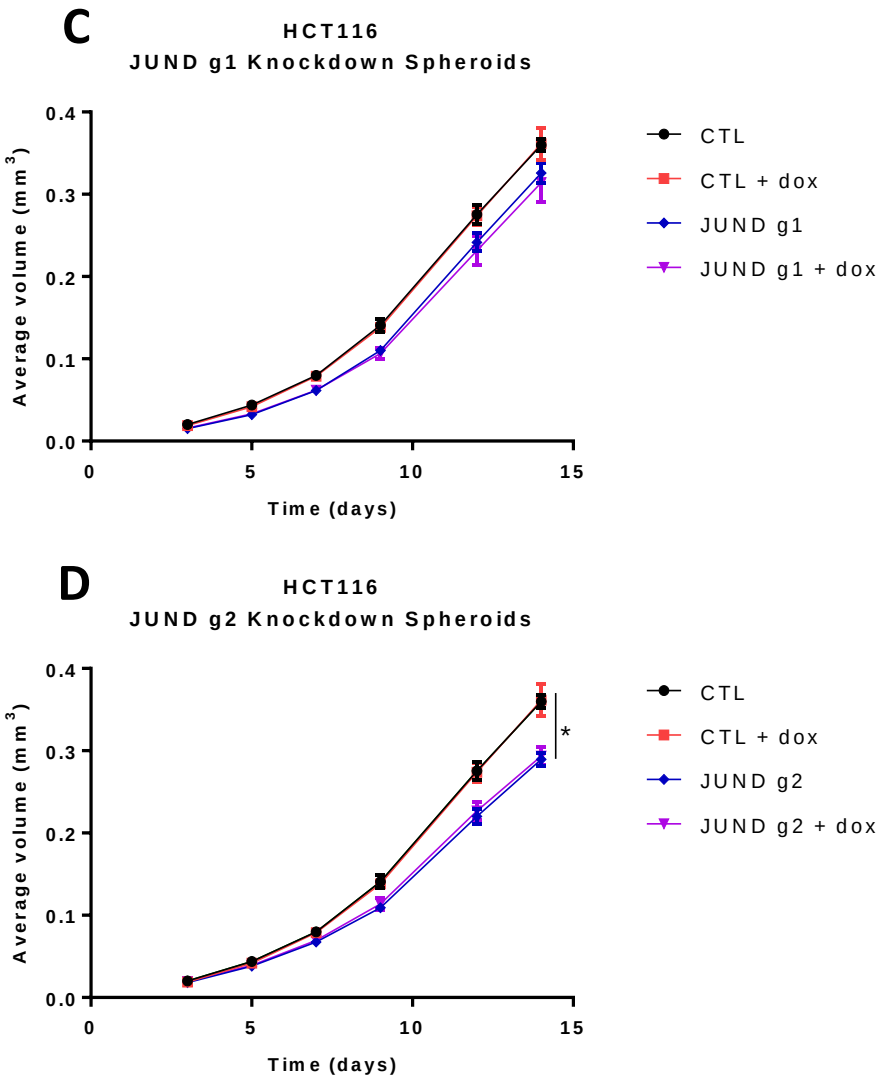

Figure 3.19 Effect of JUND knockdown on 3D spheroid growth in HCT116. (A) Representative images of control and JUND-g1 knockdown spheroids in HCT116. (B) Representative images of control and JUND-g2 knockdown spheroids in HCT116. Spheroids were formed and imaged as described. Control and JUND spheroids are shown with their respective isogenic controls (+/- doxycycline 2 µg/ml). Images taken at 10X magnification. Scale bar represents 1mm. Analysis of spheroid average volume at the 14 day time-point for JUND-g1 (C) and JUND-g2 (D). N=3. Error bars indicate ± SEM. Data analysed using a t-test. N=3. *p<0.05, **p<0.01.

3.3.9 Effect of JUND Knockdown on Cell Survival

The potential role of JUND in cell survival was also assessed in Ls174T cells using the clonogenic assay as described for FOSL2. In this case, both JUND-g1 and JUND-g2 were used for this assay as both demonstrated a good efficiency of JUND knockdown in Ls174T. The experiment was performed simultaneously to the FOSL2 clonogenic assay and as such are compared against the same controls. Figure 3.20 demonstrates the raw and quantified data. When compared against control hypoxia + doxycycline, both JUND knockdown with JUND-g1 and JUND-g2 exhibited significantly reduced colony counts: JUND-g1 knockdown decreased survival by 65% ($p<0.0001$) and JUND-g2 by 46% ($p<0.0001$).

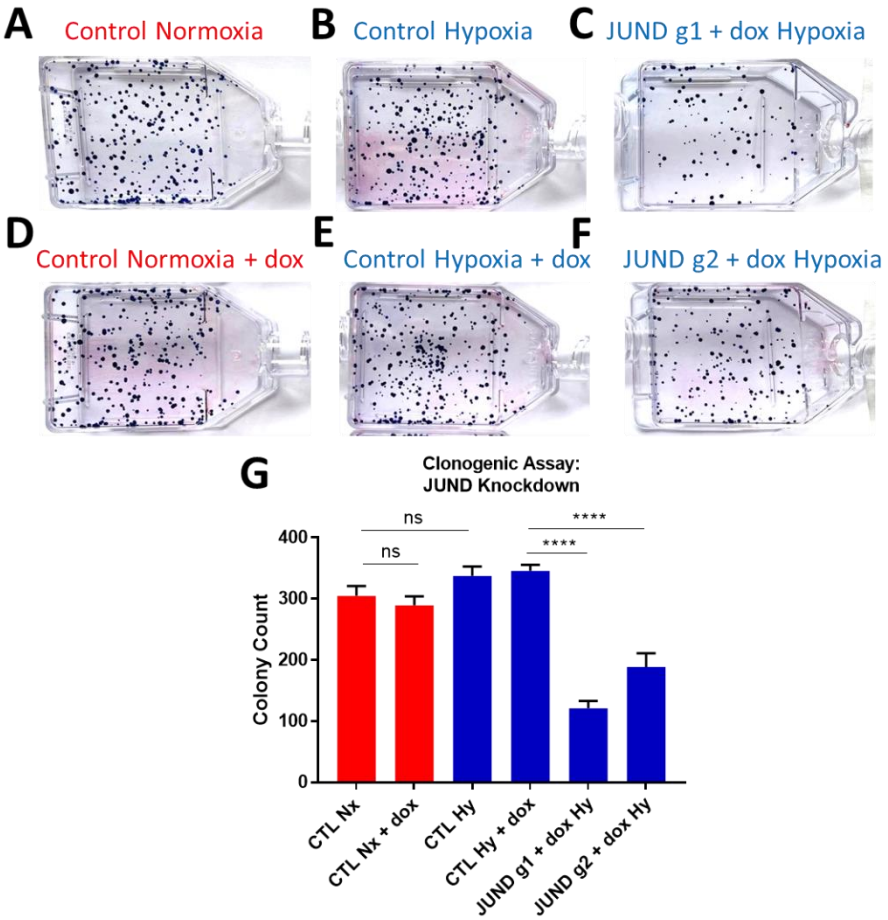

Figure 3.20 Effect of JUND knockdown on Ls174T cell survival in the clonogenic assay. JUND knockdown was induced as previously described. (A-F) depict raw data images as labelled with the colonies visible. (G) Quantification of colony counts. Error bars represent mean ± SEM. Data analysed by one-way ANOVA. **** $p<0.0001$. N=3.

3.3.10 The JUND-Associated Hypoxic Transcriptome

HCT116 JUND-g2 knockdown cell lines were selected for RNA-sequencing in order to investigate the JUND-associated hypoxic transcriptome. This is because JUND-g2 achieved a more efficient knockdown than JUND-g1 and no significant reduction in JUND was observed in the absence of doxycycline. The samples were generated simultaneously to the FOSL2 knockdown samples described previously, with the aim of analysing the FOSL2 and JUND-associated pathways individually before determining if targets and pathways were co-associated with FOSL2 and JUND in hypoxia. Thus, one set of controls was generated to be analysed against both conditions. As described for the FOSL2 samples, JUND-g2 knockdowns were generated and total RNA was extracted 24 hours after exposure to either normoxic (21% O_2) or hypoxic (1% O_2) conditions. As with the FOSL2 knockdown and control samples, all JUND RNA samples had a 260/280 ratio of above 2.0 and thus were considered free from contaminants to a level appropriate for sequencing (Table 3.7) All RIN numbers for the JUND samples were 10.0, indicating maximum RNA integrity, aside from one of the control samples which had a RIN of 9.9 (Table 3.7).

Sample	260/280 Ratio	RIN
n1 Control Normoxia	2.08	10.0
n1 Control Hypoxia	2.06	10.0
n1 JUND KD Normoxia	2.07	10.0
n1 JUND KD Hypoxia	2.07	10.0
n2 Control Normoxia	2.08	10.0
n2 Control Hypoxia	2.10	10.0
n2 JUND KD Normoxia	2.08	10.0
n2 JUND KD Hypoxia	2.08	10.0
n3 Control Normoxia	2.08	10.0
n3 Control Hypoxia	2.06	9.9
n3 JUND KD Normoxia	2.07	10.0
n3 JUND KD Hypoxia	2.06	10.0

Table 3.7 RNA purity and integrity values for HCT116 control and JUND knockdown samples submitted for RNA-sequencing

Samples were analysed by qPCR following cDNA synthesis of the RNA samples to validate an effect of knockdown prior to sequencing. Although a small increase is seen, there was no statistical increase of JUND mRNA expression in control hypoxia compared to control normoxia (Figure 3.21A). However, JUND knockdown leads to a significantly lower level of CA9 mRNA expression (37% decrease, $p<0.0001$) (Figure 3.21B), a greater effect than observed for FOSL2 knockdown.

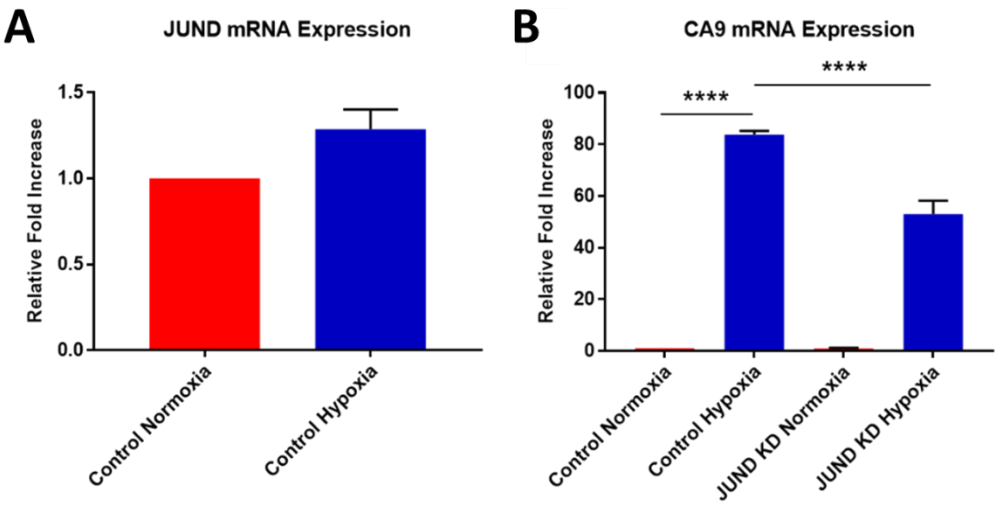

Figure 3.21 Validation of HCT116 control and JUND knockdown RNA samples prior to RNA-sequencing. RNA samples were generated as previously described following 24 hour exposure to hypoxic (1% O_2) or normoxic (21% O_2) conditions. (A) JUND mRNA expression in control hypoxia compared to normoxia samples. (B) CA9 mRNA expression in control and JUND knockdown samples in both normoxia and hypoxia. Error bars indicate ± SEM. Data analysed using a one-way ANOVA. N=3. *p<0.05, **p<0.01, ***p<0.001, ****p<0.0001.

The RNA-sequencing to investigate the JUND-associated hypoxic transcriptome was performed within the same experiment as the FOSL2 knockdown sequencing previously described. This means that the actions of both genes in hypoxia can be directly compared, and co-association analysis can be performed. As such, both knockdown conditions were compared against the same control hypoxia data previously described. Figure 3.22A shows co-expression of genes between control hypoxia and JUND knockdown hypoxia whilst Figure 3.22B displays the volcano plot for JUND knockdown in hypoxia vs control hypoxia. 251 genes were significantly upregulated upon JUND knockdown in hypoxia compared to control hypoxia, 197 genes were significantly downregulated upon JUND knockdown in hypoxia compared to control hypoxia, and 26982 genes were not significantly differentiated between the two conditions.

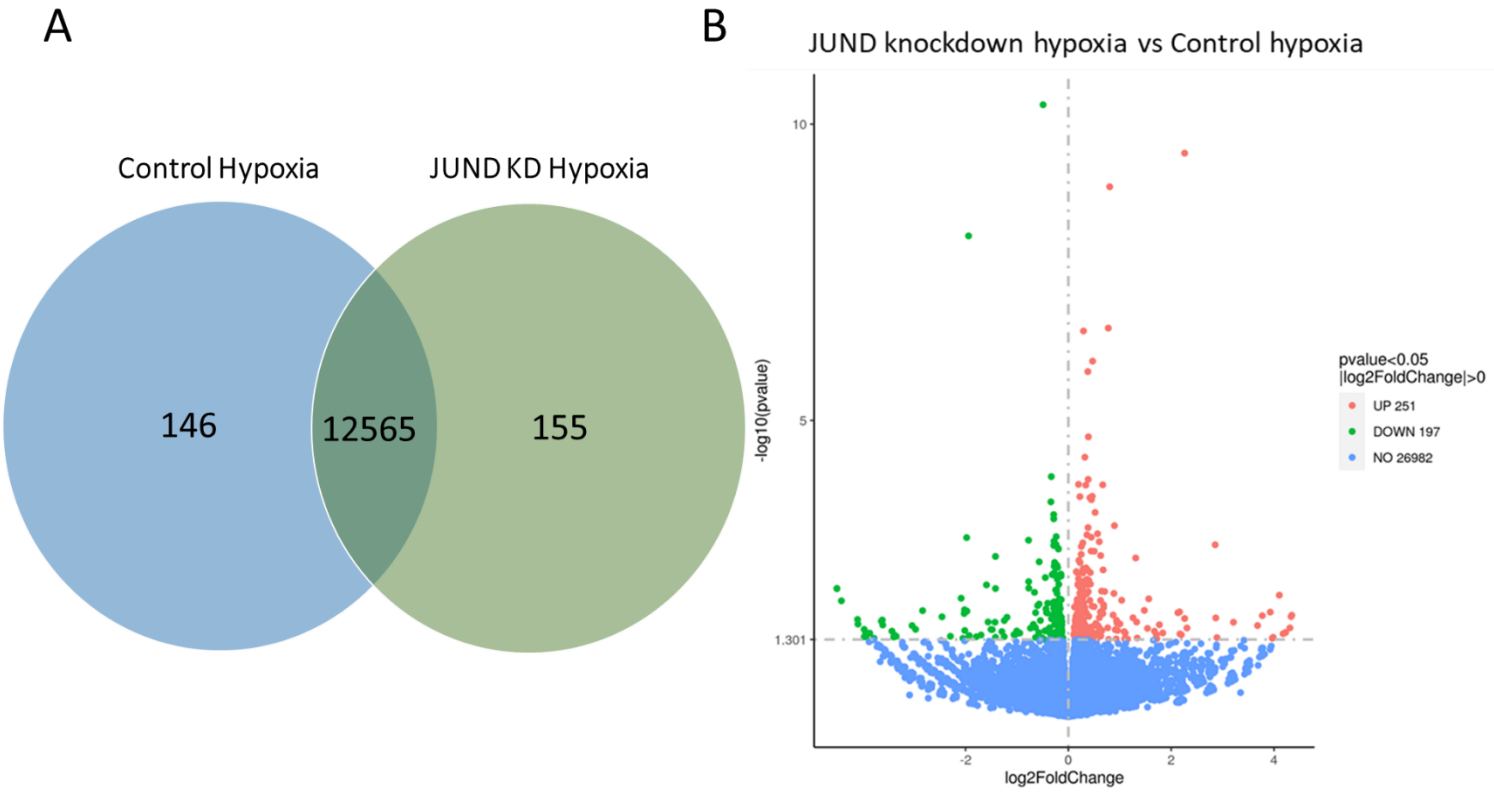

Figure 3.22 Co-expressed and differentially expressed genes between control hypoxia and JUND knockdown hypoxia. (A) Venn diagram depicting co-expressed genes. (B) Volcano plot indicating DEGs. The level of significance is given on the y-axis whilst the log2 fold change is presented on the x-axis

DEGs downregulated upon JUND knockdown in hypoxia compared to control hypoxia were further investigated, as these represent potential hypoxia-inducible JUND targets. JUND itself was present as a significantly downregulated gene in the knockdown condition (log2 fold change -0.49, p=4.70e-11). Interestingly, of the 198 DEGs significantly downregulated upon JUND knockdown compared to control hypoxia, 61 of these genes are also upregulated in control hypoxia compared to control normoxia. This means that a considerable 30% of the genes associated with JUND are hypoxia-inducible. The 61 DEGs that were both JUND-associated and hypoxia-inducible were then ordered by Log2 fold change in JUND knockdown hypoxia compared to control hypoxia, in order to identify those most associated with JUND. The top 30 of the resulting DEGs are displayed in Table 3.8.

Interestingly, the top 2 DEGs that demonstrate the greatest downregulation upon JUND knockdown are also the two showing the greatest increase in hypoxia compared to normoxia, of the genes associated with JUND, therefore representing interesting hypoxia-inducible JUND targets. These include PTPRO, a receptor-tyrosine phosphatase exhibiting downregulation upon JUND knockdown (log2 fold change -4.1, p=0.02) and hypoxic induction (log2 fold change 4.2, p=0.02). The second target is the membrane protein TMEM11, exhibiting a log2 fold change of -4.1 upon JUND knockdown (p=0.03) and a log2 fold change of 4.2 upon hypoxic induction compared to normoxia (p=0.02). Other interesting DEGs feature within the top 30 table, such as the heat shock transcription factor 4 (HS4) gene, known to activate heat-shock upon cellular stress, associated with both JUND (log2 fold 0.36, p=0.03) and hypoxia (log2 fold change 0.81, p=2.82e-06). The GTPase activating protein RGS2 is both associated with JUND (log2 fold change -0.31, p=0.004) and hypoxia (log2 fold change 0.26, p=0.02). Finally, the well-known hypoxia-inducible ANGPTL4 is also among the top 30 hypoxia-inducible JUND-associated targets, with a log2 fold change of -0.23 upon JUND knockdown (p=0.007) and a log2 fold change of 4.04 upon hypoxic induction (p=1.9e-148). Other targets not within the top 30 DEGs but worthy of note include JUND association with the DNA-damage response protein DDIT4 (log2 fold change -0.16, p=0.01), also induced by hypoxia compared to normoxia (log2 fold change 2.21, p=0). Finally, an interesting finding is that c-Jun appears in the list of genes that are significantly upregulated upon JUND knockdown in control hypoxia compared to control hypoxia (log2 fold change 0.28, p=0.004), representing a possible compensatory mechanism for loss of JUND within the cells.

Gene Name	Log2 Fold Change: JUND Knockdown Hypoxia vs Control Hypoxia	p-value	Log2 Fold Change: Control Hypoxia vs Control Normoxia	p-value
PTPRO	-4.09895	0.022932	4.169179	0.020402
TMEM211	-4.09077	0.027464	4.161512	0.024531
CYP2W1	-2.0845	0.010062	1.567748	0.034322
PTGER4P2	-1.69809	0.04192	1.599106	0.044546
H19	-1.24564	0.023951	2.669738	4.84E-05
IKBKGP1	-1.19355	0.021082	1.964699	0.000144
GPAT2P1	-0.65818	0.008001	0.603148	0.017179
LDHAP4	-0.6367	0.01763	2.04589	1.21E-11
CDHR5	-0.56817	0.012606	0.682623	0.00247
CCDC187	-0.50638	0.046916	0.865001	0.001735
JUND	-0.49107	4.7E-11	0.560562	6.81E-10
LENG9	-0.40955	0.017829	0.71518	0.000434
HSF4	-0.36321	0.03166	0.810647	2.82E-06
RGS2	-0.31426	0.004019	0.260662	0.017997
AHNAK	-0.31334	0.039613	0.494995	0.003321
NYAP1	-0.30924	0.02056	0.972035	1.41E-10
GJB3	-0.27643	0.003774	0.475839	3.43E-06
HAGH	-0.27413	0.017772	0.299739	0.009306
GNG7	-0.26792	0.027944	0.370735	0.003191
TET2	-0.26774	0.01151	0.345601	0.00177
TYMP	-0.26322	0.004106	0.44766	1.88E-05
REEP6	-0.25951	0.003942	0.447409	1.98E-06
CAMKK1	-0.25868	0.04664	0.338903	0.010133
BTBD9	-0.25471	0.020018	0.298412	0.008493
ANGPTL4	-0.22783	0.007159	4.047352	1.9E-148
KCNK5	-0.22588	0.045057	0.222799	0.04886
FRYL	-0.22294	0.002786	0.192552	0.008395
SNX33	-0.22131	0.048867	0.643042	3.68E-08
HAS3	-0.21839	0.008339	0.176907	0.032342
FAM162A	-0.21409	0.004796	1.75897	1.08E-98

Table 3.8 Top 30 DEGs associated with JUND and upregulated in hypoxia compared to normoxia. The Log2 fold change for JUND knockdown hypoxia vs control hypoxia is presented alongside the corresponding p-value, and the Log2 fold change for control hypoxia vs control normoxia is also presented alongside the corresponding p-value.

KEGG pathway analysis was used to explore which pathways are significantly downregulated upon JUND knockdown in hypoxia compared to control hypoxia. Figure 3.23 displays this as a dotplot. Interestingly, 'Ribosome' is the most important pathway associated with JUND in terms of number of genes and p-value, as with FOSL2. However, as indicated by the dot colour, none of the pathways identified reached the threshold for statistical significance and therefore were not analysed further.

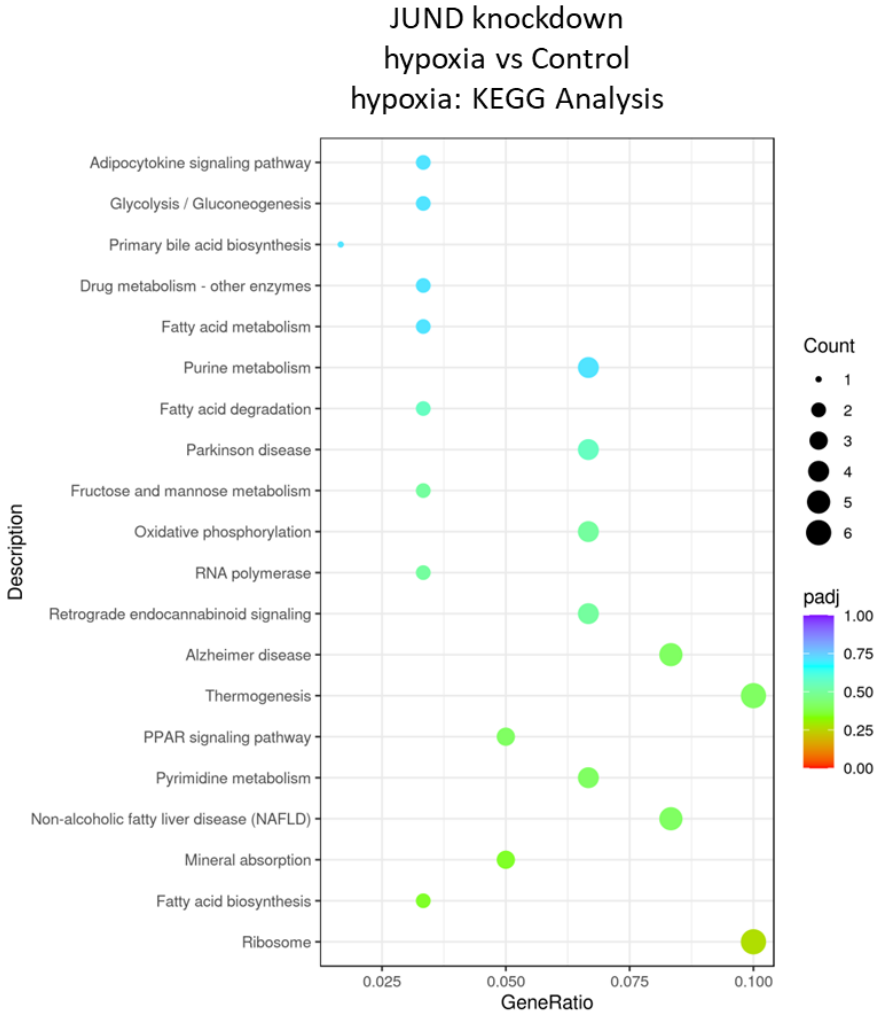

Figure 3.23 KEGG pathway analysis of downregulated genes in JUND knockdown hypoxia compared to control hypoxia. The x-axis shows the gene ratio, which reflects the number of enriched genes compared to all genes featuring in the pathway. The size of the dot shows the gene count, while the colour reflects the level of significance.

As the KEGG pathway analysis yielded no significant results, perhaps due to the smaller number of genes associated with JUND, the Gene Ontology (GO) results were also explored. Gene Ontology analysis aims to identify biological processes, molecular functions and cellular localisations of differentially expressed genes. Figure 3.24

displays a dotplot for the gene ontology terms downregulated upon JUND knockdown in hypoxia compared to control hypoxia, broken down into the 3 groups outlined above. Only 3 terms were statistically significant in the comparison, outlined in red on the figure, all members of the 'Cellular Compartment' analysis category and all associated with ribosomes. These include 'Ribosomal subunit', 'Cytosolic large ribosomal subunit' and 'Large ribosomal subunit'. However, again both the gene ontology terms and the individual DEGs comprising these were not found to be significantly upregulated in the control hypoxia vs control normoxia comparison, and therefore were not analysed further as they do not represent hypoxia-inducible JUND-associated processes.

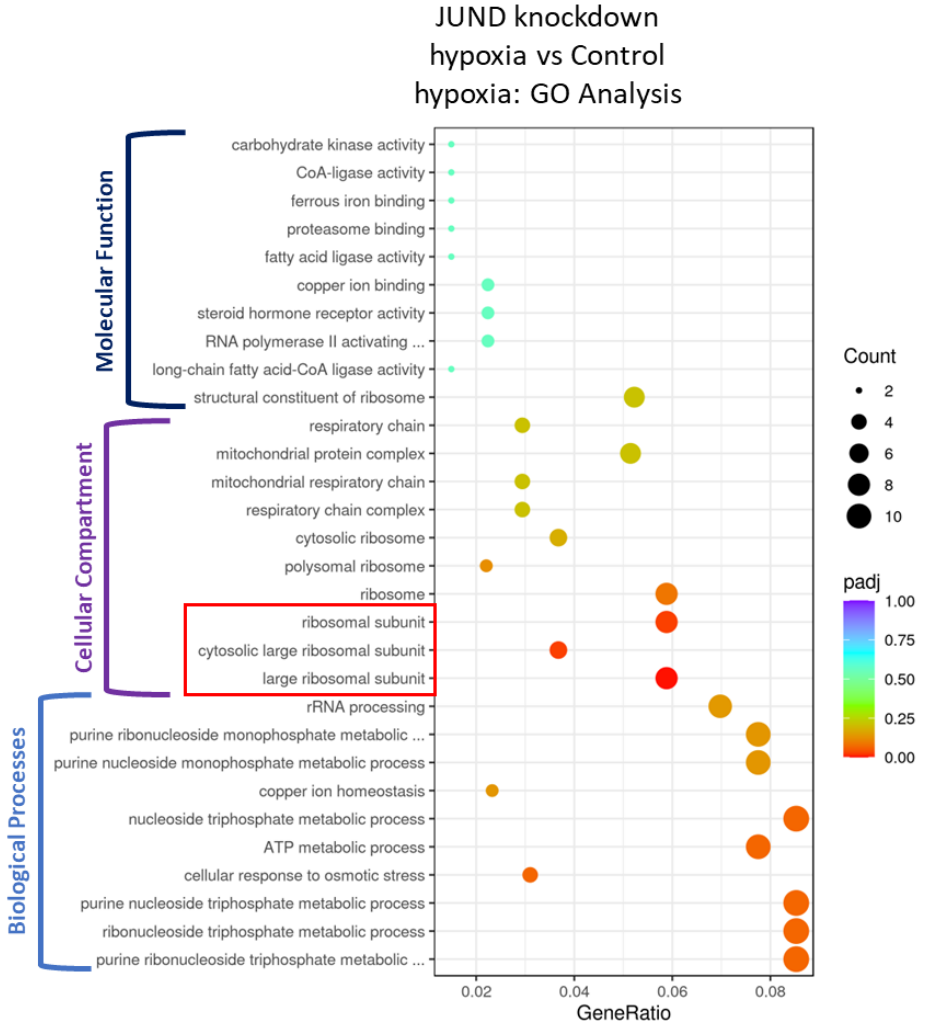

Figure 3.24 GO analysis of downregulated genes in JUND knockdown hypoxia compared to control hypoxia. The x-axis shows the gene ratio, which reflects the number of enriched genes compared to all genes featuring in the process. The size of the dot shows the gene count, while the colour reflects the level of significance. The cellular compartments highlighted in red display significantly significant terms.

3.3.11 FOSL2 and JUND Co-association with Hypoxic Targets

Analysis was performed to identify hypoxia-inducible targets that displayed a level of co-association with both FOSL2 and JUND, indicating hypoxic association with a FOSL2:JUND heterodimer. Firstly, of the 198 genes significantly downregulated upon JUND knockdown in hypoxia compared to control hypoxia, it was determined that 61 of these were also significantly downregulated upon FOSL2 knockdown in hypoxia compared to control hypoxia. Next, of the 61 genes co-associated with both FOSL2 and JUND, it was determined that 32 displayed a significant increase in control hypoxia compared to control normoxia. These 32 targets therefore represent hypoxia-inducible JUND and FOSL2 target genes, and are summarised in Table 3.9 in order of greatest hypoxic induction.

ANGPLT4 features as the DEG most increased in hypoxia compared to normoxia, with a Log2 fold increase of 4.05 (p=1.88e-148), and a degree of association with both FOSL2 and JUND. Interestingly, the gene that is eighth-most increased by hypoxia compared to normoxia of those co-associated with FOSL2 and JUND is the cytochrome P450 enzyme CYP2W1 (log2 fold change 1.57, p=0.03). This also represents the gene that is the most significantly downregulated upon both FOSL2 and JUND knockdown (log2 fold change -4.2, p=0.0006) and (log2 fold change -2.08, p=0.01) respectively. This therefore represents an interesting follow-up target as a gene exhibiting a great degree of association with both FOSL2 and JUND and a considerable log2 fold hypoxic increase. Several genes with linked function also occur, such as DDIT4 and NDRG1, both implicated in the DNA damage response as discussed in the discussion. Furthermore, JUND itself appears on the list as a gene that is hypoxia-induced and co-associated with FOSL2 and JUND, suggesting a possible feedback loop for further JUND expression upon hypoxic induction of JUND.

The list of 32 co-associated, hypoxia-induced targets were inputted into KEGG pathway software in order to identify any pathways that these genes were enriched in. While no pathways themselves were significantly enriched, possibly due to the small number of genes inputted, several modules arose demonstrating clusters of genes. For example, 8 of the DEGs are associated with ‘exosomes’: ENO2, CAPG, GNG7, REEP6, ACSL5, ANGPTL4, NDRG1 and SFN. 5 are associated with ‘Metabolic pathways’:

TYMP, ENO2, HAGH, ACSL5 and CYP2W1. Additionally, 3 genes associated with both FOSL2 and JUND are transcription factors themselves: JUND, BHLHE40 and ID1. These findings are summarised in Table 3.10.

Gene Name	Log2 Fold Change: Hypoxic Induction	p-value	Log2 Fold Change: FOSL2 Knockdown	p-value	Log2 Fold Change: JUND Knockdown	p-value
ANGPTL4	4.05	1.88E-148	-0.38758	3.8569E-06	-0.22783	0.007159
PFKFB4	2.94	9.21E-260	-0.23242	0.00015062	-0.19275	0.001486
NDRG1	2.35	1.47E-215	-0.36931	1.6218E-11	-0.13859	0.010598
DDIT4	2.21	5.48E-136	-0.24284	6.12448E-05	-0.16545	0.010556
BHLHE40	2.08	2.49E-184	-0.25195	4.07077E-05	-0.13425	0.028419
ENO2	1.82	4.34E-146	-0.33718	2.95498E-08	-0.19542	0.001451
FAM162A	1.76	1.08E-98	-0.26772	9.75636E-05	-0.21409	0.004796
CYP2W1	1.57	0.034321819	-4.20991	0.000596155	-2.0845	0.010062
TNIP1	1.40	4.32E-66	-0.18447	0.004196531	-0.13144	0.042863
NYAP1	0.97	1.41E-10	-0.31623	0.021921587	-0.30924	0.02056
ZNF395	0.94	2.83E-27	-0.1831	0.015288117	-0.16756	0.028641
NOL3	0.73	4.09E-15	-0.29868	0.000228532	-0.18854	0.034581
LENG9	0.72	0.000433649	-0.38241	0.02944912	-0.40955	0.017829
SNX33	0.64	3.68E-08	-0.2288	0.03511563	-0.22131	0.048867
JUND	0.56	6.81E-10	-0.17816	0.013387776	-0.49107	4.7E-11
TSC22D4	0.54	1.51E-09	-0.20444	0.015189639	-0.17508	0.030559
GJB3	0.48	3.43E-06	-0.23902	0.009943865	-0.27643	0.003774
CTDSP1	0.47	9.30E-12	-0.22656	0.000917196	-0.20084	0.004513
TMSB10	0.46	9.31E-18	-0.24648	5.634E-05	-0.17135	0.010313
TYMP	0.45	1.88E-05	-0.29468	0.001966839	-0.26322	0.004106
REEP6	0.45	1.98E-06	-0.26378	0.001980685	-0.25951	0.003942
H1F0	0.44	3.30E-12	-0.21203	0.000671486	-0.12632	0.035755
ACSL5	0.40	1.87E-07	-0.26649	5.19294E-05	-0.20817	0.003042
GNG7	0.37	0.003191397	-0.33649	0.004445837	-0.26792	0.027944
EMP1	0.34	0.000477342	-0.38764	6.78764E-05	-0.20713	0.024607
HAGH	0.30	0.009305943	-0.27203	0.007544021	-0.27413	0.017772
CAPG	0.25	0.001516757	-0.26671	0.002337078	-0.16737	0.04256
TSR2	0.21	0.019799214	-0.24639	0.011386085	-0.21303	0.028718
TRIOBP	0.18	0.008157353	-0.16446	0.004137393	-0.12747	0.027893
HAS3	0.18	0.032342192	-0.3928	1.23735E-06	-0.21839	0.008339
SFN	0.16	0.023379963	-0.13813	0.022987025	-0.13702	0.027295
ID1	0.14	0.009649345	-0.11212	0.02327654	-0.14079	0.004239

Table 3.9 Hypoxia-induced DEGs associated with both FOSL2 and JUND. The Log2 fold change is presented for control hypoxia vs control normoxia, FOSL2 knockdown hypoxia vs control hypoxia and JUND knockdown hypoxia vs control hypoxia, alongside corresponding p-values.

Co-regulated Genes Associated with Exosomes	
ENO2	Enolase-2
CAPG	Capping actin protein, gelsolin-like
GNG7	G protein subunit gamma 7
REEP6	Receptor accessory protein 6
ACSL5	Acyl-CoA synthetase long chain family member 5
ANGPTL4	Angiopoietin like 4
NDRG1	N-myc downstream regulated 1
SFN	Stratifin
Co-regulated Genes Associated with Metabolic Pathways	
ENO2	Enolase-2
TYMP	Thymidine phosphorylase
HAGH	Hydroxyacylglutathione hydrolase
CYP2W1	Cytochrome p450 family 2 subfamily w member 1
ACSL5	Acyl-CoA synthetase long chain family member 5
Co-regulated Genes: Transcription Factors	
JUND	Transcription factor AP1 subunit JUND
ID1	Inhibitor of DNA binding 1, HLH protein
BHLHE40	Basic helix-loop-helix family member E40

Table 3.10 Associations of co-associated FOSL2 and JUND DEGs with biological functions. Co-associated FOSL2 and JUND DEGs found to be hypoxia-inducible were associated with exosomes, metabolic pathways and transcription factors.

3.3.12 FOSL2 Knockdown Xenograft Experiment

In order to determine the role that FOSL2 plays in tumour growth in an *in vivo* setting, FOSL2 knockdown or control cells were generated *ex vivo* through doxycycline treatment as previously described and then implanted into CD1 nude mice. Both HCT116 and Ls174T control and FOSL2 gRNA-transduced cell lines were treated for 5 days with doxycycline (2 µg/ml) in order to induce Cas9 expression and subsequent cutting as previously described. FOSL2-g2-transduced lines were used for the *in vivo* experiment due to the higher level of cutting efficiency observed previously. 32 CD2 nude mice were injected subcutaneously into the flank with $2X10^6$ cells (either control or FOSL2 knockdown) in a 100µl dosing volume prepared with Matrigel. The study was identified as CSU1909 and carried out under project license number P435A9CF8. The 16 mice were used per cell line, with the experimental groups outlined in Table 3.11.

Group	Number of Mice
HCT116 Control Male	4
HCT116 Control Female	4
HCT116 FOSL2 KO Male	4
HCT116 FOSL2 KO Female	4
Ls174T Control Male	4
Ls174T Control Female	4
Ls174T FOSL2 KO Male	4
Ls174T FOSL2 KO Female	4

Table 3.11 Experimental groups for FOSL2 KD/Control HCT116 and Ls174T xenograft experiment (CSU1909).

Figure 3.25 shows the average volume (mm^3) for the 16 mice that formed the HCT116 group. Figure 3.25A shows the tumour volumes for the control and knockdown groups with genders combined. However, as gender differences were noted for the study, the male and female control or knockdown conditions are shown together for comparison in Figure 3.25B and individually in Figure 3.25C-D. From the combined gender analysis, the FOSL2 knockdown group is growing at a smaller volume than the control group from day 45 onwards. From day 59 when the last of the control group were terminated due to reaching the maximum permitted size, the control group were an average of

292mm^3 larger than the knockdown group. When separated according to gender, it is clear that this difference is occurring within the male population and not the female population. In fact, on day 48, the FOSL2 knockdown female group were growing 256mm^3 larger than the control female group.

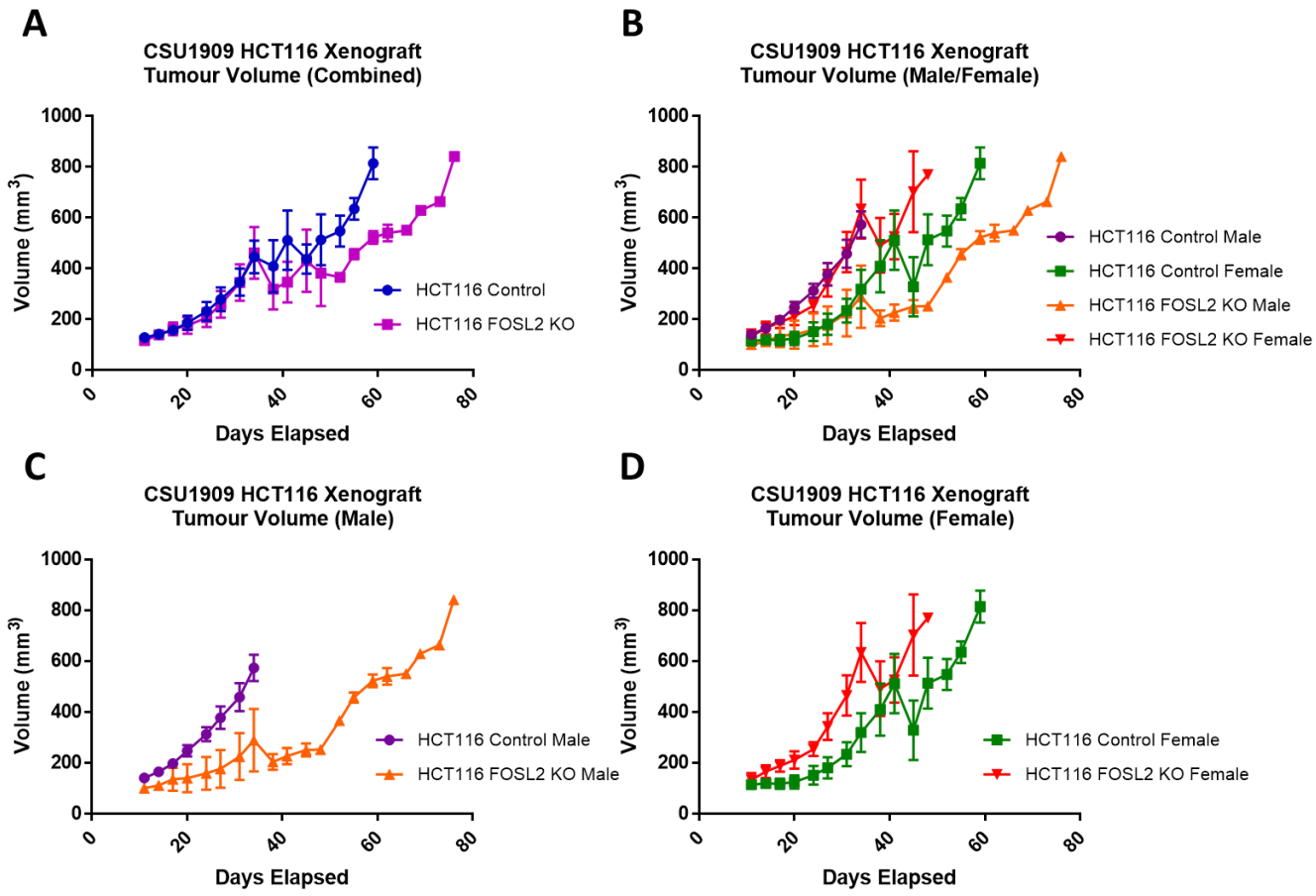

Figure 3.25 Average tumour volumes for HCT116 FOSL2 knockdown and control experiment. Tumour volumes (mm3) were measured every 3-4 days. Data is shown for control and knockdown group genders combined (A), genders shown separately (B) and individually (C-D). Data represents mean ± SEM. N=8 per group.

In order to analyse this data statistically, the growth rates of the tumours were calculated. This was performed by Log10 transforming the average volumes, performing a nonlinear regression analysis and plotting the log gradient values. The average log gradient per group was then analysed using a t-test. The growth rates calculated are presented in Figure 3.26. Figure 3.26A presents the combined-gender growth rate between the control and knockdown group whilst Figure 3.26B shows

male and female separately for comparison, and males and females are shown individually in Figure 3.26C and D respectively. No significant differences were found in the tumour growth rate between control and FOSL2 knockdown groups, when analysed either combined (p=0.4) or separately (p=0.08 males, p= 0.1 females).

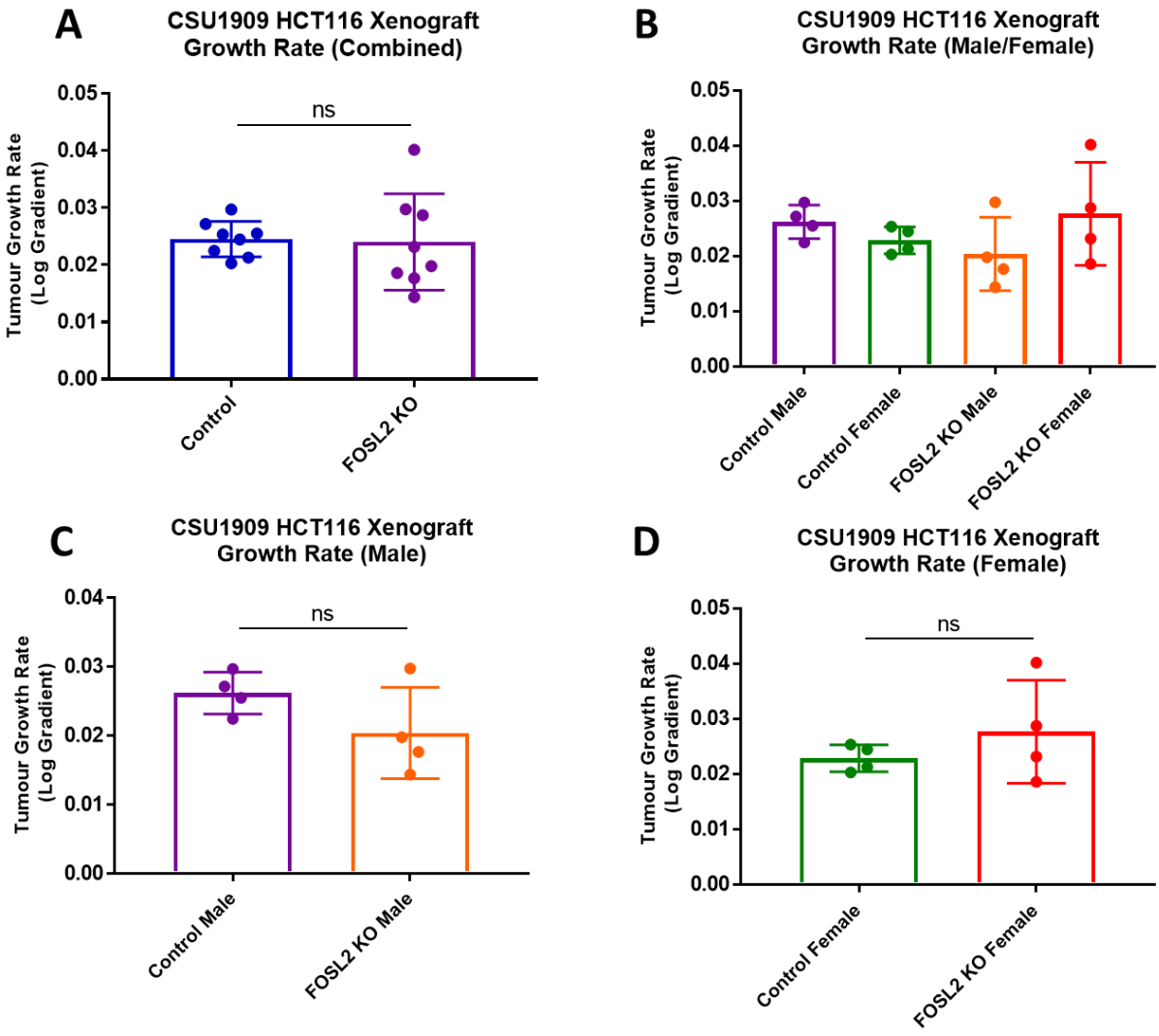

Figure 3.26 Average growth rate for HCT116 FOSL2 knockdown and control experiment. Growth rates were calculated by Log10 transforming the tumour volumes, performing a nonlinear regression and graphing the log gradient. Data is shown for control and knockdown group genders combined (A), genders shown separately (B) and individually (C-D). Data represents mean ± SEM. N=8 per group. Data analysed using a t-test.

The same analysis was performed for mice in the Ls174T control and FOSL2 knockdown groups. The average tumour volumes (mm^3) are shown in Figure 3.27. Figure 3.27A presents control against FOSL2 knockdown with genders combined; Figure 3.27B presents genders separately, whilst Figure 3.27C and D present males and females respectively. As demonstrated in the combined analysis, there is very little difference in average tumour volume between the control and knockdown conditions. At day 76, the FOSL2 knockdown tumours were an average of $76mm^3$ larger than the control tumours, however there is significant variation present. Furthermore, the Ls174T tumours did not establish and grow as well as the HCT116 tumours, which grew up to $841mm^3$ at the same time point. The issue therefore seems to be with the cell line growth within these mice as opposed to representing differences between the conditions. When genders are analysed separately, there are no differences in growth for the control and knockdown conditions in male mice (Figure 3.27C). For the female mice, at day 76 the FOSL2 knockdown mice were growing an average $98mm^3$ larger than the control mice, although there was significant variation present within the FOSL2 knockdown condition (Figure 3.27D).

The growth rates were calculated as described for HCT116 and are presented in Figure 3.28. Figure 3.28A presents the combined-gender growth rate between the control and knockdown group whilst Figure 3.28B shows male and female separately for comparison, and males and females are shown individually in Figure 3.28C and D respectively. No significant differences were found in the tumour growth rate between control and FOSL2 knockdown groups when analysed with genders combined ($p=0.4$, Figure 3.28A). No significant differences were found between control and knockdown growth rate in males ($p=0.3$, Figure 3.28C), however, FOSL2 knockdown compared to control in females were found to grow significantly faster ($p=0.008$. Figure 3.28D).

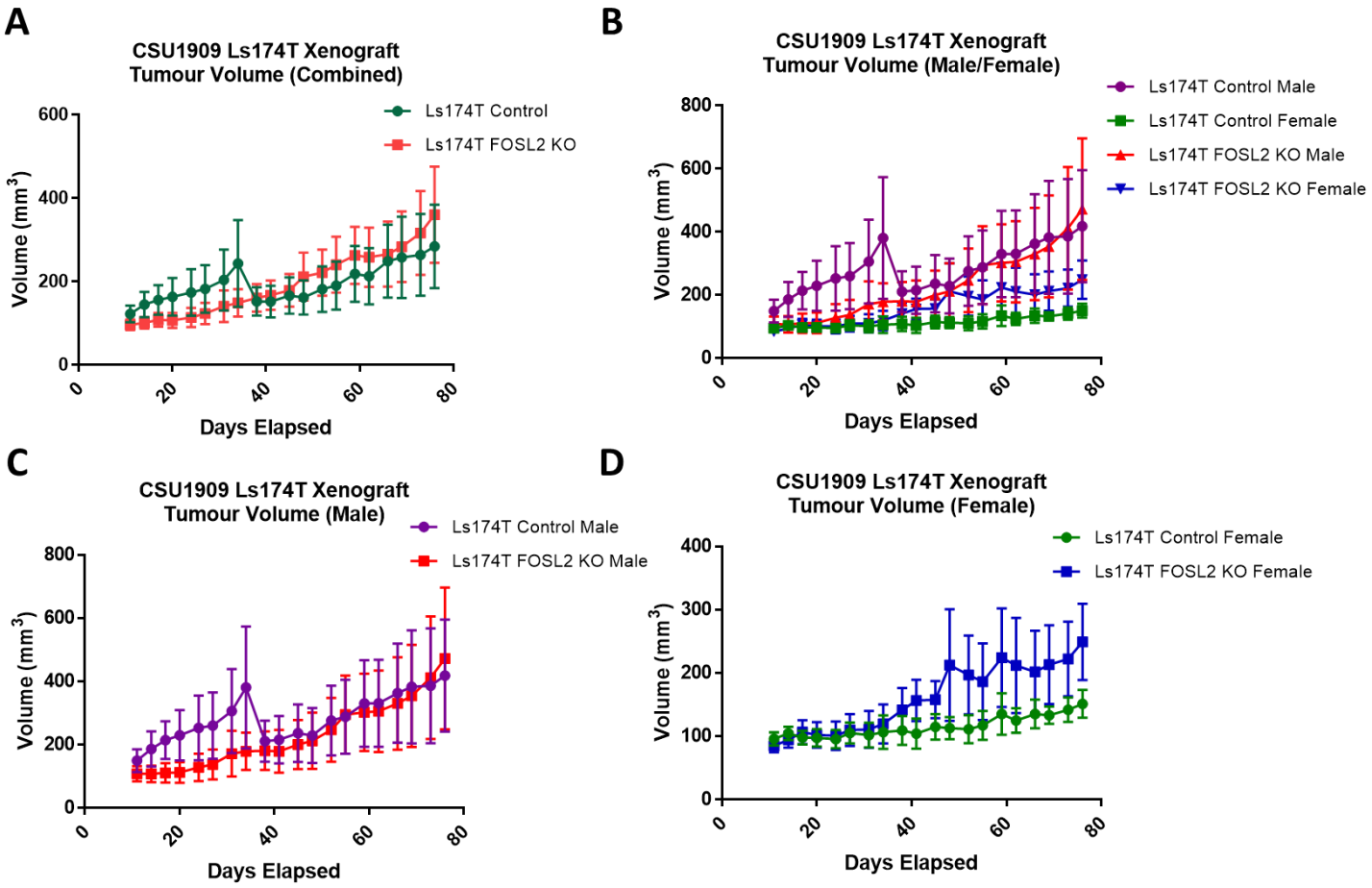

Figure 3.27 Average tumour volumes for Ls174T FOSL2 knockdown and control experiment. Tumour volumes (mm3) were measured every 3-4 days. Data is shown for control and knockdown group genders combined (A), genders shown separately (B) and individually (C-D). Data represents mean ± SEM. N=8 per group.

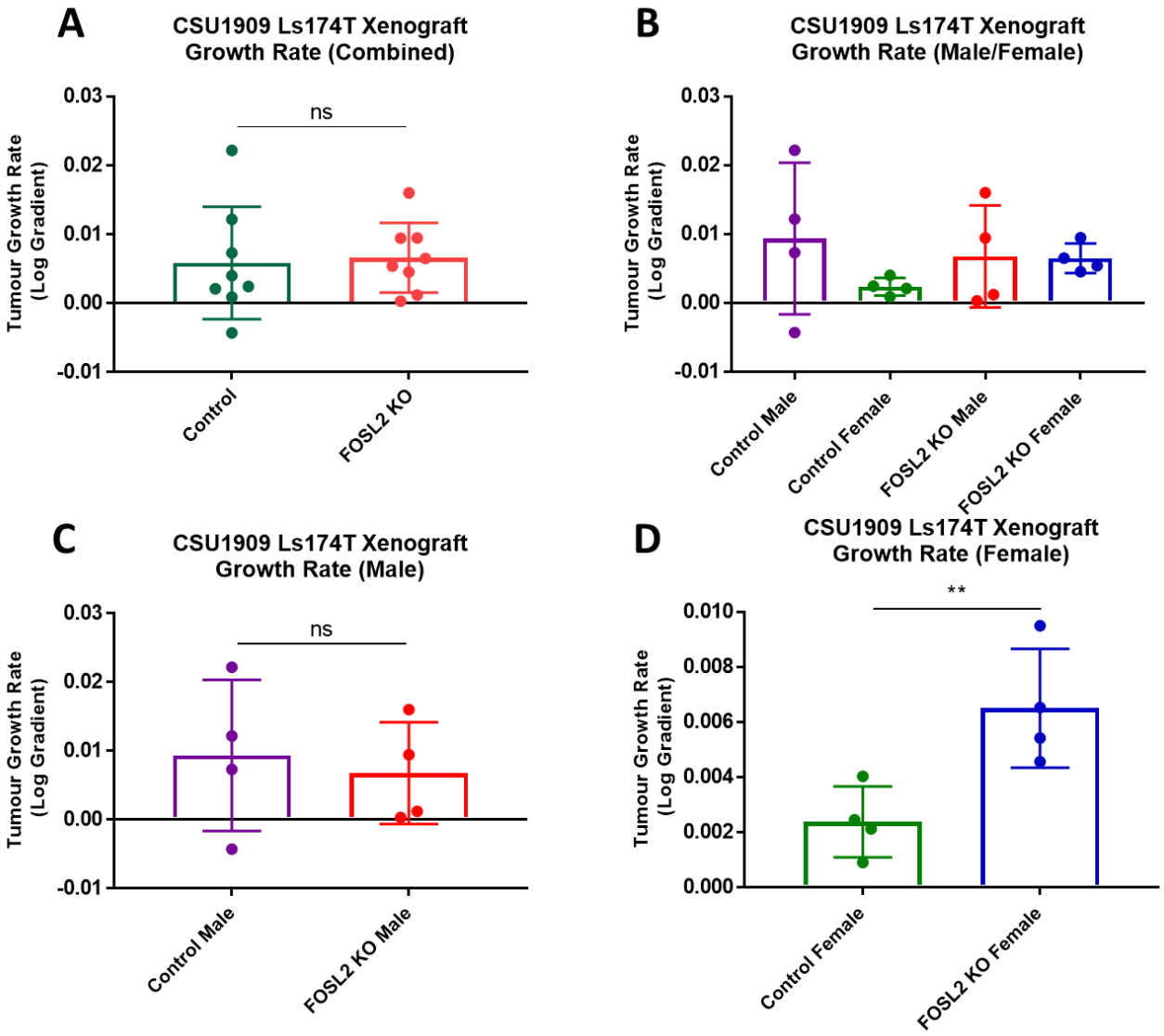

Figure 3.28 Average growth rate for Ls174T FOSL2 knockdown and control experiment. Growth rates were calculated by Log10 transforming the tumour volumes, performing a nonlinear regression and graphing the log gradient. Data is shown for control and knockdown group genders combined (A), genders shown separately (B) and individually (C-D). Data represents mean ± SEM. N=8 per group. Data analysed using a t-test. **p<0.01.

In order to investigate whether FOSL2 was associated with hypoxia within tumour xenografts as in cancer cell lines, protein was extracted from 32 frozen tumour samples. As CSU1909 completed only just prior to completion of this project, material was used from a prior xenograft experiment (CSU1869D) completed by Eric Vancauwenberghe in HCT116 cells. The experiment utilised 16 control clones (8 for each control 1 and control 2) and 16 FOSL2 knockdown clones (8 per group, KD 1 and KD 2. These were generated in the same way as the knockdown clones generated in

this study. Results from this study were similar in terms of tumour growth, where a clear gender difference was apparent. This was hypothesised as being due to clonal effects which is why the newer pooled approach was utilised for CSU1909. However, the material is still relevant to investigate due to similar findings between both experiments. Thus, western blots were performed to see if FOSL2 was associating with CA9 in an *in vivo* setting, and whether there was any difference in this between gender. Blots are shown in Figure 3.29, with FOSL2 and CA9 probed for as well as β-actin utilised as a loading control.

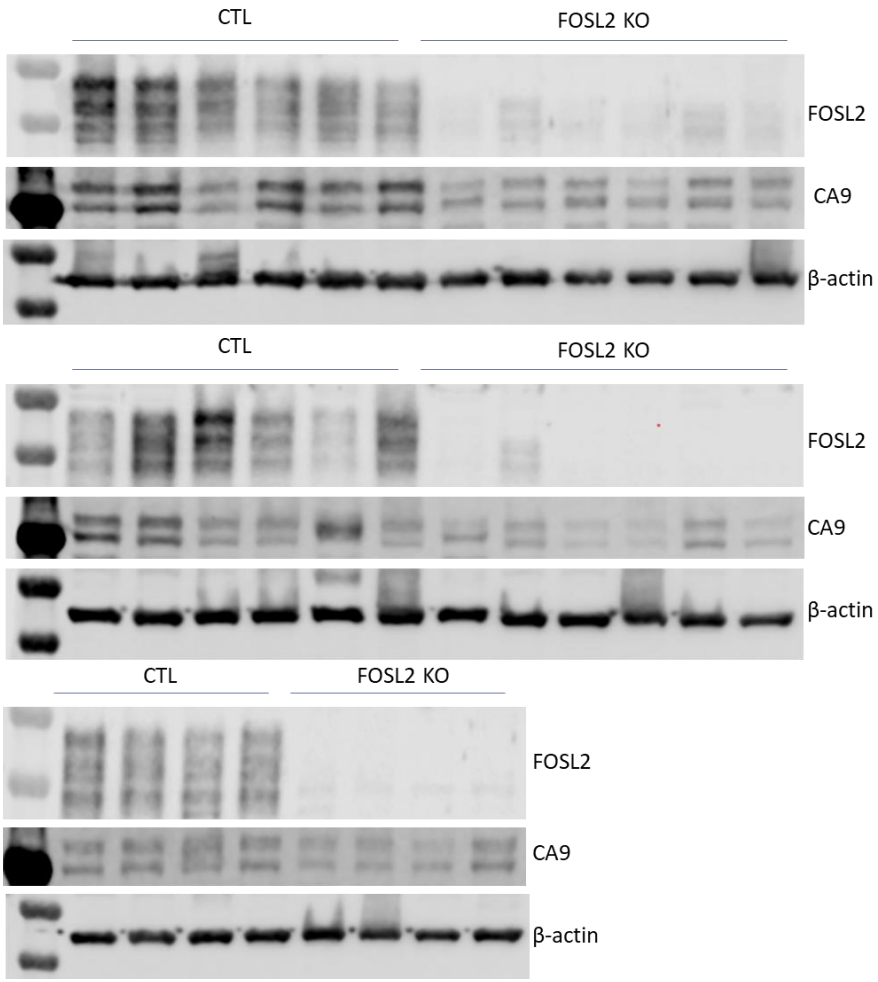

Figure 3.29 Western blots showing FOSL2 and CA9 expression in HCT116 control and FOSL2 knockdown clone tumours (CSU1869D).

Quantification analysis of FOSL2 and CA9 expression across these 32 control and FOSL2 knockdown samples is shown in Figure 3.30. It was found that when analysed with genders combined, CA9 expression was significantly lower (44% decreased) in the FOSL2 knockdown condition compared to control ($p=0.0002$, Figure 3.30A). When males and females were analysed individually, a significant decrease of CA9 expression upon FOSL2 knockdown was still apparent in both males and females (Figure 3.30B). CA9 expression in male FOSL2 knockdowns compared to male controls was 52% lower ($p=0.009$) and in females CA9 expression was 39% lower ($p=0.01$). CA9 was therefore associated with FOSL2 across both genders, although to a greater extent in the male mice. Analysis for FOSL2 expression is also shown to examine whether knockdown levels were maintained within the mice and if this was equal between males and females. When males and females are combined, the FOSL2 knockdown group showed a 94% reduction in FOSL2 ($p<0.0001$, Figure 3.30C). For male mice, FOSL2 expression in the knockdowns was 94% lower than the controls ($p=0.0001$), whilst for female mice, FOSL2 expression in the knockdowns was 93% reduced compared to controls ($p=0.001$), Figure 3.30D.

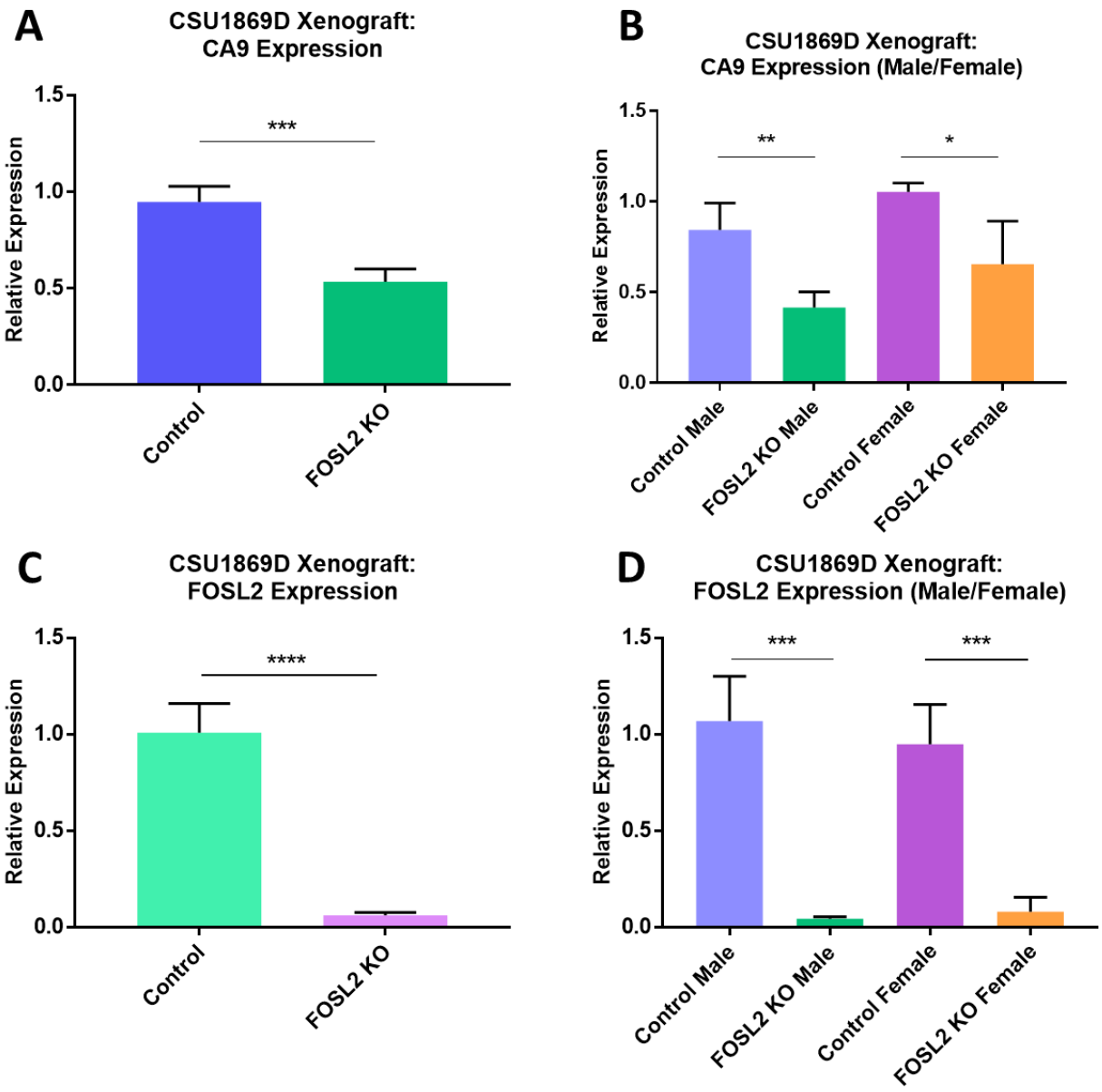

Figure 3.30 Analysis of CA9 and FOSL2 expression in HCT116 control and FOSL2 knockdown tumour samples. (A) Quantification of CA9 expression with genders combined. (B) Quantification of CA9 expression with gender analysed individually. (C) Quantification of FOSL2 expression with genders combined. (D) Quantification of FOSL2 expression with gender analysed individually. Error bars indicate ± SEM. Data analysed using a one-way ANOVA. N=3. *p<0.05, **p<0.01, ***p<0.001, ****p<0.0001.

3.4 Discussion

3.4.1 Phenotypic Role of FOSL2 and JUND in CRC

The aim of this chapter was to investigate the role of FOSL2 and JUND in hypoxia in colorectal cancer, something that has not been previously explored within the literature. Initially, FOSL2 and JUND were both found to be significantly upregulated in hypoxia (1% O_2) compared to normoxia (21% O_2) at both the 24 hour and 48 hour time-point in Ls174T cells. Importantly, no significant differences were found in FOSL2 or JUND expression between normoxia at 21% O_2 and physoxia (8.5% O_2), validating the use of normoxic oxygen concentrations for further experiments. The use of a hypoxic time-course is important in the study of transcription factor induction, as transcription factor expression varies according to both time of hypoxic induction and oxygen concentration. For example, HIF1 is known to be rapidly induced by acute or transient hypoxia, whereas HIF2 has been found to be activated by chronic hypoxia[223]. The use of the hypoxic time-course therefore enabled the selection of the suitable 24 hour time-point for the later RNA-sequencing experiment.

An inducible CRISPR-Cas9 system was optimised in order to generate inducible JUND and FOSL2 knockdown cell lines. This was to attempt to overcome some of the issues faced when generating CRISPR-Cas9 knockdown clones, mainly the clonal heterogeneity arising from this. Additionally, by being able to switch on the knockdown with doxycycline in a fresh batch of cells that had not previously been exposed to doxycycline, the effect of the knockdown could be observed before the cells had initiated any compensatory mechanisms to overcome the knockdown. The main limitation of this model was the reduced knockdown efficiency achieved. For FOSL2, only one gRNA achieved around a 70% knockdown and so multiple guides could not be used within experiments.

The inducible knockdown cell lines generated were used to establish phenotypic effects of FOSL2 and JUND in order to justify later RNA-sequencing. In HCT116, FOSL2 knockdown was found to significantly reduce the volume of spheroids compared to both the control with and without doxycycline, indicating a potential role for FOSL2 in

tumour growth and providing justification for the later *in vivo* study conducted within this project. For JUND, two gRNAs were utilised within the experiment. JUND-g1 produced no significant differences, however knockdown of JUND with JUND-g2 produced spheroids that grew significantly smaller than the control with or without doxycycline. Concerningly, this effect was also seen in the isogenic JUND-g2 without doxycycline control. This suggests some form of leakiness within the system, whereby cutting is occurring after the lentiviral gRNA enters the cells in the absence of doxycycline. This effect would need to be explored further in order to make robust conclusions on the role of JUND in spheroid growth.

In Ls174T cells, the role of FOSL2 and JUND in cell survival was investigated using the clonogenic assay, measured as number of colonies. By using the isogenic control with and without doxycycline, it was established that the doxycycline itself was not effecting cell survival. Additionally, there were no significant differences between control normoxia and hypoxia, suggesting that the hypoxic condition was not effecting cell survival. It was found that the FOSL2 knockdown in hypoxia (using the most efficient targeting gRNA) significantly reduced cell survival by 42% compared to control plus doxycycline in hypoxia. JUND was also found to significantly reduce cell survival with both guide 1 and guide 2, by 65% and 46% respectively. This indicates a potential role for both subunits in CRC survival. The role of AP1 in cell survival is complex, with both pro- and anti-apoptotic mechanisms described in a highly cell type-dependent manner[224]. However, more information is needed in order for this conclusion to be robust. The effect on cell survival was only established in hypoxia, the knockdown in normoxia would need to be included to ascertain whether the effect is present in both normoxia and hypoxia or if it is hypoxia-specific.

3.4.2 FOSL2-Associated Hypoxic Transcriptome

RNA-sequencing was performed in order to identify hypoxia-inducible targets and pathways associated with FOSL2. This was explored by analysing both the top differentially expressed genes associated with both FOSL2 and hypoxia, and also to analyse pathways that these genes may be enriched in. Several DEGs of interest

appear on the list as possible mechanisms of FOSL2 contribution to CRC pathogenesis, with current lack of evidence of association with FOSL2 presenting them as novel targets. For example, two sphingolipid-associated genes are among those most associated with FOSL2 and induced by hypoxia. These include DEGS2, involved in the biosynthesis of phytosphingolipids, and has been found to promote CRC tumourigenesis and metastasis via altered m6A-depdendent alteration[225]. SGPP2 also features, and is responsible for catalysing dephosphorylation of sphingosine-1-phosphate to sphingosine. It is mainly expressed in the GI tract and has been associated with ulcerative colitis[226], a risk factor for CRC, as well as with tumour growth and metastasis in gastric cancer[227]. Sphingolipids are well-known to have roles in cancer cell signalling[228] and are also known to be altered upon tumour hypoxia[229]. Another gene of interest associated with both FOSL2 and hypoxia is matrix metalloproteinase 14 (MMP14), which is upregulated in various cancers including CRC where it is associated with poor prognosis through promotion of invasion and metastasis[230]. These genes therefore present interesting potential FOSL2-associated hypoxic targets contributing to CRC pathogenesis.

KEGG pathway analysis revealed 4 overlapping pathways between control hypoxia and control normoxia, and FOSL2 knockdown hypoxia compared to control hypoxia, representing FOSL2-associated hypoxia-inducible pathways. These include Central carbon metabolism in cancer, Biosynthesis of amino acids, Fructose and mannose metabolism, and Carbon metabolism. Despite being grouped into multiple pathways, many of the DEGs were overlapping between pathways and therefore represent a group of core FOSL2-associated metabolic genes. These include many enzymes involved in the glycolytic pathway, such as ENO1, PGAM1, TPI1, ALDOC, PKM and PFKL. Other genes such as hexokinase 1 (HK1) are involved in additional metabolic pathways, for example HK1 phosphorylates glucose to produce G6P, the initial step in glucose utilisation, but also phosphorylates substrates such as D-fructose and D-mannose and therefore features in fructose and mannose metabolism. It is well known that tumour hypoxia induces a metabolic shift away from oxidative phosphorylation and toward glycolysis, known as the Warburg effect. Canonically, HIF1α regulates many of the glycolytic genes and therefore plays a major role in tumour metabolism[231]. Other

transcription factors have been found to regulate aspects of glycolysis such as SP transcription factors[232] and SIX1[233]. However, the role of FOSL2 in regulating tumour glycolysis has not been defined and therefore represents a novel mechanism of FOSL2-mediated hypoxic metabolism.

3.4.3 JUND-Associated Hypoxic Transcriptome

RNA-sequencing of JUND knockdown cells compared against the same controls as for FOSL2 identified JUND as a less important regulator of the hypoxic transcriptional response than FOSL2. While 872 genes were downregulated upon FOSL2 knockdown in hypoxia compared to control hypoxia, just 197 genes were downregulated upon JUND knockdown. Furthermore, when these genes were cross-referenced against genes upregulated in control hypoxia compared to control normoxia, just 61 genes were found to be both hypoxia-induced and JUND-associated. Interestingly, while many genes associated with cancer (including CRC) featured in the top DEGs associated with FOSL2, the highest associated with JUND was in fact a known tumour suppressor gene. The protein tyrosine phosphatase receptor O (PTPRO) has been found to act as a tumour suppressor gene, where it is downregulated in many cancers including CRC[234–236]. However, functions of PTPRO under hypoxic conditions remains to be elucidated as with many targets identified. CDHR5 is another potential tumour suppressor featuring in the top JUND-associated DEGs. CDHR5 is a member of the cadherin family of proteins involved in cell-cell adhesion. Loss of CDHR5 has been associated with disease progression in clear cell renal cell carcinoma and in colon cancer cells[237,238].

Despite the low number of hypoxia-regulated genes downregulated upon JUND knockdown, KEGG pathway analysis was investigated to see whether there were any enriched pathways resulting from the identified DEGs. While 13 pathways were associated with FOSL2, 4 of which overlapped with the control hypoxia upregulations, no significant pathway enrichments were identified upon JUND knockdown.

3.4.4 FOSL2 and JUND Co-associated Hypoxic Targets

Despite the lack of significant pathways enriched upon JUND knockdown, the JUND-associated DEGs were cross-referenced against the FOSL2-associated DEGs in order to investigate if any interesting targets were potentially hypoxia-induced and associated with a FOSL2-JUND heterodimer. It was determined that 32 DEGs were associated with both FOSL2 and JUND and were also upregulated in hypoxia compared to normoxia. Interestingly, hypoxia-inducible genes known to play a role in cancer progression were found to be co- associated with FOSL2 and JUND, such as ANGPTL4 and DDIT4. ANGPTL4 is a known pro-metastatic factor in several cancer types[239], whilst DDIT4 is induced by hypoxia and regulates stress responses, and has been associated with advanced pathological features in CRC[240]. FOSL2 was identified as associating with a number of metabolic genes, and PFKFB4 (6-phosphofructo-2-kinase/fructose-2,6-biphosphatase 4) was found to be associated with both FOSL2 and JUND. PFKFB4 is a key glycolytic enzyme known to be upregulated in hypoxia and contributes to the pathogenesis of many cancers including breast, lung, prostate and colon[241]. This therefore represents a novel AP1 target co-associated with both FOSL2 and JUND that contributes to the pathogenesis of CRC.

Another gene of interest displaying almost the highest log2 fold reductions upon both FOSL2 and JUND knockdown is the cytochrome P450 enzyme CYP2W1, involved in metabolising both endogenous and exogenous agents and found to be highly expressed in colon tumours[242]. CYP2W1 is particularly relevant within the field of hypoxic tumour research due to its metabolism of benzothiazoles, and in bio-activation of hypoxia-activated prodrugs. For example, CYP2W1 is involved in the hypoxic reduction of hypoxia-selective AQ4N to AQ4[243]. Thus, the significant downregulation of CYP2W1 by FOSL2 and JUND (also upregulated by hypoxia) is likely to reduce the efficacy of HAP drugs relying on these mechanisms. HAP efficacy has not been as great as expected within clinical trials, perhaps in part due to the lack of suitable biomarkers to predict therapy outcome.

3.4.5 Role of FOSL2 in Tumour Growth *in vivo*

Finally, the role of FOSL2 in tumour growth *in vivo* was investigated through a xenograft experiment involving 32 mice across 2 cell lines: Ls174T and HCT116. FOSL2 knockdown or control cell lines generated as previously described were injected subcutaneously into the flank of the mice and tumours were measured every 3 days until they reached maximum size, upon which the mice were termed. The results of the experiment contradicted the earlier results from the *in vitro* spheroid experiment. For HCT116, the experiment was more successful in the male than the female mice, with male control cells growing to a larger size than the FOSL2 knockdown male mice. For females, the opposite effect was observed. Tumour growth rates were calculated in order to perform statistical analysis, and no significant differences were found when genders were combined or analysed individually. The Ls174T results are less robust given the lack of successful growth of this cell line within the mice. For example, the control female tumours never grew to beyond 200mm^3, where larger growth would have been anticipated. No significant decrease was observed upon FOSL2 knockdown compared to control in males or females. In fact for the female mice, FOSL2 knockdown mice grew significantly faster than the control female mice.

Due to these potential gender differences arising, the role of FOSL2 in hormone signalling was considered, however this has not been elucidated and remains unclear. One study identified high expression of FOSL2 within breast CAFs, associated with angiogenesis and clinical progression in breast cancer patients. The increased FOSL2 in breast CAFs was found to be regulated by estrogen/cAMP/PKA signalling. This was partly demonstrated through an experiment indicating that a higher level of FOSL2 was detected in immortalized or primary normal fibroblasts stimulated by estrogen[244]. Other studies have focussed on plasticisers released from microplastics and the impact these compounds have on breast cancer through the activation of estrogen signalling. Interestingly, two studies identified that FOSL2 was upregulated by ESR1 (estrogen-receptor 1) activation by bisphenolic compounds released from microplastics. FOSL2 upregulation among other genes was linked to pathways such as invasion, migration and cancer progression[245,246].

It is important to consider whether the model used was suitable for investigating the importance of FOSL2 in cancer. As a sub-cutaneous approach, metastasis was not measured, only the growth of the tumour which FOSL2 may not be regulating. For future work, the *in vivo* experiment could be performed using an intraperitoneal injection of labelled tumour cells in order to observe metastasis around the mouse and into distant organs[247]. Furthermore, if FOSL2 is mediating pro-metastatic effects through the immune cells as suggested in Chapter 4, these effects may not be recapitulated within the mouse model given their immunocompromised status.

4.0 Investigating the Clinical Relevance of FOSL2 in CRC

4.1 Introduction

4.1.1 AP1 as a Prognostic Biomarker in Cancer

The potential role of the AP1 transcription factor as a prognostic biomarker has been investigated across a range of cancers. In breast cancer, the role of AP1 has been studied due to the potential indirect interaction of oestrogen receptors with other transcriptional regulators. A study which provided a systematic evaluation of the expression of all AP1 family members in breast cancer found that the mRNA expression of FOSL1, FOSL2, JUNB and JUND were significantly higher in tumour compared to adjacent tissues[248]. On the other hand, levels of c-Fos and c-Jun were significantly lower within the tumour samples. In terms of CRC, no study to date has profiled the expression levels of AP1 subunits in CRC compared to normal tissue as has been performed for breast cancer. Subunits have, however, been linked to the pathophysiology of CRC. For example, c-Fos has been found to enhance expression of IL-6 and VEGFA in colon cancer cells, leading to the induction of angiogenesis[249]. Interestingly, expression of AP1 subunits in cancer has also been linked to favourable prognosis in addition to poor prognosis, highlighting the complex and context-dependent nature of AP1 in cancer. In gastric cancer , it was found that a loss of c-Fos was associated with advanced stage, metastasis and poor prognosis. This tumour suppressor activity in gastric cancer was attributed to the role of c-Fos in regulating pro-apoptotic genes[250].

It is of importance to consider the prognostic significance of FOSL2 in cancer as described to date. Interestingly, FOSL2 has been identified as a potential biomarker of poor prognosis in non-small cell lung cancer (NSCLC). One study has described hepatocyte growth factor (HGF) and its receptor tyrosine kinase (MET)-induced phosphorylation and upregulation of FOSL2 via ERK1/2 in NSCLC. FOSL2 subsequently promoted SNAI2 transcription, leading to EMT, invasion and migration. High expression of FOSL2 was correlated with advanced tumour stage and metastasis[251].

Whilst the prognostic impact of FOSL2 expression in colorectal cancer has not been fully elucidated, one study has identified FOSL2 as a pro-metastatic factor in colon cancer. In particular, miR-143 was shown to be a miRNA-regulator of FOSL2 expression, with miR-143-mediated downregulation of FOSL2 leading to increased chemosensitivity in KRAS-mutant tumour cells as well as a less invasive phenotype[252].

4.1.2 AP1 Inhibitors to Target Cancer

Due to the described importance of the role of AP1 in cancer, it is unsurprising that AP1 is an attractive therapeutic target with decades of research into potential clinical inhibitors. While AP1-regulated pathways may be inhibited by upstream kinase inhibitors, such as the ERK1/2 inhibitor GDC-0994, the further upstream in the pathway that the therapeutic intervention targets, the greater the nonspecific effects due to effecting multiple terminal effectors[253]. Furthermore, as it has been established that some AP1 subunits may be oncogenic whilst others are tumour suppressive depending on the cellular context, selective antagonism of a subunit or specific dimer known to be driving malignancy would be the ultimate therapeutic goal for specificity[254].

Several therapeutic options for targeting AP1 have been explored based on the structure and mechanism of action of the AP1 transcription factor. These include preventing AP1 from interacting with the DNA through the bZip domain, or preventing interaction with partners through the transactivation domain. Small molecules targeting the TRE specifically have been explored. These include the MLN944 sequence-specific DNA intercalator that interacts with the 5'-ATGCAT-3' palindromic TRE sequence through its phenazine rings to induce a right-handed twist of the DNA helix[255]. It was found to inhibit c-Jun binding to the AP1 recognition site, leading to inhibition of transcription and reported efficacy in *ex vivo* models of cancer[256,257]. However, specificity is a concern among DNA binding molecules, with MLN944 also found to modulate oestrogen receptor-α-DNA binding at the estrogen response element[258]. TRE-binding retinoids have also been explored for their potential to inhibit AP1 DNA-binding. SR11302 represents a synthetic retinoid that selectively inhibits AP-

1 TRE activity without activating the retinoic acid response element (RARE) and has shown anti-tumour activity *in vivo*[259,260].

Another mechanism for targeting the protein-DNA interaction with enhanced specificity for an individual AP1 subunit is to target the subunit DNA-binding domain (DBD) rather than the TRE binding site. An example of a small molecule developed to inhibit the DNA binding of c-Fos-c-Jun specifically without affecting binding of the other subunits is known as T-5224. T-5224 has progressed the furthest clinically of all AP1 inhibitors, and has reached phase II clinical trial for efficacy in arthritis[261,262]. Whilst some anti-tumour activity has been demonstrated, further clinical research is needed for the use of T-5224 in cancer therapy[263]. In addition to small molecule inhibitors, peptidic inhibitors designed to target the full bZip domain have also been in development. Targeting the full bZip domain is desirable, as targeting the DBD alone does not prevent protein dimerisation; it is possible for dimers to form, ready to bind DNA when DBD-bound antagonists dissociate. One such peptide developed is termed A-Fos, which works by forming heterodimers with the full bZip domain of c-Jun through the leucine zipper and an acidic extension. This leads to obstructed binding of c-Jun:A-Fos to the target DNA[264]. A-Fos has been shown to effectively antagonise c-Jun DNA binding, and also to inhibit AP1 transactivation in a hepatoma cell line[265].

It is likely that as more knowledge is obtained on specific dimers driving certain pathways in cancer, inhibitors targeting specific protein-protein interactions between AP1 members may become more clinically relevant. In terms of targeting the leucine zipper (LZ) domain, peptide inhibitors are more suitable than small molecules due to the large surface area and lack of defined binding pockets. Much work has gone into developing peptides with a high affinity for LZ domains of c-Jun and c-Fos. One example is an anti-Jun and anti-Fos superzipper (SZ) peptide, demonstrated to bind to the LZ of both c-Jun and c-Fos[266]. During development it was found that a simple point mutation within the c-Jun LZ domain sequence was able to generate more extensive binding forces with interacting partners. Inhibitors against the FOSL2 LZ are yet to be investigated. Figure 4.1 summarises these AP-1-targeting therapeutic approaches.

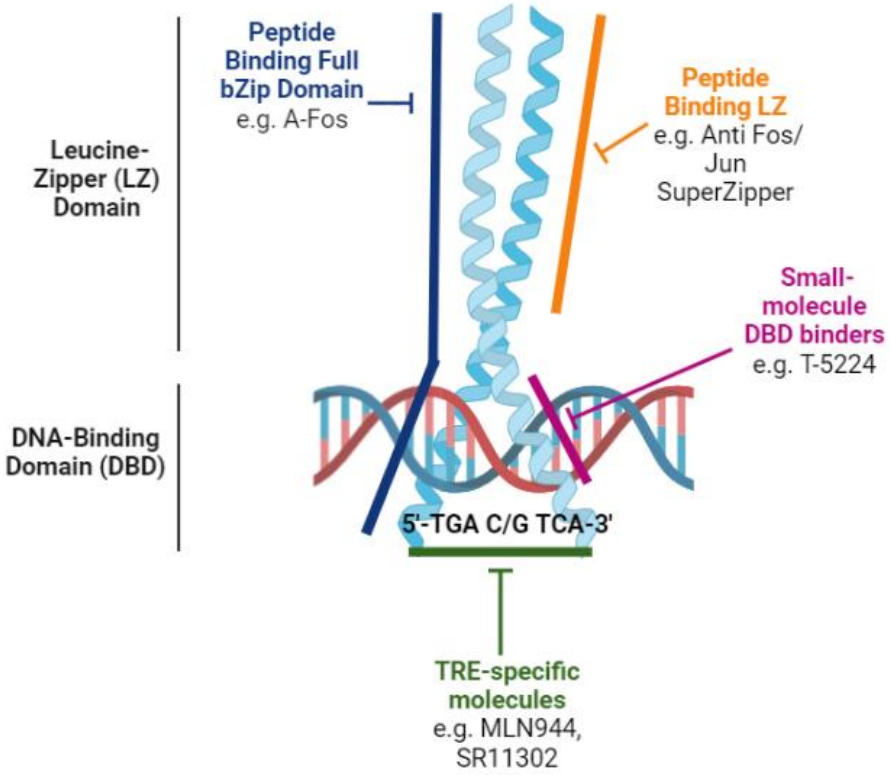

Figure 4.1 Summary of current AP-1-targeting approaches. Figure created in BioRender.

4.2 Aims and hypotheses

The role of FOSL2 as a prognostic biomarker in colorectal cancer is poorly defined. I hypothesise that, through the analysis of a large human colorectal tissue micro-array, FOSL2 will be identified as a prognostic biomarker associated with poor patient survival in CRC. Furthermore, I hypothesise that FOSL2 expression will be significantly correlated with clinicopathological variables such as tumour stage and metastasis.

In order to test these hypotheses I will use the following aims:

1. Perform H-scoring of FOSL2 expression in a large human CRC tissue micro-array consisting of tumour biopsies from over 1000 patients.
2. Correlate FOSL2 expression to clinicopathological parameters including survival, tumour grade and metastasis.
3. Correlate FOSL2 expression to additional protein markers of interest such as nuclear cMyc and CA9.
4. Analyse gender differences arising within clinicopathological variables according to FOSL2 expression.

4.3 Results

4.3.1 H-Scoring Method for Immunohistochemistry

A colorectal cancer tissue micro-array consisting of 15 slides was stained for FOSL2 expression by Declan Sculthorpe following antibody optimisation by Eric Vancauwenberghe. The scanned images of the slides were provided to myself which I proceeded to view and analyse within QuPath. Around 260-280 tumour cores were present on each TMA slide. In total, tumour cores were analysed from 1017 different patient samples, with 4 tumour cores per patient giving a total of 4068 cores that were analysed manually by myself over a 6 month period. The TMA slides were organised into rows, with each row consisting of 12 cores from 3 patients. 4 cores were provided from each patient biopsy. These include a luminal section, a middle section, an advancing edge section and finally a section from the adjacent normal tissue. Figure 4.2 demonstrates an example TMA slide for perspective (Figure 4.2A) alongside this organisation of tumour cores (Figure 4.2B-E). Tumour cores were scored blindly, without having access to the clinical characteristic data provided for the TMA.

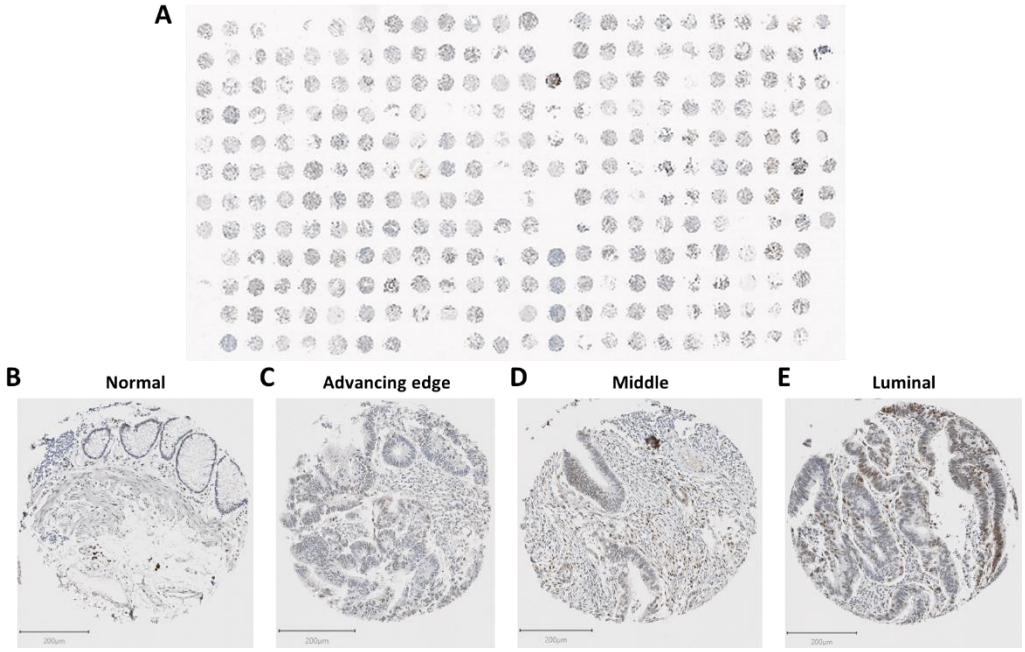

Figure 4.2 Organisation of the colorectal cancer TMA slides. (A) An example image of a TMA slide consisting of around 250 CRC tumour cores. 4 cores are provided per patient from the following regions: adjacent normal (B), advancing edge (C), middle (D) and luminal (E).

In order to accurately score the TMA for FOSL2 expression, the first step involved familiarisation with the histopathology of CRC under the instruction of clinical histopathologist Dr Abhik Mukherjee. It is of vital importance to be able to accurately recognise tumour epithelium from other histological features, and also to distinguish tumour epithelium from normal epithelium. This ensures that areas of normal epithelium are not mistakenly scored as tumour and vice versa. Figure 4.3 displays example cores for normal epithelium (Figure 4.3A-C) at 5X magnification with a magnified 40x image shown in Figure 4.3D. The normal colonic epithelium is organised into glands (also known as crypts or tubules) which appear elliptical or spherical when sections are taken. Epithelial cells form an organised monolayer around the central lumen. In tumour samples, the epithelium becomes disorganised and multi-layered. Examples of tumour cores are shown in Figure 4.3E-G, with a magnified version of a tumour gland shown in Figure 4.3H. Figure 4.3I-J present examples of cores classified as normal but clearly present both normal and tumour epithelium, it is therefore important that the tumour tissue is not mistakenly scored as normal colon. Finally, Figure 4.3K-L demonstrate examples of cores which are classified as tumour but contain no epithelium, just stroma is present which therefore cannot be scored as epithelium.

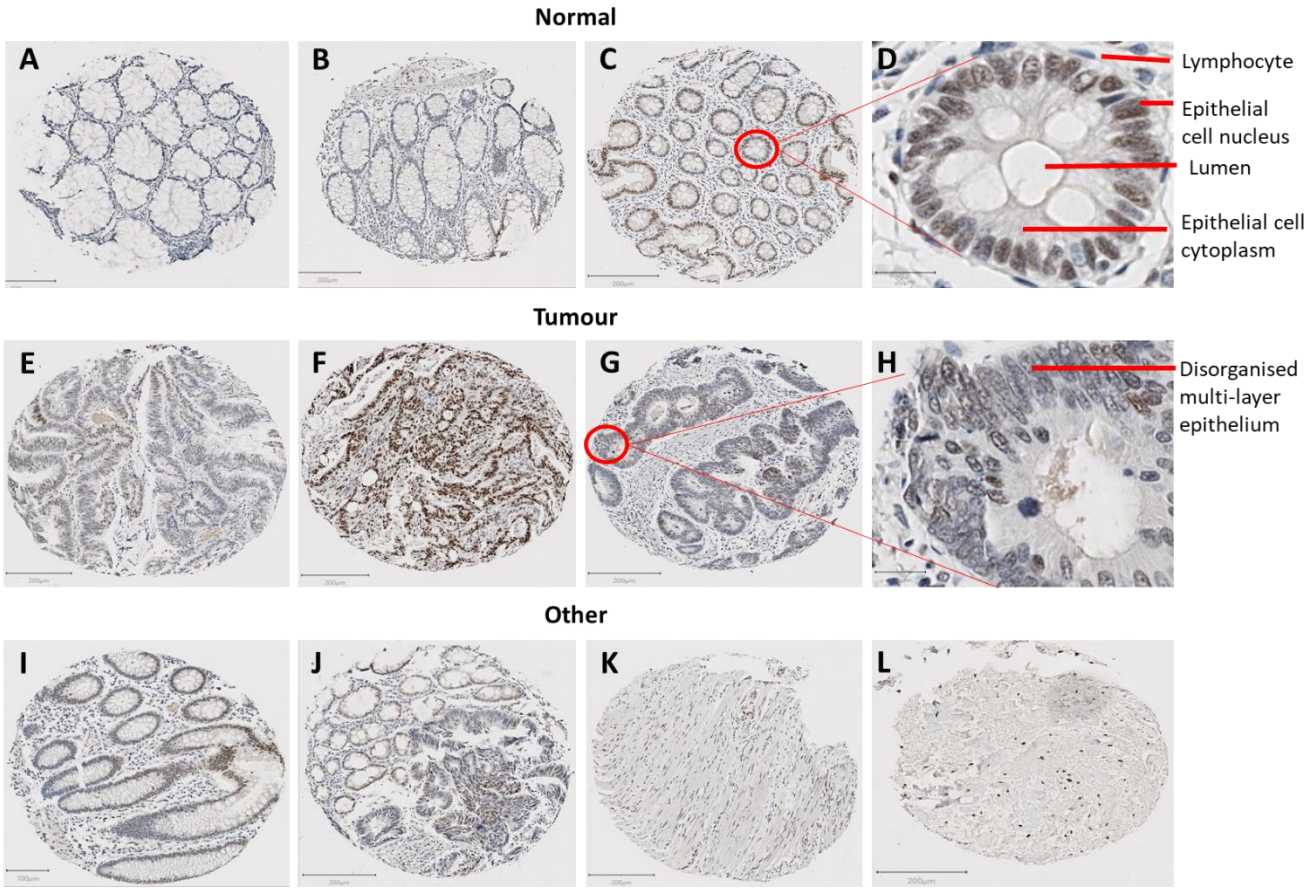

Figure 4.3 Distinguishing tumour from normal colonic epithelium. (A-C) Examples of normal colon tissue distinguished by well-organised glands, with a magnified 40x image of a gland depicted in (D). (E-G) Examples of tumour colon tissue distinguished disorganised and multi-layered epithelium, with a magnified 40x image of a gland depicted in (H). (I-J) Examples of cores containing both normal and tumour regions of epithelium. (K-L) Examples of cores classified as tumour but containing only stroma.

For the H-scoring method of immunohistochemical analysis, the cells identified as epithelial as discussed above are categorised by a staining intensity score. As the FOSL2 staining yielded a good differential staining pattern, 4 intensities were defined. These were categorised as 0 (negative staining) followed by 1-3 representing increasing intensity of staining. Epithelial cells representing each defined intensity score are presented in Figure 4.4. Finally, in order to obtain the H-score for each core, the percentage of each staining intensity within the epithelium was estimated. The calculation shown in Figure 4.5A was used to calculate the overall H-score (ranging from 0-300), with example scores shown in Figure 4.5B-D.

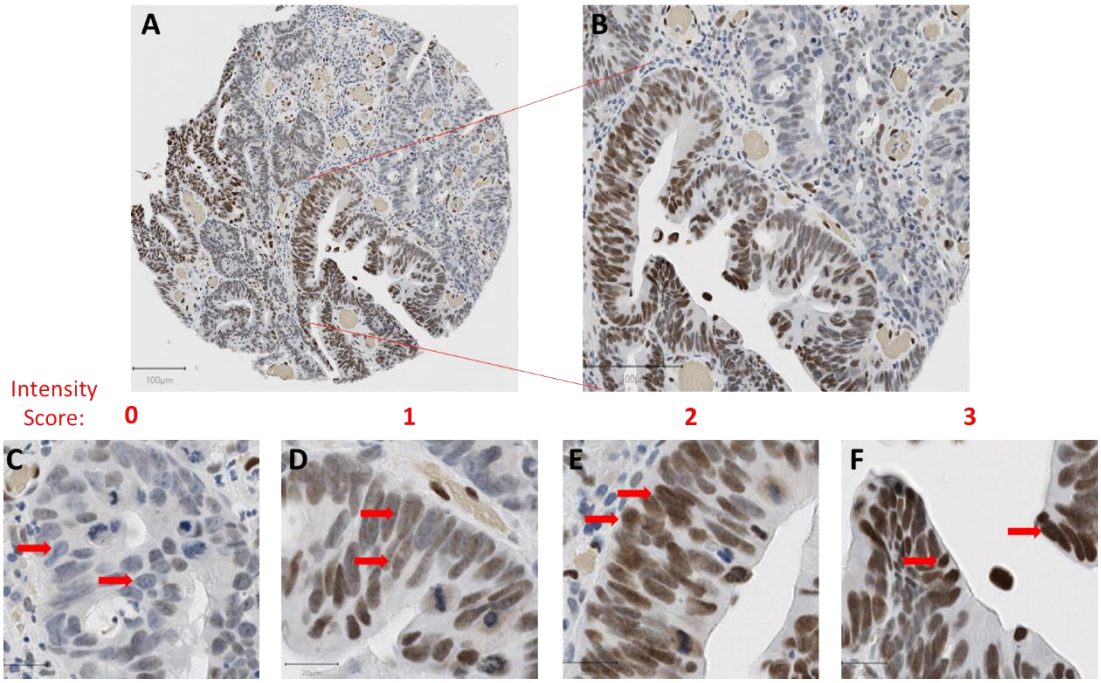

Figure 4.4 Categorising FOSL2 stain intensity scores for the H-scoring method. (A) A representative tumour core displaying FOSL2 stain intensities of all defined levels, with the selected region magnified in (B). Stain intensity levels of 0 or negative (C), 1 (D), 2 (E) and 3 (F). Red arrows point to cells displaying the given intensity. Scale bar represents 20µM for C-F.

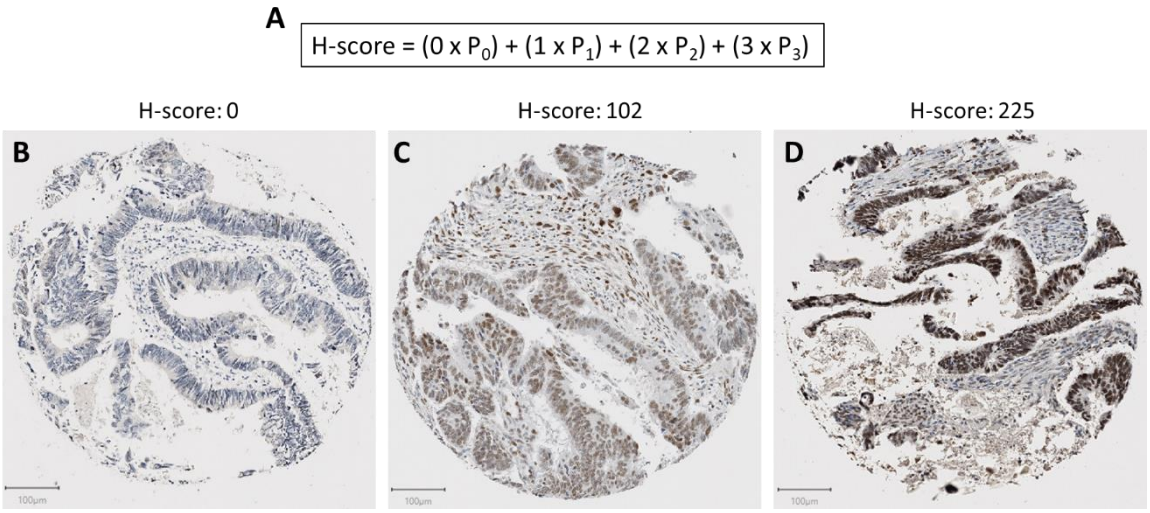

Figure 4.5 Calculating the H-score. (A) Calculation used to calculate the H-score based on the percentage estimates for each staining intensity as defined in Figure 4.4. (B-D) Example H-scores for 3 tumour cores ranging from 0 to 225.

4.3.2 FOSL2 Clinical Associations Across the Whole Tumour

The H-scores of the 1017 CRC tumour cores were established using the calculation as described. This spreadsheet was then passed on to Declan Sculthorpe to analyse and cross-tabulate these scores against the information on clinical characteristics that the group holds for the CRC TMA within SPSS. The summary statistics for the dataset as a whole (normal and tumour cores together) are presented in Table 4.1. Of the 1017 cores present across the 15 slides, 912 were successfully scored and 105 were considering missing. This is due to cores that were either washed away or contained, for example, only stroma and no epithelium as depicted in Figure 4.3. H-score values ranged from a minimum of 0 to a maximum of 253, with an average score of 48, presenting data that is distributed toward the lower staining values. This means that the data is positively skewed, with a skewness value of 1.156. The kurtosis is 0.768, indicating a slightly leptokurtic distribution. The distribution of the dataset is presented graphically in the histogram in Figure 4.6.

FOSL2 Summary Statistics

N	Valid	912
	Missing	105
Mean		48.8388
Median		31.0000
Mode		.00
Skewness		1.156
Std. Error of Skewness		.081
Kurtosis		.768
Std. Error of Kurtosis		.162
Minimum		.00
Maximum		253.00
Percentiles	25	9.0000
	33.33333333	15.0000
	50	31.0000
	66.66666667	58.0000
	75	77.7500

Table 4.1. Descriptive statistics for FOSL2 H-scores valid for analysis.

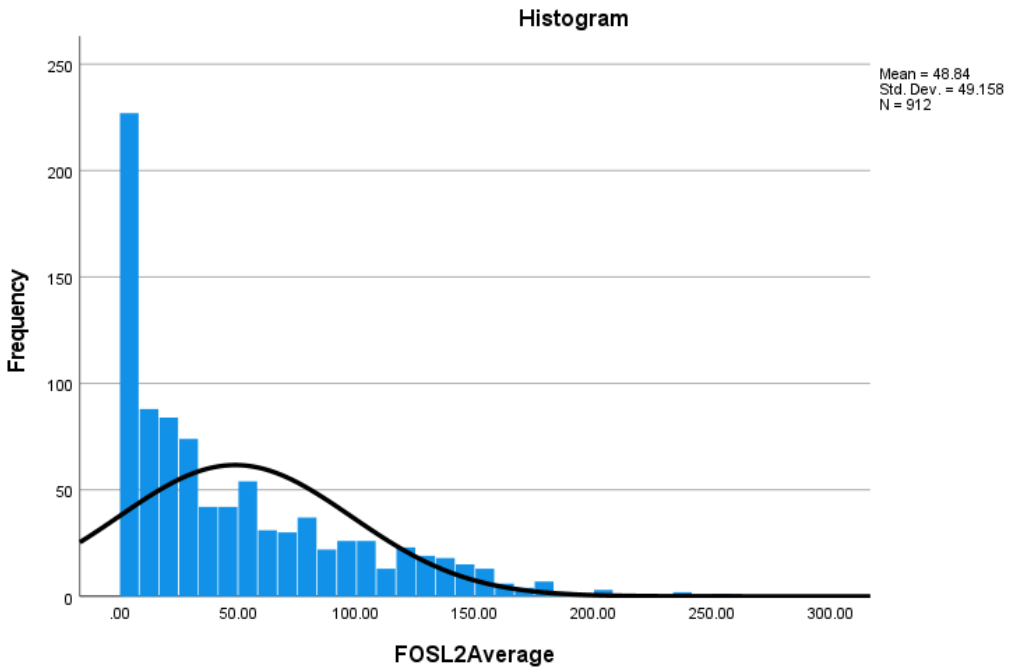

Figure 4.6 Histogram depicting the distribution of FOSL2 H-scores.

In order to characterise how FOSL2 expression correlates with clinical variables, H-scores for FOSL2 were divided into two groups which were defined as the lowest FOSL2-expressing tertile against all other expressors. The reason for this method of analysis was due to the fact that, as demonstrated by the histogram, the data is not normally distributed. Therefore, the median value cannot be used for the cut-off to separate 2 groups of FOSL2 expressors. Tertiles were therefore selected for the data. The lowest tertile was assigned the value of '1' whilst all other expressors (the highest two-thirds of H-scores) were assigned the value of '2' allowing for binary analysis. The reason for the selection of lowest FOSL2 expression against all others was that this method of analysis yielded results with more significant p-values. However, as discussed after this method, highest expressors vs all others was also used for comparison. The data was analysed against clinical variables using the chi-squared statistical test as the data represents two independent categorical variables. Table 4.2 lists all of the clinical variables and associated categories that the data was cross-tabulated against. These include the generic parameters such as gender, age, survival status and information about tumour grade, location and metastasis. Other parameters analysed include vascular invasion (EMVI, invasion beyond muscularis propria), perineural invasion (tumour presence in space surrounding a nerve) and

lymphovascular invasion (tumour cells within vascular or lymphatic spaces). The tumour edge is defined as infiltrative (with protrusions) or pushing (rounded) and tumour budding refers to single or clusters of cells at the invasive margin. Peri-tumoural lymphocytes are defined as lymphocytes surrounding the tumour. Finally, MMR status refers to mismatch repair proficiency or deficiency.

Clinicopathological Variable	Categories
Gender	Female
	Male
Age	Under 50
	Over 50
3-year Survival Status	Alive
	Deceased
5-year Survival Status	Alive
	Deceased
Disease Recurrence	No Recurrence
	Recurrence
Tumour Location	Right Colon
	Left Colon
	Rectum
	Transverse Colon
Tumour Stage	T1
	T2
	T3
	T4
Nodal Stage	N0
	N1
	N2
Metastasis	Absent
	Present
Tumour Grade	G1
	G2
	G3
Vascular Invasion (EMVI)	Absent
	Present
Perineural Invasion	Absent
	Present
Lymphovascular Invasion	Absent
	Present
Tumour Edge	Infiltrative
	Pushing
Tumour Budding	Low
	High
Peritumoral Lymphocytes	Inconspicuous
	Conspicuous
MMR Status	Proficient
	Deficient

Table 4.2. Clinicopathological variables that FOSL2 expression was analysed against including their respective categories.

Initially, the analysis was performed by combining FOSL2 H-scores across the tumour samples taken per patient and comparing the lowest tertile against all others by performing a Chi-squared test as previously described. These were cross-tabulated against all clinicopathological variables listed in Table 4.2. Across all samples averaged, 5 correlations with clinicopathological variables were statistically significant, shown in a graph format in Figure 4.7. The adjusted residual values are presented with the p-value for the association. The adjusted residues are the raw residuals (the difference between the observed and expected counts) divided by an estimate of the standard error. An adjusted residual that is more than 2.0 indicates that the number of cases in that cell is significantly larger than would be expected if the null hypothesis were true. Positive adjusted residual values represent greater than expected effects and therefore represent the direction of the statistical significance. These include gender, where the lowest tertile of FOSL2 expression were statistically associated with being male, and conversely the higher expression of FOSL2 (all other expressors) with female ($p=0.004$) (Figure 4.7A). The 5-year survival status demonstrated that the lowest expressors were statistically significantly associated with the deceased category and the highest expressors with alive ($p=0.02$) (Figure 4.7B). This is supported by findings from the tumour stage, where the lowest expressors were most likely to be tumour stage 3. However, higher FOSL2 expression was associated with tumour stages 1, 2 and 4 ($p=0.024$) (Figure 4.7E). For the tumour edge characteristic, higher FOSL2 expression was associated with an infiltrative phenotype whereas lower FOSL2 expression was associated with a pushing phenotype ($p<0.001$) (Figure 4.7C). Finally, low levels of tumour budding were associated with low FOSL2 expression whilst high levels were associated with higher levels of FOSL2 expression ($p<0.001$) (Figure 4.7D).

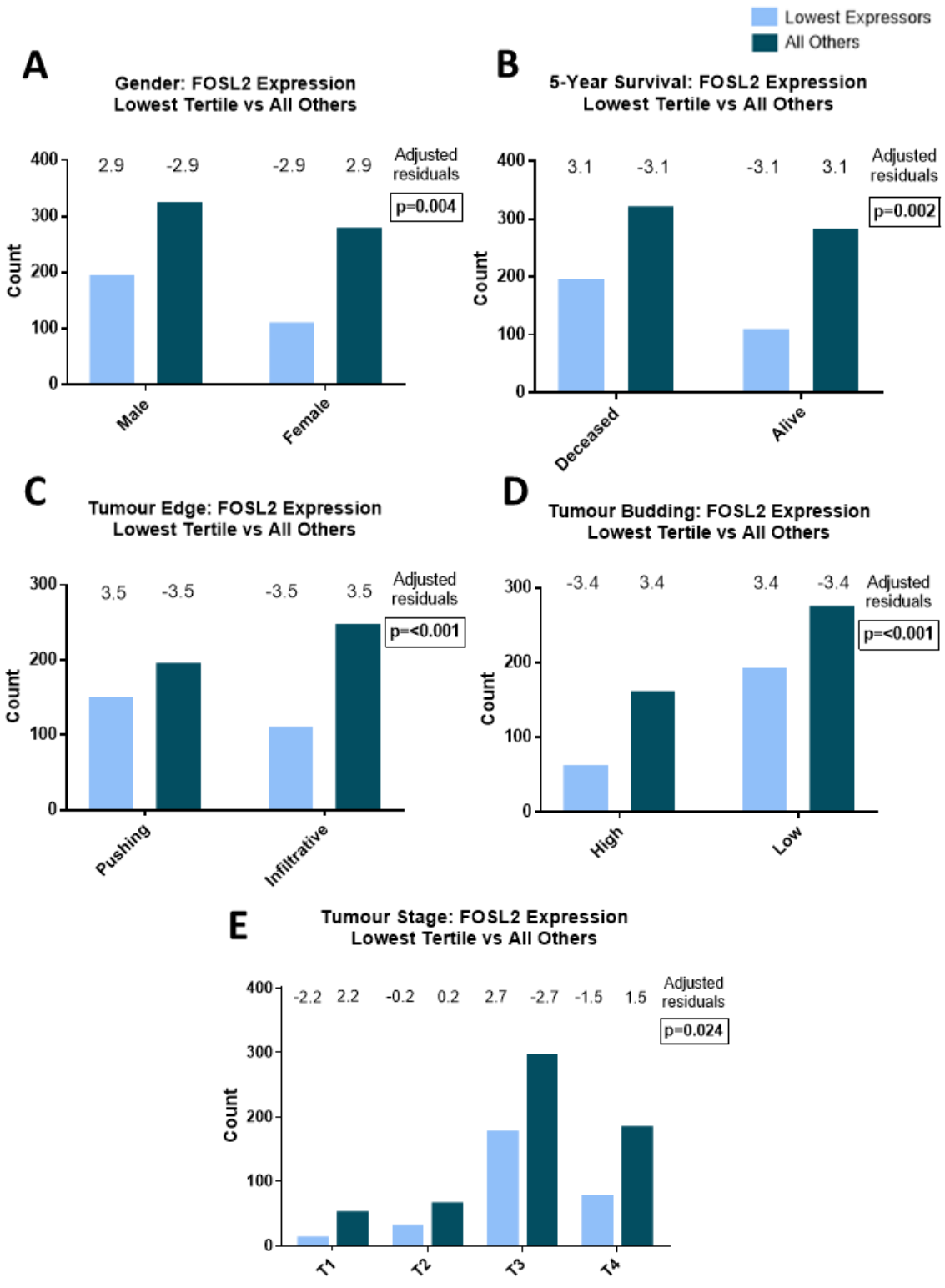

Figure 4.7 Statistically significant associations of FOSL2 expression averaged across all tumour regions. Data were analysed using the chi-squared statistical test with adjusted residuals and p-value shown. The positive adjusted residual indicates direction of significance.

In addition to correlating with clinicopathological variables as stated, the average FOSL2 H-scores were also used to generate a Kaplan-Meier plot to investigate the correlation between FOSL2 expression and patient survival (Figure 4.8). In line with the above findings, lower expression of FOSL2 is associated with a worse patient outcome and decreased survival while conversely, higher FOSL2 expression is associated with better survival.

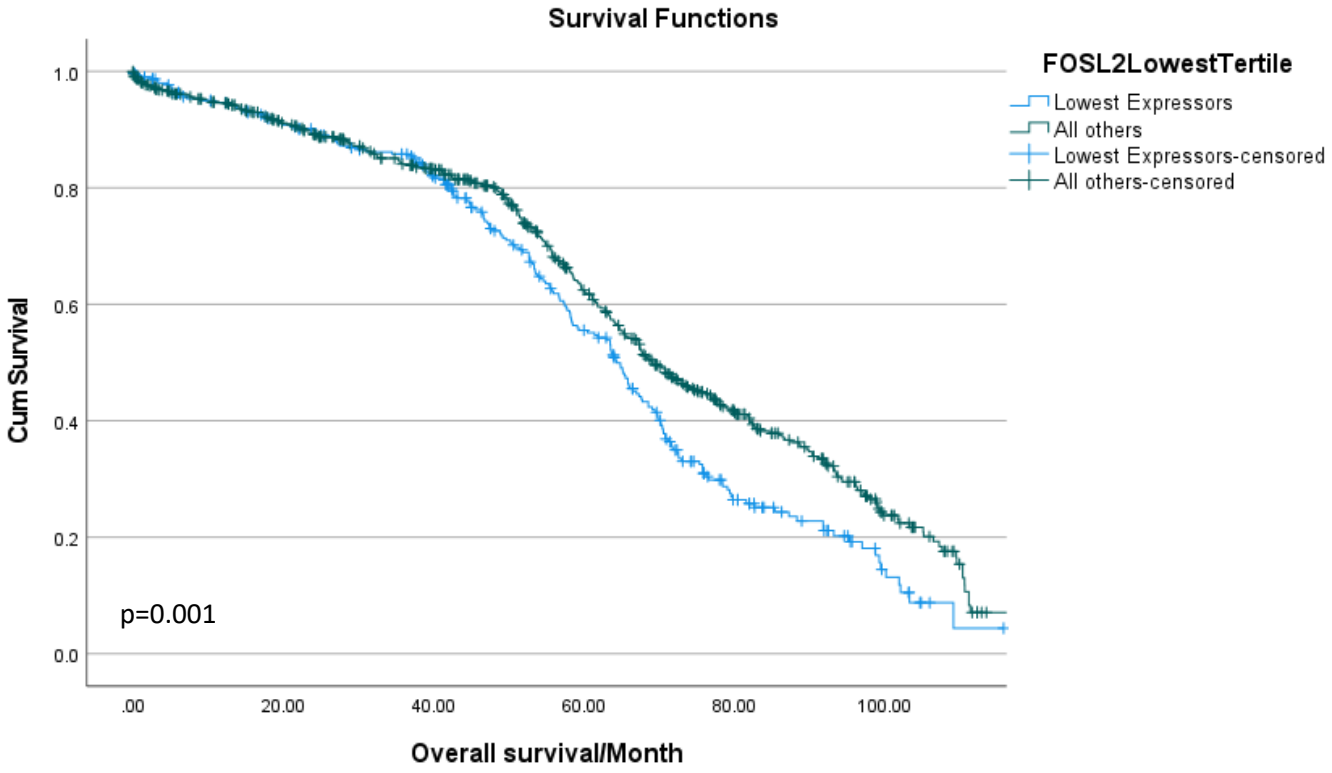

Figure 4.8 Kaplan-Meier plot of cumulative survival against overall survival/month for FOSL2 expression.

4.3.3 FOSL2 Clinical Associations in the Tumour Centre

The above results demonstrate significant findings for FOSL2 expression when taken across all tumour regions. The next analysis performed was to look at different regions of the tumour and cross-tabulate these FOSL2 H-scores against the same clinicopathological variables, allowing us to determine where the significances identified in the previous analysis are arising from. Three statistically significant associations between FOSL2 expression and clinical variables in the central tumour were identified (Figure 4.9). Firstly, lowest FOSL2 expressors were significantly associated with the deceased category for 5-year survival, and conversely the highest FOSL2 expressors with 'alive' (p=0.015, Figure 4.9A). This was found also across the whole tumour (Figure 4.7) and also in the Kaplan-Meier analysis. Interestingly, low FOSL2 expression was clinically associated with the absence of perineural invasion, whilst higher FOSL2 expression is associated with the presence of perineural invasion (p=0.045, Figure 4.9B). Finally for the central tumour analysis, low FOSL2 expression was associated with low levels of tumour budding, whilst higher levels of FOSL2 were associated with high tumour budding (p=0.004, Figure 4.9C).

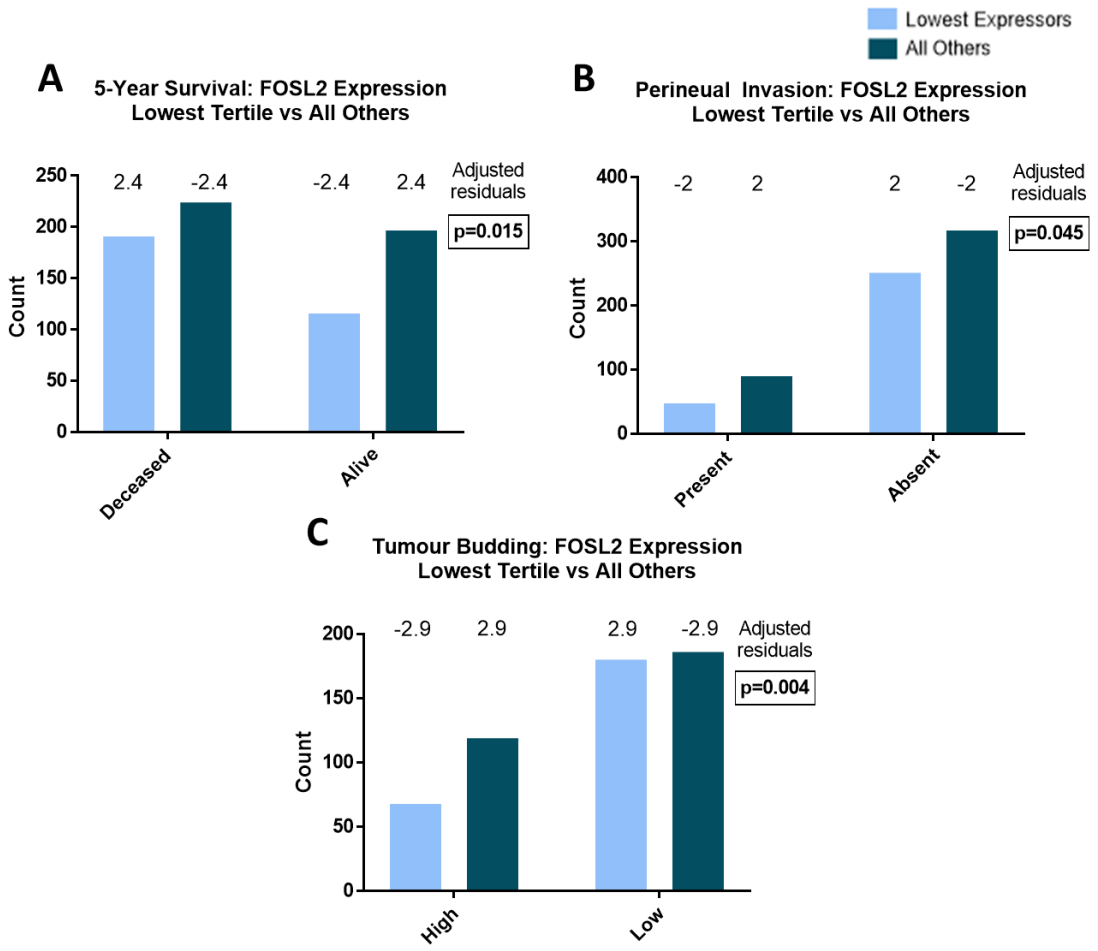

Figure 4.9 Statistically significant associations of FOSL2 expression in the central tumour. Data were analysed using the chi-squared statistical test with adjusted residuals and p-value shown. The positive adjusted residual indicates direction of significance.

4.3.4 FOSL2 Clinical Associations in the Advancing Edge

Finally, the analysis of FOSL2 expression against clinical variables was performed for H-scores obtained from the advancing edge samples. Two significant associations were identified for this region (Figure 4.10). Firstly, at the advancing edge, gender was found as a significant association as per the average tumour results, with low FOSL2 expression was associated with being male whilst higher expression was associated with females (p=0.006, Figure 4.10A). Next, the tumour edge phenotype came up at the advancing edge, where low FOSL2 expression was associated with a pushing edge phenotype whilst higher FOSL2 expression was associated with an infiltrative edge phenotype (p=0.008, Figure 4.10B).

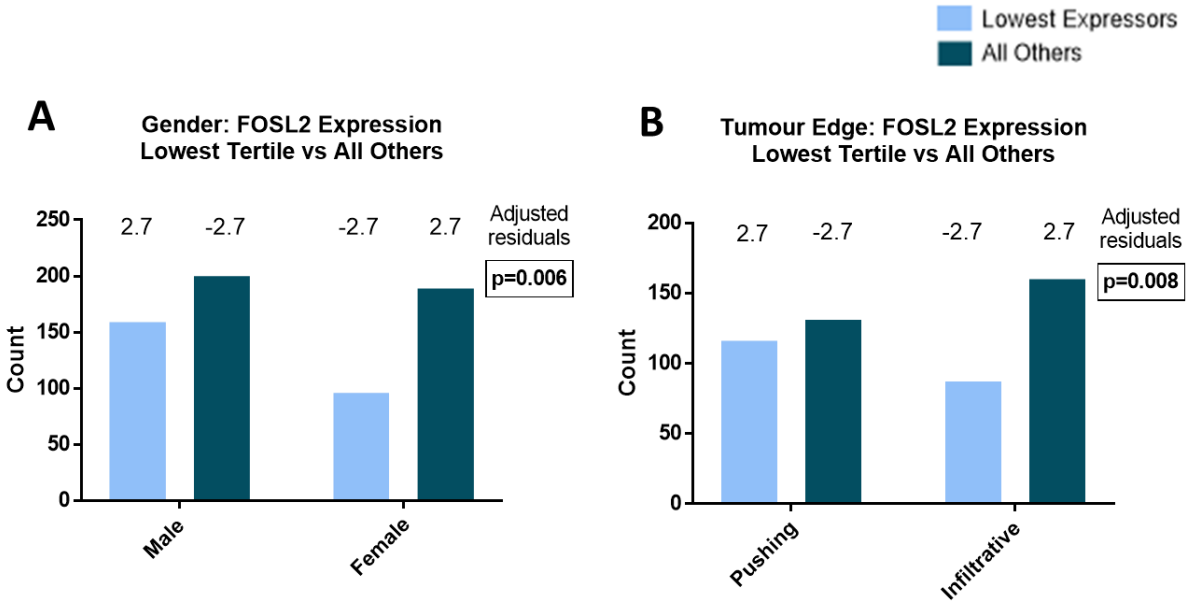

Figure 4.10 Statistically significant associations of FOSL2 expression at the advancing edge of the tumour. Data were analysed using the chi-squared statistical test with adjusted residuals and p-value shown. The positive adjusted residual indicates direction of significance.

4.3.5 FOSL2 Clinical Associations in Immune Cell Staining

In addition to H-scoring the tumour and normal epithelium for the TMA, the presence or absence of FOSL2 staining of the immune cells was also documented for each tumour core. These were not H-scored due to the lack of differential staining intensity, but a clear absence or presence of FOSL2 staining within these cells was easily identified and the subsequent binary analysis was then performed against the same clinicopathological variables. Figure 4.11 depicts an example of immune cell staining for FOSL2. Figure 4.11A shows a 5X magnification image of a tumour core with clear immune cell staining for FOSL2, as seen in the 20X magnification in Figure 4.11B. Conversely, Figure 4.11C shows a clear example of the absence of FOSL2 staining of the immune cells, seen more clearly in the 20X magnification in Figure 4.11D.

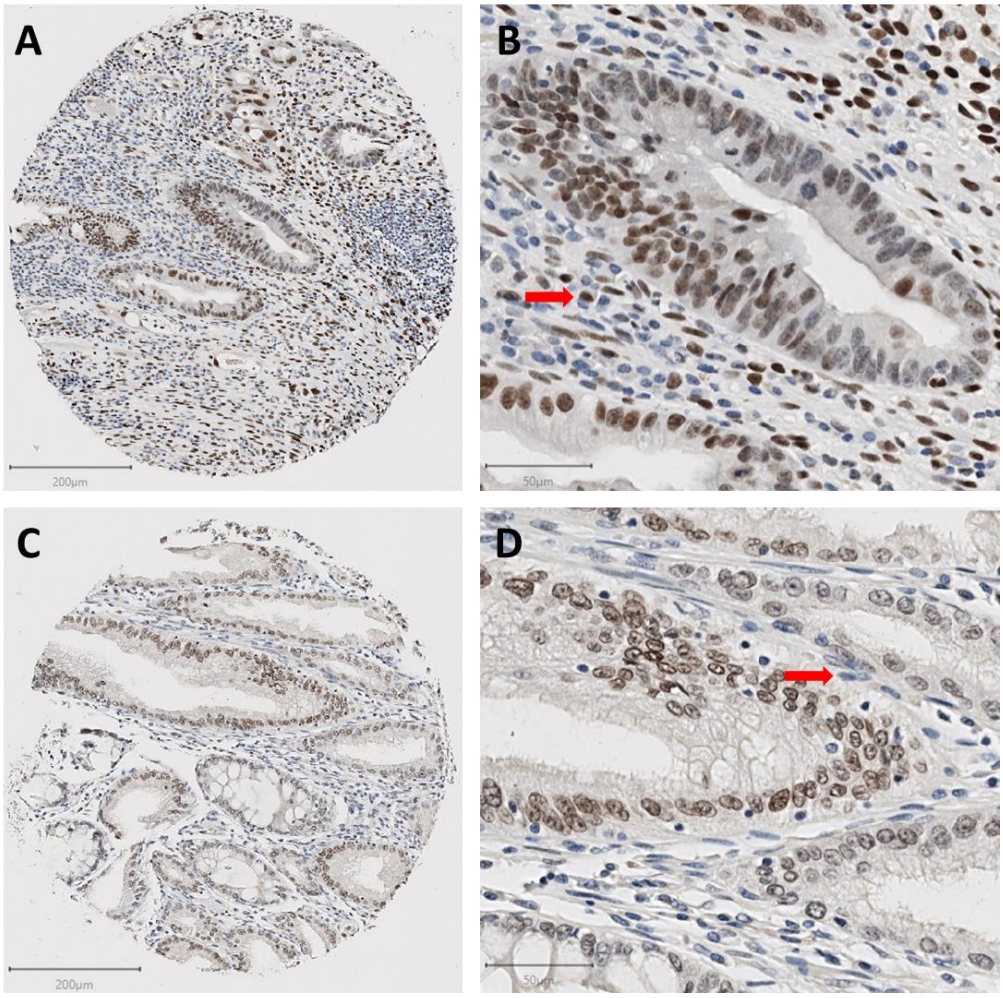

Figure 4.11 Example immune cell staining for FOSL2. (A) A 5X magnification of a tumour core depicting clear FOSL2 staining within immune cells, seen more clearly in the 20X image (B). (C) A 5X magnification of a tumour core depicting clear absence of FOSL2 staining within immune cells, seen more clearly in the 20X image (D).

The presence or absence of FOSL2 immune cell staining was analysed against the same clinicopathological variables as described for the epithelium. For luminal tumour cores, one statistically significant association was found for immune cell FOSL2 staining. Presence of immune cell staining was associated with a deficient MMR, whilst absence of immune cell staining was associated with MMR proficiency (p=0.007, Figure 4.12).

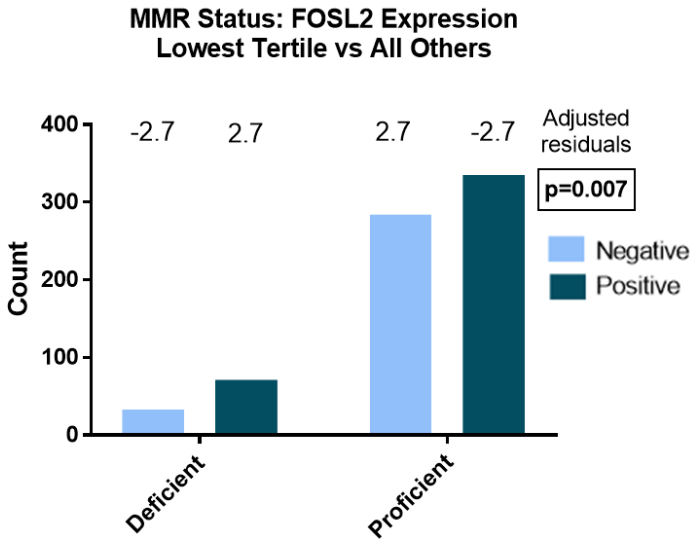

Figure 4.12 Statistically significant associations of FOSL2 absence or presence of immune cell staining in the luminal cores. Data were analysed using the chi-squared statistical test with adjusted residuals and p-value shown. The positive adjusted residual indicates direction of significance.

For tumour cores taken from the advancing edge of the tumour, 4 statistically significant associations were found between clinicopathological variables and FOSL2 presence or absence of immune cell staining, shown in Figure 4.13. Interestingly, positive FOSL2 staining of immune cells was significantly associated with the presence of metastasis, whilst negative staining was associated with absence of metastasis (p<0.001, Figure 4.13A). Regarding the phenotype of the tumour edge, positive immune cell FOSL2 staining was associated with an infiltrative tumour edge, whilst negative staining was associated with a pushing edge (p<0.001, Figure 4.13B). For tumour budding, positive FOSL2 immune cell staining was associated with high levels of tumour budding, whereas an absence of staining was associated with low levels of tumour budding (p=0.041, Figure 4.13C). Finally, positive immune cell FOSL2 staining

was associated with inconspicuous peritumoural lymphocytes, whereas negative immune cell staining was associated with conspicuous peritumoural lymphocytes (p=0.040, Figure 4.13D).

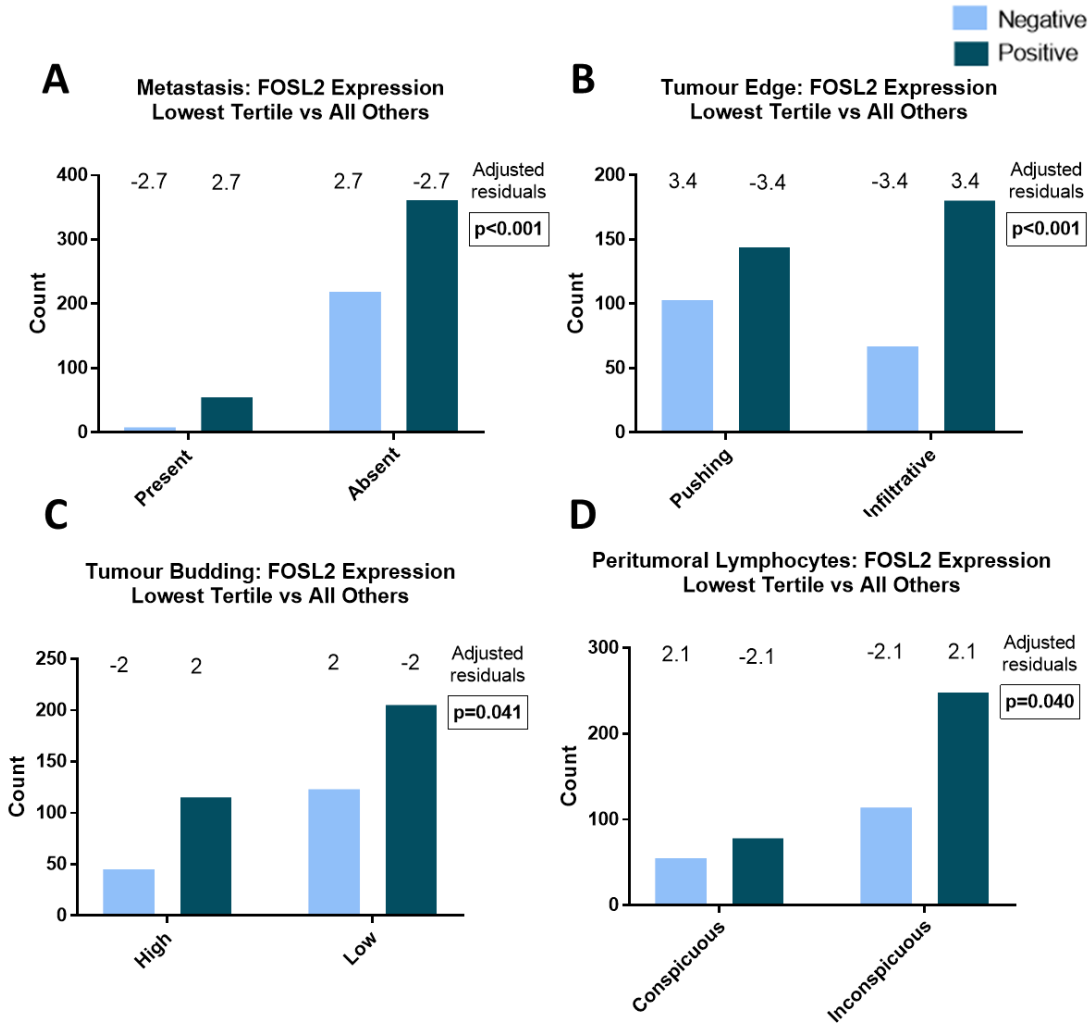

Figure 4.13 Statistically significant associations of FOSL2 absence or presence of immune cell staining at the tumour advancing edge. Data were analysed using the chi-squared statistical test with adjusted residuals and p-value shown. The positive adjusted residual indicates direction of significance.

4.3.6 Alternative Method of Analysis

As described toward the beginning of this chapter, the analysis was carried out by comparing low FOSL2 expressors vs all others due to this method yielding more significant p-values. The analysis was also carried out by splitting the highest FOSL2 expressor tertile against all others in order to see if similar conclusions could be drawn. Table 4.3 demonstrates statistically significant results yielded by this method of

analysis (for the tumour as an average).

Clinicopathological Variable	Average FOSL2 H-Score (Highest Tertile vs All Others Expression)		Adjusted residuals		p-value	Phenotype Associated with High FOSL2 Expression
	Highest Expressors (%)	All Others (%)	Highest Expressors	All Others		
Gender					**0.01**	**Female**
Female	113 (28.9%)	278 (71.1%)	2.4	-2.4		
Male	115 (22.1%)	406 (77.9%)	-2.4	2.4		
3-Year Survival Status					**0.03**	**Dead**
Alive	154 (23.2%)	509 (76.8%)	-2.0	2.0		
Dead	74 (29.7%)	175 (70.3%)	2.0	-2.0		
Tumour Stage					**0.02**	**Early Stage**
Early	53 (31.4%)	116 (68.6%)	2.1	-2.1		
Late	175 (23.6%)	568 (76.4%)	-2.1	2.1		
Tumour Budding					**0.007**	**High**
Low	92 (19.6%)	377 (80.4%)	-2.6	2.6		
High	64 (28.4%)	161 (71.6%)	2.6	-2.6		

Table 4.3 Statistically significant associations of FOSL2 expression across the average of the tumour regions when comparing the highest FOSL2 expressor tertile vs all others. Data were analysed using the chi-squared statistical test with adjusted residuals and p-value shown. The positive adjusted residual indicates direction of significance.

When compared to the previous method of analysis using lowest expressors vs all others, the gender 'Female' is still statistically significantly associated with high levels of FOSL2 expression (p=0.01). Interestingly, 3-year survival status becomes significantly associated with FOSL2 expression when performing the analysis this way around, with high FOSL2 associated with being dead after 3 years (p=0.03). Similarly to the previous analysis, high levels of FOSL2 are also associated with early tumour stage (p=0.02) and high levels of tumour budding (p=0.007), although the association of FOSL2 with an infiltrating tumour edge no longer features as statistically significant.

4.3.7 Clinicopathological Analysis Split by Gender

Additional analysis was performed in order to identify if statistically significant associations of FOSL2 expression were attributable to one gender over the other. Table 4.4 shows statistically significant associations of FOSL2 expression (highest expressors vs all others) when studying samples from male patients only. As evident, most of the associations that appeared in the previous analysis are no longer statistically significant. However, in the male population, high FOSL2 expression is associated with high tumour grade (p=0.004).

Clinicopathological Variable	Average FOSL2 H-Score (Highest Tertile vs All Others Expression)		Adjusted residuals		p-value	Phenotype Associated with High FOSL2 Expression
	Highest Expressors (%)	All Others (%)	Highest Expressors	All Others		
Tumour Grade					**0.004**	**High Grade**
Low	99 (20.5%)	383 (79.5%)	-3.0	3.0		
High	16 (41%)	23 (59%)	3.0	-3.0		

Table 4.4 Statistically significant associations of FOSL2 expression across the average of the tumour regions when comparing male highest FOSL2 expressor tertile vs all others. Data were analysed using the chi-squared statistical test with adjusted residuals and p-value shown. The positive adjusted residual indicates direction of significance.

Table 4.5 shows statistically significant associations of FOSL2 expression (highest expressors vs all others) when studying samples from female patients only. It is clear that most of the statistical significance arising from the combined analysis is attributable to female patients. This time, high FOSL2 expression is significantly associated with being dead for 3-year survival analysis (p=0.03) and for overall survival analysis (p=0.006). Additionally, in the female population, high FOSL2 expressors are associated with early tumour stage (p=0.05) and high levels of tumour budding (p=0.03).

Clinicopathological Variable	Average FOSL2 H-Score (Highest Tertile vs All Others Expression)		Adjusted residuals		p-value	Phenotype Associated with High FOSL2 Expression
	Highest Expressors (%)	All Others (%)	Highest Expressors	All Others		
3-Year Survival Status					**0.03**	**Dead**
Alive	75 (26.1%)	212 (73.9%)	-2.0	2.0		
Dead	38 (36.5%)	66 (63.5%)	2.0	-2.0		
Overall Survival Status					**0.006**	**Dead**
Alive	18 (18.6%)	79 (81.4%)	-2.6	2.6		
Dead	95 (32.3%)	199 (67.7%)	2.6	-2.6		
Tumour Stage					**0.05**	**Early Stage**
Early	26 (38.2%)	42 (61.8%)	1.9	-1.9		
Late	87 (26.9%)	236 (73.1%)	-1.9	1.9		
Tumour Budding					**0.03**	**High**
Low	47 (23.7%)	151 (76.3%)	-2.1	2.1		
High	34 (35.4%)	62 (64.6%)	2.1	-2.1		

Table 4.5 Statistically significant associations of FOSL2 expression across the average of the tumour regions when comparing female highest FOSL2 expressor tertile vs all others. Data were analysed using the chi-squared statistical test with adjusted residuals and p-value shown. The positive adjusted residual indicates direction of significance.

4.3.8 FOSL2 Correlation with Additional Markers

Finally, the expression of FOSL2 was correlated with several other proteins of interest that had been stained and H-scored previously on the same TMA, and so this data was readily available for use. Importantly, CA9 had previously been stained and scored on this TMA and was of importance due to its role as a hypoxic marker. It was found that, as indicated by the previous *in vitro* data, low CA9 expression was significantly correlated with low FOSL2 expression and conversely, high CA9 with high FOSL2 expression (p=0.002, Figure 4.14A). This correlation was found when FOSL2 scores across the whole tumour were analysed. This significant correlation remained when cores from the centre of the tumour were analysed (p=0.02, Figure 4.14B) where CA9 would play the most important role. The association was lost at the advancing edge of the tumour, where CA9 would not be playing a significant role. 2 other statistically significant results were identified when FOSL2 expression across the whole tumour was cross-tabulated with other markers previously studied. As shown in Figure 4.14C, low levels expression of membrane-bound β-catenin were statistically significantly associated with high levels of FOSL2, and conversely, high levels of membrane-bound β-catenin with low levels of FOSL2 (p=0.02). Finally, Figure 4.14D presents the final association where low levels of FOSL2 were statistically significantly associated with low levels of nuclear cMyc, and conversely high levels of FOSL2 with high levels of nuclear cMyc (p=0.008). Table 4.6 summarises all statistically significant findings resulting from the TMA analysis.

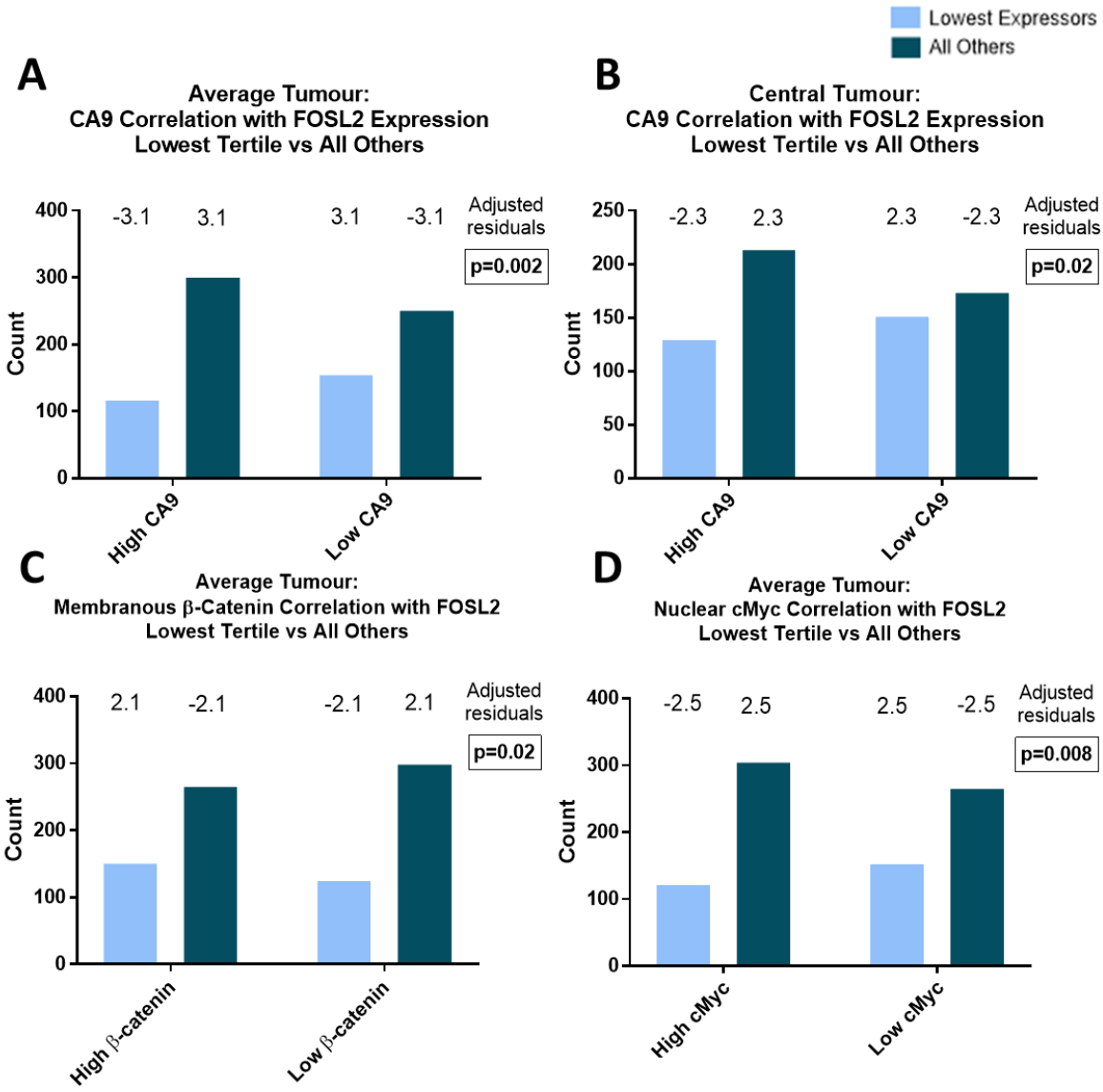

Figure 4.14 Statistically significant associations of FOSL2 expression with additional markers. Data were analysed using the chi-squared statistical test with adjusted residuals and p-value shown. The positive adjusted residual indicates direction of significance.

FOSL2 Expression in Epithelium				
Clinicopathological Variable	**Phenotype Associated with High FOSL2 Expression**	**Tumour Region**		
		Average (All Regions)	**Central**	**Advancing Edge**
Gender	Female	p=0.004		p=0.006
5-Year Survival	Alive	p=0.002	p=0.015	
Tumour Edge	Infiltrative	p<0.001		p=0.008
Tumour Budding	High	p<0.001	p=0.004	
Tumour Stage	Stage 1 Stage 4	p=0.024		
Perineural Invasion	Presence		p=0.045	
FOSL2 Staining in Immune Cells				
Clinicopathological Variable	**Phenotype Associated with Positive FOSL2 Staining**	**Tumour Region**		
		Average (All Regions)	**Luminal**	**Advancing Edge**
MMR Status	Deficiency		p=0.007	
Metastasis	Present			p<0.001
Tumour Edge	Infiltrative			p<0.001
Tumour Budding	High			p=0.041
Peritumoral Lymphocytes	Inconspicuous			p=0.04
FOSL2 Correlation with Additional Markers				
Marker	**Expression Associated with High FOSL2**	**Tumour Region**		
		Average (All Regions)	**Central**	**Advancing Edge**
CA9	High	p=0.002	p=0.02	
Membranous β-catenin	Low	p=0.02		
Nuclear cMyc	High	p=0.008		

Table 4.6. A summary of all statistically significant results when analysing FOSL2 expression associations with clinicopathological variables.

4.4 Discussion

4.4.1 Association of FOSL2 with Pro-Metastatic Variables

The use of a large colorectal cancer tissue micro-array was used to assess the correlation of FOSL2 expression with a broad range of clinicopathological variables. This allowed for analysis of data from biopsies obtained from over a thousand CRC patients and is therefore an extremely valuable research tool. In terms of methodological limitations, it has been suggested that 0.6mm biopsies of paraffin-embedded tissue may not represent the full region of the tumour accurately. However, many studies have validated the accuracy and clinical relevance of the technique, comparing IHC findings from TMAs with corresponding larger sections from solid tumours, the vast majority of which finding a high level of concordance between the two[267]. However, for this project, H-scoring was performed without digital assistance or bioinformatic software. This is due to limitations in software currently available to us, for example the inability to accurately discern between normal and tumour epithelium. It was therefore decided alongside clinical histopathologist Dr Abhik Mukherjee to score the TMA using manual techniques.

Interestingly, high FOSL2 expression was associated with several clinicopathological variables that are intrinsically linked to invasion and metastasis. These include high levels of tumour budding, correlated in the average and central tumour, and an 'infiltrative' tumour edge phenotype, correlated in the average and advancing edge samples. Tumour budding has been recognised as a marker of aggressive tumour behaviour, and therefore supplements the current TNM staging system as an 'additional prognostic factor' in CRC[268]. The process of tumour budding involves the detachment of clusters of up to five tumour cells at the invasive front of CRC, allowing invasion of the peritumoural tissue and subsequent invasion into lymphatic and blood vessels. Tumour budding has been linked to epithelial-to-mesenchymal transition (EMT), which is also associated with the activation of Wnt signalling[269]. In tumour-budding cells, β-catenin is found highly expressed in the nuclei of cells as opposed to the cytoplasm or membrane, alongside expression of target genes such as ZEB1 and SLUG, indicating an activation of Wnt signalling[270]. This represents a very interesting

link to FOSL2, as high FOSL2 was correlated with high levels of tumour budding. Furthermore, high levels of FOSL2 were significantly correlated with low levels of membrane-bound β-catenin when cross-tabulated against other markers analysed on the same TMA. This implies higher levels of β-catenin in the nucleus, potentially through regulation by FOSL2, providing a possible mechanistic link to the associated phenotype of tumour budding. Further analysis of this is necessary to confirm higher levels of β-catenin in the nucleus by association with FOSL2. Interestingly, the tumour budding phenotype has been shown to be associated with tumour hypoxia associated with hypovascularisation, which may be associated with FOSL2 under hypoxic conditions[271].

Within the tumour epithelium, high FOSL2 was also correlated with an 'infiltrative' advancing edge phenotype. It is known that an infiltrative edge is a hallmark of aggressive tumours, and as such has been classified as an independent adverse prognostic indicator[272]. Finally within the central tumour regions, FOSL2 was also associated with perineural invasion (PNI). PNI is defined as invasion spreading in or around neural tissue and along nerve sheaths, and unsurprisingly is associated with poor prognosis[273]. Despite significant associations with tumour budding, infiltrative edge and PNI, FOSL2 expression within tumour epithelium was not correlated with metastasis, although there was an association with tumour stage 4. Within the field, the presence of additional clinicopathological factors including tumour budding, infiltrative edge and perineural or lymphovascular invasion is being increasingly recognised to determine an accurate prognosis alongside the classical TNM system. This is because patients with a lower TNM stage have been found to exhibit a worse prognosis than patients of a higher tumour stage when these additional factors are present[272]. Thus, despite not being involved in metastasis directly within the tumour epithelium, it is possible that FOSL2 may be initiating the early stages of invasion through these defined mechanisms of tumour budding and local invasion of nerve or lymphatic tissue. Future work for the role of FOSL2 in CRC may therefore seek to determine the regulation of invasion by FOSL2 in tumour hypoxia, and hypoxia is a known driver of invasion and metastasis. Importantly, high levels of FOSL2 were correlated with high CA9 within the central tumour, demonstrating that FOSL2 is

localising to and exerting effects within the hypoxic regions of tumours as hypothesised. An interesting follow-up would be to stain the same TMA for markers that distinguish between the CMS1-4 subtypes, and to see if FOSL2 plays a more important role in certain subtypes, and if certain subtypes were more hypoxic (correlated with CA9) than others.

4.4.2 Association of FOSL2 with Patient Survival

A significant association was found between high FOSL2 expression and 'alive' status for 5-year survival. It is important to consider several factors involved in the complexity of the AP1 transcription factor, and future work will need to fully elucidate the mechanisms involved. For example, it is well known that AP1 subunits have the capability of acting as either oncogenes or tumour suppressors in a context-dependent manner. In fact, research has highlighted a novel class of proteins which are able to function as 'double agents' in terms of performing both oncogenic and tumour suppressor roles depending on the cellular context, and more than half of these were identified to be transcription factors[274]. In the case of c-Jun, one of the most well-known oncogenic AP1 subunits, c-Jun also has the capacity to perform tumour suppressor roles depending on the context. For example, c-Jun works with FOSL1 to upregulate the expression of tumour suppressor $p14^{ARF}$/$p19^{ARF}$ in the context of over-expressed H-Ras[275]. The oncogenic and tumour suppressor functions of FOSL2 in both cancer and hypoxia are less well elucidated. As FOSL2 does not act alone, it would be of great importance to characterise the FOSL2 interactome within tumours, and how dimerisation partners and dynamics (and subsequent FOSL2-associated transcriptomes) changes across tumour regions and also tumour stage. It is possible that a molecular switch exists, where FOSL2 goes from hypoxia-induced regulation of invasion to performing a more tumour suppressive role. In addition to this, it is important to consider that the TMA was measuring FOSL2 expression, and not activation status. As previously described, it is the phosphorylated and activated form of FOSL2 that mediates its transcriptional functions. It may be increased, non-activated FOSL2 that antagonises the formation of alternative AP1 dimers, whilst a lower level of activated FOSL2 mediates its oncogenic functions.

4.4.3 Role of FOSL2 in Immune Cells

In addition to identifying the clinical associations of FOSL2 expression within the tumour epithelium, results were also obtained for FOSL2 positive or negative staining within the lymphocytes and stromal cells surrounding the epithelium. The results were very interesting, as it was found that FOSL2-positive lymphocyte staining was significantly associated with metastasis, infiltrative edge, high tumour budding and inconspicuous peritumoural lymphocytes at the advancing edge tumour cores. This raises the interesting and unexplored possibility that FOSL2 within the tumour-associated immune cells may be regulating aggressive and metastatic tumour phenotypes, which warrants further investigation. Interestingly, FOSL2 has been identified in the literature as playing a role in cancer-associated stroma. For example, increased FOSL2 in breast cancer-associated fibroblasts (CAFs) has been associated with VEGF-independent angiogenesis and clinical progression in patients, as well as tumour growth *in vivo*[244]. In lung cancer, FOSL2 has been identified as regulating a switch from M1 to M2-tumour associated macrophages (TAMs), influencing lung tumour development and poor patient prognosis through regulation by β-catenin[276]. In colorectal cancer, TAMs have been shown to promote tumour proliferation, invasion and metastasis[277].

5.0 Investigating the Role of FOSL2 in Hypoxic Phospho-Signalling

5.1 Introduction

5.1.1 Targeting Signal Transduction in CRC

Whilst a variety of signalling pathways are disrupted in cancer, kinase signalling cascades are of particular therapeutic importance due to the prevalence of cancer-driving mutations occurring within this category of proteins, alongside their enhanced targetability[278]. Many genes commonly mutated in cancer, including CRC, encode members of the PI3K-Akt and MAPK pathways. Both pathways lie downstream of RAS signalling, where a RAS-GTPase is activated by a receptor tyrosine kinase (RTK). KRAS mutations are found across all subtypes of CRC, most notably in 68% of CMS3 tumours[46,279]. PI3Ks may be activated by RAS and catalyse the phosphorylation of PIP2 to PIP3, which serves as a second messenger for a variety of downstream pathways[280]. Conversely, PTEN acts as a tumour suppressor by catalysing the dephosphorylation of PIP3 and therefore serves as a negative regulator of PI3K signalling. PIK3CA activating mutations and PTEN mutations and deletions are common events in CRC, which, when combined, are found in around 40% of large bowel tumours[281–283].

The mitogen-activated protein kinase (MAPK) pathway is another pathway downstream of RAS signalling that is implicated in many cancers including CRC[284]. Activation of RAS as described above in turn leads to the activation of a series of MAPKs, beginning with a MAPKKK such as Raf1, followed by a MAPKK such as MEK1/2 and finally a MAPK such as ERK1/2[285]. Activated MAPKs are able to translocate to the nucleus, where they are involved in the phosphorylation of a number of transcription factors including STAT1 and c-Myc that in turn regulate the transcription of genes involved in many different cellular processes[286]. The BRAF V600E mutation is commonly found in CRCs, occurring in around 8% of cases and is associated with poor prognosis. The mutation leads to conformational changes within the catalytic domain

of the enzyme, leading to constitutively activated BRAF independently of upstream RAS activation[287,288].

EGFR has been a favourable target for mCRC due to overexpression in many cancers including colorectal cancer. However, monoclonal antibodies targeting EGFR such as cetuximab show limited efficacy in a subset of patients[289,290]. This is due to oncogenic mutations in genes encoding downstream signalling transducers leading to primary intrinsic resistance to EGFR inhibition. For example, mutant KRAS is now a predictor of resistance to anti-EGFR therapy, allowing for a more targeted approach[291]. This is further compounded by the genomic instability often present in many CRCs, leading to the alteration of different kinases within the same signal transduction pathway, reducing the efficacy of certain targeted treatments[292]. Similarly, mono-therapeutic inhibitors to BRAF such as vemurafenib have shown limited efficacy in BRAF-mutant CRC[293,294]. To circumvent these effects, combination therapies have been shown to improve clinical outcomes by preventing therapeutic resistance. For example, BRAF inhibition combined with an EGFR or MEK inhibitor improves the suppression of the ERK/MAPK pathway but must be balanced with accumulating toxicities and side effects[295]. Interestingly, even CRCs that are wild-type for KRAS, BRAF, PI3KCA and HER2 have been shown to activate compensatory mechanisms to bypass EGFR blockade.

5.1.2 Signal Transduction in Hypoxia

Growth factors induced by HIF signalling cause activation of pathways downstream of their respective receptor. This includes VEGF, the well-known HIF1α target that regulates angiogenesis[296]. Other targets of HIF1α are able to activate signal transduction pathways in a ligand-independent manner. For example, caveolin-1 (CAV1) is a direct transcriptional target of HIF1α and HIF2α, and upregulation is associated with poor prognosis. In hypoxia, the formation of caveolae increases due to upregulation of CAV1, allowing ligand-independent activation of EGFR and consequential downstream signalling[297]. However, other proteins are likely to be regulating signal transduction in hypoxia in a HIF-independent manner. For example,

whilst VEGF-A is known to be HIF-regulated, VEGF-C is upregulated in cancers including breast and lung and yet harbours no known HRE[298].

A complex interplay exists between HIFs and hypoxic signal transduction whereby the previously described signalling pathways themselves are able to regulate HIF transcription factors. For instance, HIFα levels are influenced by translational regulation occurring through the nutrient and energy-sensing mTOR complexes, where HIF1α is regulated through mTORC1 and mTORC2, whilst HIF2α is primarily regulated by mTORC2[299]. Downstream of these complexes, STAT3 phosphorylation by mTORC1 in hypoxic conditions is able to induce HIF1α mRNA expression, demonstrating HIF regulation by the PI3K-mTOR axis[300]. Additional mediators of this pathway may also be implicated in HIF regulation. For example, GSK3β is another substrate of Akt that has been shown to regulate the degradation of HIF1α independently of pVHL[301]. The MAPK pathway is also able to regulate HIF signalling, primarily at the level of transactivation. Phosphorylation of HIF1α or co-activator p300 by p38 induces HIF activation by promoting formation of the HIF complex and enhancing p300 transactivation[302].

5.1.3 AP1 Signalling

The previously described MAPK pathway is the primary regulator of AP1. AP1 transcriptional activity can be induced by a variety of stimuli and environmental cues, including growth factors, neurotransmitters, polypeptide hormones, cytokines, bacterial and viral infections and the phorbol ester tumour promoter TPA[303]. The transcription of the Fos and Jun genes are regulated by the MAPKs (JNKs, ERKs and p38). JNKs themselves are activated by upstream MKK4 and MKK7, whilst the ERKs are activated by MEK1/2. The expression of Fos subunits is induced by TCFs, which are activated through phosphorylation by ERK, JNK and p38[304]. On the other hand, expression of JUN is induced by ATF2, MEF2C and JUN, activated through phosphorylation by p38 and JNK[304]. This is demonstrated in Figure 5.1.

In addition to transcriptional regulation, AP1 is subject to regulation by post-translational modification, in particular regulation of activity by phosphorylation. As

with other TFs, phosphorylation of AP1 may regulate various levels of activity including DNA binding, transactivation and dimerization[305]. Kinases observed to regulate AP1 activity by phosphorylation include casein kinase 2 (CK2), GSK3β and RSK2. Serum and growth factor-activated ERK1/2 may also directly phosphorylate c-Jun, FOSL1 and FOSL2[305,306]. However, phosphorylation of different subunits may have opposing effects. For example, phosphorylation of c-Jun on a serine residue adjacent to the C-terminal binding domain has been found to inhibit c-Jun DNA binding activity, whilst phosphorylation of FOSL1 and FOSL2 enhances their DNA binding in conjunction with c-Jun[185].

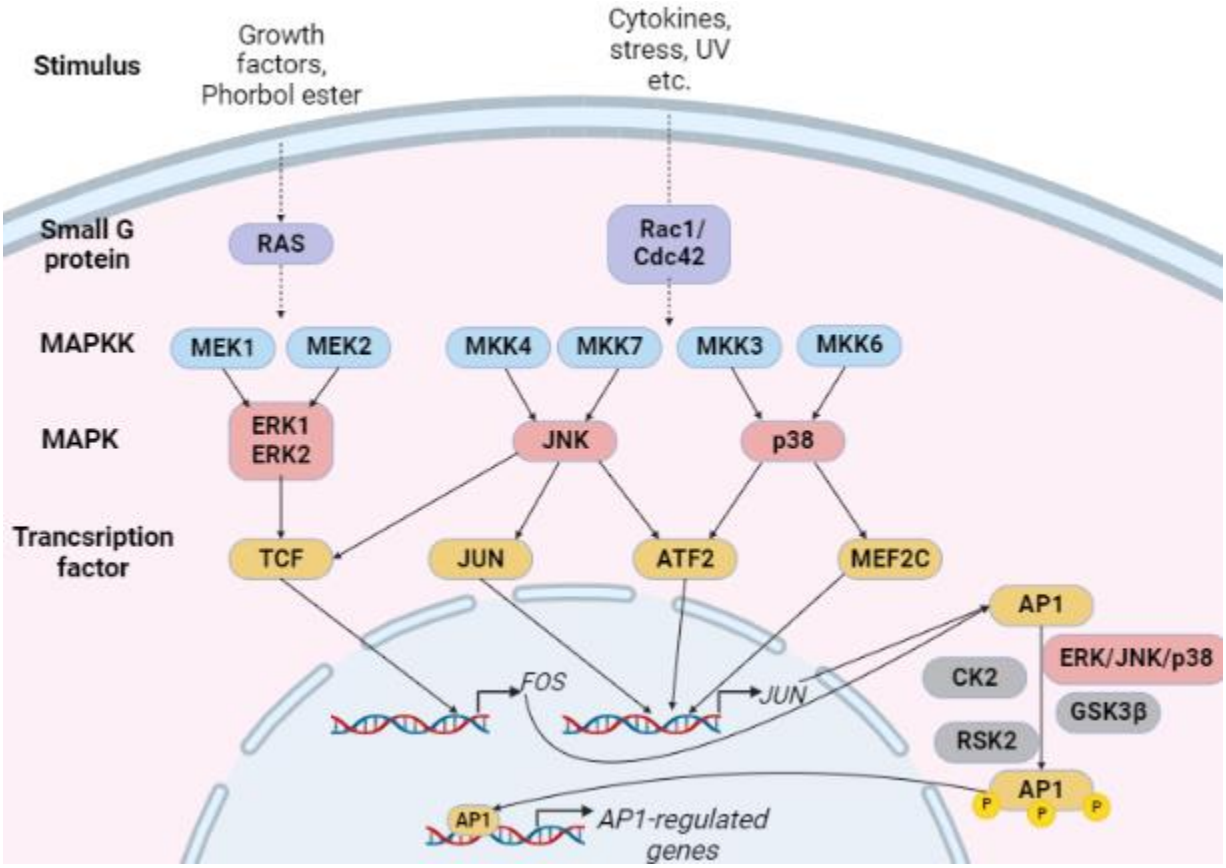

Figure 5.1. Regulation of AP1 expression and activity by the MAPK pathway. The transcription of Fos and Jun genes is regulated by the MAPK pathway upon stimulation of receptor tyrosine kinases by extracellular stimuli. Adaptor molecules bind to the activated receptor and promote the formation of activated Ras-GTP. Upon activation, the catalytic domain of Ras interacts with and activates MEK proteins. ERK and JNK play a role in the activation of the TCF and JUN transcription factors, which contribute to the transcriptional activation of Fos and Jun subunits. Within the cytoplasm, AP1 subunits are phosphorylated by a number of proteins, leading to activation and downstream expression of AP1 target genes. Figure created in BioRender.

5.2 Aims and hypotheses

The role that FOSL2 plays in regulating the hypoxic response in colorectal cancer has not yet been characterised. I hypothesise that FOSL2 will be activated in hypoxic conditions in CRC cell lines, demonstrated through investigating FOSL2 phosphorylation and localisation status. I hypothesise that several phospho-signalling pathways will be upregulated in hypoxic compared to normoxic conditions, and FOSL2 will be associated with elements of hypoxic phospho-signalling, both independently of and in co-association with HIF1 and HIF2.

In order to test these hypotheses I will use the following aims:

1. Determine the level of FOSL2 phosphorylation following exposure to multiple time-points of hypoxia (1% O_2) or normoxia (21% O_2) in Ls174T and HCT116.
2. Investigate the localisation of FOSL2 by immunofluorescence following exposure to 24 hours hypoxia (1% O_2) or normoxia (21% O_2) in Ls174T and HCT116.
3. Use CRISPR-Cas9 to generate HIF1α and HIF2α knockdown clones to test the HIF-dependency or HIF-independency of FOSL2-associated targets.
4. Complete a phospho-kinase array experiment using an Ls174T control clone in normoxia (21% O_2) and hypoxia (1% O_2) and Ls174T HIF1α, HIF2α and FOSL2 knockdown clones in hypoxia at a 24 hour time-point.
    a. Investigate the phospho-signalling targets induced by hypoxia compared to normoxia.
    b. Investigate phospho-signalling pathways associated with HIF1α and HIF2α in hypoxia.
    c. Investigate phospho-signalling pathways associated with FOSL2 in hypoxia.
5. Validate key changes identified in the phospho-array in Ls174T and HCT116.

5.3 Results

5.3.1 FOSL2 Phosphorylation in Hypoxia

In order to investigate FOSL2 activation under hypoxic conditions, FOSL2 phosphorylation levels were measured. Due to the lack of a commercially available phospho-FOSL2 antibody, the Phos-Tag Acrylamide system was used in order to separate phosphorylated from non-phosphorylated proteins, as outlined in Methods. HCT116 and Ls174T wild-type cells, representing CMS4 and CMS3 colorectal cancer subtypes respectively, were seeded in 0.5% FBS [v/v] medium and exposed to hypoxic (1% O_2) or normoxic (21% O_2) conditions for various time-points: 2, 6, 12 and 24 hours prior to protein extraction. Figure 5.2 shows representative Phos-Tag blots for HCT116 (A) and Ls174T (B). The dephosphorylation control in the first lane represents a sample treated with lambda protein phosphatase in order to degrade phosphorylated residues and to aid in identification of the correct phosphorylated protein band. Both HCT116 and Ls174T show reduced phosphorylation in this negative control compared to the 2hr normoxic control (33% and 48% respectively). When normalised to the 2hr normoxic condition, both cell lines show an upregulation of p-FOSL2 at both the 12 hour and 24 hour hypoxic time-points. For HCT116 this is a 2.8-fold increase at 12 hours hypoxia and a 2.7-fold increase at 24 hours hypoxia (Figure 5.2C). Fos Ls174T a 2.4-fold increase in p-FOSL2 is observed at 12 hours hypoxia and a 1.7-fold increase is observable at 24 hours hypoxia (Figure 5.2D). These values represent the average of N=2 replicates and so statistical significance cannot be obtained, due to Phos-Tag reagent shortages at the end of the project.

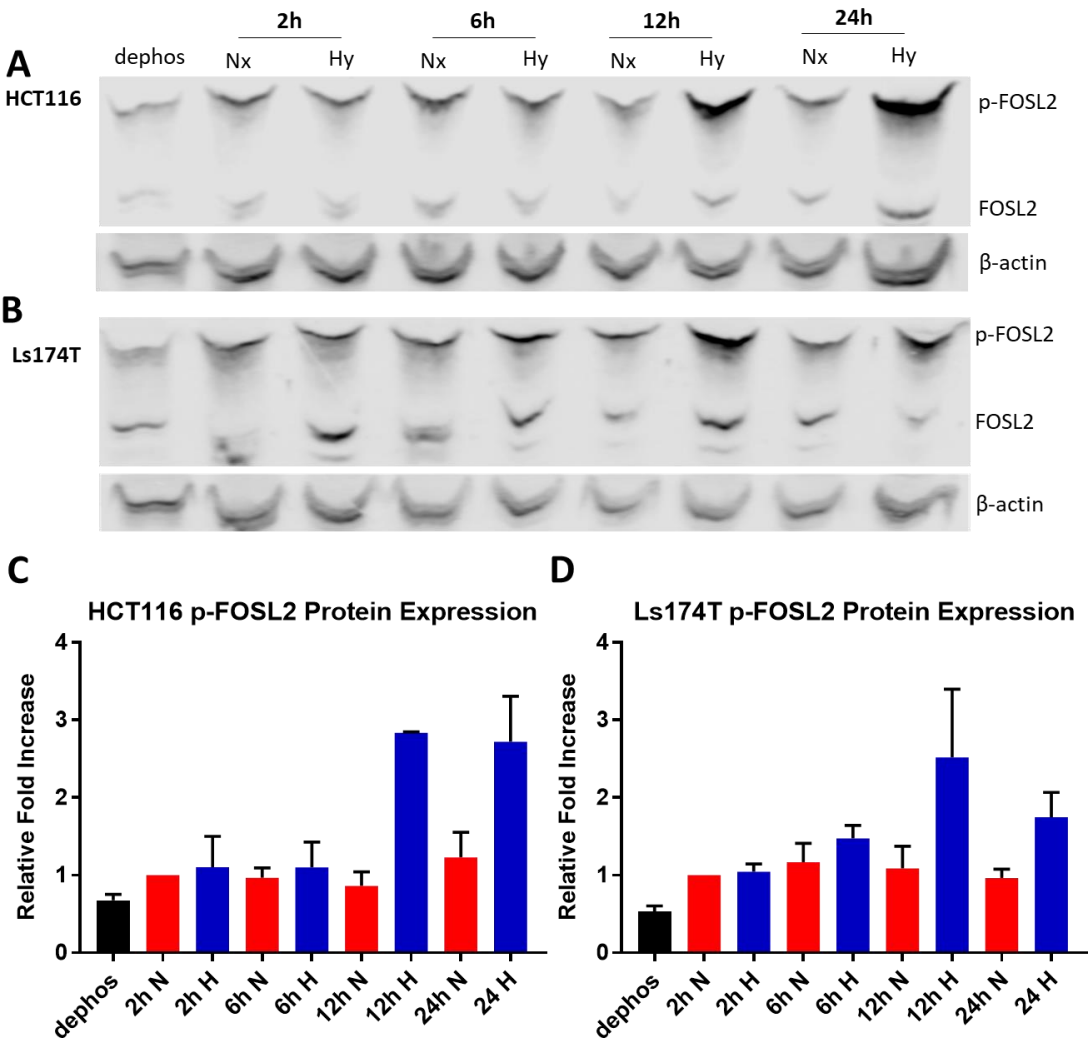

Figure 5.2. Phosphorylated FOSL2 protein levels under normoxic (21% O_2) or hypoxic (1% O_2) conditions in HCT116 and Ls174T cell lines across multiple time-points. Representative Phos-Tag immunoblot images of p-FOSL2 in HCT116 (A) and Ls174T (B). (C) Quantification of HCT116 p-FOSL2 expression. (D) Quantification of Ls174T p-FOSL2 expression. Error bars indicate ± SEM. N=2.

5.3.2 FOSL2 Localisation in Hypoxia

As FOSL2 phosphorylation is increased in hypoxia, and FOSL2 is a transcription factor acting within the nucleus to regulate target gene expression, it was hypothesised that increased activation in hypoxia may be inducing a shift in FOSL2 localisation from the cytoplasm and into the nucleus. In order to test this hypothesis, both HCT116 and Ls174T wild-type cells were seeded into 8-well chamber slides in either 10% [v/v] or 0.5% [v/v] FBS-containing medium, in order to investigate FOSL2 localisation and to exclude the possibility that changes observed are due to growth factor presence within

the FBS that are inducing FOSL2 activation. After cell adherence, slides were placed in either hypoxic (1% O_2) or normoxic (21% O_2) conditions for 24 hours prior to fixation and staining as per Methods. The 24 hour time point was selected as there was an induction of FOSL2 phosphorylation at the 24 hour hypoxic time point in both HCT116 and Ls174T as discussed. FOSL2 knockdown clones were used for each cell line in order to demonstrate specificity of antibody binding.

It was found that across both normoxic and hypoxic conditions, FOSL2 was localised exclusively to the nucleus in both HCT116 (Figure 5.3) and Ls174T (Figure 5.4), and cytoplasmic staining was not detectable. This localisation of FOSL2 in the nuclear region is again validated later in the project with the staining of the tissue micro array, where FOSL2 was found only in nuclear regions. In both cell lines, an apparent increase in intensity of FOSL2 staining is visible in the hypoxic condition compared to normoxia, a finding that is validated by western blotting later in this chapter. The localisation of FOSL2 is also not altered between 10% [v/v] and 0.5% [v/v] FBS conditions.

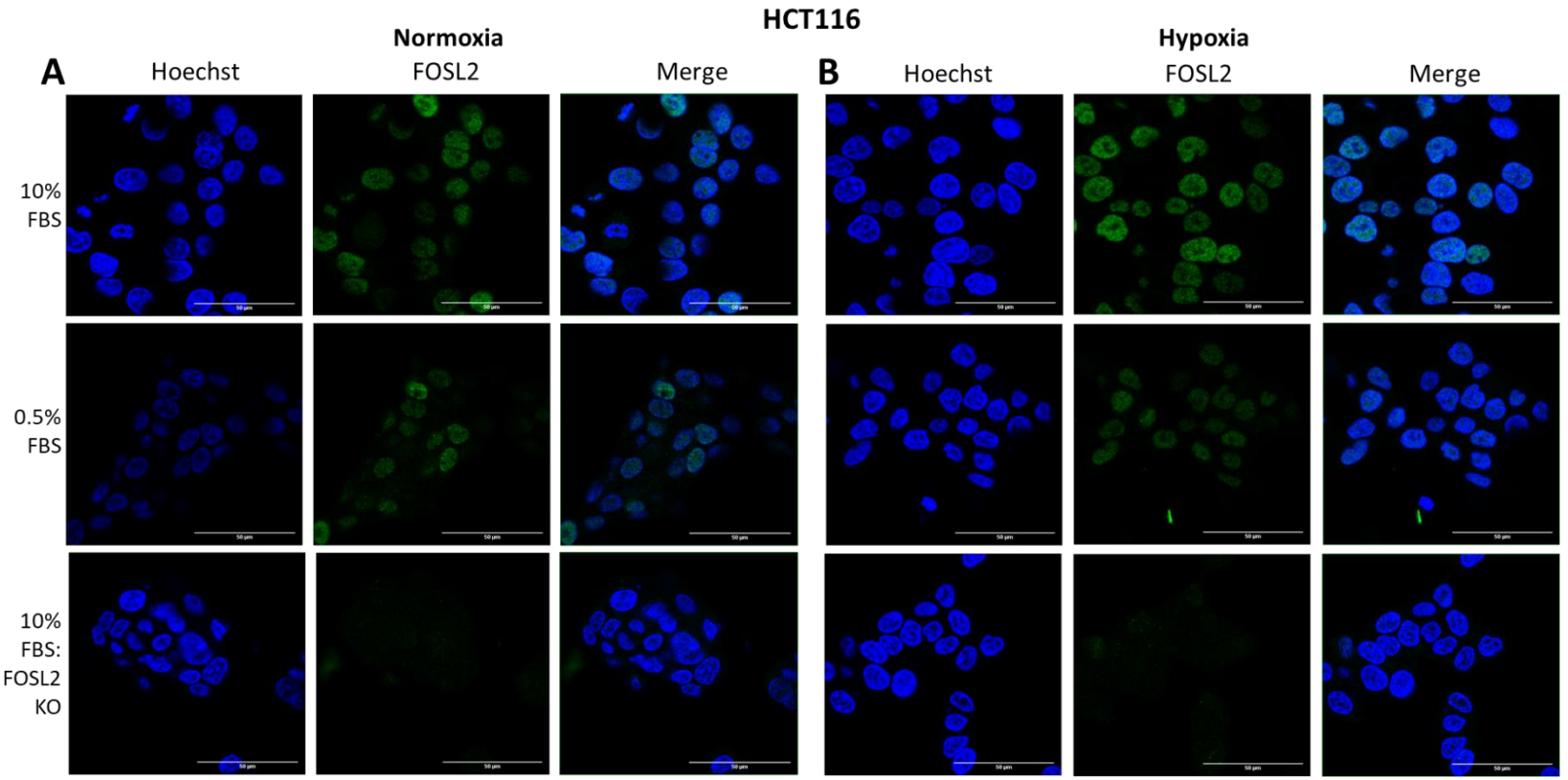

Figure 5.3. Representative images of FOSL2 localisation in normoxic (A, 21% O_2) or hypoxic (B, 1% O_2) conditions in HCT116. HCT116 wild-type cells were grown in 10% FBS (top panel) or 0.5% FBS (centre panel) during the normoxic or hypoxic 24 hour incubation. FOSL2 knockdown cells are used in the bottom panel to demonstrate antibody specificity. Nuclei are stained with Hoechst. Images taken at 63X magnification. Scale bar represents 50µM. N=3.

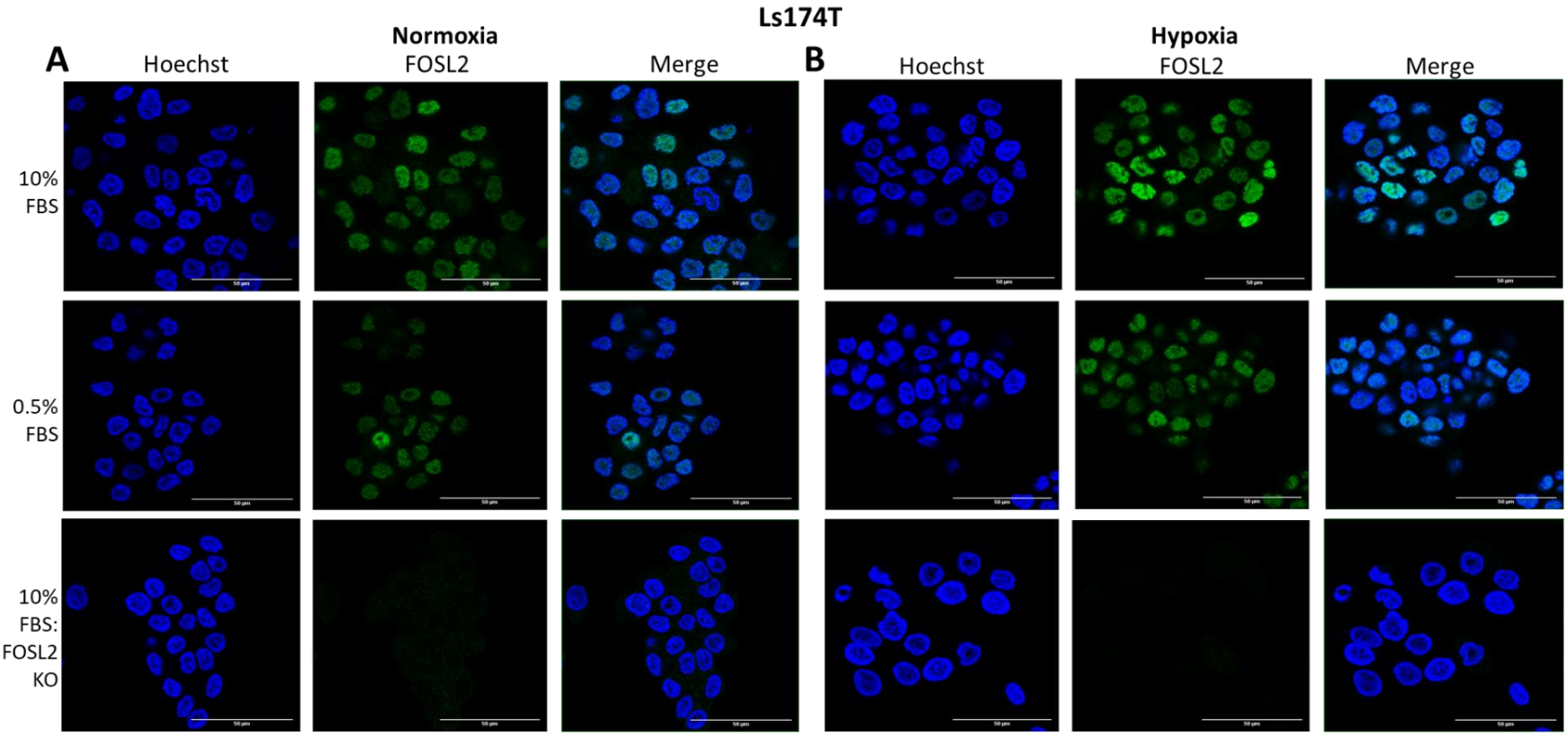

Figure 5.4. Representative images of FOSL2 localisation in normoxic (A, 21% O_2) or hypoxic (B, 1% O_2) conditions in Ls174T. Ls174T wild-type cells were grown in 10% FBS (top panel) or 0.5% FBS (centre panel) during the normoxic or hypoxic 24 hour incubation. FOSL2 knockdown cells are used in the bottom panel to demonstrate antibody specificity. Nuclei are stained with Hoechst. Images taken at 63X magnification. Scale bar represents 50µM. N=3.

5.3.3 Generation of HIF1α and HIF2α knockdown clones

To investigate the HIF-dependent or HIF-independent role of FOSL2 in hypoxic signalling, HIF1α and HIF2α knockdown clones were generated. Ls174T iCas9-expressing cells were transfected with synthetic gRNAs against either HIF1α or HIF2α as described in Methods. Three pre-designed gRNA sequences were selected per gene, in order to maximise the chances of at least two efficient guides per gene for experimental use. Ls174T iCas9 cells were split into 7 conditions for transfection: negative control (transfection with a non-targeting gRNA sequence), HIF1α-targeting g1, g2 and g3 and HIF2α-targeting g1, g2 and g3 sequences. Protein was extracted from the transfected pools shortly after transfection and cells were frozen down early to prevent compensation effects or the loss of the gene knockdown within the cell population.

Representative western blots are shown for the HIF1α (Figure 5.5A) and HIF2α (Figure 5.5B) knockdown pools with their respective quantification in Figure 5.5C and Figure 5.5D. For HIF1α, when normalised to expression in the negative control, HIF1α-g1 and HIF1α-g2 were the most effective, achieving a pooled 51% and 77% knockdown respectively. The HIF1α-g3 was ineffective and in fact exhibited an increased HIF1α expression compared to the control, which may have been due to over-confluence of the dishes prior to protein extraction. For HIF2α, HIF2α-g1 was the least effective, achieving only 12% knockdown, whereas HIF2α-g2 and HIF2α-g3 achieved 61% and 82% HIF2α knockdown respectively.

The two most efficient targeting sequences per gene as outlined above were taken forward for single clone selection, as described in Methods. Figure 5.5 shows a representative western blot of 2 control and 7 prospective knockdown clones for HIF1α (Figure 5.5E) and HIF2α (Figure 5.5F). A number of clones could be eliminated based on this screening, for example clones 2, 3 and 6 for HIF1α and clones 1, 2, 3 and 6 for HIF2α. Clones that appeared to be gene knockdowns through western blotting were taken forwards for DNA sequencing to confirm gene knockdown status, as described below.

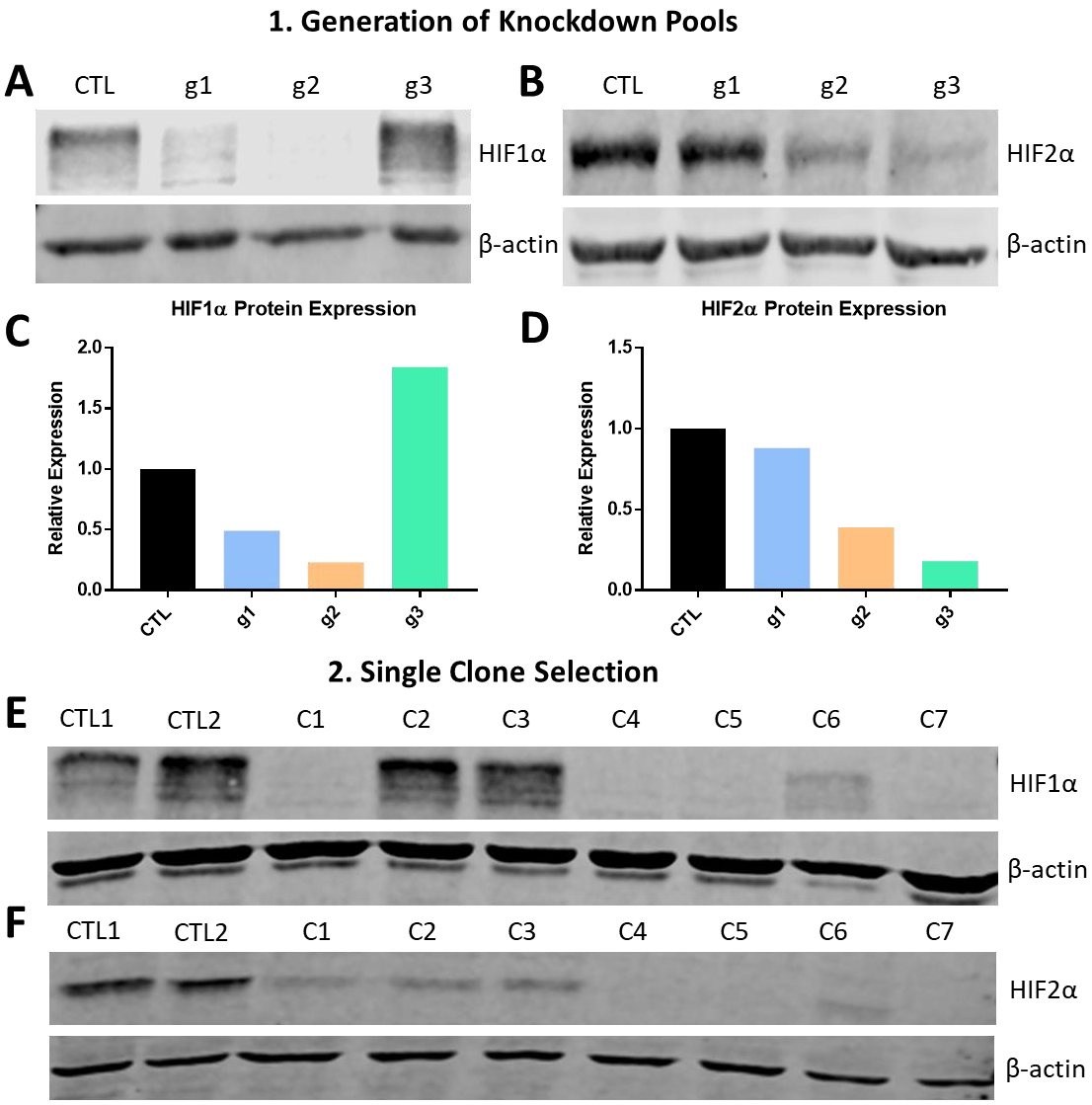

Figure 5.5. Generation of HIF1α and HIF2α knockdown cell lines in Ls174T. Firstly, knockdown pools were generated by lipotransfection of synthetic gRNAs (g1-g3) into cells expressing Cas9 under a doxycycline-inducible promoter. Representative immunoblots of resulting HIF1α (A) and HIF2α (B) pools are shown, with respective quantification in (C) and (D). The most efficient pool was used for single clone selection, with representative immunoblots of controls and single clones (C1-C7) shown for HIF1α (E) and HIF2α (F).

Apparent HIF1α and HIF2α knockdown clones underwent DNA extraction and submission for Sanger DNA sequencing at the Nottingham Deep-SEQ facility in order to confirm cutting at the predicted site. Figure 5.6 depicts chromatograms from a HIF1α (Figure 5.6A) and a HIF2α (Figure 5.6B) knockdown clone that were selected for the following experiment in this chapter, shown against the same sequence in the

control clone. The gRNA sequence and adjacent PAM site is highlighted. The HIF1α clone features a 1bp insertion within the cutting site, and the HIF2α clone features a 2bp deletion. Both of these are frameshift mutations, altering the triplet reading code for all subsequent codons. Frameshift indels such as these frequently lead to premature stop codons and have a greater functional impact than 'in-frame' indels. However, in the absence of a total knockdown, truncated protein may remain and perform functions within the cell as a dominant negative form of the protein. For this project, the term 'knockdown' is used due to the absence of identifying absolute gene knockdowns.

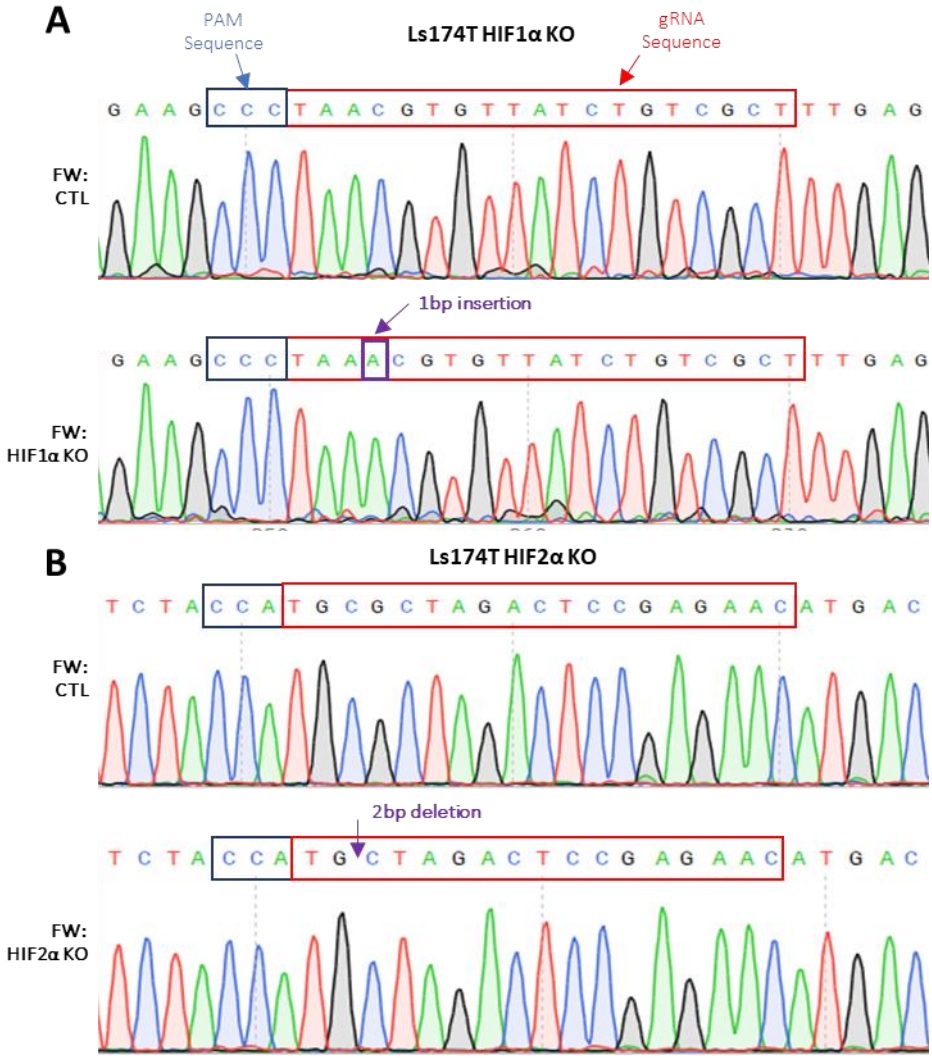

Figure 5.6. Validation of Ls174T HIF1α and HIF2α knockdown clones by Sanger sequencing. (A) Representative chromatograms obtained from Sanger sequencing of an Ls174T HIF1α knockdown clone, with the top panel depicting the control forward sequence and the bottom panel showing the knockdown sequence with a 1bp insertion. (B) Representative chromatograms obtained from an Ls174T HIF2α knockdown clone, with the top panel depicting the control forward sequence and the bottom panel showing the knockdown sequence with a 2bp deletion.

5.3.4 Investigating the role of HIF1α, HIF2α and FOSL2 in hypoxic phospho-signalling

In order to investigate the role that phosphorylated FOSL2 is playing in associating with hypoxic phospho-signalling pathways, a phospho kinase array experiment was performed, as described in Methods. This allowed for the simultaneous detection and

quantification of 48 phosphorylated proteins across multiple experimental conditions, to investigate which targets and pathways FOSL2 may be associated with in hypoxia in Ls174T cells. Additionally, HIF1α and HIF2α knockdown clones were included within the experiment so that it could be determined whether FOSL2 was associated with targets in a HIF-dependent or HIF-independent manner. The HIF clones used were those validated and described above. The FOSL2 knockdown clone used was kindly generated by Eric Vancauwenberghe of the McIntyre group using the same method and validation techniques as described for the HIF clones.

Figure 5.7 describes the experimental process. The conditions selected were the Ls174T control clone in both normoxia (21% O_2, 24 hours) and hypoxia (1% O_2, 24 hours), and the HIF1α, HIF2α and FOSL2 knockdown clones in hypoxia (Figure 5.7A). After experimental samples were generated, a small amount of the lysate was used to confirm that the knockdown conditions were maintained and that the hypoxic conditions were hypoxic, prior to starting the experiment. Figure 5.7B and 5.7C show confirmation of the HIF1α and HIF2α knockdowns respectively, as well as the HIF induction in the control conditions to confirm that the hypoxic condition is showing HIF induction. Figure 5.7D shows that FOSL2 expression is increased in hypoxia compared to normoxia, and that there is no FOSL2 expression in the knockdown conditions. Figure 5.7E and 5.7F demonstrate an example of how the raw data appears after chemi-luminescent detection in the control normoxia and control hypoxia conditions respectively. The larger reference spots are highlighted, as well as an example target (phospho-Erk1/2), demonstrating target duplicate spots which were later quantified using densitometry analysis.

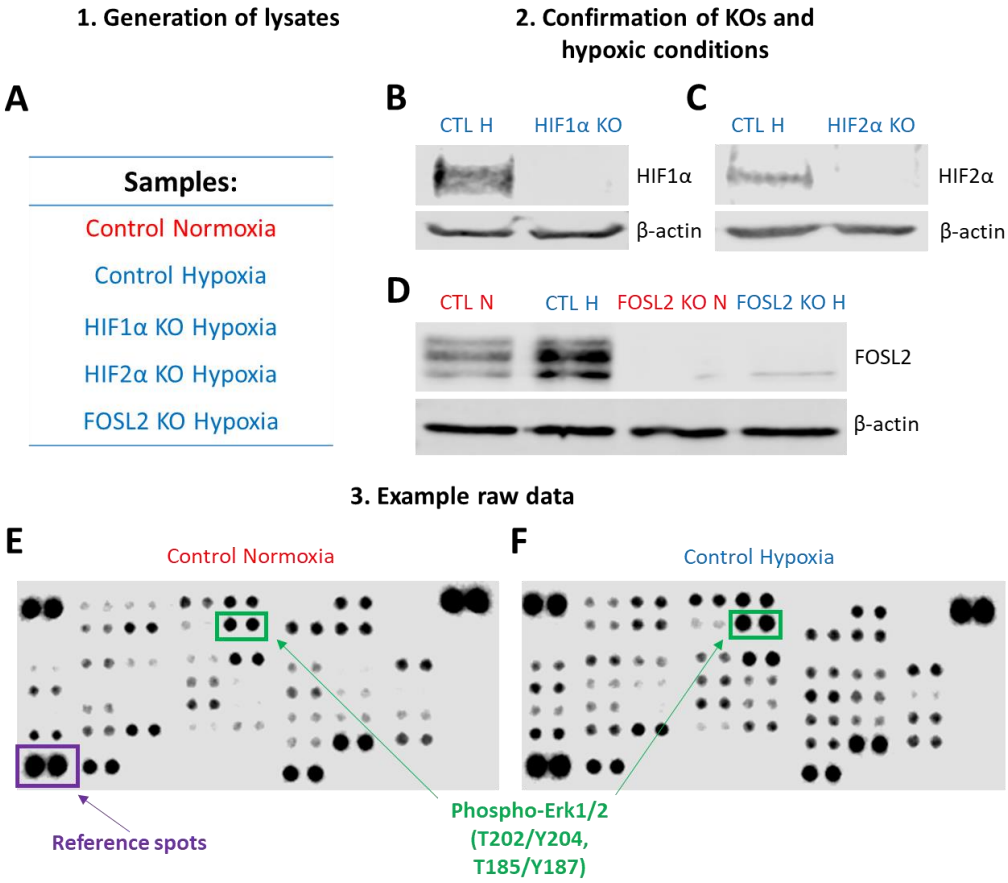

Figure 5.7. Experimental process for the phospho-kinase array experiment. (A) A table showing the experimental conditions selected for the experiment (B-D) Representative western blots confirming HIF1α, HIF2α and FOSL2 knockdown conditions as well as the presence of hypoxia. (E-F) Example images of experimental raw data for control normoxia and control hypoxia, depicting reference spots and an example target spotted in duplicate.

The phospho-kinase signalling array was repeated three times in order for three independent biological replicates to be included in the analysis. The two raw signal values for each target protein were averaged, and for the first analysis, values for the control hypoxia condition were normalised to control normoxia and the Log2 fold changes were calculated, to investigate how phospho-signalling is altered in hypoxia (Figure 5.8). Between the completion of three experimental repeats the composition of the commercial kit changed, and so where error bars are not present, only one repeat was performed for that target.

It was found that phospho-signalling was almost globally induced by hypoxia in comparison to normoxia. Of the 48 target proteins included, 45 of these were increased in hypoxia (94% of all targets) and just 3 of these were decreased (6% of targets). Of the 3 targets that were decreased in hypoxia, two were phosphorylation sites present on p53: the S46 site showed almost no decrease compared to normoxia (-0.01 log2 fold change), whereas the S392 site showed a -0.47 log2 fold change compared to normoxia. The other target decreased in hypoxia was RSK1/2 (S221/S227), which demonstrated a -0.27 log2 fold change. All other phospho-proteins showed an average of an induction in hypoxia compared to normoxia across the 3 repeats. The top 5 targets with the most prominent log2 fold increase in hypoxia were as follows: Fyn Y420 (1.5), HSP27 S78/S82 (1.26), TOR S2448 (1.4), ERK1/2 T202/Y204, T185/Y187 (1.15) and STAT5a Y694 (1.38). In terms of statistical significance, just 2 of the phospho-proteins showed a significant increase in log2 fold change in hypoxia compared to normoxia: WNK1 T60 (0.47, p=0.03) and STAT6 Y641 (0.3, p= 0.04). This is due to variation between the biological repeats, with one repeat appearing to be less hypoxic than the others. Additionally, variation is common within phospho-studies due to the dynamic nature of the post-translational modification, and additional variation may have arisen due to the kit composition change between replicates.

The next analysis performed was to compare phospho-signalling associations of HIF1α and HIF2α in hypoxia. To investigate this, both HIF1α and HIF2α knockdown conditions were normalised to the control hypoxia condition, and the log2 fold changes are presented graphically (Figure 5.9). Interestingly, HIF2α was found to play a more prominent role than HIF1α in terms of associations with hypoxic phospho-signalling. Of the 48 phospho-targets studied, 43 (89%) were increased upon knockdown of HIF1α compared to control hypoxia. 3 targets were unchanged: STAT1 Y701, STAT3 S727 and RSK1/2/3 S380/S386/S377, and 2 targets were slightly downregulated: PRAS40 T246 (log2 fold -0.08) and Chk-2 T68 (log2 fold -0.1), although the p-values for the downregulations were non-significant. The targets with most increased log2 fold changes upon HIF1α knockdown included: STAT3 Y705 (0.66, p=0.0008), β-catenin (0.6, p=0.002) and PDGF Rβ (0.54, p=0.006). However, for the scope of this study, the

downregulated targets would be of most interest as potential HIF-associated targets of hypoxic signalling.

As apparent also in Figure 5.9, HIF2α was found to play a more prominent role in associations with hypoxic phospho-signalling than HIF1α in Ls174T cells at the 24 hour hypoxic time-point as the experiment was performed, and there was no evidence of target co-associations by both HIFs. Of the 48 targets investigated, 50% (24 targets) were upregulated and 50% were downregulated upon knockdown of HIF2α. Of the more relevant downregulations, the phospho-targets with the greatest log2 fold change upon HIF2α knockdown in hypoxia compared to control hypoxia include β-catenin (-1.8, p=<0.000001). β-catenin along with HSP60 are both targets for which total protein levels are measured by the array as opposed to specific phosphorylation residues. The other statistically significant downregulation was the S473 site of Akt1/2/3 (-1.23, p=0.000071). Other large but non-significant downregulations included RSK1/2 S221/S227 with a log2 fold change of -1, and Hck Y411 with a log2 fold change of -1.42.

After establishing the pattern of phospho-signalling associations with HIF1α and HIF2α in hypoxia, the next analysis performed was to normalise the FOSL2 knockdown values to control hypoxia values in order to establish the pattern of association with FOSL2 and to compare this to the HIFs. As shown in Figure 5.10, the pattern of association with FOSL2 in hypoxia is more similar to that of HIF2α than HIF1α; of the 48 phospho-targets investigated, 17 targets were upregulated upon FOSL2 knockdown in hypoxia, although no upregulations were statistically significant and none with a log2 fold change above 0.55. 31 targets showed a downregulation upon FOSL2 knockdown, suggesting an association to some extent with FOSL2. The largest downregulation upon FOSL2 knockdown was Hck Y411 with a log2 fold change of -1.23, although this finding represents n=1 due to the changing of the kit composition by the company between replicates and so significance could not be determined. Statistically significant downregulations were identified as follows: PYK2 Y402 (-0.60, p= 0.006), CREB S133 (-0.68, p=0.002), PRAS40 T246 (-0.57, p=0.01), RSK1/2 S221/S227 (-0.61, p=0.006), STAT3 S727 (-0.49, p=0.02), p70 6S kinase T421/S424 (-0.44, p=0.04) and HSP60 total protein (-0.43, p=0.05).

The global signalling changes induced by knockdown of HIF1α, HIF2α and FOSL2 in hypoxia compared to control hypoxia are summarised in the heatmap shown in Figure 5.11, where the blue represents downregulations and it is clear to see the more prominent role played by both HIF2α and FOSL2 as opposed to HIF1α.

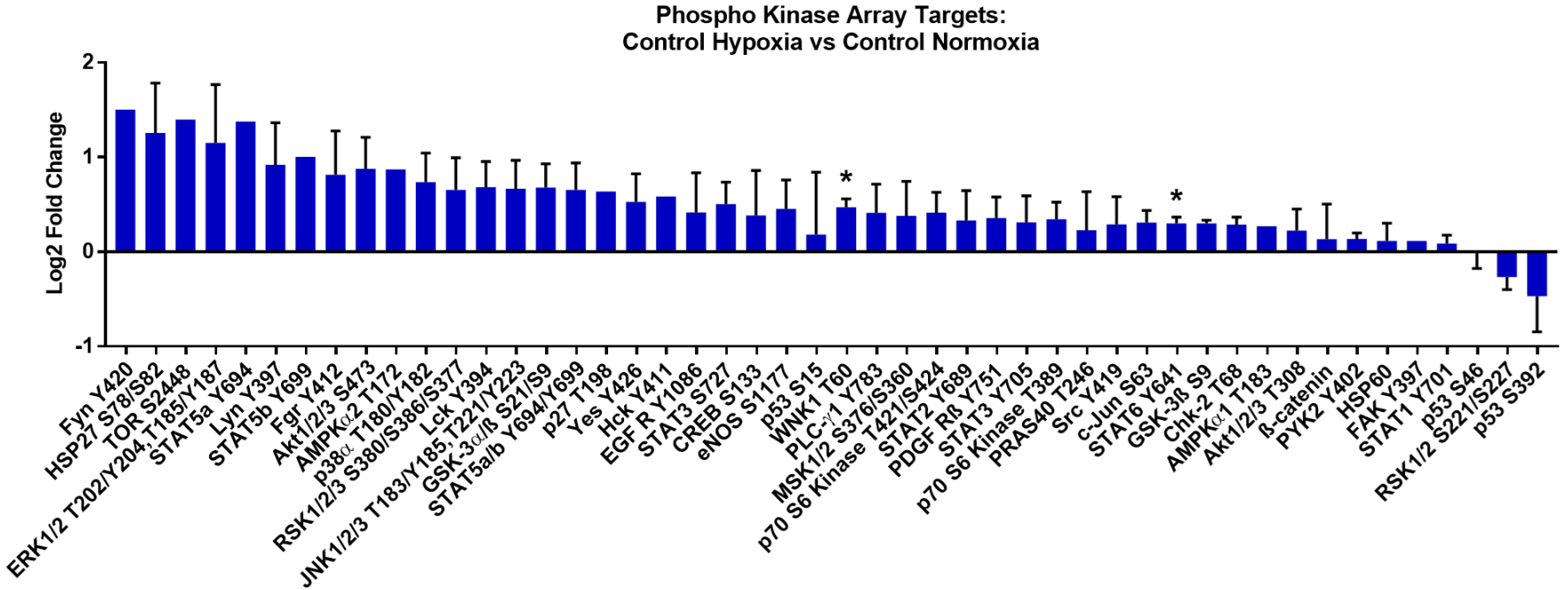

Figure 5.8 Phospho-kinase array targets normalising control hypoxia (1% O_2) to control normoxia (21% O_2) in Ls174T cells. Densitometry analysis was performed on the raw data images as described above. Log2 fold changes are presented for each target when control hypoxia is normalised to control normoxia values. Error bars indicate ± SEM. Data analysed using a one-way ANOVA. N=3. *p<0.05.

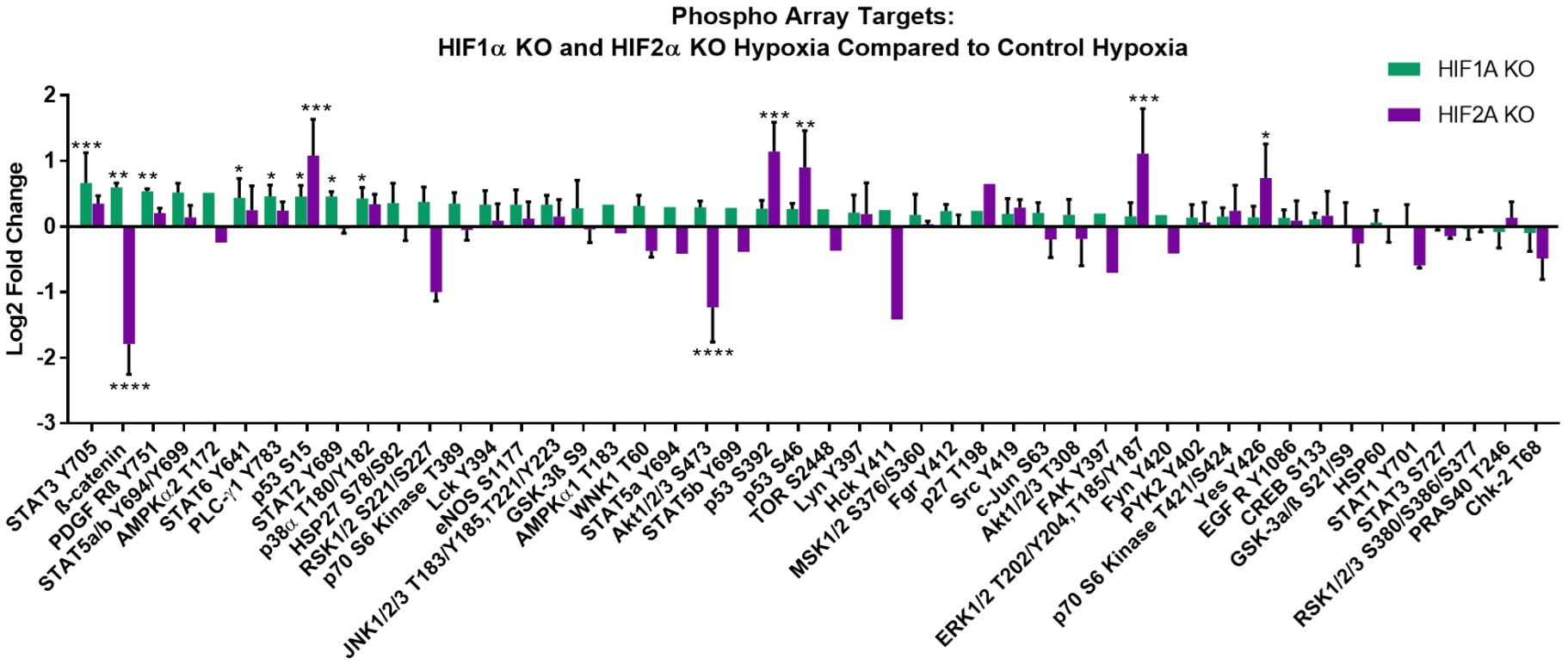

Figure 5.9 Phospho-kinase array targets normalising HIF1α knockdown and HIF2α knockdown hypoxia conditions to control hypoxia in Ls174T cells. Densitometry analysis was performed on the raw data images as described above. Log2 fold changes are presented for each target when HIF1α or HIF2α knockdown values are normalised to control hypoxia. Error bars indicate ± SEM. Data analysed using a one-way ANOVA. N=3. *p<0.05, **p<0.01, ***p<0.001, ****p<0.0001.

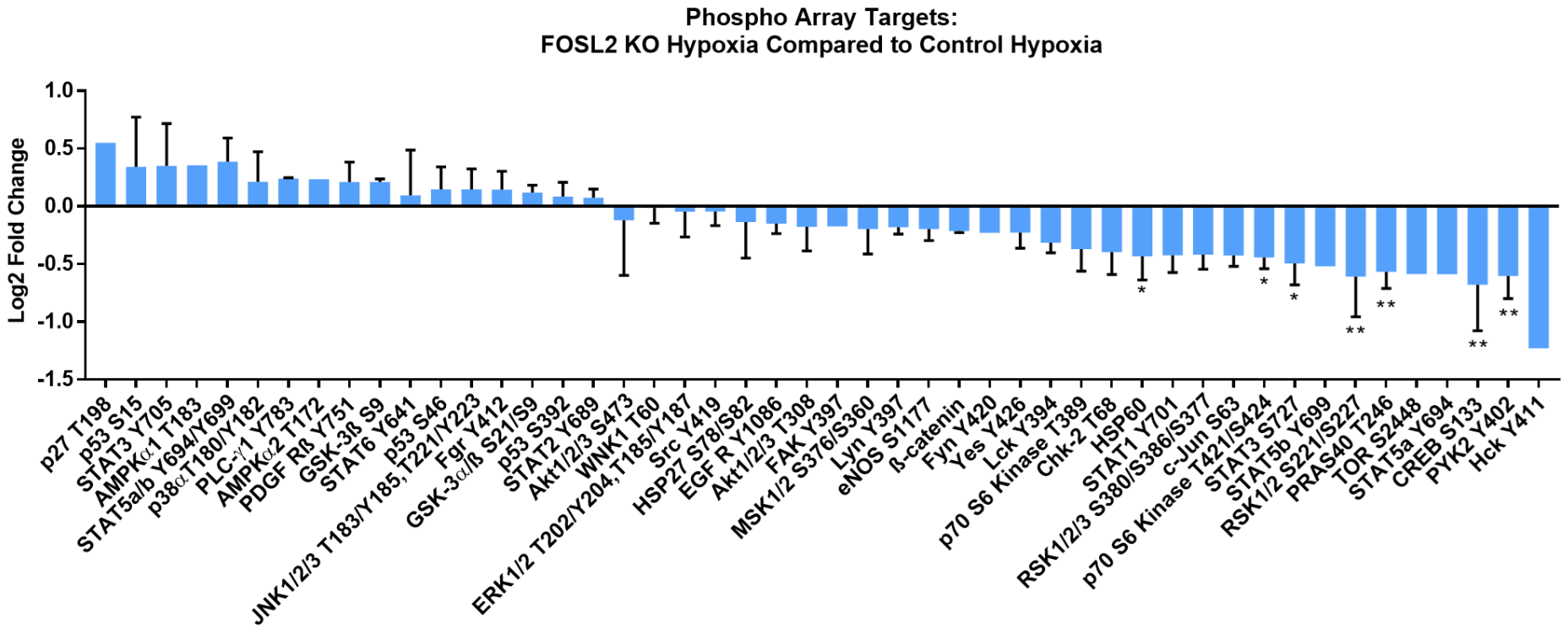

Figure 5.10 Phospho-kinase array targets normalising FOSL2 knockdown hypoxia to control hypoxia in Ls174T cells. Densitometry analysis was performed on the raw data images as described above. Log2 fold changes are presented for each target when FOSL2 knockdown values are normalised to control hypoxia. Error bars indicate ± SEM. Data analysed using a one-way ANOVA. N=3. *p<0.05, **p<0.01, ***p<0.001, ****p<0.0001.

Target	Phosphorylation Site	HIF1A KO	HIF2A KO	FOSL2 KO
STAT3	Y705	1.76	1.28	1.36
β-catenin	N/A	1.51	0.32	0.86
PDGF Rβ	Y751	1.45	1.16	1.17
STAT5a/b	Y694/Y699	1.45	1.12	1.33
STAT6	Y641	1.42	1.27	1.15
PLC-γ1	Y783	1.40	1.19	1.18
p53	S15	1.39	2.46	1.37
STAT2	Y689	1.38	0.98	1.06
p38α	T180/Y182	1.37	1.28	1.20
HSP27	S78/S82	1.34	1.00	0.95
RSK1/2	S221/S227	1.31	0.50	0.69
p70 S6 Kinase	T389	1.29	0.98	0.79
Lck	Y394	1.29	1.10	0.81
eNOS	S1177	1.29	1.12	0.88
JNK1/2/3	T183/Y185,T221/Y223	1.27	1.15	1.12
GSK-3β	S9	1.27	0.98	1.16
WNK1	T60	1.26	0.78	1.00
Akt1/2/3	S473	1.23	0.49	1.02
p53	S392	1.22	2.43	1.07
p53	S46	1.21	2.19	1.13
Lyn	Y397	1.20	1.28	0.88
MSK1/2	S376/S360	1.19	1.03	0.89
Fgr	Y412	1.18	1.03	1.12
Src	Y419	1.17	1.23	0.98
c-Jun	S63	1.17	0.90	0.75
Akt1/2/3	T308	1.17	0.95	0.90
ERK1/2	T202/Y204,T185/Y187	1.13	2.60	0.99
PYK2	Y402	1.12	1.09	0.67
p70 S6 Kinase	T421/S424	1.12	1.26	0.74
Yes	Y426	1.12	1.87	0.86
EGF R	Y1086	1.10	1.12	0.90
CREB	S133	1.09	1.20	0.67
GSK-3α/β	S21/S9	1.07	0.89	1.09
HSP60	N/A	1.06	1.02	0.76
STAT1	Y701	1.03	0.66	0.75
STAT3	S727	0.99	0.90	0.72
RSK1/2/3	S380/S386/S377	0.99	0.99	0.75
PRAS40	T246	0.98	1.13	0.68
Chk-2	T68	0.97	0.75	0.77

Figure 5.11 Heatmap depicting changes induced by HIF1α, HIF2α and FOSL2 knockdown in hypoxia normalised to control hypoxia. Densitometry analysis was performed on the raw data images as described above. The values presented in the heatmap represent the average of the target for each knockdown condition in hypoxia normalised to control hypoxia. Values of 1 are equivalent to control hypoxia (white), values below 1 represent downregulations (blue), values above 1 are indicative of upregulations (red).

The statistically significant changes induced in hypoxia upon FOSL2 knockdown as listed above were re-plotted alongside the HIF1α and HIF2α knockdown values for these targets in order to determine HIF-dependency or -independency of associations (Figure 5.12). These findings are summarised in Table 5.1, where significant FOSL2-associated targets are listed in order of Log2 fold change upon FOSL2 knockdown.

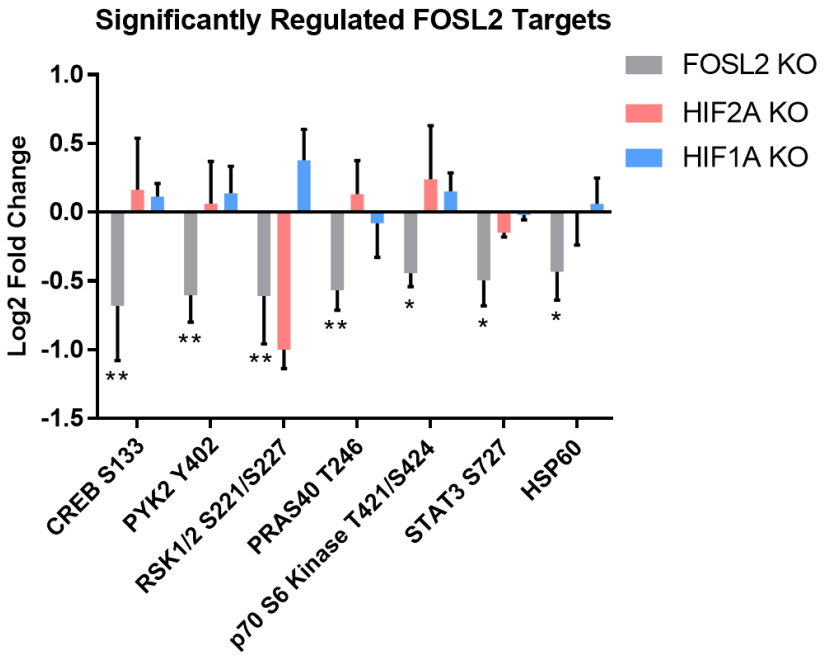

Figure 5.12 Significant FOSL2-associated targets alongside values for HIF1α and HIF2α knockdown conditions. Log2 fold changes are presented for each target when FOSL2, HIF1α and HIF2α knockdown values are normalised to control hypoxia. Error bars indicate ± SEM. Data analysed using a one-way ANOVA. N=3. *p<0.05, **p<0.01.

Target Protein	Phosphorylation Site	Result of Phosphorylation	FOSL2 KO Log2 Fold Change	Log2 Fold Change Control Hypoxia vs Normoxia	Regulation by HIFs?
CREB	S133	Transcriptional activation (co-activator recruitment)	-0.68 p=0.002	0.38	No
RSK1/2	S221/S227	Activation of RSK1/2	-0.60 p=0.006	-0.27	HIF2α (-1.00, n=2)
PYK2	Y402	Enzymatic activation	-0.60 p=0.006	0.14	No
PRAS40	T246	Dissociation from mTORC1; upregulates mTORC1 activity	-0.57 p=0.01	0.23	HIF1α (-0.08, p=ns)
STAT3	S727	Transcriptional activation	-0.50 p=0.02	0.50	HIF2α (-0.14, p=ns)
P70 S6 Kinase	T421/S424	Activation of p70 S6 kinase	-0.44 p=0.04	0.34	No
HSP60	N/A (total)	N/A (total protein)	-0.43 p=0.05	0.11	No

Table 5.1 Significant FOSL2-associated target parameters. The table indicates the target protein, site and result of phosphorylation as well as log2 fold change upon FOSL2 knockdown, induction in hypoxia and associations with HIFs.

As demonstrated by Table 5.1, the largest log2 fold change induced by FOSL2 knockdown is reduced phosphorylation of CREB S133, which also demonstrates the second highest log2 fold increase in control hypoxia compared to control normoxia (0.38) and therefore represents an interesting target of hypoxic FOSL2 signalling. Furthermore, as with most other targets listed, this association is occurring independently of HIF1α and HIF2α. The only co-associations of these targets appears through HIF1α in the association with PRAS40 T246 although this is very minimal with a log2 fold change of just -0.08 and statistically non-significant. Similarly, both RSK1/2 S221/S227 and STAT3 S727 appear to exhibit some degree of co-association with HIF2α although these are non-significant and minimal in the case of STAT3 S727. For RSK1/2 S221/S227, HIF2α knockdown induces a log2 fold change of -1, even larger than that for FOSL2 knockdown (-0.6). However, this represents the only target listed that is not induced by control hypoxia compared to control normoxia, and therefore does not represent an interesting target in the context of hypoxic signalling.

Figure 5.13 represents a simplified schematic diagram including these significant FOSL2-associated targets and where they fit into phospho-signalling pathways. HSP60 (total) is not included although in itself represents an interesting finding as HSP60 is involved in regulation of HIF1α protein stability, and so this could represent an indirect mechanism for FOSL2 regulation of the HIFs themselves. As shown, FOSL2 is associated with the activation of various members of the mTOR and ERK signalling pathways at multiple effector levels. These include PYK2 which functions upstream of the ERK signalling cascade to promote its activation, and RSK1/2 which, following activation by ERK1/2, are able to in turn activate transcriptional targets such as CREB. CREB works alongside other activated transcription factors including STAT3 to activate pathways that are implicated in cancer, including survival, proliferation and apoptosis. Activation of PRAS40 at residue T246 is able to promote mTORC1 signalling, and p70S6K acts downstream of this complex to activate protein translation when activated by phosphorylation. Also shown is FOSL2 itself which is regulated by ERK1/2. Interestingly, FOSL2 regulation of upstream ERK1/2 activators such as PYK2 may represent a positive feedback system for FOSL2 activation.

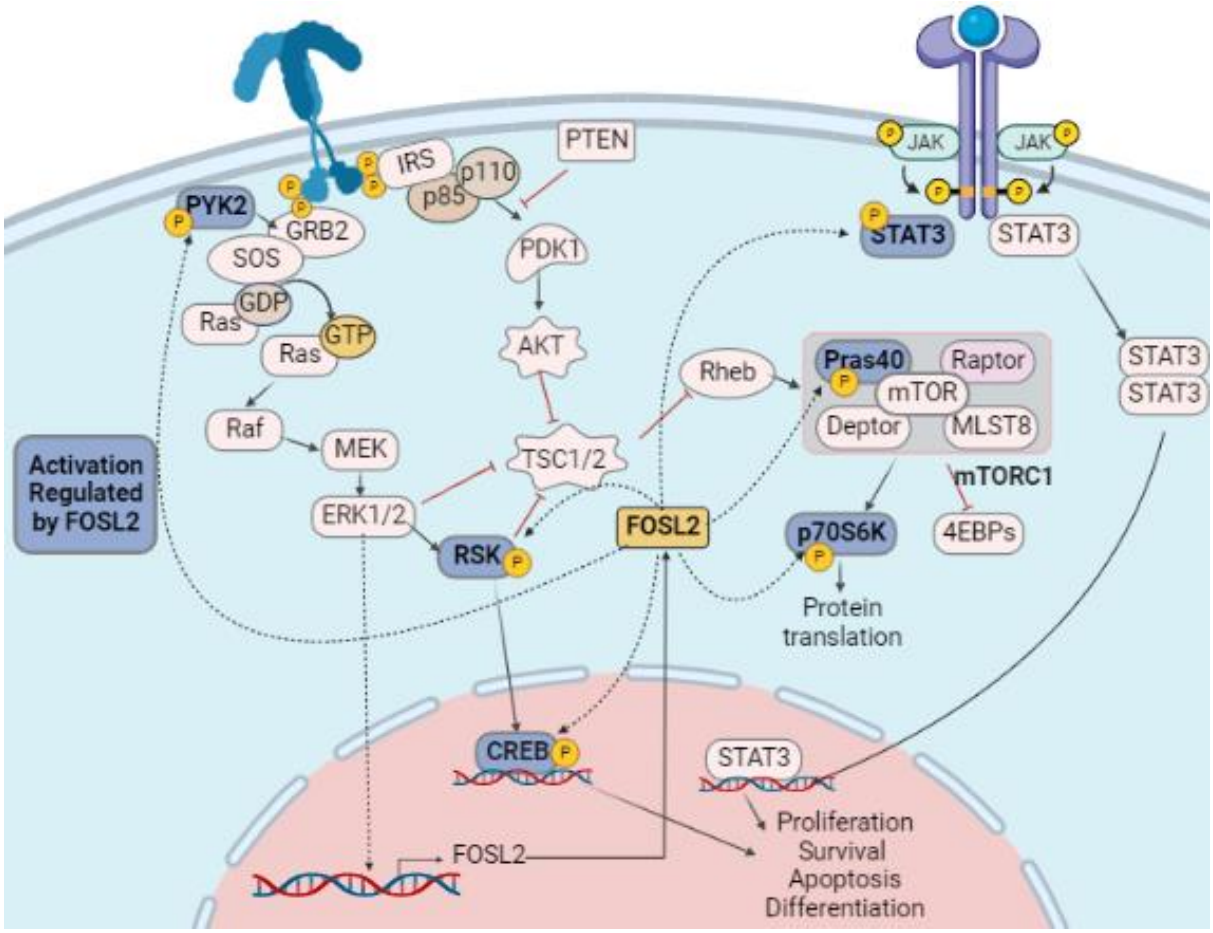

Figure 5.13 Schematic diagram demonstrating FOSL2 association with phospho-signalling pathways. FOSL2 is associated with the activation of various members of the mTOR and ERK signalling pathways at multiple effector levels. These include PYK2 which promotes activation of ERK1/2 signalling, and RSK1/2 which are able to in turn activate transcriptional targets such as CREB. CREB works alongside other activated transcription factors including STAT3 to activate pathways that are implicated in cancer. Activation of PRAS40 at residue T246 is able to promote mTORC1 signalling, and p70S6K acts downstream of this complex to activate protein translation when activated by phosphorylation. Figure created in BioRender.

Finally, select targets from the phospho-kinase array were validated by western blot in both Ls174T and HCT116 cell lines. This is because the array itself was performed in Ls174T, although it was performed in clones (control or knockdown) as opposed to wild-type or pooled populations. It was therefore to be determined whether changes identified would also be seen in the wild-type versions of these cells and were not simply clonal effects. Furthermore, HCT116 was included as a cell line representing a distinct colorectal cancer subtype (CMS4) and so it was useful to compare whether changes may feature across different subtypes or present as subtype-specific. Initially,

a focus of this experiment was to investigate potential upstream regulators of FOSL2 in hypoxia by identifying key changes induced in control hypoxia compared to normoxia. Thus, ERK1/2 was selected as the canonical FOSL2 regulator for validation of hypoxic induction in order to determine whether the known inducer of FOSL2 is upregulated in hypoxia or whether it is likely that there are alternative mechanisms of FOSL2 regulation in hypoxia compared to normoxia. Based on some preliminary bioinformatic analysis, Akt1/2/3 S473 was also selected for validation as a potential upstream regulator of FOSL2 in hypoxia. Subsequently, due to the global level of hypoxic upregulations and the lack of a specific model to test FOSL2 regulation, analysis shifted toward changes that were induced by FOSL2 itself. However, the validation of these two targets still serves an important purpose to indicate that changes observed in the array were maintained using a phospho-antibody from a different company and in wild-type cells, demonstrating that the experiment and its conclusions can be considered robust.

Figure 5.14 demonstrates the validation of these targets in Ls174T. Validation was performed in wild-type cells seeded either in 0.5% or 10% FBS [v/v] and in normoxia (21% O_2) or hypoxia (1% O_2) for 24 hours as that was the time point that the array was performed at. The array was performed with cells seeded in 10% FBS [v/v] as per the protocol, but the 0.5% FBS [v/v] conditions were included in the validation to ensure changes seen are not due to the composition of the FBS. Figure 5.14A shows representative western blots for p-Akt (S473) alongside total Akt, with 3 quantifications shown in Figure 5.14C-E. p-Akt(S473) was significantly upregulated in hypoxia compared to normoxia in both 0.5% and 10% FBS [v/v] conditions when normalised to β-actin. When normalised to the relative normoxic condition, p-Akt (S473) was 1.37-fold increased in hypoxia ($p=0.01$) in 10% FBS conditions and 1.81-fold increased in hypoxia ($p=0.003$) in 0.5% FBS. Similarly, when the analysis was performed to normalise p-Akt (S473) to total Akt, p-Akt (S473) was 1.62-fold higher in hypoxia compared to normoxia in 10% FBS ($p<0.0001$) and 1.65-fold higher in hypoxia compared to normoxia in 0.5% FBS ($p=0.0002$). Finally, no significant increases in hypoxia were found when normalising total Akt levels to β-actin, demonstrating that levels of p-Akt (473) are increasing in hypoxia and not levels of total Akt. These findings

support validation of the array, where Akt (S473) was the target with the 9th highest hypoxic induction compared to control normoxia (0.88 Log2 fold increase).

Figure 5.14B shows representative western blots for p-Erk1/2 (T202/Y204, T185/Y187) alongside total Erk1/2, with 3 quantifications shown in Figure 5.14F-H. It was found that p-Erk1/2 (T202/Y204, T185/Y187) is significantly upregulated in hypoxia compared to normoxia at the 10% FBS condition when normalised to β-actin with a 1.74-fold increase (p=0.03). This validates the array as the experiment was performed at 10% FBS. However, the same significant hypoxic induction was not apparent at the 0.5% FBS condition. Similarly, when p-Erk1/2 (T202/Y204, T185/Y187) was normalised to total Erk1/2, a significant induction was found in hypoxia compared to normoxia in the 10% FBS condition (1.79-fold increase, p=0.001), but no significant differences were found between the two at 0.5% FBS. Finally, no significant differences were found when normalising total Erk1/2 to β-actin, demonstrating that phospho-levels are increasing but not total protein levels.

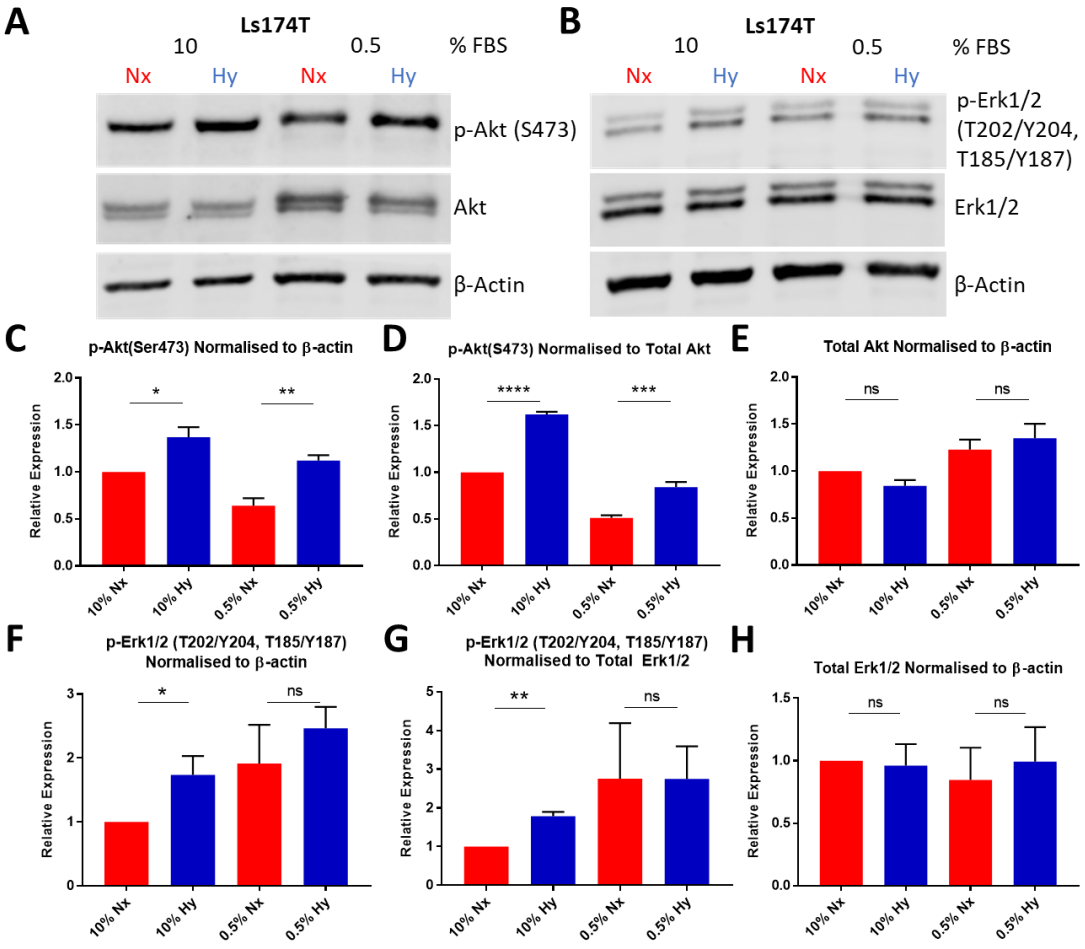

Figure 5.14 Validation of phospho-array target hypoxic induction in Ls174T in 10% and 0.5% FBS. Representative western blots are shown at 24 hours normoxia (21% O_2) or hypoxia (1% O_2) at 10% and 0.5% FBS conditions for p-Akt (S473) alongside total Akt (A) or p-Erk1/2 (T202/Y204, T185, Y187) alongside total Erk1/2 (B). (C-E) Quantifications for p-Akt and total Akt. (F-H) Quantifications for p-Erk1/2 and total Erk1/2. Error bars indicate ± SEM. Data analysed using a one-way ANOVA. N=3. *p<0.05, **p<0.01, ***p<0.001, ****p<0.0001.

Figure 5.15 represents the validation of the same targets but this time in wild-type HCT116 cells, representing the CMS4 colorectal cancer subtype. Figure 5.15A shows representative western blots for p-Akt (S473) alongside total Akt, with 3 quantifications shown in Figure 5.15C-E. p-Akt(S473) was significantly upregulated in hypoxia compared to normoxia in both 0.5% and 10% FBS [v/v] conditions when normalised to β-actin. When normalised to the relative normoxic condition, p-Akt (S473) was 3.2-fold increased in hypoxia (p=0.03) in 10% FBS conditions and 2.7-fold increased in hypoxia (p=0.02) in 0.5% FBS. Similarly, when the analysis was performed

to normalise p-Akt (S473) to total Akt, p-Akt (S473) was 3.5-fold higher in hypoxia compared to normoxia in 10% FBS (p=0.05) and 2.7-fold higher in hypoxia compared to normoxia in 0.5% FBS (p=0.04). Finally, no significant increases in hypoxia were found when normalising total Akt levels to β-actin, demonstrating that levels of p-Akt (473) are increasing in hypoxia and not levels of total Akt. This represents an important validation of the array, as not only were the clonal inductions maintained in wild-type Ls174T cells, but they were also applicable to HCT116 cells representing a distinct CRC subtype. Despite this, no significant differences were found between normoxia and hypoxia across any condition for p-Erk1/2 (T202/Y204, T185, Y187) in HCT116 cells (Figure 5.15F-H), and so this demonstrates a target for which findings in Ls174T are not applicable to HCT116. This is an interesting result in itself as FOSL2 is activated in hypoxia in HCT116 as described earlier, and so if this is not through the canonical Erk1/2 regulator, alternative mechanisms may be regulating FOSL2 in hypoxia in alternative CRC subtypes such as CMS4.

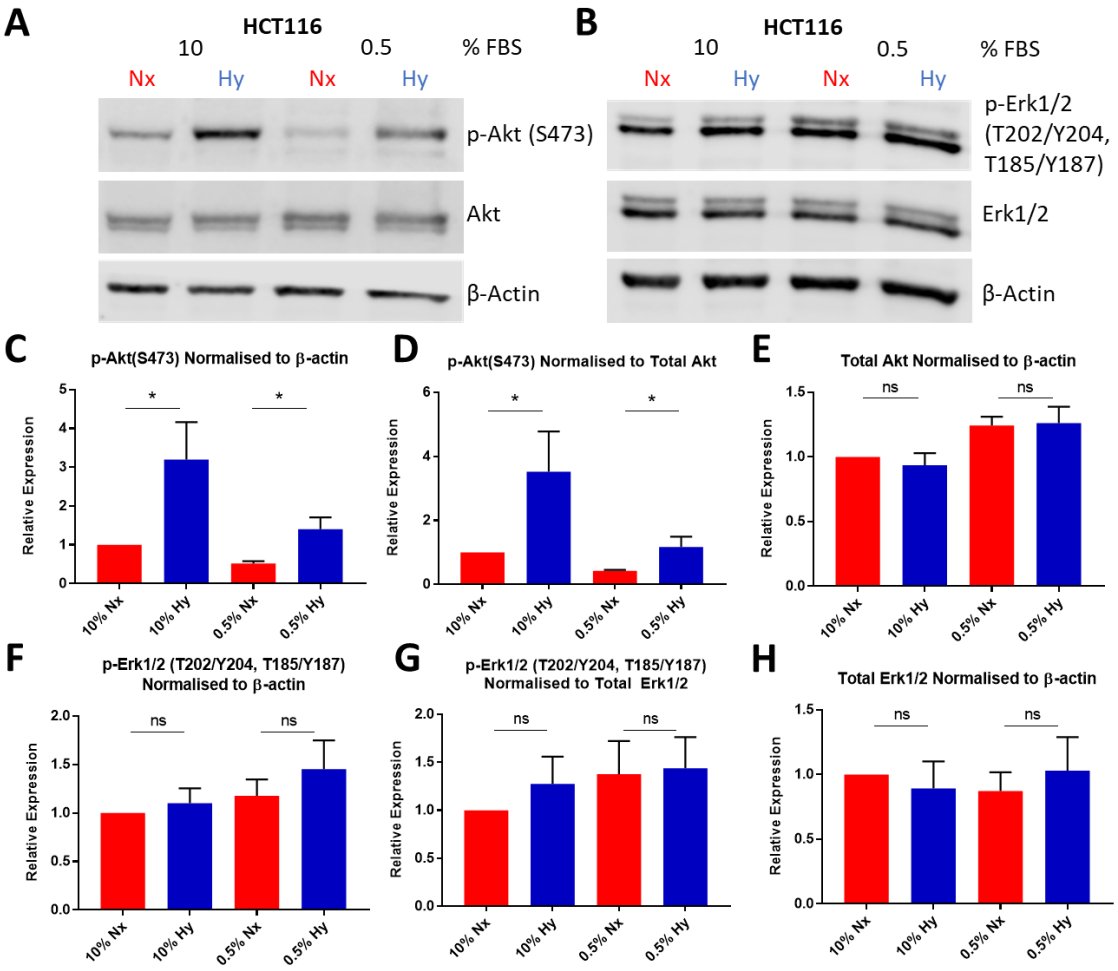

Figure 5.15 Validation of phospho-array target hypoxic induction in HCT116 in 10% and 0.5% FBS. Representative western blots are shown at 24 hours normoxia (21% O_2) or hypoxia (1% O_2) at 10% and 0.5% FBS conditions for p-Akt (S473) alongside total Akt (A) or p-Erk1/2 (T202/Y204, T185/Y187) alongside total Erk1/2 (B). (C-E) Quantifications for p-Akt and total Akt. (F-H) Quantifications for p-Erk1/2 and total Erk1/2. Data analysed using a one-way ANOVA. N=3. *p<0.05, **p<0.01, ***p<0.001, ****p<0.0001.

5.4 Discussion

5.4.1 FOSL2 Phosphorylation in Hypoxia

This chapter began by investigating the phosphorylation of FOSL2 in hypoxia (1% O_2) and normoxia (21% O_2) at multiple time-points in Ls174T and HCT116 cell lines, representing CMS3 and CMS4 respectively. When studying phosphorylation and signalling pathways, care was taken to seed cells in 0.5% FBS conditions to observe the true impact of hypoxia and avoid growth factors within the serum from stimulating the investigated targets. Despite representing n=2 due to reagent supply issues, a convincing upregulation of p-FOSL2 was observed in both cell lines at the 12 hour hypoxia time-point (2.8 and 2.4-fold increase for HCT116 and Ls174T respectively) and for HCT116 at the 24-hour time point (2.7-fold increase). An additional biological replicate is needed to confirm these findings. However, it would be logical that FOSL2 activity is increased in hypoxia due to the later conclusion that FOSL2 is an important regulator of the hypoxic transcriptome. Important future work would confirm the FOSL2 activation status in hypoxia using an alternative approach in order to add robustness to the conclusion. For instance, the use of a promoter-regulated luciferase assay containing AP1 response elements to observe if increased activity is found in hypoxia.

Phosphorylation of transcription factors can alter their activity by a range of mechanisms. Phosphorylation can result in transcriptional repression rather than activation, for example Akt-mediated phosphorylation of the FOXO transcription factors inhibits their activation of pro-apoptotic genes and therefore enhances cell survival[307]. In terms of AP1, phosphorylation can regulate multiple levels of activity, including dimerization, DNA binding and transactivation[305]. The phosphorylation of JUN subunits is well characterised whilst the mechanisms and outcomes of the FOS subunits remains to be fully elucidated. For c-Jun, five phosphorylation sites have been identified on serine and threonine residues, which regulate activity by distinct mechanisms[308]. JNK-mediated phosphorylation of c-Jun N-terminal domain at S63/S73 enhances the interaction of c-Jun with co-activators, promoting transactivation of target genes. On the other hand, phosphorylation of c-Jun on T91/T93 releases target

genes from transcriptional repression[309–311]. Site-specific phosphorylation is therefore important to establish the fine-tuned multi-faceted transcriptional regulation of AP1 subunits. The phosphorylation of subunits within the transactivation domains can also help to establish differential gene expression of the different transcription factors. For example, it has been observed that the N-terminal transactivation domains of c-Jun and JunD show greater divergence than their functional domains. The local sequence contexts of MAPK phospho-acceptor sites present in the N-terminus of JunD are essentially identical to those present in c-Jun[312]. Whilst phosphorylation of c-Jun is primarily responsive to JNKs, the N-terminal domain of JunD is phosphorylated upon transient activation of ERK1/2[313]. Interestingly, it has been found that substrate specificity for MAPKs may be determined by distinct targeting domains known as docking sites and not just the sequence flanking the phospho-acceptor site. These sites are able to enhance the efficiency of phosphorylation by mediating the interaction of kinase and substrate[312]. Regulation of FOSL2 by phosphorylation is less well determined, and it would be important to investigate the sites of FOSL2 phosphorylation, and to investigate the presence of kinase docking sites to infer regulatory mechanisms, both of which may be achieved by utilising bioinformatics tools.

It was hypothesised that the phosphorylation of FOSL2 observed in hypoxia induced a localisation shift in FOSL2 from cytoplasm to nucleus. However, as Figures 5.3 and 5.4 show, FOSL2 localisation remained exclusively nuclear between normoxic and hypoxic conditions. This nuclear localisation of FOSL2 was also confirmed in the tissue micro-array as discussed in Chapter 4. The next steps would therefore be to measure other parameters of transcriptional activation such as DNA binding (for example by ELISA) and dimerisation which could be achieved by Co-IP, and to observe how these differ between normoxic and hypoxic conditions. It would be interesting to measure these parameters in the presence and absence of inhibitors against predicted kinase regulators of FOSL2. ERK1/2 is the canonical activator of FOSL2 as described above, however it would be important to establish whether alternative mechanisms of regulation exist in hypoxia that lead to FOSL2 mediating important aspects of the hypoxic response. During the validation of the phospho-kinase array experiment, it

was found that levels of phospho-ERK1/2 (T202/Y204, T185/Y187) were significantly upregulated in Ls174T in hypoxia compared to normoxia (Figure 5.14), yet this was not apparent in HCT116 (Figure 5.15) despite p-FOSL2 upregulation in hypoxia in HCT116. It would therefore be interesting to consider whether alternative mechanisms of FOSL2 regulation in hypoxia are present across different CRC molecular subtypes.

5.4.2 HIF-Associated Hypoxic Signalling

Hypoxia-induced signal transduction was investigated through a phospho-kinase array which allowed for the simultaneous measurement of the phosphorylation of 48 target proteins involved in key signalling pathways. This experiment was performed in Ls174T at 24 hours normoxia (21% O_2) or hypoxia (1% O_2) and utilised CRISPR-Cas9-generated knockdown clones for HIF1α, HIF2α and FOSL2 alongside a non-targeting control clone. Interestingly, an almost global upregulation of phospho-signalling was found to occur in hypoxia compared to normoxia (94% of targets). Members of the Akt and MAPK signalling pathways are known to be increased in hypoxia and also serve to regulate HIF signalling as previously described[302]. However, it is also important to consider the site-specific phosphorylation of targets and the divergent role that this may play in signalling. For example, whilst both Akt activating phosphorylations are increased in hypoxia, the Akt1/2/3 S473 site is increased considerably more than the Akt1/2/3 T308 site (0.88 and 0.22 log2 fold changes respectively), an interesting finding as T308 is considered the more important marker for Akt activation[314]. Whilst the divergent roles of the activations are not yet fully elucidated, the S473 phosphorylation has been implicated in GLUT4 translocation and may therefore play a role in hypoxic glucose metabolism[315]. Akt1/2/3 S473 phosphorylation is regulated by the mTORC2 complex, downstream of which are increased cell growth and survival pathways[315]. Interestingly, it has been demonstrated that reactive oxygen species, mediated by $p22^{phox}$-based Nox oxidases have a role in the activation of Akt on S473, a site phosphorylated by the mTORC2 complex, which in turn goes on to regulate HIF2α stability in hypoxia[316]. TOR itself is the third most increased phosphorylation in hypoxia on the S2448 residue, enabling interactions to occur between other mTOR complex proteins.

HSP27 S78/S82 is the second highest upregulated target in hypoxia compared to normoxia. Interestingly, HSP27 is upregulated in many cancers and is associated with aggressiveness and poor prognosis[317]. HSP27 has been found to be upregulated by MET inhibition through a pathway dependent on MAPK/ERK signalling and HIF1α[318]. It has been found that inhibiting HSP27 inhibits progression and metastasis of CRC[319]. Other prominent upregulations in hypoxic signalling include phosphorylation of the STAT family of transcription factors. Both STAT5a and STAT5b activating phosphorylations on Y694 and Y699 feature in the top 10 largest fold inductions in hypoxia. This is an interesting finding as although STAT5 has been associated with solid tumours and early research highlighted induction by hypoxia[320,321], the association of STAT5 in hypoxic colorectal tumours has not been characterised. Both STAT3 residues (Y705 and Y727) are also upregulated in hypoxia compared to normoxia, which is well characterised in hypoxic CRC and has also been identified as a regulator of HIF1α[322,323]. Despite the global upregulation of hypoxic phospho-signalling, only two upregulations were found to be statistically significant (WNK1 T60 and STAT6 Y641), both representing relatively small log2 fold changes in hypoxia. This is due to significant variation present in one replicate of the phospho array, where the commercial kit was discontinued and replaced with a substitute. Any alteration in buffer or reagent composition is likely to influence phosphorylation levels.

HIF1α and HIF2α knockdown clones in hypoxia were normalised to control hypoxia in order to determine their associations with phospho-signalling in hypoxia. Interestingly, there was no significant downregulation of any target phosphorylation upon HIF1α knockdown compared to control hypoxia. Conversely, a number of targets were upregulated upon HIF1α knockdown, although the interests of this investigation was to study downregulations in order to identify potential targetable kinase signalling induced in hypoxia in CRC. On the other hand, HIF2α knockdown was found to significantly reduce β-catenin expression by -1.8 log2 fold change, which in the array was measured as total protein as opposed to a specific phosphorylation site. This is supported by previous research which found that HIF2α was required for β-catenin activation and subsequent proliferation in renal cell carcinoma[324]. The activity of β-catenin has also been shown to be upregulated by HIF2α in pancreatic cancer[325],

however this relationship is less well characterised in CRC despite the importance of Wnt signalling in CRC pathology. The other target significantly downregulated upon HIF2α knockdown was Akt1/2/3 S473. This is an interesting and undefined interaction in CRC, as both HIF2α and Akt1/2/3 activation are regulated by mTORC2[299,315]. It is therefore possible that some form of regulatory loop exists whereby mTORC2 is regulated by HIF2α, which then serves to phosphorylate and activate HIF2α and Akt1/2/3 S473.

5.4.3 FOSL2 Association with Hypoxic Signalling

Finally, the FOSL2 knockdown condition in hypoxia was normalised to control hypoxia in order to identify hypoxic phospho-signalling associated with FOSL2 in Ls174T cells. Several significant downregulations were identified upon knockdown of FOSL2, all of which occurred in the most part independently of the HIFs aside from RSK1/2 S221/S227 which occurred in co-association with HIF2α. This is an interesting finding as it presents FOSL2 as a novel regulator of hypoxic cell signalling independently of the HIFs. As presented in the Results, HSP60 association with FOSL2 could represent an indirect mechanism for FOSL2 regulation of the HIFs themselves, as HSP60 is a chaperone protein known to regulate HIF1α stability. The association of STAT3 S727 with FOSL2 is also a novel finding which could present a mechanism for FOSL2 regulation of HIF1α due to HIF1α regulation by STAT3 as mentioned previously[322]. The interplay between hypoxia and mTOR signalling has been discussed, and FOSL2 association with both PRAS40 T246 (known to promote mTORC1 signalling) and downstream p70S6K (T421/S424) presents a novel mechanism for FOSL2 association with mTOR signalling in colorectal cancer. Future work would involve the validation of these targets as associated with FOSL2 in additional cell lines and alternative FOSL2 knockdown models. As this work was performed in single knockdown clones (as discussed later), it would be important to repeat the work in pooled populations in order to determine that effects seen are not clonal in nature and represent true changes.

6.0 Discussion and Future Directions

6.1 Overall Conclusions

This project sought to characterise the role that the AP1 subunits FOSL2 and JUND play in the regulation of the hypoxic response in colorectal cancer. This was based on preliminary data in the form of a lentiviral shRNA colorectal cancer viability screen, that identified AP1 as a significant mediator of hypoxic cell survival. The main findings are summarised here.

It was found that the expression of FOSL2 and JUND protein was significantly increased in hypoxia (1% O_2) compared to normoxia (21% O_2) in Ls174T cells at both the 24 and 48 hour hypoxic time-points. An inducible CRISPR-Cas9 system was then optimised in order to study the impact of FOSL2 and JUND knockdown in CRC cell lines. In HCT116, it was found that FOSL2 knockdown significantly reduced average spheroid volume, independently of doxycycline treatment. JUND knockdown with JUND-g2 also led to a significantly smaller spheroid volume, although this was not seen with JUND-g1 and was also seen in the JUND-g2 minus doxycycline control, therefore more work is needed for the conclusion to be robust. In the cell survival clonogenic assay, FOSL2 knockdown was found to reduce cell survival by 42% in hypoxia, while for JUND survival was significantly decreased by 65% and 46% in JUND-g1 and JUND-g2 respectively. However, the corresponding normoxia knockdown conditions were not included and so it cannot be concluded whether this effect is hypoxia-specific.

Given the phenotypic effects identified, the hypoxic transcriptomes of FOSL2 and JUND were then explored using RNA-sequencing. FOSL2 was found to be a novel regulator of the hypoxic transcriptome, associating with 333 DEGs that were also upregulated in control hypoxia compared to control normoxia. Several of these DEGs are known to play important roles in the pathogenesis of cancers including colorectal cancer, such as MMP14. In terms of pathway analysis, FOSL2 was found to be a novel regulator of hypoxia-inducible metabolic genes featuring in several metabolic pathways, such as ALDOC, HK1 and PFKL. Interestingly, JUND was found to play a less

significant role in the associations with the hypoxic response, with only 61 DEGs identified that were both JUND-associated and induced by hypoxia. In fact, some of the top JUND-associated genes were tumour suppressor genes, such as PTPRO and CDHR5. The co-association of hypoxia-inducible DEGs by both FOSL2 and JUND were explored, and both were found to associate with JUND itself, ANGPTL4 and, interestingly, the CYP2W1 enzyme required for the activation of many HAPs[243]. Some of the co-associated genes are associated with cancer, such as DDIT4 and PFKFB4[240,241].

As FOSL2 was clearly mediating the greater effect on the hypoxic response compared to JUND, FOSL2 expression analysis was carried out on a large human CRC tissue micro array in order to assess clinical relevance. FOSL2 expression was associated with 'alive' 5-year survival status as opposed to poorer survival as hypothesised. Despite this, FOSL2 expression was also significantly associated with a number of pro-metastatic clinicopathological variables, such as high levels of tumour budding and an infiltrative tumour edge phenotype. Interestingly, the association of FOSL2 expression with pro-metastatic variables was found in FOSL2-positive immune cell staining as well as in the tumour epithelium. Importantly, FOSL2 expression was also correlated with CA9 expression, supporting the hypothesis of a role in tumour hypoxia. FOSL2 knockdown cell lines were investigated *in vivo* for their effect on sub-cutaneous tumour cell growth but no significant differences were found between knockdown cell lines and control cell lines in either Ls174T or HCT116.

Finally, the role of FOSL2 in hypoxic phospho-signalling was explored. This was due to the fact that clinically, transcription factors represent notoriously difficult targets. Comparatively, small-molecule inhibitors against kinases show great efficacy. Thus, the signalling pathways associated with FOSL2 were explored in order to identify what oncogenic mechanisms could be inhibited through targeting the upstream signalling resulting in FOSL2 activation. Phospho-FOSL2 was found to be upregulated in hypoxia (1% O_2) compared to normoxia (21% O_2) at the 12 and 24 hour time-points in both Ls174T and HCT116, suggesting FOSL2 activation in hypoxia. No differences were found in the localisation of FOSL2 between normoxia and hypoxia, which remained exclusively nuclear. HIF1α, HIF2α and FOSL2 knockdown clones were used in a phospho array experiment, where phospho-signalling proteins were found to be

almost globally upregulated in hypoxia. Interestingly, HIF2α was found to play a more important role in associating with phospho-proteins than HIF1α, including targets such as β-catenin. 7 phospho-proteins were found to be significantly downregulated upon FOSL2 knockdown, largely independently of the HIFs. FOSL2 was demonstrated to be involved in the activation of various members of the mTOR and ERK signalling pathways at multiple effector levels.

6.2 Future Directions

6.2.1 Validating the Role of FOSL2 as a Hypoxic Target in CRC

This project identified FOSL2 as a novel regulator of the hypoxic response in CRC through phenotypic effects, transcriptome and phospho-signalling analysis. Future work would aim to characterise in more detail the specific targets of FOSL2 in hypoxia that mediate its phenotypic effects. For example, the RNA-sequencing identified novel top hypoxia-inducible FOSL2-associated DEGs implicated in cancer, such as DEGS2 and SGPP2[225–227]. Furthermore, FOSL2 was found to associate with a number of metabolic genes involved in glycolysis, an important feature of hypoxic tumour metabolism[231]. It would therefore be important to validate this novel role of FOSL2 and to observe if HIF1α is dependent on FOSL2 for the regulation of glycolysis in CRC. The phospho-kinase signalling array also identified novel targets of FOSL2, this time whereby FOSL2 was regulating levels of protein phosphorylation. These included STAT3 and HSP60, important in the hypoxic response[322], among other members of mTOR and ERK pathways. It would be important to explore the mechanism of FOSL2 activation of these signalling proteins. The RNA-sequencing did not reveal any upstream kinases associated with FOSL2 at the expression level, although the array and sequencing were performed in Ls174T and HCT116 respectively and so are not directly comparable.

Another important follow-up investigation arising from the results of this project would be to explore the role of FOSL2 in the regulation of invasion and metastasis. Results from the TMA suggested a significant association between FOSL2 expression and pro-metastatic variables within the tumour epithelium. These included tumour

budding and infiltrative tumour edge. In addition to this, the RNA-sequencing identified MMP14 as one of the FOSL2-associated targets most induced by hypoxia. MMPs including MMP14 have been linked to cell proliferation and invasion in many cancers including CRC[230,326]. This would therefore be an important novel FOSL2 target to validate from the sequencing. An additional mechanism for FOSL2-associated invasion and metastasis may be through FOSL2 regulation of β-catenin, expressed highly in the nuclei of tumour-budding cells upon activation of Wnt signalling[270]. The TMA analysis revealed high FOSL2 correlated with low levels of membrane-bound β-catenin, implying higher levels within the nucleus and possible activation of Wnt signalling, leading to induction of EMT. This is further supported by the RNA-sequencing, where Delta/Notch-like epidermal growth factor (EGF)-related receptor (DNER) was found to be significantly associated with FOSL2 and induced by hypoxia. DNER is known to regulate EMT via the Wnt/β-catenin pathway and is associated with cancers including breast[327]. This therefore represents robust justification for further analysis into the regulation of invasion and metastasis by FOSL2 via the Wnt/β-catenin pathway.

Further experiments of interest would therefore be to examine the effect of FOSL2 knockdown on invasion and cell migration *in vitro*. If FOSL2 mediates tumourigenic effects through regulation of an invasive phenotype, it may explain why no significant results were yielded from the FOSL2 knockdown *in vivo* experiment. It is possible that FOSL2 is not playing a role in tumour growth, and therefore an intraperitoneal (IP) injection model may have been more relevant in order to study tumour metastasis. This hypothesis is supported by the literature, where in colorectal cancer, FOSL2 silencing inhibited cell migration and invasion *in vitro*[252]. A study in non-small cell lung cancer has also confirmed this, where FOSL2 was found to regulate EMT and metastasis[328].

Finally, future work could involve the use of kinase inhibitors to inhibit FOSL2 activation and subsequent regulation of the pro-tumourigenic pathways listed above. This is an attractive therapeutic possibility given the difficulty in targeting transcription factors directly. As previously described, AP1 inhibitors themselves have not yet been clinically approved[303]. Dual-mechanism ERK1/2 inhibitors have been developed which

block ERK1/2 phosphorylation by MEK1/2 and prevent nuclear accumulation of ERK1/2[329]. Future work would involve the use of ERK1/2 inhibitors currently undergoing clinical trial to observe whether the malignant phenotypes associated with FOSL2 were significantly reduced. Many of the MAPK family members were significantly increased in control hypoxia compared to control normoxia, representing these as potential ready-targetable hypoxic mediators.

6.2.2 Investigating the FOSL2 Hypoxic Interactome

Unanswered questions remain on how FOSL2 is associated with target genes in a hypoxia-dependent manner. It is highly likely that the dimer compositions of FOSL2 is altered under hypoxic conditions, that drives the transactivation of alternative genes. However, without investigating the normoxic vs hypoxic interactome of FOSL2, it is very difficult to decipher this due to the complex nature of AP1. Additionally, the transcriptomic analysis of FOSL2 knockdown alone is ignoring the role of the FOSL2 binding partner, and therefore important information is likely to be missed. Initially, co-immunoprecipitation experiments could be performed in order to analyse which JUN subunits exhibit increased binding to FOSL2 under hypoxic conditions. The results of the RNA-sequencing imply that this is unlikely to be JUND, where only a small number of DEGs overlapped between the two, and so it would be interesting to explore whether FOSL2 may be heterodimerising with c-Jun or JUNB in hypoxia.

Additionally, it would be beneficial to explore the FOSL2 hypoxic interactome more broadly. For example, through rapid immunoprecipitation mass spectrometry of endogenous proteins (RIME)[330], the transcriptional complexes formed that include FOSL2 could be compared in normoxia and hypoxia. In addition to identifying heterodimerisation partners or hypoxia-specific cofactors, such technology may also uncover any non-canonical roles of FOSL2 in hypoxia, as has been identified for other transcription factors. For example, in hypoxic breast cancer cells, a novel role for HIF1 was identified in the recruitment of TRIM28 and DNA-dependent protein kinase (DNA-PK) to HRE sites to release paused pol II, enabling recruitment of CDK9 and mediating productive transcriptional elongation[331]. HIF2α was also found to have a novel role in

hypoxia, whereby HIF2α forms a complex with RNA-binding protein RBM4 and cap-binding eIF4A2, with a RNA-HRE recruiting this complex to mRNAs for active translation[332].

RIME techniques can also be used in parallel with ChIP-SEQ in order to identify the regions of chromatin to which a transcription factor binds. This would be of great interest in the study of FOSL2, in order to identify whether or not the binding distribution alters between normoxic and hypoxic conditions. ChIP-SEQ carried out on other additional AP1 subunits could also help to establish which heterodimers are involved in regulating specific genes. Interestingly, AP1 has been found to bind and exert transcriptional regulatory effects through distal enhancer regions as opposed to gene promoter regions. In KRAS-mutant CRC, ARID1A was identified as a cofactor for AP1 bound to enhancer sites, with the loss of the ARID1A cofactor leading to transcriptional deregulation and impaired proliferation[333]. It has also been suggested that AP1 may be acting as a pioneer factor at such enhancer sites, through the regulation of chromatin accessibility[334]. In mammary cancers, hyperactivated AP1 was found to promote chromatin accessibility at the IL-6 locus, associated with angiogenesis and metastasis[335]. Thus, large-scale 'omics' techniques would provide invaluable mechanistic information about the role of FOSL2 in hypoxia, such as interacting partners (RIME), distribution of binding sites (ChIP-SEQ) and regulation of chromatin accessibility (ATAC-seq).

6.2.3 Investigating the Role of JUND in Associating with the Hypoxic Response

The findings related to the role of JUND in CRC and the hypoxic response within this project highlight the complexities involved with the study of a complex heterodimeric transcription factor such as AP1. While JUND initially seemed to be exerting a phenotypic effect as identified through JUND knockdown, the results were contentious and not supported by the RNA-sequencing data. The effect on spheroid growth was identified in only one guide RNA, with no difference in the other guide RNA. Furthermore, the significant reduction in cell survival as measured through the clonogenic assay was identified only in hypoxia and therefore may not be hypoxia-

specific. It is also important to note that identified effects through knockdown of an AP1 subunit may represent compensatory effects rather than a true effect of the subunit. This notion is supported by the RNA-sequencing data, whereby c-Jun expression was found to be significantly upregulated upon JUND knockdown. It is therefore important to establish in future work involving AP1 knockdowns which dimer compositions are forming as a result of this, and the influence this is having on the observed phenotype.

6.3 Limitations of Methodology

Several limitations of methodology ought to be acknowledged when considering the conclusions drawn from this project. These include the use of the colorectal cancer cell lines that were utilised for the *in vitro* data produced in chapters 1 and 2. Whilst cancer cell lines are useful tools to model aspects of tumour phenotypes and response to drugs, it is accepted that they are not a model with a great deal of clinical relevance. This means that conclusions drawn regarding tumour behaviour identified in 2D monolayer culture of cell lines often do not translate into more realistic 3D models featuring aspects of the TME, or indeed into patient tumours. This is supported by studies that have identified a lack of correlation between cancer cell lines and the tumour type they represent[336]. To combat this, some studies have attempted to select cancer cell lines based on gene expression profiles aligning well to human tumours[337]. Ideally, this work could be validated in patient-derived organoids, which are 3D cultures more accurately simulating tumour characteristics and recapitulating tumour heterogeneity[338]. A model like this could therefore bridge the gap between cell line and animal models for future work.

In addition to the model of cell line, the selection of cell lines used in the study may pose a further limitation. If the work was to be repeated, I would screen a larger panel of CRC cell lines initially for expression of FOSL2 and JUND in normoxia and hypoxia in order to see in which cell lines AP1 may be most important in hypoxia. Additionally, the two main cell lines used for experiments were Ls174T, representing the colorectal cancer CMS3 subtype, and HCT116, representing CMS4. This is useful in order to see if results found within experiments are applicable to more than one CRC cell line

generally or are the result of a cell-line effect. However, in order to truly draw conclusions about molecular subtypes, more than one cell line per subtype would need to be included within the study. Whilst knockdown cell lines were generated in 2 cell lines per CMS3 and CMS4 (4 cell lines in total), a lack of gRNA efficiency across all cell lines meant that just one per subtype was taken forward for experiments. If more time was available, the CRISPR-Cas9 approach would be optimised across more cell lines in order to observe trends across molecular subtype categories. Finally, it would be useful to include a 'normal' colon cell line within experiments in order to see which mechanisms were tumour specific, and which were applicable to the colon in general.

Another limitation to consider is the defined oxygen concentrations used within experiments and how they relate to tumour physiology. 'Normoxia' at 21% O_2 describes normal levels of oxygen within tissue culture flasks, however it is becoming increasingly scrutinised within the field of hypoxic research as this does not represent an accurate comparator for the levels of physiological tissue oxygenation. The oxygen concentration within tissues is significantly less than 21%, ranging from 3.4-6.8% and with an average of around 6.1% O_2[339]. Across the intestine, oxygen concentrations range from 3.5-6% O_2. It would therefore be much more physiologically accurate to replace normoxia at 21% O_2 with physoxia at 5-6% O_2 for the experiments performed in this study. Physoxia was used for this reason alongside normoxia and hypoxia for the FOSL2 and JUND protein expression time-courses and no significant differences were found in baseline FOSL2 or JUND expression between physoxia and normoxia. However, this does not mean that the activation status or downstream transcriptomes regulated by these genes are not different between physoxia and normoxia, and so for the large-scale experiments performed in this project such as the phospho-kinase array and RNA-sequencing, physoxia would be a more appropriate condition. Future validation of targets identified through these experiments would therefore include physoxic conditions.

7.0 Appendix

7.1 Supplementary Experimental Information

1. qPCR Primer Sequences

Target	Sequence
β-actin	**F:** ATTGGCAATGAGCGGTTC
	R: GGATGCCACAGGACTCCAT
CA9	**F:** CTTGGAAGAAATCGCTGAGG
	R: TGGAAGTAGCGGCTGAAGTC
SORBS1	**F:** ATTCCCAAGCCTTTCCATCAG
	R: TTTTGCTGTTCTCGATTGTGTTG
DEPTOR	**F:** CCTACCCAAACTGTTTTGTCGC
	R: CGGTCTGCTAATTTCTGCATGAG
PCK1	**F:** GCTGGTGTCCCTCTAGTCTATG
	R: GGTATTTGCCGAAGTTGTAG
FOSL2	**F:** TATCCCGGGAACTTTGACAC
	R: GACGCTTCTCCTCCTCTTCA
JUND	**F:** GCAAGCTGGAGCGCATCT
	R: ACTCAGTACGCGGGCAC

2. DNA Primers Flanking gRNA Sites: (For sequencing the cutting site)

Target	Sequence
HIF1α g1	**F:** ATTGGCAATGAGCGGTTC
	R: GGATGCCACAGGACTCCAT
HIF1α g2	**F:** CTTGGAAGAAATCGCTGAGG
	R: TGGAAGTAGCGGCTGAAGTC
HIF1α g3	**F:** ATTCCCAAGCCTTTCCATCAG
	R: TTTTGCTGTTCTCGATTGTGTTG
HIF2α g1	**F:** CCTACCCAAACTGTTTTGTCGC
	R: CGGTCTGCTAATTTCTGCATGAG
HIF2α g2	**F:** GCTGGTGTCCCTCTAGTCTATG
	R: GGTATTTGCCGAAGTTGTAG

HIF2α g3	**F:** TATCCCGGGAACTTTGACAC
	R: GACGCTTCTCCTCCTCTTCA

3. Western Blot Buffer Recipes

10X TBS (1L)

24g Tris Base

88g NaCl

Dissolve in 900ml dH_2O, adjust pH7.6, make up to 1L final volume.

1X TBS-T (1L)

100ml 10X TBS

900ml dH_2O

1ml Tween-20

1X 5%-BSA-TBS-T [w/v] (100ml)

5g BSA

100ml 1X TBS-T

1X 3%-BSA-TBS-T [w/v] (100ml)

3g Milk Powder

100ml 1X TBS-T

10X Running Buffer (1L)

30.3g Tris Base

144.4g Glycine

10g SDS

Prepare to 1L with dH_2O.

1X Transfer Buffer (1L)

200ml 5X Bio-Rad Transfer Buffer

200ml 100% EtOH

600ml dH_2O

4. Western Blot Hand-Cast Gel Recipes

Reagents per 1 x 1mm gel:

Reagent	% Resolving Gel			6% Stacking Gel
	8	10	12	
dH_2O	4.2ml	3.8ml	3.4ml	2.9ml
40% Acrylamide	1.6ml	2ml	2.4ml	750µl
1.5M Tris pH8.8	2ml	2ml	2ml	N/A
0.5M Tris pH6.8	N/A	N/A	N/A	1.25ml
10% SDS	80µl	80µl	80µl	50µl
10% APS	80µl	80µl	80µl	50µl
TEMED	8µl	8µl	8µl	5µl

5. Phos-Tag Reagent Recipes

5mmol/L Phos-Tag Solution containing 3% [w/w] methanol

10mg Phos-Tag AAL-107

100µl Methanol

3.2ml dH_2O

10mmol/L $ZnCl_2$ Solution (always prepared fresh) (500ml)

0.7g $ZnCl_2$

500ml dH_2O

1.4mol/L Bis-Tris/HCl Solution, pH6.8 (100ml)

29.9g Bis-Tris base

10ml 6.0mol/L HCl

Prepare to 100ml with dH_2O

0.5mol/L Sodium Bisulfite Solution (100ml)

5.3g $NaHSO_3$

Prepare in 100ml dH_2O

5X Running Buffer, pH7.8 (500ml)

30.0g Tris Base

52.3g MOPS

25ml 10% SDS [w/v]

Prepare to 500ml with dH_2O

1X Running Buffer (500ml)

100ml 5X Running Buffer

5ml 0.5mol/L Sodium Bisulfite

Prepare to 500ml with dH_2O

6. Phos-Tag Reagent Recipes

Reagents per 1 x 1mm gel:

Reagent	8% Resolving Gel (50µM Phos-Tag)	4% Stacking Gel
dH_2O	3.7ml	3.2ml
40% Acrylamide	1.4ml	500µl
1.54M Bis-Tris	1.75ml	1.25ml
5mM Phos-Tag	70µl	N/A
10mM $ZnCl2_2$	70µl	N/A
10% APS	70µl	50µl
TEMED	7µl	5µl

7.2 Professional Internship Placement: Reflective Statement

Note to Examiners:

This statement is included as an appendix to the thesis in order that the thesis accurately captures the PhD training experienced by the candidate as a BBSRC Doctoral Training Partnership student.

The Professional Internship for PhD Students is a compulsory 3-month placement which must be undertaken by DTP students. It is usually centred on a specific project and must not be related to the PhD project. This reflective statement is designed to capture the skills development which has taken place during the student's placement and the impact on their career plans it has had.

PIP Reflective Statement

I completed my PIP from 1st March 2021 – 23rd April 2021 (a total duration of 8 weeks). While the initial guidelines are for students to complete a 3 month placement, additional flexibility was granted due to the lost lab time that students faced due to COVID, and so I was able to complete an 8 week placement instead. I completed my virtual placement at CamBioScience (a brand of the OBRIZUM Group company), under the supervision of Dr Michelle Ware. CamBioScience is an educational technology brand which works with life science experts in order to run various courses and conferences for scientists across many disciplines. The courses provided by CamBioScience include on-demand online courses in CRISPR and 3D cell model technologies, as well as live courses held throughout the year.

The project that I worked on with CamBioScience was primarily focussed on improving and adding content to the on-demand CRISPR course and the 3D cell models course, which was suitable for me given my background in molecular biology and a basic understanding of the course content. Before being able to make course improvements, I had to understand how the OBRIZUM platform worked. The platform is unique in that it provides an adaptive, personalised learning experience through algorithms. Therefore my first task was to spend time completing all 3 on-demand courses, noting extensive platform and course feedback as I went along. This involved completing a large questionnaire and sending this feedback on to the technology team to consider. Following on from this, I was given training in basic video editing using the OpenShot software, and in generating closed captions using the Trint software. I spent a large amount of time sifting through a backlog of currently unused video footage and PowerPoint slides from previous live courses, editing the content and adding this to the platform. Another part of this was question creation, as platform users are assessed by questions on each piece of content they are shown. Halfway through my placement, CamBioScience prepared for the launch of their new Merck course, in

digital PCR and sequencing. I played an important role in getting the content and questions for this course ready within a strict deadline.

I completed an array of placement outcomes during my 8 weeks with CamBioScience. These include providing the aforementioned platform and course feedback to various different members of the company. This feedback is now being considered and will hopefully help to improve the online user experience. In addition to this, I was able to edit many new videos for both the online CRISPR and 3D cell models courses. These videos were in a diverse range of cutting-edge topics, such as CRISPR base editing, deadCas9 technologies, and CRISPR screening. The content that I was able to create can now be added into the courses in the subsequent months. This new content features in each monthly member's newsletter and encourages users to either re-engage with their course or to renew their subscriptions. Other outcomes of my placement include helping with the delivery of content for CamBioScience's new Merck course, which was time-sensitive and involved quality control checking all content before being added to the platform. While these formed the main outcomes of my placement, I was also involved in small projects throughout. For example, another intern and I collaboratively created a platform Q&A and user guide to help with the user experience. I was also involved with a mini-project that aimed to investigate the platform's 'Flashcard feature', which had been added into the platform with little understanding of its function. After some testing I was able to consolidate some ideas and feed these back to the team.

I learned a variety of skills during my placement. On a superficial level, the course content itself was invaluable in providing theoretical and practical advice for my own CRISPR experiments in the lab. I also learned how to use several types of software, including Trint and Openshot, in order to edit videos which is a completely new skill for me. In addition to these things, I gained and improved on a number of transferable skills. These include project management, as I was granted a large amount of independence to achieve my project outcomes. While difficult at first, I soon came up with an organised system of listing tasks by priority, which I will continue into my PhD. Time management was also important, especially relating to the Merck course where we only had several days to get the content in order before the course launch. During this time especially I developed my team working skills, as myself and 3 others were working on collaborative online documents to continually update each other on the project. Finally, I feel like I developed my presenting skills. I was involved with weekly meetings with members from different departments including technical and sales, and I frequently reported back my progress to them.

My placement time with CamBioScience was incredibly useful for me on many levels. I learned a huge variety of skills including those relating to the laboratory, technical online skills, and many transferable skills listed above. I was able to network with team members from different departments and backgrounds and gained significant insight from their own journeys out of academia and into the company. The placement has

encouraged me to consider options not only outside of academia but outside of the laboratory.

8.0 Bibliography

1. SadiKDvic, B., Al-Romaih, K., Squire, J. & Zielenska, M. Cause and Consequences of Genetic and Epigenetic Alterations in Human Cancer. *Curr. Genomics* **9**, 394–408 (2008).
2. Hollstein, M., Sidransky, D., Vogelstein, B. & Harris, C. C. p53 Mutations in Human Cancers. *Science* **253**, 49–53
3. Olivier, M. *et al. Li-Fraumeni and Related Syndromes: Correlation between Tumor Type, Family Structure, and TP53 Genotype 1*. *CANCER RESEARCH* **63**, (2003).
4. Gerlinger, M. *et al.* Intratumor heterogeneity and branched evolution revealed by multiregion sequencing. *N. Engl. J. Med.* **366**, 883–892 (2012).
5. Sharma, A. *et al.* Non-Genetic Intra-Tumor Heterogeneity Is a Major Predictor of Phenotypic Heterogeneity and Ongoing Evolutionary Dynamics in Lung Tumors. *Cell Rep.* **29**, 2164-2174.e5 (2019).
6. Hanahan, D. & Weinberg, R. A. The hallmarks of cancer. *Cell* **100**, 57–70 (2000).
7. Hanahan, D. & Weinberg, R. A. Hallmarks of Cancer: The Next Generation. *Cell* **144**, 646–674 (2011).
8. Quail, D. F. & Joyce, J. A. Microenvironmental regulation of tumor progression and metastasis. *Nature Medicine* **19**, 1423–1437 (2013).
9. Malanchi, I. *et al.* Interactions between cancer stem cells and their niche govern metastatic colonization. *Nature* **481**, 85–91 (2012).
10. Straussman, R. *et al.* Tumour micro-environment elicits innate resistance to RAF inhibitors through HGF secretion. *Nature* **487**, 500–504 (2012).
11. Sung, H. *et al.* Global Cancer Statistics 2020: GLOBOCAN Estimates of Incidence and Mortality Worldwide for 36 Cancers in 185 Countries. *CA. Cancer J. Clin.* **71**, 209–249 (2021).
12. Center, M. M., Jemal, A., Smith, R. A. & Ward, E. Worldwide Variations in Colorectal Cancer. *CA. Cancer J. Clin.* **59**, 366–378 (2009).
13. Bray, F. *et al.* Global cancer statistics 2018: GLOBOCAN estimates of incidence and mortality worldwide for 36 cancers in 185 countries. *CA. Cancer J. Clin.* **68**, 394–424 (2018).
14. Xi, Y. & Xu, P. Global colorectal cancer burden in 2020 and projections to 2040. *Transl. Oncol.* **14**, 101174 (2021).
15. White, A. *et al.* A review of sex-related differences in colorectal cancer incidence, screening uptake, routes to diagnosis, cancer stage and survival in

the UK. *BMC Cancer* **18**, 906 (2018).

16. Rawla, P., Sunkara, T. & Barsouk, A. Epidemiology of colorectal cancer: incidence, mortality, survival, and risk factors. *Przegląd Gastroenterol.* **14**, 89 (2019).

17. Fearon, E. R. & Vogelstein, B. A genetic model for colorectal tumorigenesis. *Cell* **61**, 759–767 (1990).

18. Conteduca, V., Sansonno, D., Russi, S. & Dammacco, F. Precancerous colorectal lesions (Review). *Int. J. Oncol.* **43**, 973–984 (2013).

19. Stewart, S. L., Wike, J. M., Kato, I., Lewis, D. R. & Michaud, F. A population-based study of colorectal cancer histology in the United States, 1998-2001. *Cancer* **107**, 1128–1141 (2006).

20. Lynch, H. T. & de la Chapelle, A. Hereditary Colorectal Cancer. *N. Engl. J. Med.* **348**, 919–932 (2003).

21. Jasperson, K. W., Tuohy, T. M., Neklason, D. W. & Burt, R. W. Hereditary and Familial Colon Cancer. *Gastroenterology* **138**, 2044–2058 (2010).

22. Fearnhead, N. S. The ABC of APC. *Hum. Mol. Genet.* **10**, 721–733 (2001).

23. MacDonald, B. T., Tamai, K. & He, X. Wnt/β-Catenin Signaling: Components, Mechanisms, and Diseases. *Developmental Cell* **17**, 9–26 (2009).

24. Kwong, L. N. & Dove, W. F. APC and its modifiers in colon cancer. *Adv. Exp. Med. Biol.* **656**, 85 (2009).

25. Boland, C. R. & Goel, A. Microsatellite Instability in Colorectal Cancer. *Gastroenterology* **138**, 2073 (2010).

26. Boland, C. R. *et al.* A National Cancer Institute Workshop on Microsatellite Instability for cancer detection and familial predisposition: development of international criteria for the determination of microsatellite instability in colorectal cancer. *Cancer Res.* **58**, 5248–57 (1998).

27. Thibodeau, S. N., Bren, G. & Schaid, D. Microsatellite Instability in Cancer of the Proximal Colon. *Science* **260**, 816–819

28. Jiricny, J. The multifaceted mismatch-repair system. *Nature Reviews Molecular Cell Biology* **7**, 335–346 (2006).

29. Herman, J. G. *et al.* Incidence and functional consequences of hMLH1 promoter hypermethylation in colorectal carcinoma. *Proc. Natl. Acad. Sci. U. S. A.* **95**, 6870–6875 (1998).

30. Nguyen, H. T. & Duong, H. Q. The molecular characteristics of colorectal cancer: Implications for diagnosis and therapy (review). *Oncology Letters* **16**, 9–18 (2018).

31. Ogino, S. *et al.* CpG island methylator phenotype (CIMP) of colorectal cancer is best characterised by quantitative DNA methylation analysis and prospective cohort studies. *Gut* **55**, 1000–1006 (2006).

32. Weisenberger, D. J. *et al.* CpG island methylator phenotype underlies sporadic microsatellite instability and is tightly associated with BRAF mutation in colorectal cancer. *Nat. Genet.* **38**, 787–793 (2006).

33. Shen, L. *et al.* Integrated genetic and epigenetic analysis identifies three different subclasses of colon cancer. *Proc. Natl. Acad. Sci. U. S. A.* **104**, 18654–18659 (2007).

34. Lengauer, C., Kinzler, K. W. & Vogelstein, B. Genetic instability in colorectal cancers. *Nature* **386**, 623–627 (1997).

35. Thiagalingam, S. *et al.* Mechanisms underlying losses of heterozygosity in human colorectal cancers. *Proc. Natl. Acad. Sci. U. S. A.* **98**, 2698–2702 (2001).

36. Walther, A., Houlston, R. & Tomlinson, I. Association between chromosomal instability and prognosis in colorectal cancer: A meta-analysis. *Gut* **57**, 941–950 (2008).

37. Powell, S. M. *et al.* APC mutations occur early during colorectal tumorigenesis. *Nature* **359**, 235–237 (1992).

38. Ogino, S. *et al.* Prognostic significance and molecular associations of 18q loss of heterozygosity: A cohort study of microsatellite stable colorectal cancers. *J. Clin. Oncol.* **27**, 4591–4598 (2009).

39. Jen, J. *et al.* Allelic Loss of Chromosome 18q and Prognosis in Colorectal Cancer. *N. Engl. J. Med.* **331**, 213–221 (1994).

40. Fleming, N. I. *et al.* SMAD2, SMAD3 and SMAD4 mutations in colorectal cancer. *Cancer Res.* **73**, 725–735 (2013).

41. Zhang, B. *et al.* Antimetastatic Role of Smad4 Signaling in Colorectal Cancer. *Gastroenterology* **138**, 969 (2010).

42. Pino, M. S. & Chung, D. C. The Chromosomal Instability Pathway in Colon Cancer. *Gastroenterology* **138**, 2059–2072 (2010).

43. Muzny, D. M. *et al.* Comprehensive molecular characterization of human colon and rectal cancer. *Nature* **487**, 330–337 (2012).

44. Prior, I. A., Lewis, P. D. & Mattos, C. A comprehensive survey of ras mutations in cancer. *Cancer Research* **72**, 2457–2467 (2012).

45. Singh, M. P., Rai, S., Pandey, A., Singh, N. K. & Srivastava, S. Molecular subtypes of colorectal cancer: An emerging therapeutic opportunity for personalized medicine. *Genes and Diseases* (2019). doi:10.1016/j.gendis.2019.10.013

46. Guinney, J. *et al.* The consensus molecular subtypes of colorectal cancer. *Nat. Med. 2015 2111* **21**, 1350–1356 (2015).

47. Berg, K. C. G. *et al.* Multi-omics of 34 colorectal cancer cell lines - a resource for biomedical studies. *Mol. Cancer* **16**, 1–16 (2017).

48. Le, D. T. *et al.* Mismatch repair deficiency predicts response of solid tumors to

PD-1 blockade. *Science* **357**, 409–413 (2017).

49. Saltz, L. B. *et al.* Phase II trial of cetuximab in patients with refractory colorectal cancer that expresses the epidermal growth factor receptor. *J. Clin. Oncol.* **22**, 1201–1208 (2004).

50. Moroni, M. *et al.* Gene copy number for epidermal growth factor receptor (EGFR) and clinical response to antiEGFR treatment in colorectal cancer: A cohort study. *Lancet Oncol.* **6**, 279–286 (2005).

51. Amado, R. G. *et al.* Wild-type KRAS is required for panitumumab efficacy in patients with metastatic colorectal cancer. *J. Clin. Oncol.* **26**, 1626–1634 (2008).

52. Karapetis, C. S. *et al.* K-ras mutations and benefit from cetuximab in advanced colorectal cancer. *N. Engl. J. Med.* **359**, 1757–1765 (2008).

53. Benvenuti, S. *et al.* Oncogenic activation of the RAS/RAF signaling pathway impairs the response of metastatic colorectal cancers to anti-epidermal growth factor receptor antibody therapies. *Cancer Res.* **67**, 2643–2648 (2007).

54. Schmoll, H. J. *et al.* Esmo consensus guidelines for management of patients with colon and rectal cancer. A personalized approach to clinical decision making. *Ann. Oncol.* **23**, 2479–2516 (2012).

55. Cunningham, D. *et al.* Cetuximab monotherapy and cetuximab plus irinotecan in irinotecan- refractory metastatic colorectal cancer. *N. Engl. J. Med.* **351**, 337–345 (2004).

56. Van Cutsem, E. *et al.* Open-label phase III trial of panitumumab plus best supportive care compared with best supportive care alone in patients with chemotherapy- refractory metastatic colorectal cancer. *J. Clin. Oncol.* **25**, 1658–1664 (2007).

57. Russo, M. *et al.* Tumor heterogeneity and Lesion-Specific response to targeted therapy in colorectal cancer. *Cancer Discov.* **6**, 147–153 (2016).

58. Van Emburgh, B. O., Sartore-Bianchi, A., Di Nicolantonio, F., Siena, S. & Bardelli, A. Acquired resistance to EGFR-targeted therapies incolorectal cancer. *Molecular Oncology* **8**, 1084–1094 (2014).

59. Pufall, M. A. & Kaplan, C. D. Mechanisms of eukaryotic transcription. *Genome Biol.* **14**, 1–3 (2013).

60. Haberle, V. & Stark, A. Eukaryotic core promoters and the functional basis of transcription initiation. *Nat. Rev. Mol. Cell Biol. 2018 1910* **19**, 621–637 (2018).

61. Winston, F. Control of eukaryotic transcription elongation. *Genome Biol.* **2**, reviews1006.1 (2001).

62. Arimbasseri, A. G., Rijal, K. & Maraia, R. J. Transcription termination by the eukaryotic RNA polymerase III. *Biochim. Biophys. Acta* **1829**, 318 (2013).

63. Lambert, M., Jambon, S., Depauw, S. & David-Cordonnier, M. H. Targeting

Transcription Factors for Cancer Treatment. *Mol. 2018, Vol. 23, Page 1479* **23**, 1479 (2018).

64. Sever, R. & Brugge, J. S. Signal Transduction in Cancer. *Cold Spring Harb. Perspect. Med.* **5**, (2015).

65. Ozaki, T. & Nakagawara, A. Role of p53 in Cell Death and Human Cancers. *Cancers (Basel).* **3**, 994 (2011).

66. Lee, H. K., Lee, D. S. & Park, J. C. Nuclear factor I-C regulates E-cadherin via control of KLF4 in breast cancer. *BMC Cancer* **15**, 1–11 (2015).

67. Shen, L., Shi, Q. & Wang, W. Double agents: genes with both oncogenic and tumor-suppressor functions. *Oncog. 2018 73* **7**, 1–14 (2018).

68. Xu, H. *et al.* Transcription factors in colorectal cancer: molecular mechanism and therapeutic implications. *Oncogene 2020 409* **40**, 1555–1569 (2020).

69. Yu, L. L. *et al.* Nuclear factor-kB p65 (RelA) transcription factor is constitutively activated in human colorectal carcinoma tissue. *World J. Gastroenterol.* **10**, 3255 (2004).

70. Slattery, M. L. *et al.* The NF-κB signalling pathway in colorectal cancer: associations between dysregulated gene and miRNA expression. *J. Cancer Res. Clin. Oncol.* **144**, 269 (2018).

71. Vaiopoulos, A. G., Athanasoula, K. C. & Papavassiliou, A. G. NF-κB in colorectal cancer. *J. Mol. Med. (Berl).* **91**, 1029–1037 (2013).

72. Greten, F. R. *et al.* IKKβ links inflammation and tumorigenesis in a mouse model of colitis-associated cancer. *Cell* **118**, 285–296 (2004).

73. Li, J. *et al.* Effects and mechanism of STAT3 silencing on the growth and apoptosis of colorectal cancer cells. *Oncol. Lett.* **16**, 5575–5582 (2018).

74. Corvinus, F. M. *et al.* Persistent STAT3 activation in colon cancer is associated with enhanced cell proliferation and tumor growth. *Neoplasia* **7**, 545–555 (2005).

75. Xiong, H. *et al.* Inhibition of JAK1, 2/STAT3 signaling induces apoptosis, cell cycle arrest, and reduces tumor cell invasion in colorectal cancer cells. *Neoplasia* **10**, 287–297 (2008).

76. Tripathi, M. K. *et al.* Nuclear factor of activated T-cell activity is associated with metastatic capacity in colon cancer. *Cancer Res.* **74**, 6947–6957 (2014).

77. Steven, A. *et al.* Colorectal Carcinogenesis: Connecting K-RAS-Induced Transformation and CREB Activity In Vitro and In Vivo. *Mol. Cancer Res.* **13**, 1248–1262 (2015).

78. Iacopetta, B. TP53 mutation in colorectal cancer. *Hum. Mutat.* **21**, 271–276 (2003).

79. Schulz-Heddergott, R. *et al.* Therapeutic Ablation of Gain-of-Function Mutant p53 in Colorectal Cancer Inhibits Stat3-Mediated Tumor Growth and Invasion.

Cancer Cell **34**, 298-314.e7 (2018).

80. McKeown, S. R. Defining normoxia, physoxia and hypoxia in tumours-implications for treatment response. *Br. J. Radiol.* **87**, (2014).

81. Vaupel, P., Kallinowski, F. & Okunieff, P. Blood flow, oxygen and nutrient supply, and metabolic microenvironment of human tumors: a review. *Cancer Res.* **49**, 6449–65 (1989).

82. Vaupel, P. & Harrison, L. Tumor Hypoxia: Causative Factors, Compensatory Mechanisms, and Cellular Response. *Oncologist* **9**, 4–9 (2004).

83. Vaupel, P. & Med, M. A. The Role of Hypoxia-Induced Factors in Tumor Progression. *Oncologist* **9**, 10–17 (2004).

84. Nishida, N., Yano, H., Nishida, T., Kamura, T. & KDjiro, M. Angiogenesis in Cancer. *Vasc. Health Risk Manag.* **2**, 213 (2006).

85. Prabhakar, N. R. Oxygen sensing during intermittent hypoxia: cellular and molecular mechanisms. *J. Appl. Physiol.* **90**, 1986–1994 (2001).

86. Kimura, H. *et al.* Fluctuations in red cell flux in tumor microvessels can lead to transient hypoxia and reoxygenation in tumor parenchyma. *Cancer Res.* **56**, 5522–5528 (1996).

87. Semenza, G. L. Oxygen Sensing, Hypoxia-Inducible Factors, and Disease Pathophysiology. *Annu. Rev. Pathol. Mech. Dis.* **9**, 47–71 (2014).

88. Vaupel, P. & Med, M. A. Hypoxia and Aggressive Tumor Phenotype: Implications for Therapy and Prognosis. *Oncologist* **13**, 21–26 (2008).

89. Minchinton, A. I. & Tannock, I. F. Drug penetration in solid tumours. *Nature Reviews Cancer* **6**, 583–592 (2006).

90. Tannock, I. Response of Aerobic and Hypoxie Cells in a Solid Tumor to Adriamycin and Cyclophosphamide and Interaction of the Drugs with Radiation1.

91. Gardner, L. B. *et al.* Hypoxia inhibits G1/S transition through regulation of p27 expression. *J. Biol. Chem.* **276**, 7919–7926 (2001).

92. Graeber, T. G. *et al.* Hypoxia-mediated selection of cells with diminished apoptotic potential in solid tumours. *Nature* **379**, 88–91 (1996).

93. Comerford, K. M. *et al.* Hypoxia-inducible Factor-1-dependent Regulation of the Multidrug Resistance (MDR1) Gene 1. *CANCER Res.* **62**, 3387–3394 (2002).

94. Chen, J. *et al.* HIF-1α Inhibition Reverses Multidrug Resistance in Colon Cancer Cells via Downregulation of MDR1/P-Glycoprotein. *PLoS One* **9**, e98882 (2014).

95. GRAY, L. H., CONGER, A. D., EBERT, M., HORNSEY, S. & SCOTT, O. C. The concentration of oxygen dissolved in tissues at the time of irradiation as a factor in radiotherapy. *Br. J. Radiol.* **26**, 638–648 (1953).

96. Brown, J. M. Tumor Hypoxia in Cancer Therapy. *Methods in Enzymology* **435**,

295–321 (2007).

97. Vaupel, P. Tumor microenvironmental physiology and its implications for radiation oncology. *Semin. Radiat. Oncol.* **14**, 198–206 (2004).

98. Kaelin, W. G. & Ratcliffe, P. J. Oxygen Sensing by Metazoans: The Central Role of the HIF Hydroxylase Pathway. *Molecular Cell* **30**, 393–402 (2008).

99. Semenza, G. L. Hypoxia-inducible factors in physiology and medicine. *Cell* **148**, 399–408 (2012).

100. Ema, M. *et al.* A novel bHLH-PAS factor with close sequence similarity to hypoxia-inducible factor 1α regulates the VEGF expression and is potentially involved in lung and vascular development. *Proc. Natl. Acad. Sci. U. S. A.* **94**, 4273–4278 (1997).

101. Wenger, R. H., Stiehl, D. P. & Camenisch, G. Integration of oxygen signaling at the consensus HRE. *Science's STKE : signal transduction knowledge environment* **2005**, (2005).

102. Makino, Y., Kanopka, A., Wilson, W. J., Tanaka, H. & Poellinger, L. Inhibitory PAS domain protein (IPAS) is a hypoxia-inducible splicing variant of the hypoxia-inducible factor-3α locus. *J. Biol. Chem.* **277**, 32405–32408 (2002).

103. Jiang, B. H., Semenza, G. L., Bauer, C. & Marti, H. H. Hypoxia-inducible factor 1 levels vary exponentially over a physiologically relevant range of O 2 tension. *Am. J. Physiol. - Cell Physiol.* **271**, (1996).

104. Wang, G. L., Jiang, B. H., Rue, E. A. & Semenza, G. L. Hypoxia-inducible factor 1 is a basic-helix-loop-helix-PAS heterodimer regulated by cellular O2 tension. *Proc. Natl. Acad. Sci. U. S. A.* **92**, 5510–4 (1995).

105. Wiesener, M. S. *et al.* Widespread hypoxia-inducible expression of HIF-2alpha in distinct cell populations of different organs. *FASEB J.* **17**, 271–273 (2003).

106. Tian, H., McKnight, S. L. & Russell, D. W. Endothelial PAS domain protein 1 (EPAS1), a transcription factor selectively expressed in endothelial cells. *Genes Dev.* **11**, 72–82 (1997).

107. Holmquist-Mengelbier, L. *et al.* Recruitment of HIF-1α and HIF-2α to common target genes is differentially regulated in neuroblastoma: HIF-2α promotes an aggressive phenotype. *Cancer Cell* **10**, 413–423 (2006).

108. Epstein, A. C. *et al.* C. elegans EGL-9 and mammalian homologs define a family of dioxygenases that regulate HIF by prolyl hydroxylation. *Cell* **107**, 43–54 (2001).

109. Huang, L. E., Gu, J., Schau, M. & Bunn, H. F. Regulation of hypoxia-inducible factor 1α is mediated by an O2-dependent degradation domain via the ubiquitin-proteasome pathway. *Proc. Natl. Acad. Sci. U. S. A.* **95**, 7987–7992 (1998).

110. JaakKDla, P. *et al.* Targeting of HIF-α to the von Hippel-Lindau ubiquitylation complex by O2-regulated prolyl hydroxylation. *Science (80-.).* **292**, 468–472

(2001).

111. Mahon, P. C., Hirota, K. & Semenza, G. L. FIH-1: A novel protein that interacts with HIF-1α and VHL to mediate repression of HIF-1 transcriptional activity. *Genes Dev.* **15**, 2675–2686 (2001).

112. KDh, M. Y., Darnay, B. G. & Powis, G. Hypoxia-Associated Factor, a Novel E3-Ubiquitin Ligase, Binds and Ubiquitinates Hypoxia-Inducible Factor 1 , Leading to Its Oxygen-Independent Degradation. *Mol. Cell. Biol.* **28**, 7081–7095 (2008).

113. KDh, M. Y., Lemos, R., Liu, X. & Powis, G. The hypoxia-associated factor switches cells from HIF-1α- to HIF-2α-dependent signaling promoting stem cell characteristics, aggressive tumor growth and invasion. *Cancer Res.* **71**, 4015–4027 (2011).

114. Gingras, A. C., Raught, B. & Sonenberg, N. Regulation of translation initiation by FRAP/mTOR. *Genes Dev.* **15**, 807–826 (2001).

115. Masoud, G. N. & Li, W. HIF-1α pathway: role, regulation and intervention for cancer therapy. *Acta Pharm. Sin. B* **5**, 378–389 (2015).

116. Sang, N. *et al.* MAPK Signaling Up-regulates the Activity of Hypoxia-inducible Factors by Its Effects on p300. *J. Biol. Chem.* **278**, 14013 (2003).

117. Zhong, H. *et al.* Overexpression of hypoxia-inducible factor 1alpha in common human cancers and their metastases. *Cancer Res.* **59**, 5830–5 (1999).

118. Ryan, H. E. *et al. Hypoxia-inducible Factor-1 Is a Positive Factor in Solid Tumor Growth*. *CANCER RESEARCH* **60**, (2000).

119. Raval, R. R. *et al.* Contrasting Properties of Hypoxia-Inducible Factor 1 (HIF-1) and HIF-2 in von Hippel-Lindau-Associated Renal Cell Carcinoma. *Mol. Cell. Biol.* **25**, 5675–5686 (2005).

120. Imamura, T. *et al.* HIF-1α and HIF-2α have divergent roles in colon cancer. *Int. J. Cancer* **124**, 763–771 (2009).

121. Elvert, G. *et al.* Cooperative Interaction of Hypoxia-inducible Factor-2α (HIF-2α) and Ets-1 in the Transcriptional Activation of Vascular Endothelial Growth Factor Receptor-2 (Flk-1). *J. Biol. Chem.* **278**, 7520–7530 (2003).

122. Smythies, J. A. *et al.* Inherent DNA-binding specificities of the HIF-1a and HIF-2a transcription factors in chromatin. doi:10.15252/embr.201846401

123. DenKD, N. C. *et al.* Investigating hypoxic tumor physiology through gene expression patterns. *Oncogene 2003 2237* **22**, 5907–5914 (2003).

124. Lal, A. *et al.* Transcriptional Response to Hypoxia in Human Tumors. *JNCI J. Natl. Cancer Inst.* **93**, 1337–1343 (2001).

125. WyKDff, C. C., Pugh, C. W., Maxwell, P. H., Harris, A. L. & Ratcliffe, P. J. Identification of novel hypoxia dependent and independent target genes of the von Hippel-Lindau (VHL) tumour suppressor by mRNA differential expression profiling. *Oncogene* **19**, 6297–6305 (2000).

126. Semenza, G. L. Regulation of cancer cell metabolism by hypoxia-inducible factor 1. *Semin. Cancer Biol.* **19**, 12–16 (2009).

127. Semenza, G. L. *et al.* Hypoxia response elements in the aldolase A, enolase 1, and lactate dehydrogenase A gene promoters contain essential binding sites for hypoxia-inducible factor 1. *J. Biol. Chem.* **271**, 32529–37 (1996).

128. Chen, C., Pore, N., Behrooz, A., Ismail-Beigi, F. & Maity, A. Regulation of *glut1* mRNA by Hypoxia-inducible Factor-1. *J. Biol. Chem.* **276**, 9519–9525 (2001).

129. Pescador, N. *et al.* Hypoxia Promotes Glycogen Accumulation through Hypoxia Inducible Factor (HIF)-Mediated Induction of Glycogen Synthase 1. *PLoS One* **5**, 9644 (2010).

130. McIntyre, A. *et al.* Carbonic anhydrase IX promotes tumour growth and necrosis in vivo and inhibition enhances anti-VEGF therapy. *Clin. Cancer Res.* **18**, 3100 (2012).

131. Wilson, W. R. & Hay, M. P. Targeting hypoxia in cancer therapy. *Nat. Rev. Cancer 2011 116* **11**, 393–410 (2011).

132. Von Pawel, J. *et al.* Tirapazamine plus cisplatin versus cisplatin in advanced non-small-cell lung cancer: A report of the international CATAPULT I study group. Cisplatin and Tirapazamine in Subjects with Advanced Previously Untreated Non-Small-Cell Lung Tumors. *J. Clin. Oncol.* **18**, 1351–1359 (2000).

133. Borad, M. J. *et al.* Randomized Phase II Trial of Gemcitabine Plus TH-302 Versus Gemcitabine in Patients With Advanced Pancreatic Cancer. *J. Clin. Oncol.* **33**, 1475 (2015).

134. Cutsem, E. Van *et al.* MAESTRO: A randomized, double-blind phase III study of evofosfamide (Evo) in combination with gemcitabine (Gem) in previously untreated patients (pts) with metastatic or locally advanced unresectable pancreatic ductal adenocarcinoma (PDAC). *https://doi.org/10.1200/JCO.2016.34.15_suppl.4007* **34**, 4007–4007 (2016).

135. Spiegelberg, L. *et al.* Hypoxia-activated prodrugs and (lack of) clinical progress: The need for hypoxia-based biomarker patient selection in phase III clinical trials. *Clin. Transl. Radiat. Oncol.* **15**, 62 (2019).

136. Toustrup, K. *et al.* Development of a hypoxia gene expression classifier with predictive impact for hypoxic modification of radiotherapy in head and neck cancer. *Cancer Res.* **71**, 5923–5931 (2011).

137. Poon, E., Harris, A. L. & Ashcroft, M. Targeting the hypoxia-inducible factor (HIF) pathway in cancer. *Expert Rev. Mol. Med.* **11**, (2009).

138. Greenberger, L. M. *et al.* A RNA antagonist of hypoxia-inducible factor-1alpha, EZN-2968, inhibits tumor cell growth. *Mol. Cancer Ther.* **7**, 3598–3608 (2008).

139. Jeong, W. *et al.* Pilot trial of EZN-2968, an antisense oligonucleotide inhibitor of hypoxia-inducible factor-1 alpha (HIF-1α), in patients with refractory solid tumors. *Cancer Chemother. Pharmacol.* **73**, 343 (2014).

140. Reita, D. *et al.* Synergistic Anti-Tumor Effect of mTOR Inhibitors with Irinotecan on Colon Cancer Cells. *Cancers (Basel).* **11**, (2019).

141. Wang, H. *et al.* Targeting mTOR suppressed colon cancer growth through 4EBP1/eIF4E/PUMA pathway. *Cancer Gene Ther. 2019 276* **27**, 448–460 (2019).

142. Tanaka, T., Yamaguchis, J., Shojis, K. & Nangakus, M. Anthracycline Inhibits Recruitment of Hypoxia-inducible Transcription Factors and Suppresses Tumor Cell Migration and Cardiac Angiogenic Response in the Host. *J. Biol. Chem.* **287**, 34866 (2012).

143. Lee, K. A. *et al.* Anthracycline chemotherapy inhibits HIF-1 transcriptional activity and tumor-induced mobilization of circulating angiogenic cells. *Proc. Natl. Acad. Sci. U. S. A.* **106**, 2353–2358 (2009).

144. Befani, C. D. *et al.* Bortezomib represses HIF-1α protein expression and nuclear accumulation by inhibiting both PI3K/Akt/TOR and MAPK pathways in prostate cancer cells. *J. Mol. Med. (Berl).* **90**, 45–54 (2012).

145. Jing, X. *et al.* Role of hypoxia in cancer therapy by regulating the tumor microenvironment. *Mol. Cancer 2019 181* **18**, 1–15 (2019).

146. Shibuya, M. Vascular Endothelial Growth Factor (VEGF) and Its Receptor (VEGFR) Signaling in Angiogenesis: A Crucial Target for Anti- and Pro-Angiogenic Therapies. *Genes Cancer* **2**, 1097–1105 (2011).

147. Giantonio, B. J. *et al.* Bevacizumab in combination with oxaliplatin, fluorouracil, and leucovorin (FOLFOX4) for previously treated metastatic colorectal cancer: Results from the Eastern Cooperative Oncology Group Study E3200. *J. Clin. Oncol.* **25**, 1539–1544 (2007).

148. Yang, Q. *et al.* Bevacizumab plus chemotherapy as third- or later-line therapy in patients with heavily treated metastatic colorectal cancer. *Onco. Targets. Ther.* 2407 (2015). doi:10.2147/OTT.S88679

149. Lopes-Coelho, F., Martins, F., Pereira, S. A. & Serpa, J. Anti-Angiogenic Therapy: Current Challenges and Future Perspectives. *Int. J. Mol. Sci.* **22**, 3765 (2021).

150. Crawford, Y. *et al.* PDGF-C mediates the angiogenic and tumorigenic properties of fibroblasts associated with tumors refractory to anti-VEGF treatment. *Cancer Cell* **15**, 21–34 (2009).

151. Casanovas, O., Hicklin, D. J., Bergers, G. & Hanahan, D. Drug resistance by evasion of antiangiogenic targeting of VEGF signaling in late-stage pancreatic islet tumors. *Cancer Cell* **8**, 299–309 (2005).

152. Allen, E., Walters, I. B. & Hanahan, D. Brivanib, a dual FGF/VEGF inhibitor, is active both first and second line against mouse pancreatic neuroendocrine tumors developing adaptive/evasive resistance to VEGF inhibition. *Clin. Cancer Res.* **17**, 5299–5310 (2011).

153. Burbridge, M. F. *et al.* S49076 is a novel kinase inhibitor of MET, AXL, and FGFR with strong preclinical activity alone and in association with bevacizumab. *Mol. Cancer Ther.* **12**, 1749–1762 (2013).

154. Liu, T., Zhang, L., Joo, D. & Sun, S. C. NF-κB signaling in inflammation. *Signal Transduct. Target. Ther. 2017 21* **2**, 1–9 (2017).

155. Yang, M. H. *et al.* Direct regulation of TWIST by HIF-1α promotes metastasis. *Nat. Cell Biol. 2008 103* **10**, 295–305 (2008).

156. Maxwell, P. J. *et al.* HIF-1 and NF-kappaB-mediated upregulation of CXCR1 and CXCR2 expression promotes cell survival in hypoxic prostate cancer cells. *Oncogene* **26**, 7333–7345 (2007).

157. Cummins, E. P. *et al.* Prolyl hydroxylase-1 negatively regulates IkappaB kinase-beta, giving insight into hypoxia-induced NFkappaB activity. *Proc. Natl. Acad. Sci. U. S. A.* **103**, 18154–18159 (2006).

158. Van Uden, P., Kenneth, N. S. & Rocha, S. Regulation of hypoxia-inducible factor-1alpha by NF-kappaB. *Biochem. J.* **412**, 477–484 (2008).

159. Nakayama, K. cAMP-response Element-binding Protein (CREB) and NF-κB Transcription Factors Are Activated during Prolonged Hypoxia and Cooperatively Regulate the Induction of Matrix Metalloproteinase MMP1. *J. Biol. Chem.* **288**, 22584 (2013).

160. Sharrocks, A. D. The ETS-domain transcription factor family. *Nat. Rev. Mol. Cell Biol.* **2**, 827–837 (2001).

161. Peng, C. *et al.* Integrin αvβ6 and transcriptional factor Ets-1 act as prognostic indicators in colorectal cancer. *Cell Biosci.* **4**, 1–9 (2014).

162. Oikawa, M. *et al.* Hypoxia induces transcription factor ETS-1 via the activity of hypoxia-inducible factor-1. *Biochem. Biophys. Res. Commun.* **289**, 39–43 (2001).

163. ApreliKDva, O., Wood, M., Tackett, S., Chandramouli, G. V. R. & Barrett, J. C. Role of ETS transcription factors in the hypoxia-inducible factor-2 target gene selection. *Cancer Res.* **66**, 5641–5647 (2006).

164. Elvert, G. *et al.* Cooperative interaction of hypoxia-inducible factor-2alpha (HIF-2alpha) and Ets-1 in the transcriptional activation of vascular endothelial growth factor receptor-2 (Flk-1). *J. Biol. Chem.* **278**, 7520–7530 (2003).

165. Chan, Y. C., Khanna, S., Roy, S. & Sen, C. K. miR-200b targets Ets-1 and is down-regulated by hypoxia to induce angiogenic response of endothelial cells. *J. Biol. Chem.* **286**, 2047–2056 (2011).

166. Vazquez, A., Bond, E. E., Levine, A. J. & Bond, G. L. The genetics of the p53 pathway, apoptosis and cancer therapy. *Nat. Rev. Drug Discov.* **7**, 979–987 (2008).

167. Leszczynska, K. B. *et al.* Hypoxia-induced p53 modulates both apoptosis and radiosensitivity via AKT. *J. Clin. Invest.* **125**, 2385–2398 (2015).

168. Zhou, C. H., Zhang, X. P., Liu, F. & Wang, W. Modeling the interplay between the HIF-1 and p53 pathways in hypoxia. *Sci. Reports 2015 51* **5**, 1–10 (2015).

169. Alarcón, R., KDumenis, C., Geyer, R. K., Maki, C. G. & Giaccia, A. J. Hypoxia induces p53 accumulation through MDM2 down-regulation and inhibition of E6-mediated degradation. *Cancer Res.* **59**, 6046–6051 (1999).

170. Fei, P. *et al.* Bnip3L is induced by p53 under hypoxia, and its knockdown promotes tumor growth. *Cancer Cell* **6**, 597–609 (2004).

171. Ravi, R. *et al.* Regulation of tumor angiogenesis by p53-induced degradation of hypoxia-inducible factor 1α. *Genes Dev.* **14**, 34 (2000).

172. Nieminen, A. L., Qanungo, S., Schneider, E. A., Jiang, B. H. & Agani, F. H. Mdm2 and HIF-1alpha interaction in tumor cells during hypoxia. *J. Cell. Physiol.* **204**, 364–369 (2005).

173. Amelio, I. *et al.* p53 mutants cooperate with HIF-1 in transcriptional regulation of extracellular matrix components to promote tumor progression. *Proc. Natl. Acad. Sci. U. S. A.* **115**, E10869–E10878 (2018).

174. Negrini, S., Prada, I., D'Alessandro, R. & Meldolesi, J. REST: an oncogene or a tumor suppressor? *Trends Cell Biol.* **23**, 289–295 (2013).

175. Cavadas, M. A. S. *et al.* REST is a hypoxia-responsive transcriptional repressor. *Sci. Reports 2016 61* **6**, 1–13 (2016).

176. Ooi, L. & Wood, I. C. Chromatin crosstalk in development and disease: lessons from REST. *Nat. Rev. Genet. 2007 87* **8**, 544–554 (2007).

177. Conti, L. *et al.* REST controls self-renewal and tumorigenic competence of human glioblastoma cells. *PLoS One* **7**, (2012).

178. Westbrook, T. F. *et al.* A genetic screen for candidate tumor suppressors identifies REST. *Cell* **121**, 837–848 (2005).

179. Cavadas, M. A. S. *et al.* REST mediates resolution of HIF-dependent gene expression in prolonged hypoxia. *Sci. Reports 2015 51* **5**, 1–12 (2015).

180. Shneor, D., Folberg, R., Pe'Er, J., Honigman, A. & Frenkel, S. Stable knockdown of CREB, HIF-1 and HIF-2 by replication-competent retroviruses abrogates the responses to hypoxia in hepatocellular carcinoma. *Cancer Gene Ther.* **24**, 64–74 (2017).

181. Steven, A. *et al.* Hypoxia-mediated alterations and their role in the HER-2/neuregulated CREB status and localization. *Oncotarget* **7**, 52061 (2016).

182. Røe, K. *et al.* Hypoxic Tumor Kinase Signaling Mediated by STAT5A in Development of Castration-Resistant Prostate Cancer. *PLoS One* **8**, e63723 (2013).

183. Pak, S. H. *et al.* Hypoxia upregulates Hsp90α expression via STAT5b in cancer cells. *Int. J. Oncol.* **41**, 161–168 (2012).

184. Fatrai, S., Wierenga, A. T. J., Daenen, S. M. G. J., Vellenga, E. & Schuringa, J. J.

Identification of HIF2alpha as an important STAT5 target gene in human hematopoietic stem cells. *Blood* **117**, 3320–3330 (2011).

185. Shaulian, E. & Karin, M. AP-1 as a regulator of cell life and death. *Nat. Cell Biol. 2002 45* **4**, E131–E136 (2002).

186. Eferl, R. & Wagner, E. F. AP-1: a double-edged sword in tumorigenesis. *Nat. Rev. Cancer* **3**, 859–868 (2003).

187. Chinenov, Y. & Kerppola, T. K. Close encounters of many kinds: Fos-Jun interactions that mediate transcription regulatory specificity. *Oncogene* **20**, 2438–2452 (2001).

188. Ryseck, R. P. & Bravo, R. c-JUN, JUN B, and JUN D differ in their binding affinities to AP-1 and CRE consensus sequences: Effect of FOS proteins. *Oncogene* **6**, 533–542 (1991).

189. Halazonetis, T. D., Georgopoulos, K., Greenberg, M. E. & Leder, P. c-Jun dimerizes with itself and with c-Fos, forming complexes of different DNA binding affinities. *Cell* **55**, 917–924 (1988).

190. Milde-Langosch, K. The Fos family of transcription factors and their role in tumourigenesis. *Eur. J. Cancer* **41**, 2449–2461 (2005).

191. Jochum, W., Passegué, E. & Wagner, E. F. AP-1 in mouse development and tumorigenesis. *Oncogene* **20**, 2401–2412 (2001).

192. DraKDs, E. *et al.* c-Jun Expression and Activation are Restricted to CD30+ Lymphoproliferative Disorders. *Am. J. Surg. Pathol.* **31**, 447–453 (2007).

193. Eferl, R. *et al.* Liver tumor development: c-Jun antagonizes the proapoptotic activity of p53. *Cell* **112**, 181–192 (2003).

194. Young, M. R. *et al.* Transgenic mice demonstrate AP-1 (activator protein-1) transactivation is required for tumor promotion. *Proc. Natl. Acad. Sci. U. S. A.* **96**, 9827–9832 (1999).

195. Grigoriadis, A. E., Schellander, K., Wang, Z. Q. & Wagner, E. F. Osteoblasts are target cells for transformation in c-fos transgenic mice. *J. Cell Biol.* **122**, 685–701 (1993).

196. Jochum, W. *et al.* Increased bone formation and osteosclerosis in mice overexpressing the transcription factor Fra-1. *Nat. Med.* **6**, 980–984 (2000).

197. El-Fattah Ibrahim, S. A. *et al.* The role of AP-1 in self-sufficient proliferation and migration of cancer cells and its potential impact on an autocrine/paracrine loop. *Oncotarget* **9**, 34259 (2018).

198. Takagi, S., Simizu, S. & Osada, H. RECK negatively regulates matrix metalloproteinase-9 transcription. *Cancer Res.* **69**, 1502–1508 (2009).

199. Belguise, K., Kersual, N., Galtier, F. & Chalbos, D. FRA-1 expression level regulates proliferation and invasiveness of breast cancer cells. *Oncogene* **24**, 1434–1444 (2005).

200. Oliveira-Ferrer, L. *et al.* c-FOS suppresses ovarian cancer progression by changing adhesion. *Br. J. Cancer 2014 1103* **110**, 753–763 (2013).

201. Jin, S. P. *et al.* Prognostic significance of loss of c-fos protein in gastric carcinoma. *Pathol. Oncol. Res.* **13**, 284–289 (2007).

202. Passegué, E., Jochum, W., Schorpp-Kistner, M., Möhle-Steinlein, U. & Wagner, E. F. Chronic myeloid leukemia with increased granulocyte progenitors in mice lacking junB expression in the myeloid lineage. *Cell* **104**, 21–32 (2001).

203. Whitfield, J., Neame, S. J., Paquet, L., Bernard, O. & Ham, J. Dominant-negative c-Jun promotes neuronal survival by reducing BIM expression and inhibiting mitochondrial cytochrome c release. *Neuron* **29**, 629–643 (2001).

204. Rebollo, A. *et al.* Bcl-3 expression promotes cell survival following interleukin-4 deprivation and is controlled by AP1 and AP1-like transcription factors. *Mol. Cell. Biol.* **20**, 3407–3416 (2000).

205. Ashida, R. *et al.* AP-1 and colorectal cancer. *Inflammopharmacology* **13**, 113–125 (2005).

206. Yao, K. S., Xanthoudakis, S., Curran, T. & O'Dwyer, P. J. Activation of AP-1 and of a nuclear redox factor, Ref-1, in the response of HT29 colon cancer cells to hypoxia. *Mol. Cell. Biol.* **14**, 5997–6003 (1994).

207. Premkumar, D. R. *et al.* Intracellular Pathways Linking Hypoxia to Activation of c-fos and AP-1. in *Oxygen Sensing* **475**, 101–109 (Kluwer Academic Publishers, 2000).

208. Fantozzi, I. *et al.* Hypoxia increases AP-1 binding activity by enhancing capacitative Ca^{2+} entry in human pulmonary artery endothelial cells. *Am. J. Physiol. Cell. Mol. Physiol.* **285**, L1233–L1245 (2003).

209. Millhorn, D. E. *et al.* Regulation of gene expression for tyrosine hydroxylase in oxygen sensitive cells by hypoxia. *Kidney Int.* **51**, 527–535 (1997).

210. Shi, Q. *et al.* Cooperation Between Transcription Factor AP-1 and NF-kappa B in the Induction of Interleukin-8 in Human Pancreatic Adenocarcinoma Cells by Hypoxia. *J. Interf. Cytokine Res.* **19**, 1363–1371 (1999).

211. Yamashita, K., Discher, D. J., Hu, J., Bishopric, N. H. & Webster, K. A. Molecular Regulation of the Endothelin-1 Gene by Hypoxia. *J. Biol. Chem.* **276**, 12645–12653 (2001).

212. Bandyopadhyay, R. S., Phelan, M. & Faller, D. V. Hypoxia induces AP-1-regulated genes and AP-1 transcription factor binding in human endothelial and other cell types. *Biochim. Biophys. Acta* **1264**, 72–8 (1995).

213. SalniKDw, K. *et al.* The regulation of hypoxic genes by calcium involves c-Jun/AP-1, which cooperates with hypoxia-inducible factor 1 in response to hypoxia. *Mol. Cell. Biol.* **22**, 1734–41 (2002).

214. Yu, B. *et al.* c-Jun Protects Hypoxia-Inducible Factor-1 from Degradation via Its Oxygen-Dependent Degradation Domain in a Nontranscriptional Manner.

Cancer Res. **69**, 7704–7712 (2009).

215. Laderoute, K. R., Calaoagan, J. M., Knapp, M. & Johnson, R. S. Glucose Utilization Is Essential for Hypoxia-Inducible Factor 1 -Dependent Phosphorylation of c-Jun. *Mol. Cell. Biol.* **24**, 4128–4137 (2004).

216. Le, Q. T. & Courter, D. Clinical Biomarkers for Hypoxia Targeting. *Cancer Metastasis Rev.* **27**, 351 (2008).

217. Lin, W. *et al.* Characterization of Hypoxia Signature to Evaluate the Tumor Immune Microenvironment and Predict Prognosis in Glioma Groups. *Front. Oncol.* **10**, 796 (2020).

218. Yang, L. *et al.* Development and Validation of a 28-gene Hypoxia-related Prognostic Signature for Localized Prostate Cancer. *EBioMedicine* **31**, 182–189 (2018).

219. Zou, Y. F. *et al.* A signature of hypoxia-related factors reveals functional dysregulation and robustly predicts clinical outcomes in stage I/II colorectal cancer patients. *Cancer Cell Int.* **19**, (2019).

220. Yang, Y. *et al.* Prognostic value of a hypoxia-related microRNA signature in patients with colorectal cancer. *Aging (Albany. NY).* **12**, 35–52 (2020).

221. Abou Khouzam, R. *et al.* An Eight-Gene Hypoxia Signature Predicts Survival in Pancreatic Cancer and Is Associated With an Immunosuppressed Tumor Microenvironment. *Front. Immunol.* **12**, (2021).

222. Zhang, Y. *et al.* Hypoxia Constructing the Prognostic Model of Colorectal Adenocarcinoma and Related to the Immune Microenvironment. *Front. Cell Dev. Biol.* **9**, (2021).

223. KDh, M. Y. & Powis, G. Passing the baton: the HIF switch. *Trends Biochem. Sci.* **37**, 364–372 (2012).

224. Ameyar, M., Wisniewska, M. & Weitzman, J. B. A role for AP-1 in apoptosis: The case for and against. *Biochimie* **85**, 747–752 (2003).

225. Guo, W. *et al.* M6A methylation of DEGS2, a key ceramide-synthesizing enzyme, is involved in colorectal cancer progression through ceramide synthesis. *Oncogene 2021 4040* **40**, 5913–5924 (2021).

226. Huang, W. C. *et al.* Sphingosine-1-phosphate phosphatase 2 promotes disruption of mucosal integrity, and contributes to ulcerative colitis in mice and humans. *FASEB J.* **30**, 2945–2958 (2016).

227. Zhu, Y. *et al.* NUDT21 Promotes Tumor Growth and Metastasis Through Modulating SGPP2 in Human Gastric Cancer. *Front. Oncol.* **11**, (2021).

228. Ogretmen, B. Sphingolipid metabolism in cancer signalling and therapy. *Nat. Rev. Cancer 2017 181* **18**, 33–50 (2017).

229. Yin, J., Miyazaki, K., Shaner, R. L., Merrill, A. H. & Kannagi, R. Altered sphingolipid metabolism induced by tumor hypoxia -New vistas in glycolipid

tumor markers. *FEBS Lett.* **584**, 1872 (2010).

230. Cui, G., Cai, F., Ding, Z. & Gao, L. MMP14 predicts a poor prognosis in patients with colorectal cancer. *Hum. Pathol.* **83**, 36–42 (2019).

231. Robey, I. F., Lien, A. D., Welsh, S. J., Baggett, B. K. & Gillies, R. J. Hypoxia-Inducible Factor-1α and the Glycolytic Phenotype in Tumors. *Neoplasia* **7**, 324 (2005).

232. Archer, M. C. Role of Sp Transcription Factors in the Regulation of Cancer Cell Metabolism. *Genes Cancer* **2**, 712 (2011).

233. Li, L. *et al.* Transcriptional Regulation of the Warburg Effect in Cancer by SIX1. *Cancer Cell* **33**, 368-385.e7 (2018).

234. Dong, H. *et al.* PTPRO represses ERBB2-driven breast oncogenesis by dephosphorylation and endosomal internalization of ERBB2. *Oncogene 2017 363* **36**, 410–422 (2016).

235. Dai, W. *et al.* PTPRO represses colorectal cancer tumorigenesis and progression by reprogramming fatty acid metabolism. *Cancer Commun. (London, England)* **42**, (2022).

236. Xu, Y., Li, J., Wang, P., Zhang, Z. & Wang, X. LncRNA HULC promotes lung squamous cell carcinoma by regulating PTPRO via NF-κB. *J. Cell. Biochem.* **120**, 19415–19421 (2019).

237. Bläsius, F. M. *et al.* Loss of cadherin related family member 5 (CDHR5) expression in clear cell renal cell carcinoma is a prognostic marker of disease progression. *Oncotarget* **8**, 75076–75086 (2017).

238. Hinkel, I. *et al.* Cdx2 Controls Expression of the Protocadherin Mucdhl, an Inhibitor of Growth and β-Catenin Activity in Colon Cancer Cells. (2012). doi:10.1053/j.gastro.2011.12.037

239. Zhao, J. *et al.* ANGPTL4 overexpression is associated with progression and poor prognosis in breast cancer. *Oncol. Lett.* **20**, 2499 (2020).

240. Fattahi, F. *et al.* High expression of DNA damage-inducible transcript 4 (DDIT4) is associated with advanced pathological features in the patients with colorectal cancer. *Sci. Reports 2021 111* **11**, 1–17 (2021).

241. Gao, R. *et al.* PFKFB4 Promotes Breast Cancer Metastasis via Induction of Hyaluronan Production in a p38-Dependent Manner. *Cell. Physiol. Biochem.* **50**, 2108–2123 (2018).

242. Gomez, A. *et al.* Expression of CYP2W1 in colon tumors: regulation by gene methylation. *Pharmacogenomics* **8**, 1315–1325 (2007).

243. Nishida, C. R., Lee, M. & Ortiz De Montellano, P. R. Efficient hypoxic activation of the anticancer agent AQ4N by CYP2S1 and CYP2W1. *Mol. Pharmacol.* **78**, 497–502 (2010).

244. Wan, X. *et al.* FOSL2 promotes VEGF-independent angiogenesis by

transcriptionnally activating Wnt5a in breast cancer-associated fibroblasts. *Theranostics* **11**, 4975–4991 (2021).

245. Böckers, M., Paul, N. W. & Efferth, T. Bisphenolic compounds alter gene expression in MCF-7 cells through interaction with estrogen receptor α. *Toxicol. Appl. Pharmacol.* **399**, (2020).

246. Böckers, M., Paul, N. W. & Efferth, T. Organophosphate ester tri-o-cresyl phosphate interacts with estrogen receptor α in MCF-7 breast cancer cells promoting cancer growth. *Toxicol. Appl. Pharmacol.* **395**, (2020).

247. Jung, J. Human Tumor Xenograft Models for Preclinical Assessment of Anticancer Drug Development. *Toxicol. Res.* **30**, 1 (2014).

248. Kharman-Biz, A. *et al.* Expression of activator protein-1 (AP-1) family members in breast cancer. *BMC Cancer* **13**, 1–10 (2013).

249. Mar, A. C. *et al.* Interleukin-1 Receptor Type 2 Acts with c-Fos to Enhance the Expression of Interleukin-6 and Vascular Endothelial Growth Factor A in Colon Cancer Cells and Induce Angiogenesis. *J. Biol. Chem.* **290**, 22212–22224 (2015).

250. Jin, S. P. *et al.* Prognostic significance of loss of c-fos protein in gastric carcinoma. *Pathol. Oncol. Res.* **13**, 284–289 (2007).

251. Yin, J. *et al.* HGF/MET Regulated Epithelial-Mesenchymal Transitions And Metastasis By FOSL2 In Non-Small Cell Lung Cancer. *Onco. Targets. Ther.* **12**, 9227 (2019).

252. Li, S., Fang, X. dong, Wang, X. ying & Fei, B. yuan. Fos-like antigen 2 (FOSL2) promotes metastasis in colon cancer. *Exp. Cell Res.* **373**, 57–61 (2018).

253. Kidger, A. M., Sipthorp, J. & Cook, S. J. ERK1/2 inhibitors: New weapons to inhibit the RAS-regulated RAF-MEK1/2-ERK1/2 pathway. *Pharmacol. Ther.* **187**, 45–60 (2018).

254. Brennan, A., Leech, J. T., Kad, N. M. & Mason, J. M. Selective antagonism of cJun for cancer therapy. *J. Exp. Clin. Cancer Res.* **39**, 1–16 (2020).

255. Dai, J., Punchihewa, C., Mistry, P., Ooi, A. T. & Yang, D. Novel DNA bis-intercalation by MLN944, a potent clinical bisphenazine anticancer drug. *J. Biol. Chem.* **279**, 46096–46103 (2004).

256. Di Nicolantonio, F. *et al.* The ex vivo characterization of XR5944 (MLN944) against a panel of human clinical tumor samples. *Mol. Cancer Ther.* **3**, 1631–1637 (2004).

257. Byers, S. A., Schafer, B., Sappal, D. S., Brown, J. & Price, D. H. The antiproliferative agent MLN944 preferentially inhibits transcription. *Mol. Cancer Ther.* **4**, 1260–1267 (2005).

258. Lin, C., Mathad, R. I., Zhang, Z., Sidell, N. & Yang, D. Solution structure of a 2:1 complex of anticancer drug XR5944 with TFF1 estrogen response element: insights into DNA recognition by a bis-intercalator. *Nucleic Acids Res.* **42**, 6012–6024 (2014).

259. Huang, C. *et al.* Blocking activator protein-1 activity, but not activating retinoic acid response element, is required for the antitumor promotion effect of retinoic acid. *Proc. Natl. Acad. Sci. U. S. A.* **94**, 5826 (1997).

260. Mishra, D. K. & Kim, M. P. SR 11302, an AP-1 Inhibitor, Reduces Metastatic Lesion Formation in Ex Vivo 4D Lung Cancer Model. *Cancer Microenviron.* **10**, 95 (2017).

261. Izuta, S. *et al.* T-5224, a selective inhibitor of c-Fos/activator protein-1, attenuates lipopolysaccharide-induced liver injury in mice. *Biotechnol. Lett.* **34**, 2175–2182 (2012).

262. Aikawa, Y. *et al.* Treatment of arthritis with a selective inhibitor of c-Fos/activator protein-1. *Nat. Biotechnol.* **26**, 817–823 (2008).

263. Kamide, D. *et al.* Selective activator protein-1 inhibitor T-5224 prevents lymph node metastasis in an oral cancer model. *Cancer Sci.* **107**, 666–673 (2016).

264. Olive, M. *et al.* A dominant negative to activation protein-1 (AP1) that abolishes DNA binding and inhibits oncogenesis. *J. Biol. Chem.* **272**, 18586–18594 (1997).

265. Biddie, S. C. *et al.* Transcription Factor AP1 Potentiates Chromatin Accessibility and Glucocorticoid Receptor Binding. *Mol. Cell* **43**, 145 (2011).

266. Bains, N. P. S. *et al.* Zipping up transcription factors: Rational design of anti-Jun and anti-Fos peptides. *Lett. Pept. Sci. 1997 42* **4**, 67–77 (1997).

267. Simon, R., Mirlacher, M. & Sauter, G. Tissue microarrays. *Biotechniques* **36**, 98–105 (2004).

268. Lugli, A., Karamitopoulou, E. & Zlobec, I. Tumour budding: a promising parameter in colorectal cancer. *Br. J. Cancer* **106**, 1713 (2012).

269. Kalluri, R. EMT: when epithelial cells decide to become mesenchymal-like cells. *J. Clin. Invest.* **119**, 1417–1419 (2009).

270. Kirchner, T. & Brabletz, T. Patterning and Nuclear β-Catenin Expression in the Colonic Adenoma-Carcinoma Sequence : Analogies with Embryonic Gastrulation. *Am. J. Pathol.* **157**, 1113 (2000).

271. Righi, A. *et al.* Tumour budding is associated with hypoxia at the advancing front of colorectal cancer. *Histopathology* **66**, 982–990 (2015).

272. KDelzer, V. H. *et al.* The tumor border configuration of colorectal cancer as a histomorphological prognostic indicator. (2014). doi:10.3389/fonc.2014.00029

273. Liebig, C. *et al.* Perineural Invasion Is an Independent Predictor of Outcome in Colorectal Cancer. *J. Clin. Oncol.* **27**, 5131 (2009).

274. Shen, L., Shi, Q. & Wang, W. Double agents: genes with both oncogenic and tumor-suppressor functions. *Oncog. 2018 73* **7**, 1–14 (2018).

275. Ameyar-Zazoua, M. *et al.* AP-1 dimers regulate transcription of the p14/p19ARF tumor suppressor gene. *Oncogene 2005 2414* **24**, 2298–2306

(2005).

276. Sarode, P. *et al.* Reprogramming of tumor-associated macrophages by targeting β-catenin/FOSL2/ARID5A signaling: A potential treatment of lung cancer. *Sci. Adv.* **6**, (2020).

277. Wang, H., Tian, T. & Zhang, J. Tumor-Associated Macrophages (TAMs) in Colorectal Cancer (CRC): From Mechanism to Therapy and Prognosis. *Int. J. Mol. Sci.* **22**, (2021).

278. Bhullar, K. S. *et al.* Kinase-targeted cancer therapies: progress, challenges and future directions. *Mol. Cancer 2018 171* **17**, 1–20 (2018).

279. Zhu, G., Pei, L., Xia, H., Tang, Q. & Bi, F. Role of oncogenic KRAS in the prognosis, diagnosis and treatment of colorectal cancer. *Mol. Cancer 2021 201* **20**, 1–17 (2021).

280. Fruman, D. A. *et al.* The PI3K pathway in human disease. *Cell* **170**, 605 (2017).

281. Hamada, T., Nowak, J. A. & Ogino, S. PIK3CA mutation and colorectal cancer precision medicine. *Oncotarget* **8**, 22305 (2017).

282. Samuels, Y. *et al.* High frequency of mutations of the PIK3CA gene in human cancers. *Science* **304**, 554 (2004).

283. Zhou, X. P. *et al.* PTEN mutational spectra, expression levels, and subcellular localization in microsatellite stable and unstable colorectal cancers. *Am. J. Pathol.* **161**, 439–447 (2002).

284. Dhillon, A. S., Hagan, S., Rath, O. & KDlch, W. MAP kinase signalling pathways in cancer. *Oncogene 2007 2622* **26**, 3279–3290 (2007).

285. Morrison, D. K. MAP Kinase Pathways. *Cold Spring Harb. Perspect. Biol.* **4**, (2012).

286. KDvarik, P. *et al.* Stress-induced phosphorylation of STAT1 at Ser727 requires p38mitogen-activated protein kinase whereas IFN-γ uses a differentsignaling pathway. *Proc. Natl. Acad. Sci. U. S. A.* **96**, 13956 (1999).

287. Smeby, J. *et al.* CMS-dependent prognostic impact of KRAS and BRAFV600E mutations in primary colorectal cancer. *Ann. Oncol.* **29**, 1227 (2018).

288. Davies, H. *et al.* Mutations of the BRAF gene in human cancer. *Nature* **417**, 949–954 (2002).

289. Maughan, T. S. *et al.* Addition of cetuximab to oxaliplatin-based first-line combination chemotherapy for treatment of advanced colorectal cancer: Results of the randomised phase 3 MRC COIN trial. *Lancet* **377**, 2103–2114 (2011).

290. Douillard, J.-Y. *et al.* Panitumumab-FOLFOX4 Treatment and RAS Mutations in Colorectal Cancer A BS T R AC T. *N Engl J Med* **369**, 1023–1057 (2013).

291. Li, Q. H. *et al.* Anti-EGFR therapy in metastatic colorectal cancer: mechanisms and potential regimens of drug resistance. *Gastroenterol. Rep.* **8**, 179–191

(2020).

292. Xie, Y. H., Chen, Y. X. & Fang, J. Y. Comprehensive review of targeted therapy for colorectal cancer. *Signal Transduct. Target. Ther. 2020 51* **5**, 1–30 (2020).

293. KDpetz, S. *et al.* Phase II Pilot Study of Vemurafenib in Patients With Metastatic BRAF-Mutated Colorectal Cancer. *J. Clin. Oncol.* **33**, 4032–4038 (2015).

294. Corcoran, R. B. *et al.* EGFR-mediated re-activation of MAPK signaling contributes to insensitivity of BRAF mutant colorectal cancers to RAF inhibition with vemurafenib. *Cancer Discov.* **2**, 227–235 (2012).

295. Corcoran, R. B. *et al.* Combined BRAF, EGFR, and MEK Inhibition in Patients With BRAFV600E-Mutant Colorectal Cancer. *Cancer Discov.* **8**, 428 (2018).

296. Forsythe, J. A. *et al.* Activation of vascular endothelial growth factor gene transcription by hypoxia-inducible factor 1. *Mol. Cell. Biol.* **16**, 4604–4613 (1996).

297. Wang, Y. *et al.* Hypoxia promotes ligand-independent EGF receptor signaling via hypoxia-inducible factor-mediated upregulation of caveolin-1. *Proc. Natl. Acad. Sci. U. S. A.* **109**, 4892–4897 (2012).

298. Simiantonaki, N. *et al.* Hypoxia-induced epithelial VEGF-C/VEGFR-3 upregulation in carcinoma cell lines. *Int. J. Oncol.* **32**, 585–592 (2008).

299. Toschi, A., Lee, E., Gadi, N., Ohh, M. & Foster, D. A. Differential dependence of hypoxia-inducible factors 1 alpha and 2 alpha on mTORC1 and mTORC2. *J. Biol. Chem.* **283**, 34495–34499 (2008).

300. Dodd, K. M., Yang, J., Shen, M. H., Sampson, J. R. & Tee, A. R. mTORC1 drives HIF-1α and VEGF-A signalling via multiple mechanisms involving 4E-BP1, S6K1 and STAT3. *Oncogene* **34**, 2239 (2015).

301. Flügel, D., Görlach, A., Michiels, C. & Kietzmann, T. Glycogen synthase kinase 3 phosphorylates hypoxia-inducible factor 1alpha and mediates its destabilization in a VHL-independent manner. *Mol. Cell. Biol.* **27**, 3253–3265 (2007).

302. Sang, N. *et al.* MAPK signaling up-regulates the activity of hypoxia-inducible factors by its effects on p300. *J. Biol. Chem.* **278**, 14013–14019 (2003).

303. Ye, N., Ding, Y., Wild, C., Shen, Q. & Zhou, J. Small molecule inhibitors targeting activator protein 1 (AP-1). *J. Med. Chem.* **57**, 6930–6948 (2014).

304. Eferl, R. & Wagner, E. F. AP-1: a double-edged sword in tumorigenesis. *Nat. Rev. Cancer* **3**, 859–868 (2003).

305. Gazon, H., Barbeau, B., Mesnard, J. M. & Peloponese, J. M. Hijacking of the AP-1 signaling pathway during development of ATL. *Front. Microbiol.* **8**, 2686 (2018).

306. KDul, D. *et al.* PTEN down regulates AP-1 and targets c-fos in human glioma

cells via PI3-kinase/Akt pathway. *Mol. Cell. Biochem.* **300**, 77–87 (2007).

307. Zhang, X., Tang, N., Hadden, T. J. & Rishi, A. K. Akt, FoxO and regulation of apoptosis. *Biochim. Biophys. Acta - Mol. Cell Res.* **1813**, 1978–1986 (2011).

308. Garces de Los Fayos Alonso, I. *et al.* The Role of Activator Protein-1 (AP-1) Family Members in CD30-Positive Lymphomas. *Cancers (Basel).* **10**, (2018).

309. Baker, S. J. *et al.* Jun is phosphorylated by several protein kinases at the same sites that are modified in serum-stimulated fibroblasts. *Mol. Cell. Biol.* **12**, 4694 (1992).

310. Smeal, T., Binetruy, B., Mercola, D. A., Birrer, M. & Karin, M. Oncogenic and transcriptional cooperation with Ha-Ras requires phosphorylation of c-Jun on serines 63 and 73. *Nature* **354**, 494–496 (1991).

311. Ogawa, S. *et al.* A nuclear receptor corepressor transcriptional checkpoint controlling activator protein 1-dependent gene networks required for macrophage activation. *Proc. Natl. Acad. Sci. U. S. A.* **101**, 14461–14466 (2004).

312. Vinciguerra, M. *et al.* Differential Phosphorylation of c-Jun and JunD in Response to the Epidermal Growth Factor Is Determined by the Structure of MAPK Targeting Sequences. *J. Biol. Chem.* **279**, 9634–9641 (2004).

313. Gallo, A. *et al.* Menin uncouples Elk-1, JunD and c-Jun phosphorylation from MAP kinase activation. *Oncogene* **21**, 6434–6445 (2002).

314. Vincent, E. E. *et al.* Akt phosphorylation on Thr308 but not on Ser473 correlates with Akt protein kinase activity in human non-small cell lung cancer. *Br. J. Cancer* **104**, 1755 (2011).

315. VadlaKDnda, L., Dash, A., Pasupuleti, M., Kumar, K. A. & Reddanna, P. The Paradox of Akt-mTOR Interactions. *Front. Oncol.* **3**, (2013).

316. Nayak, B. K. *et al.* Stabilization of HIF-2alpha through redox regulation of mTORC2 activation and initiation of mRNA translation. *Oncogene* **32**, 3147 (2013).

317. Seul-Ki, C., Kam, H., Kye-Young, K., In Park, S. & Yun-Sil, L. Targeting Heat Shock Protein 27 in Cancer: A Druggable Target for Cancer Treatment? *Cancers (Basel).* **11**, (2019).

318. Musiani, D. *et al.* Heat-shock protein 27 (HSP27, HSPB1) is up-regulated by MET kinase inhibitors and confers resistance to MET-targeted therapy. *FASEB J.* **28**, 4055–4067 (2014).

319. Huang, C. Y., Wei, P. L., Chen, W. Y., Chang, W. C. & Chang, Y. J. Silencing Heat Shock Protein 27 Inhibits the Progression and Metastasis of Colorectal Cancer (CRC) by Maintaining the Stability of Stromal Interaction Molecule 1 (STIM1) Proteins. *Cells* **7**, (2018).

320. Joung, Y. H. *et al.* Hypoxia activates signal transducers and activators of transcription 5 (STAT5) and increases its binding activity to the GAS element in

mammary epithelial cells. *Exp. Mol. Med.* **35**, 350–357 (2003).

321. Røe, K. *et al.* Hypoxic Tumor Kinase Signaling Mediated by STAT5A in Development of Castration-Resistant Prostate Cancer. *PLoS One* **8**, e63723 (2013).

322. Tang, Y., Weng, X., Liu, C., Li, X. & Chen, C. Hypoxia Enhances Activity and Malignant Behaviors of Colorectal Cancer Cells through the STAT3/MicroRNA-19a/PTEN/PI3K/AKT Axis. *Anal. Cell. Pathol. (Amst).* **2021**, (2021).

323. Zhao, F. L. & Qin, C. F. EGF promotes HIF-1α expression in colorectal cancer cells and tumor metastasis by regulating phosphorylation of STAT3. *Eur. Rev. Med. Pharmacol. Sci.* **23**, 1055–1062 (2019).

324. Choi, H., Chun, Y. S., Kim, T. Y. & Park, J. W. HIF-2alpha enhances beta-catenin/TCF-driven transcription by interacting with beta-catenin. *Cancer Res.* **70**, 10101–10111 (2010).

325. Zhang, Q. *et al.* Hypoxia-inducible factor-2α promotes tumor progression and has crosstalk with Wnt/β-catenin signaling in pancreatic cancer. *Mol. Cancer* **16**, 1–14 (2017).

326. Claesson-Welsh, L. How the matrix metalloproteinase MMP14 contributes to the progression of colorectal cancer. *J. Clin. Invest.* **130**, 1093–1095 (2020).

327. Wang, Z. *et al.* DNER promotes epithelial–mesenchymal transition and prevents chemosensitivity through the Wnt/β-catenin pathway in breast cancer. *Cell Death Dis.* **11**, (2020).

328. Yin, J. *et al.* HGF/MET Regulated Epithelial-Mesenchymal Transitions And Metastasis By FOSL2 In Non-Small Cell Lung Cancer. *Onco. Targets. Ther.* **12**, 9227 (2019).

329. Kidger, A. M. *et al.* Dual-mechanism ERK1/2 inhibitors exploit a distinct binding mode to block phosphorylation and nuclear accumulation of ERK1/2. *Mol. Cancer Ther.* **19**, 525–539 (2020).

330. Mohammed, H. *et al.* Rapid immunoprecipitation mass spectrometry of endogenous proteins (RIME) for analysis of chromatin complexes. *Nat. Protoc.* **11**, 316–326 (2016).

331. Yang, Y. *et al.* HIF-1 Interacts with TRIM28 and DNA-PK to release paused RNA polymerase II and activate target gene transcription in response to hypoxia. *Nat. Commun.* **13**, (2022).

332. Uniacke, J. *et al.* An oxygen-regulated switch in the protein synthesis machinery. *Nat. 2012 4867401* **486**, 126–129 (2012).

333. Sen, M. *et al.* ARID1A facilitates KRAS signaling-regulated enhancer activity in an AP1-dependent manner in colorectal cancer cells. *Clin. Epigenetics* **11**, 1–16 (2019).

334. Bejjani, F., Evanno, E., Zibara, K., Piechaczyk, M. & Jariel-Encontre, I. The AP-1 transcriptional complex: Local switch or remote command? *Biochim. Biophys.*

acta. Rev. cancer **1872**, 11–23 (2019).

335. Ndlovu, 'Matladi N. *et al.* Hyperactivated NF-κB and AP-1 Transcription Factors Promote Highly Accessible Chromatin and Constitutive Transcription across the Interleukin-6 Gene Promoter in Metastatic Breast Cancer Cells. *Mol. Cell. Biol.* **29**, 5488 (2009).

336. Gillet, J. P. *et al.* Redefining the relevance of established cancer cell lines to the study of mechanisms of clinical anti-cancer drug resistance. *Proc. Natl. Acad. Sci. U. S. A.* **108**, 18708–18713 (2011).

337. Dancik, G. M., Ru, Y., Owens, C. R. & Theodorescu, D. A framework to select clinically relevant cancer cell lines for investigation by establishing their molecular similarity with primary human cancers. *Cancer Res.* **71**, 7398–7409 (2011).

338. Luo, L., Ma, Y., Zheng, Y., Su, J. & Huang, G. Application Progress of Organoids in Colorectal Cancer. *Front. Cell Dev. Biol.* **10**, 307 (2022).

339. McKeown, S. R. Defining normoxia, physoxia and hypoxia in tumours—implications for treatment response. *Br. J. Radiol.* **87**, (2014).